Sulfur Cycling in the Water Columns of Lakes and Oceans

Thesis by

Alexandra Atlee Phillips

In Partial Fulfillment of the Requirements

for the degree of

Doctor of Philosophy

CALIFORNIA INSTITUTE OF TECHNOLOGY

Pasadena, California

2021

(Defended April 29, 2021)

Alexandra Atlee Phillips
ORCID: 0000-0001-5959-5238

ACKNOWLEDGEMENTS

On my first day as a graduate student at Caltech, a professor joked that PhD's in GPS were often "raised by a village." Now, at the finish line of this nearly six-year journey, I am realizing just how large my village was.

I have to start with my fellow first years in the basement office horribly (but aptly) nicknamed "the pit." Maddie, we suffered through those P-Chem sets together and nearly broke each other in the process, but I could never have done it without you. Usha, you knew exactly when it was time for a tea and banana bread break. We got each other through the worst moments of our PhD's—I'm so thankful you were in my village. Sujung, thank you for the countless climbing sessions; Hao, for the many lessons on mass spectrometry; Gray, for all things microbiology; Joe, for all things geology; and Lee, for conversations to step away from science.

At Caltech, I was lucky to be in the lab of Alex Sessions, who always had an open door for my never-ending inquiries about running mass spectrometers or derivatization reactions in the lab. I've never encountered a professor so generous with their time. Thank you for the countless edits to my manuscripts and the endless advice on my research projects. I'm grateful for the scientist you helped me become. The Sessions Lab had a somewhat secret second PI, who I somehow bothered with even more questions. Fenfang, I would never have finished this PhD without you. Both because of how often you saved my samples and because of the friendship you offered when I needed it most—thank you. To all lab technicians, support staff, and administrators at GPS, you are immensely appreciated.

My committee is filled with other wonderful professors. John, thank you for your open door for conversations about isotopes, careers, and science fiction. Jared, I appreciate the many hallway conversations about photography and the even longer office chats about microbes in Mono Lake. Jess, your knowledge of oceanography and willingness to share your insights have been instrumental to my thesis. Julie, thank you for coming in at the last hour to share your expertise for my final chapter. To other professors at Caltech: Woody, George, Victoria, even though you are not members of my committee, you were part of the village that raised me. From looking at rocks and minerals in your offices, to developing ideas in reading groups, to taking field trips to salty lakes—I have learned so much from your mentorship. Larry, I know you aren't a professor, but I looked up to you just the same. Thank you for making the too hot (or too freezing) days on a small boat so enjoyable, for always being ready to grab a post-fieldwork beer at Mono Lake café, and for your positive feedback when I needed it the most.

My village was also filled with incredible graduate students and post-docs. Preston, thank you for rescuing me throughout my thesis, even if you still aren't convinced

that organic sulfur is interesting. Ted and Frankie, I owe you so many beers. Thanks for always being there for science, for sulfur, for tennis, for everything. Grace and Yoni, you were the best and worst office mates ever—the best for the conversations, the meals, the laughs—and the worst for my productivity. Danie and Elise, how would I have survived Mono Lake trips without you both? Miquela, thank you for being the best exercise/coloring/coffee buddy anyone could ask for. Mak, I don't think anyone at Caltech has seen so many of my tears as you—thank you for being there. Shae, Hannah, Elliott, Elle, Tony, Reto, Paula, Karli, Morgan, Max, Holly, Dan, Gabriella, Selva, Eryn, and everyone I'm forgetting to name—thank you for putting up with my constant requests for manuscript and figure edits, for keeping my spirits high, for your help in the lab, for your friendship, for all of it.

I dedicated a lot of my free time as a graduate student to the greater scientific community, through outreach centered in diversity, equity, and inclusion. But in all honesty, this work has given me more than I could ever provide. The staff at the Caltech Y has been like a second department, coaxing my passion for science policy and supporting my new endeavors for RISE summer programs. Liz, thank you for turning my crazy ideas into reality. While I am thanking people for taking my insane ideas and running with them, I must turn to the staff at AGU, especially Victoria and Liz. Thank you for helping me launch the Wonder Fund, for paying the open-access fees of my science policy paper, for supporting Mujeres Haciendo Ciencia and Women Doing Science. To my incredible international team at Women Doing Science, you know what you do for the page and me. Thank you for believing in this mission. Thank you to Westridge for trusting me to mentor three of your wonderful high school students: Brenna, Hannah, and Audrey. It has been an immense pleasure to work with you all.

To my friends and family: Brittney, Halle, Sara, Ben, Blaire, Andrew, Alejandra, Tom, Sherry, Mom, Dad—I don't know how to thank you all for the decades of love and support you have shown me. The care packages, the weekend trips, the home cooked meals, the much-needed occasional alcoholic beverage…my village may be centered at Caltech, but its roots are with you. Mom, thank you for being the first one to show me what a scientist could look like. I hope I have made you all proud.

Finally, Dr. Alexander Weber Spott (this is a full name moment), I could not have made it through this journey without you. Thank you for joining me in the lab at 2 a.m. before fieldwork and learning what "acid-washing" entailed. Thank you for ordering food to my apartment door when I was too stressed to remember to feed myself. Thank you for driving to Pasadena literally every two weeks for six years just so we could spend our weekends together. Thank you for spending hours with me as I verbally processed my results and outlined my papers. I'm not sure you completely understand sulfur isotopes, but you might as well be a coauthor on all my publications. You are a wonderful engineer, scientist, fiancé, cat dad, climbing buddy, barista, and all-around adventure partner. I love you.

ABSTRACT

Sulfur is a critical bioelement central to many of Earth's biogeochemical cycles. Studies of sulfur have overwhelmingly focused on sediments, where transformations between organic and inorganic sulfur phases drive short-term biological reactions and long-term climate cycles. However, sulfur cycling in the water column is just as dynamic and exerts similar controls over biogeochemical cycles in lakes and oceans – although the exact dynamics are only beginning to be understood. This thesis provides new understanding of sulfur cycling in aquatic environments through three chapters that span laboratory developments and field observations. Chapter 1 presents a time-series in enigmatic Mono Lake, CA, where the temporal dynamics of sulfur cycling microbes was investigated. This study, published in *Geobiology,* highlights the dependency of sulfate reduction and oxidation on lake chemistry and the need for studies to move beyond "snapshots" of microbial diversity. Chapter 2, published in *Rapid Communications in Mass Spectrometry,* presents development of a highly sensitive (1-10 μg S) mass spectrometry technique that allows, for the first time, sulfur isotope measurements of amino acids. These new measurements permitted discovery of new connections between metabolism and sulfur isotope signatures. Chapter 3 further applies these novel methods, making the first sulfur isotope measurements of marine dissolved organic matter. The data indicated that marine organic sulfur is entirely produced by phytoplankton and implied that heterotrophic bacteria rapidly and efficiently recycle reduced sulfur compounds, even in the water column. Taken together, these three chapters significantly advanced available tools for studying sulfur in the environment and expanded our understanding of modern aquatic sulfur cycling. The final chapter represents a departure from oceans, lakes, mass spectrometry, and sulfur. Here, I evaluate the success and impacts of my outreach project, the popular Women Doing Science Instagram, in portraying diverse, international women scientists, noting the powerful potential for social media to bolster STEM identity for graduate students.

PUBLISHED CONTENT AND CONTRIBUTIONS

Phillips, A.A., Speth, D.R., Miller, L.G., Wang, X.T., Wu, F., Medeiros, P.M., Monteverde, D.R., Osburn, M.R., Berelson, W.M., Betts, H.L., Wijker, R.S., Mullin, S.W., Johnson, H.A., Orphan, V.J., Fischer, W.W., Geobiology Course 2017, Geobiology Course 2018, Sessions, A.L. Microbial succession and dynamics in meromictic Mono Lake, California. Geobiology. doi: 10.1111/gbi.12437

A.A.P. participated in the conception of the project, data analysis, and sample collection and was the primary author on the manuscript.

Phillips, A.A., Wu, F., Sessions, A.L., 2021. Sulfur isotope analysis of cysteine and methionine via preparatory liquid chromatography and elemental analyzer isotope ratio mass spectrometry. Rapid Communications in Mass Spectrometry 35, e9007. doi: 10.1002/rcm.9007.

A.A.P. helped design the project, analyzed samples, iterated on methods development, interpreted the results, and was the primary author of the manuscript.

TABLE OF CONTENTS

INTRODUCTION

Studies on the cycling of sulfur, a critical bioelement, have overwhelmingly focused on sediments, where transformations are important drivers for both short-term biology (Canfield, 2001; Jørgensen et al., 2019) and long-term climate (Berner, 1987). However, sulfur cycling in aquatic systems, especially of organic sulfur, is just as dynamic and holds a large influence on global biogeochemical cycles. This thesis presents three chapters on aquatic sulfur cycling to address this gap, from the water column of Mono Lake to novel laboratory measurements to organic sulfur in the modern ocean.

In the last decade, there has been a growing recognition that organic sulfur plays a central role in the biology of lakes and oceans. Studies in low sulfate environments like Lake Superior found that organic sulfur produced in the water column is the dominant substrate for microbial sulfate reduction, linking sulfur cycling in the water columns to sediment processes (Fakhraee et al., 2017). Links between sulfur and carbon cycles were identified in freshwater bacteria that host a novel synthesis pathway for methionine that releases hydrocarbons like methane (North et al., 2020). In the ocean, common marine heterotrophs have lost the ability to assimilate sulfate, and are entirely reliant on scavenging organic sulfur from their environment (Tripp et al., 2008; Dupont et al., 2012). Genomic surveys have found that these are not isolated findings, identifying a diverse suite of marine microbes capable of transforming sulfur metabolites (Moran and Durham, 2019). Taken together, these recent results support the realization of a decidedly active role of organic sulfur in aquatic ecosystems.

These pivotal studies that shine a spotlight on organic sulfur in lakes and oceans have largely focused on chemical quantifications or genetic surveys. Isotope

investigations, meanwhile, have been severely limited due to difficulties in analytical chemistry and instrumentation (Ksionzek et al., 2016; Pohlabeln et al., 2017; Raven et al., 2020). Luckily, creative new solutions have been developed for the latter problem through innovations in mass spectrometry systems (*e.g.,* GC-MC-ICP-MS, EA-IRMS; Raven et al., 2015; Sayle et al., 2019). However, their applications to *organic* sulfur compounds remain hindered by the former, analytical chemistry. Sulfur compounds, especially polar metabolites relevant to biology, are extremely redox sensitive. The same properties that make them ideal for controlling oxidation and reduction reactions in our cells make them difficult to recover in the laboratory (Rampler et al., 2012). There is a distinct need to bridge the gaps between isolation and measurement of organic sulfur compounds. Expanding sulfur isotope investigations to include these tricky organic species could help answer outstanding questions in aquatic systems that chemical and biological investigations have failed to resolve. For instance, sulfur isotope compositions could be leveraged for mass balance calculations to finally close the marine sulfur cycle (Ksionzek et al., 2016).

This thesis probes the role of sulfur in aquatic biogeochemical cycles, with a focus on measuring organic components. The first chapter examines the important role sulfur plays in Mono Lake, combining biological and chemical data over a time series investigation (Phillips et al., 2021). The second chapter presents a novel method of measuring the sulfur isotope composition of individual organic molecules, such as the amino acids cysteine and methionine, on a mass spectrometry system optimized for S (Phillips et al., 2021). The third chapter applies the same method to determine the sulfur isotope values of dissolved organic matter in the ocean.

Chapters 1 and 3 directly examine sulfur cycling in the water column of a hypersaline lake and the modern ocean. Both reveal the dynamic nature of biotic sulfur cycling in aquatic ecosystems: for example, the temporal dependency of sulfate reduction on lake chemistry and the role of marine phytoplankton in supplying reduced sulfur

for heterotrophs. Chapters 2 and 3 highlight the power of sulfur isotopes as tools to investigate organic sulfur – the rewards of solving difficult analytical chemistry separations. Both compound-specific investigations of amino acids and bulk measurements of marine organic matter demonstrate that metabolism does indeed discriminate systematically against heavy sulfur isotopes. Together, these studies support a paradigm shift in the understanding of sulfur, especially organic sulfur, in water columns: that sulfur cycling is not decidedly inactive bur rather full of highly dynamic processes that are just beginning to be uncovered.

The analytical tools developed in this thesis are applicable beyond the water columns of lakes and oceans. For example, compound-specific isotope analysis of cysteine and methionine may unlock novel liver cancer biomarkers (Albalat et al., 2016), offer more constrained paleodiet indicators for ancient civilizations (Fourel et al., 2015), or inform soil scientists about the efficiency of sulfur in fertilizer (Tcherkez and Tea, 2013). Studies of Mono Lake's extreme chemistry may inform policy makers about the unintended consequences of freshwater diversions in drought-ridden states. We can use our understanding of organic sulfur from the modern ocean to teach us lessons of the past, better constraining models that rely on sulfur to unravel the history of Earth's climate.

The last chapter of this thesis is a departure from lakes, oceans, sulfur, and mass spectrometry. For many students, especially those from marginalized groups (*e.g.*, women, people of color), diversity, equity, and inclusion (DEI) work is as integral to their science as time in the lab or field. Until academic systems reward these services, it is difficult to imagine closing gender or racial gaps across the "leaky pipeline" (Domingo et al., 2020). This chapter takes a small step towards recognizing the scientific merit of graduate outreach work, discussing a case study of depicting diversity on social media. I founded Women Doing Science in 2018 to showcase daily stories and images of the myriad identities of women in STEM from around the

world. Analysis of the Instagram page revealed that posts indeed reflect diverse, international female scientists. Further, online audiences not only rewarded diversity with higher engagement, but also specifically sought it out on Instagram. This highlights the power of social media to portray role models with intersectional identities for students that may lack real-life examples in their family or university. Further, it demonstrates the importance of diverse representation in STEM, a lesson that can be translated to mitigate racial and gender imbalances within academic structures.

BIBLIOGRAPHY

Albalat, E., Telouk, P., Balter, V., Fujii, T., Bondanese, V.P., Plissonnier, M.-L., Vlaeminck-Guillem, V., Baccheta, J., Thiam, N., Miossec, P., Zoulim, F., Puisieux, A., Albarède, F., 2016. Sulfur isotope analysis by MC-ICP-MS and application to small medical samples. Journal of Analytical Atomic Spectrometry 31, 1002–1011.

Berner, R.A., 1987. Models for carbon and sulfur cycles and atmospheric oxygen; application to Paleozoic geologic history. American Journal of Science 287, 177–196.

Canfield, D.E., 2001. Biogeochemistry of Sulfur Isotopes. Reviews in Mineralogy and Geochemistry 43, 607–636.

Domingo, C.R., Gerber, N.C., Harris, D., Mamo, L., Pasion, S.G., Rebanal, R.D., Rosser, S.V., 2020. More service or more advancement: Institutional barriers to academic success for women and women of color faculty at a large public comprehensive minority-serving state university. Journal of Diversity in Higher Education.

Dupont, C.L., Rusch, D.B., Yooseph, S., Lombardo, M.-J., Alexander Richter, R., Valas, R., Novotny, M., Yee-Greenbaum, J., Selengut, J.D., Haft, D.H., Halpern, A.L., Lasken, R.S., Nealson, K., Friedman, R., Craig Venter, J., 2012. Genomic insights to SAR86, an abundant and uncultivated marine bacterial lineage. The ISME Journal 6, 1186–1199.

Fakhraee, M., Li, J., Katsev, S., 2017. Significant role of organic sulfur in supporting sedimentary sulfate reduction in low-sulfate environments. Geochimica et Cosmochimica Acta 213, 502–516.

Fourel, F., Lécuyer, C., Balter, V., 2015. New Frontiers for Sulfur Isotopic Analyses. Procedia Earth and Planetary Science, 11th Applied Isotope Geochemistery Conference AIG-11 13, 232–239.

Jørgensen, B.B., Findlay, A.J., Pellerin, A., 2019. The Biogeochemical Sulfur Cycle of Marine Sediments. Frontiers in Microbiology 10.

Ksionzek, K.B., Lechtenfeld, O.J., McCallister, S.L., Schmitt-Kopplin, P., Geuer, J.K., Geibert, W., Koch, B.P., 2016. Dissolved organic sulfur in the ocean: Biogeochemistry of a petagram inventory. Science 354, 456–459.

Moran, M.A., Durham, B.P., 2019. Sulfur metabolites in the pelagic ocean. Nature Reviews Microbiology 17, 665–678.

North, J.A., Narrowe, A.B., Xiong, W., Byerly, K.M., Zhao, G., Young, S.J., Murali, S., Wildenthal, J.A., Cannon, W.R., Wrighton, K.C., Hettich, R.L., Tabita, F.R., 2020. A nitrogenase-like enzyme system catalyzes methionine, ethylene, and methane biogenesis. Science 369, 1094–1098.

Peterson, B.J., Howarth, R.W., Garritt, R.H., 1985. Multiple Stable Isotopes Used to Trace the Flow of Organic Matter in Estuarine Food Webs. Science 227, 1361–1363.

Phillips, A.A., Speth, D.R., Miller, L.G., Wang, X.T., Wu, F., Medeiros, P.M., Monteverde, D.R., Osburn, M.R., Berelson, W.M., Betts, H.L., Wijker, R.S., Mullin, S.W., Johnson, H.A., Orphan, V.J., Fischer, W.W., Sessions, A.L., Geobiology Course 2017, Geobiology Course 2018, 2021. Microbial succession and dynamics in meromictic Mono Lake, California. Geobiology.

Phillips, A.A., Wu, F., Sessions, A.L., 2021. Sulfur isotope analysis of cysteine and methionine via preparatory liquid chromatography and elemental analyzer isotope ratio mass spectrometry. Rapid Communications in Mass Spectrometry 35, e9007.

Pohlabeln, A.M., Gomez-Saez, G.V., Noriega-Ortega, B.E., Dittmar, T., 2017. Experimental Evidence for Abiotic Sulfurization of Marine Dissolved Organic Matter. Frontiers in Marine Science 4.

Rampler, E., Dalik, T., Stingeder, G., Hann, S., Koellensperger, G., 2012. Sulfur containing amino acids – challenge of accurate quantification. Journal of Analytical Atomic Spectrometry 27, 1018–1023.

Raven, M.R., Adkins, J.F., Werne, J.P., Lyons, T.W., Sessions, A.L., 2015. Sulfur isotopic composition of individual organic compounds from Cariaco Basin sediments. Organic Geochemistry 80, 53–59.

Raven, M.R., Keil, R.G., Webb, S.M., 2020. Microbial sulfate reduction and organic sulfur formation in sinking marine particles. Science.

Sayle, K.L., Brodie, C.R., Cook, G.T., Hamilton, W.D., 2019. Sequential measurement of δ15N, δ13C and δ34S values in archaeological bone collagen at the Scottish Universities Environmental Research Centre (SUERC): A new analytical frontier. Rapid Communications in Mass Spectrometry 33, 1258–1266.

Tcherkez, G., Tea, I., 2013. 32S/34S isotope fractionation in plant sulphur metabolism. New Phytologist 200, 44–53.

Tripp, H.J., Kitner, J.B., Schwalbach, M.S., Dacey, J.W.H., Wilhelm, L.J., Giovannoni, S.J., 2008. SAR11 marine bacteria require exogenous reduced sulphur for growth. Nature 452, 741–744.

Chapter 1

MICROBIAL SUCCESSION AND DYNAMICS IN MEROMICTIC MONO LAKE, CALIFORNIA

Phillips, A.A., Speth, D.R., Miller, L.G., Wang, X.T., Wu, F., Medeiros, P.M., Monteverde, D.R., Osburn, M.R., Berelson, W.M., Betts, H.L., Wijker, R.S., Mullin, S.W., Johnson, H.A., Orphan, V.J., Fischer, W.W., Geobiology Course 2017, Geobiology Course 2018, Sessions, A.L. Microbial succession and dynamics in meromictic Mono Lake, California. Geobiology. doi: https://doi.org/10.1111/gbi.12437

ABSTRACT

Mono Lake is a closed-basin, hypersaline, alkaline lake located in Eastern Sierra Nevada, California, that is dominated by microbial life. This unique ecosystem offers a natural laboratory for probing microbial community responses to environmental change. In 2017, a heavy snowpack and subsequent runoff led Mono Lake to transition from annually mixed (monomictic) to indefinitely stratified (meromictic). We followed microbial succession during this limnological shift, establishing a two-year (2017–2018) water-column time series of geochemical and microbiological data. Following meromictic conditions, anoxia persisted below the chemocline and reduced compounds such as sulfide and ammonium increased in concentration from near 0 to ~400 and ~150 μM, respectively, throughout 2018. We observed significant microbial succession, with trends varying by water depth. In the epilimnion (above the chemocline), aerobic heterotrophs were displaced by phototrophic genera when a large bloom of cyanobacteria appeared in fall 2018. Bacteria in the hypolimnion (below the chemocline) had a delayed, but systematic, response reflecting colonization by sediment "seed bank" communities. Phototrophic sulfide-oxidizing bacteria appeared first in summer 2017, followed by

microbes associated with anaerobic fermentation in spring 2018, and eventually sulfate-reducing taxa by fall 2018. This slow shift indicated that multi-year meromixis was required to establish a sulfate-reducing community in Mono Lake, although sulfide oxidizers thrive throughout mixing regimes. The abundant green alga *Picocystis* remained the dominant primary producer during the meromixis event, abundant throughout the water column including in the hypolimnion despite the absence of light and prevalence of sulfide. Our study adds to the growing literature describing microbial resistance and resilience during lake mixing events related to climatic events and environmental change.

SUMMARY STATEMENT

We investigated microbial succession in hypersaline, alkaline Mono Lake, California, following a climatic perturbation. By combining geochemical and microbiological data, we were able to link depth-dependent microbial community shifts to limnological changes.

1 | INTRODUCTION

The interplay between microbial communities, biogeochemical cycling, and changing environmental conditions is of long-standing interest. Related questions such as the pace and dynamics of microbial succession have been less explored, presumably due to the inherent difficulty of observing natural ecosystems in the midst of dramatic changes. Existing studies of aquatic microbial succession in lakes have focused mainly on loss of stratification, presumably for practical reasons of timing and access. These studies (Hollibaugh et al., 2001; Jones et al., 2008; Shade et al., 2011, 2012) suggested that aquatic communities were generally quite stable in the face of disturbance due to mixing, with high resistance and resilience. We are not aware of any previously published time series examining succession across the onset of stratification and anoxia. Given that climate models and field observations alike suggest future increases in lake

stratification with global warming (Peeters et al., 2002; Arvola et al., 2009), this represents a significant knowledge gap. Here, we report a two-year time series (2017–2018) of microbial diversity and geochemistry from Mono Lake, California, that captures one such transition—the lake's shift from annually mixed (monomictic) to indefinitely stratified (meromictic), following an exceptionally large snowmelt in 2017. This dataset provided a unique opportunity to study both shifts in microbial composition and lake geochemistry that accompany the onset of stratification, as well as the timing of these changes.

Mono Lake is a hypersaline (~85 ppt, ~3x seawater salinity), alkaline (pH 9.8), closed-basin lake located in the eastern Sierra Nevada Mountains of California, USA (38°N, 119°W; Figure 1). Water enters the lake primarily from snowmelt via streams (Wilson Creek, Mill Creek, Rush Creek, Lee Vining Creek) and exits by evaporation (~1 m/yr). This hydrologic condition, combined with weathering of Sierran granite in the lake's watershed, produces the high salinity and pH characteristic of Mono Lake (Garrels and Mackenzie, 1967). These properties also tightly tie lake levels and water chemistry to climate, with modern and Pleistocene high stands correlated with wet Sierra Nevada conditions (Benson et al., 1998). Further, primary productivity in Mono Lake is extremely high (269–1060 g C m^{-2} yr^{-1}) due largely to the activity of the green alga *Picocystis* sp. strain ML (Jellison and Melack, 1993). The brine shrimp *Artemia monica* is the predominant metazoan predator in Mono Lake, feeding on *Picocystis* and in turn supplying a food source to hundreds of thousands of migrating birds that flock to the lake annually on the Pacific Flyway (Wiens et al., 1993). Thus, despite its modest size and extreme chemistry, Mono Lake serves an essential ecological role beyond the Sierra Nevada. Seasonal surveys of primary production, *Artemia*, and birds such as grebes, gulls, and phalaropes have been conducted since at least 1980 (Cooper et al., 1984; Melack et al., 2017), though they have not provided much insight into Mono Lake's microbial community.

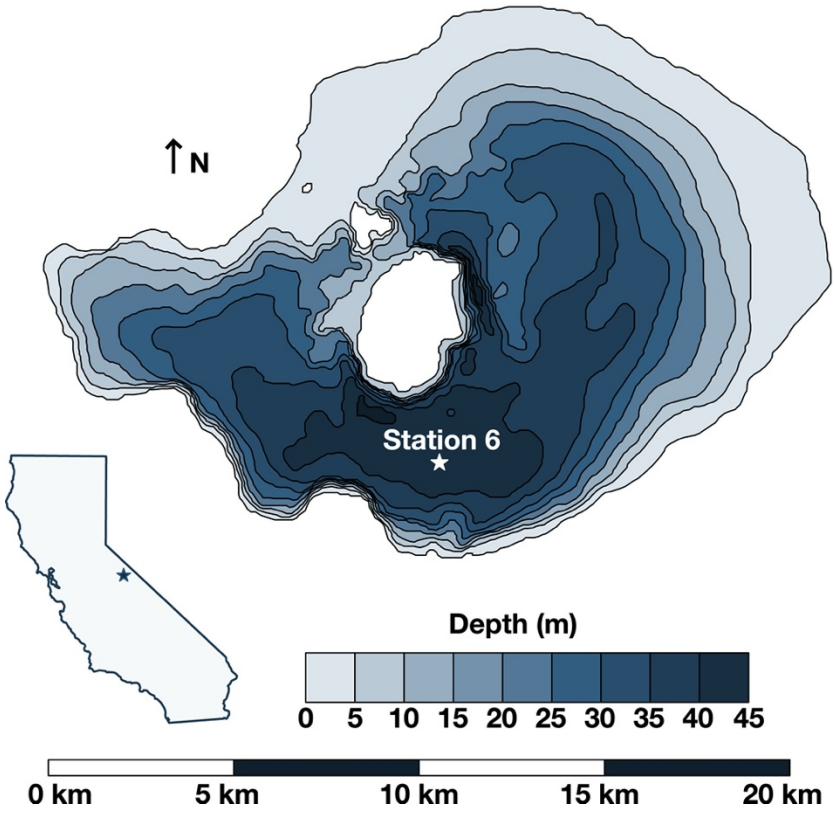

Figure 1 *Bathymetric map of Mono Lake after* (Bruce et al., 2008)*. Location is indicated on the California map insert with a blue star. All samples were collected from Station 6 in the south basin, marked with a white star. White areas on the map correspond to Paoha island (larger island) and Negit Island to the north.*

Mono Lake is typically monomictic, with thermally driven summer stratification disrupted by winter, wind-driven overturn. However, in years with very high spring–summer freshwater inputs, often correlated with El Niño–Southern Oscillation (ENSO) events, a buoyant layer with >10 ppt lower salinity can form at the surface of the lake that withstands winter mixing. This leads to protracted stratification that can continue for five or more years, depending on continued water balance and storm severity. During this time, the hypolimnion becomes euxinic, with sulfide concentrations reaching hundreds of micromolar (Miller et al., 1993). For example, following the deep snow pack associated with the 1982 ENSO, summer melting brought a 2.6 m lake level rise that triggered persistent stratification from 1983

through 1989 (Melack et al., 2017). Mono Lake was again meromictic from 1996 to 2004 and from 2006 to 2008. It has since remained monomictic until the exceptional snow year of 2017 when our study began.

Although there have been numerous studies of Mono Lake, none have yet captured the microbial response to the onset of meromixis with high-throughput sequencing. (Hollibaugh et al. (2001) quantified bacterial clades using denaturing gradient gel electrophoresis (DGGE) but found no evidence for microbial community restructuring between 1994 and 1995 when the lake became meromictic. Further DGGE studies conducted between 2000 and 2006, as part of the Mono Lake Microbial Observatory, cataloged responses of particular metabolic clades including aerobic methanotrophs (Carini et al., 2005), sulfate reducers (Scholten et al., 2005), nitrifiers (Carini and Joye, 2008), and methylotrophs (Nercessian et al., 2005). Recently, two studies of Mono Lake have used next-generation sequencing technology, including 16S rRNA gene amplicon sequencing, environmental metagenomics, and transcriptomics (Edwardson and Hollibaugh, 2017; Stamps et al., 2018), but these investigations focused on single time points. To supplement this literature, we monitored Mono Lake at the onset of a new meromictic period that began in 2017. Our two-year (thus far) time series reflects six seasonal sampling dates with physical, chemical, and biological data to characterize Mono Lake during this transition.

2 | METHODS

2.1 | Water Sampling

All water sampling was conducted at “Station 6” (37.95739 N, −119.0316 W), a representative site in the deepest part of the south basin, marked by a buoy (Figure 1). Samples were collected on May 23, June 22, and September 19, 2017 (hereafter referred to as spring 2017, summer 2017, and fall 2017, respectively), and May 8, June 13, and October 9, 2018 (spring 2018, summer 2018, and fall

2018, respectively). Sampling was preceded by measurements of conductivity, temperature, dissolved oxygen, and photosynthetically active radiation (PAR) using a SeaBird SBE 19 CTD cast to 35 m depth. Salinity profiles were initially calculated from conductivity after Jellison et al. (1999). While this produced accurate bottom-water salinity estimates (as compared to handheld refractometer measurements of 86 ± 2 ppt; Atago S-28E), it also yielded sharp fluctuations in salinity across the thermocline, which we do not believe are physically plausible and which made interpreting the structure of the chemocline difficult. Instead, we used the default SeaBird seawater calibration of our CTD, then scaled each profile linearly to a bottom-water salinity of 86. This produced a smoother chemocline structure (Figure 2a), but potentially at the expense of less accurate surface salinity values. Discrete water samples were collected using a 5-L Niskin bottle or a 2" diameter submersible well pump at five to eight depths. When the pump was used, water flowed through the pump and tubing at each depth for at least two minutes before sampling. *Artemia monica* (brine shrimp) were removed from sampled water using a 10-μm Nitex-screen filter. Water aliquots were taken for dissolved inorganic carbon (DIC), dissolved organic carbon (DOC), dissolved organic nitrogen (DON), sulfate and sulfide, nutrients and major ions, particulate organic carbon (POC) and fatty acids (FAs), 16S rRNA gene amplicon sequencing, and incubations. Not all parameters were sampled on all dates, as described in Table S1.

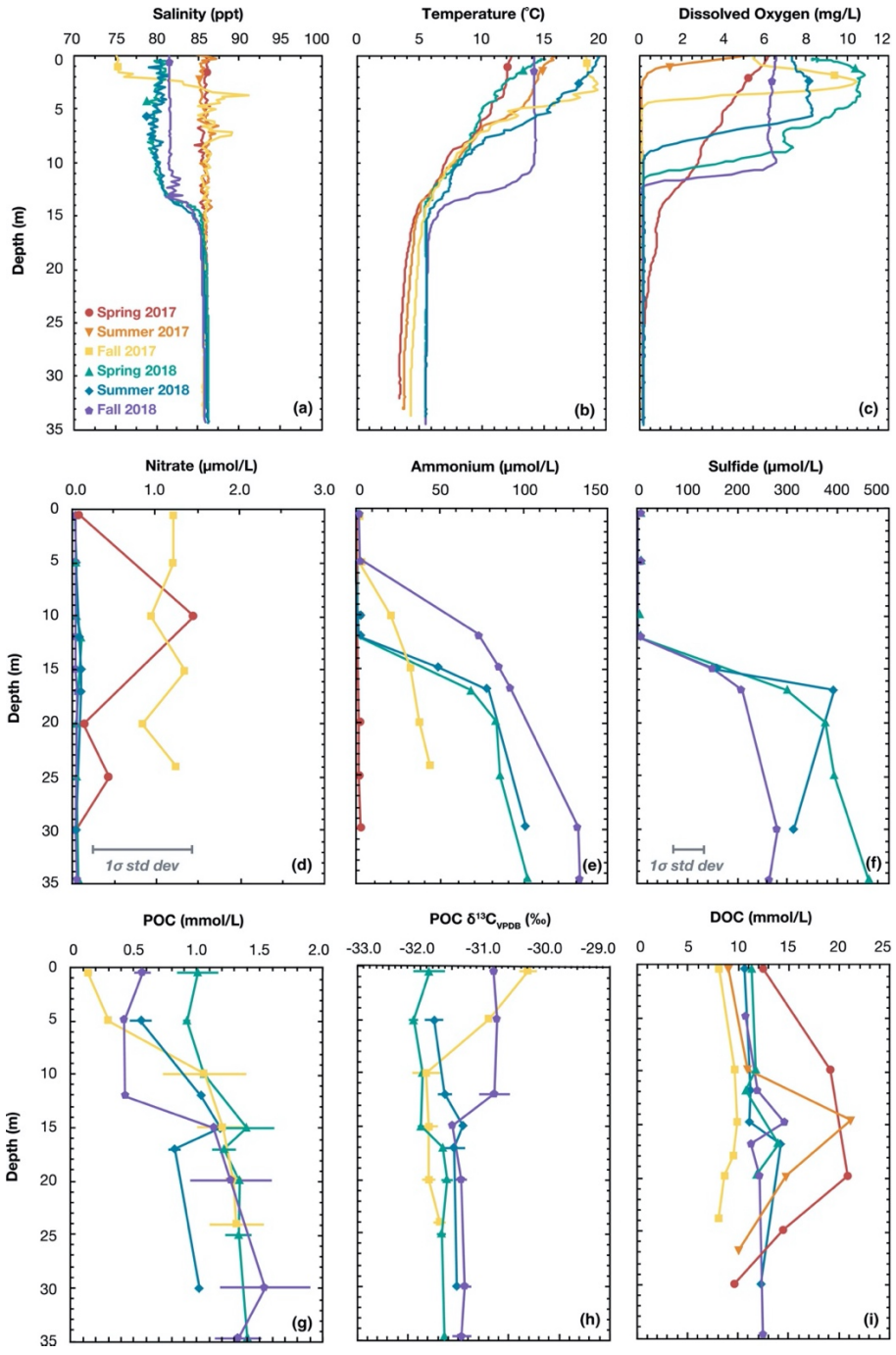

Figure 2 *Vertical profiles of (a) salinity, (b) temperature, (c) dissolved oxygen, (d) nitrate, (e) ammonium, (f) sulfide, (g) particulate organic carbon (POC) (h), POC* $\delta^{13}C_{VPDB}$*, and (i) dissolved organic carbon (DOC) concentrations at Station 6, Mono Lake, CA. Profiles were measured in spring 2017 (red circles), summer 2017*

(orange inverted triangles), fall 2017 (yellow squares), spring 2018 (green triangles), summer 2018 (blue diamonds), and fall 2018 (purple pentagons)

2.2 l Geochemical measurements

2.2.1 l Sulfide and sulfate

Water (7 ml) was immediately preserved for sulfide analysis by filtering through a 0.22-μm polyvinylidene difluoride (PVDF) syringe filter into a 15-ml falcon tube containing 3 ml zinc acetate (1 M), precipitating zinc sulfide and zinc carbonate. Samples were kept at room temperature until analysis. Concentrations were measured using a modified spectrophotometric assay (Cline, 1969) at Caltech, described in detail in the SI. Replicate measurements yielded typical 1σ standard deviations of 30 μM.

Water (10 ml) was subsampled on the boat for dissolved sulfate by filtering through a 0.22 μm PVDF syringe filter into a 15-ml falcon tube containing 200 μl hydrochloric acid (3 M). HCl was added to volatilize H_2S and to suppress biological activity. Samples were stored at room temperature until analysis. Sulfate concentrations were measured with a Dionex Ion Chromatography System 2000 equipped with an AS29-Fast (4 μm diameter) column at Caltech, yielding 1σ standard deviations of 1.5 mM for sample replicates (~1.2% rsd).

2.2.2 l Nutrients and major ions

Water (50 ml) from the POM filtrate (see below) was subsampled on shore into 50-ml falcon tubes and frozen at –20°C until shipment on dry ice to Scripps Institution of Oceanography Nimitz Marine Facility for nutrient analysis. There, phosphate, silica, nitrate, nitrite, and ammonium concentrations were analyzed by modified colorimetric assays (Armstrong et al., 1967; Bernhardt and Wilhelms, 1967) on a SEAL Analytical segmented continuous-flow AutoAnalyzer 3. Nutrient standards

yielded 1σ standard deviations of 1 μM for nitrate, phosphate, and ammonium and 0.01 μM for nitrite and silica. For cation measurements, an additional 15 ml of filtered water was subsampled into 15-ml falcon tubes and kept frozen until analysis. Concentrations of K^{+}, Mg^{2+}, Ca^{2+}, Si^{4+}, Sr^{2+}, Li^{2+}, Fe^{2+}, and Mn^{2+} were analyzed on a Thermo Element2 high-resolution inductively coupled plasma mass spectrometer (HR-ICP-MS) at the University of Southern California, using external calibration. The calibration standards had major ion ratios similar to Mono Lake water. IAPSO (International Association for the Physical Sciences of the Ocean) standard seawater was analyzed as a reference.

2.2.3 l Dissolved inorganic carbon (DIC)

Water for DIC analysis was collected directly from the Niskin bottle on the boat and filtered through a 0.22-μM polyether sulfone (PES) syringe filter into 15-ml falcon tubes until overflowing. For analysis, 0.1–0.4 g water was injected into an evacuated, 10-ml Exetainer and 5 ml of 10% phosphoric acid was added. The evolved CO_2 was analyzed following (Subhas et al., 2015). Exetainer gases were purged with N_2 flushing through a mass control valve into a mixing bag (Liaison-Picarro). Gas was fed via N_2 carrier to a Picarro Cavity Ring Down Spectrometer (G2131-i) at University of Southern California for analysis of total ^{12}C and ^{13}C. Weighed $CaCO_3$ working standards were used for calibration. Replicate samples yielded 1σ standard deviations of ±4 μM DIC (at 2000 μM) and 0.15‰ for $\delta^{13}C_{VCDT}$.

2.2.4 l Dissolved organic carbon (DOC)

On the boat, 500 ml of water was subsampled for DOC analysis into acid-cleaned 1-L amber bottles (Nalgene, HDPE) and placed on ice. Directly after returning to the lake shore, this water was filtered through pre-washed 0.22 μm PES syringe filters into acid-washed 60-ml amber bottles (Nalgene) and frozen at –20°C. Immediately before analysis, samples were thawed and acidified to pH 2 with 10 M hydrochloric acid (HCl). DOC concentrations were measured with a Shimadzu

TOC-L_{CPH} analyzer at University of Georgia. Potassium hydrogen phthalate was used as a standard for the DOC calibration curve (prepared the same day). Internal blanks and ultrapure water (>18.2 MΩ) blanks were also analyzed at the same time. Analytical accuracy and precision were tested against the Consensus Reference Material after Hansell (2005). 1σ standard deviations of triplicate samples varied but were never above 0.15 μM.

2.2.5 l Dissolved organic nitrogen (DON)

Water samples for total DON were collected and filtered through 0.22 μM PES syringe filters into 15-ml falcon tubes and placed on ice on the boat. Total dissolved nitrogen (TDN) concentrations were measured by oxidizing all reduced N species to nitrate with alkaline persulfate solution (Nydahl, 1978; Wang et al., 2015), followed by quantification of the resulting nitrate with the chemiluminescence method (Braman and Hendrix, 1989) at Princeton. In a pre-combusted 4-ml glass vial, 0.1 ml of Mono Lake water was combined with 1 ml persulfate oxidizing reagent (1 g recrystallized low-N $K_2S_2O_8$ and ACS grade 1.5 g NaOH in 100 ml ultrapure water) and autoclaved for 1 hr. DON concentration was calculated by subtracting the concentrations of nitrate and ammonium/ammonia from the concentration of TDN. The nitrogen concentration of blanks (persulfate oxidizing reagent) was <0.3 µM. 1σ standard deviations for replicate DON concentration measurements were <2%.

2.2.6 l Particulate organic matter (POM)

Water (3–5 L) from each depth was collected in acid-cleaned, 10-L high-density polyethylene (HDPE) carboys on the boat. Within three hours after sampling, ~2 L subsamples from these jugs were filtered on shore using a Cole-Parmer Masterflex l/P peristaltic pump (model 77602-10) through pre-combusted 0.7 μm × 147 mm OD GF/F filters in a Whatman stainless-steel filter holder via Masterflex Tygon E-LFL pump tubing (l/P 73, 9.5 mm ID). Filters containing POM were rinsed with ~1 L

of 85 g/L NaCl salt solution in ultrapure water to remove dissolved carbonate and sulfate and then frozen until lyophilization. Freeze-dried filters were subsampled for POC via 1/16 inch diameter hole punch. Filter punches were exposed to fumes of 12 M HCl for one week to remove DIC. Three decarbonated hole punches were folded into 9 mm × 5 mm tin capsules (OEA Labs) and combusted to CO_2 with a Thermo Fisher Scientific Flash Elemental Analyzer (EA) Isolink CN connected to a Delta V Plus Isotope Ratio Mass Spectrometer (IRMS) via a ConFlo IV Universal Interface at Caltech. A calibrated in-house standard (urea, $\delta^{13}C_{VPDB} = -27.8‰$) was used for isotope calibration and concentration calculations. 1σ standard deviations were variable but typically ~0.10 mM, and are plotted as the error bars of Figure 2g.

2.2.7 l Fatty acids (FAs)

Cultured *Picocystis* biomass and Mono Lake POM were analyzed for fatty acid compositions via gas chromatography–mass spectrometry (GC-MS) at Caltech. *Picocystis* biomass (~10 mg) was freeze-dried, then ground in a solvent-washed mortar and pestle. Freeze-dried POM filters were cut in half, with one half archived while the other was extracted. Samples were extracted and derivatized as methyl esters following standard protocols described in the SI.

2.3 l Microbiology

2.3.1 l *Picocystis* cultures

We obtained *Picocystis* sp. strain ML pure culture (Roesler et al., 2002) from R. Oremland (USGS) and grew cells in batch culture under white light on a rotary shaker at 180 rpm and 30°C. L1 minimal medium was prepared and used as described in (Guillard and Hargraves, 1993), substituting artificial seawater (35 g/L Instant Ocean Sea Salt) in place of filtered natural seawater. The growth medium was supplemented with salt to reach 70 g/L NaCl. Cell growth was monitored by

measuring absorbance at 600 nm, and purity was checked by microscopy. Cultures were harvested in the late exponential phase (OD 0.4–0.6) and stored at –25°C until lyophilization, extraction, and analysis.

2.3.2 l Sulfate reduction incubations

Incubations for sulfate-reducing potential were started in fall 2018 by addition of 30 ml Mono Lake water from 12, 17, 20, and 35 m water depth to N_2-sparged 60-ml serum bottles with blue butyl stoppers at the time of sampling. Samples were kept on ice overnight until return to Caltech, when they were incubated at 4°C in the dark. Incubations were conducted in duplicate with four conditions: lactate addition (2 mM final concentration), pyruvate addition (2 mM final concentration), no addition, and killed control. Killed controls were autoclaved 48 hr after sample addition. Incubations were monitored by measuring dissolved sulfide concentration using the Cline assay (described in SI) at three days, two weeks, one month, and six months.

2.3.3 l 16S rRNA Illumina TAG sequencing

Water samples for high-throughput Illumina 16S rRNA gene amplicon sequencing were collected in 50-ml falcon tubes and stored on ice or at 4°C for ~24 hr until benchtop centrifugation (5250 *g*, 20 min, 4°C). Supernatant was discarded until a pellet and ~1 ml liquid remained. Pellets were resuspended and transferred to 2-ml tubes and centrifuged (16 000 *g*, 10 min). Supernatant was decanted, and pellets were kept at –20°C until DNA extraction following Zhou et al. (1996; details available in the SI). Following the initial PCR, amplicons were barcoded using Illumina Nextera P5/P7 primers and pooled prior to sequencing and subsequent sample demultiplexing at Laragen Inc. Sequence data were analyzed using QIIME 1.8.0 (Caporaso et al., 2010), with a 99% OTU cutoff and taxonomic assignment using the SILVA138 NR99 database (Quast et al., 2013). OTU counts were binned by taxonomic assignment at the genus rank. Using R, counts for each genus were

normalized to relative abundance per dataset. After normalization, chloroplasts (representing mainly the eukaryote *Picocystis*) and fully unassigned sequences (<90% identity to any SILVA sequence) were removed for clarity, and the data were binned in 3 groups: genera represented by >1% of the sequences of any one sample, genera represented by 0.1%–1% of the sequences of any one sample, and genera not present in more than 0.1% in any sample. The resulting abundance tables were used to generate heat maps in MATLAB. Statistical analyses (NMDS, ANOSIM, ADONIS, Pearson correlation, SIMPER) were carried out in R using the *vegan* package (Oksanen et al., 2020). Alpha diversity was analyzed by rarefying each sample to 1,370 sequence depth using QIIME 1.8.0 and calculating richness (number of distinct OTUs), evenness (Shannon equitability), and diversity (Shannon–Wiener Index) following (Shannon and Weaver, 1949).

3 | RESULTS

3.1 | Physical and chemical properties

Salinity was vertically well mixed (~86 ppt) in spring and summer 2017 (Figure 2a). A lens (~1 m) of less saline (75 ppt) surface water developed by the fall. Mono Lake typically overturns in the winter, but the lake remained stratified throughout 2018. Temperature structure exhibited seasonable variability, although the base of the thermocline remained at ~15 m (Figure 2b). Dissolved oxygen profiles (Figure 2c) indicated that in spring 2017 at the start of our time series, the lake was oxic at the surface and dysoxic at depth. In summer 2017, a significant oxycline developed at 3 m, which progressively deepened throughout our time series. After and including summer 2017, no detectable O_2 was measured below the chemocline. These profiles demonstrate monomictic conditions in the spring and summer of 2017 with a shift to meromixis in the winter of 2017–18.

Dissolved sulfate (~105 mM), silica (540 ± 60 μM), and phosphate (697 ± 44 μM) remained high throughout the time series (Table S2), while nitrite remained very

low (<0.3 μM). In contrast, nitrate, ammonium, and sulfide concentrations changed with prolonged stratification. Nitrate decreased from its maximum of 1.45 μM in fall 2017 to <0.01 μM by fall 2018 (Figure 2d). Ammonium (Figure 2e) was low (<4 μM) in spring 2017, while the lake was fully mixed, but gradually increased below the chemocline, reaching 141 μM by fall 2018. Sulfide was not measured in 2017, but throughout 2018, it accumulated below the chemocline, reaching a maximum concentration of 464 μM (Figure 2f). Major cations (K^+, Mg^{2+}, Ca^{2+}, Si^{4+}, Sr^{2+}, Li^{2+}, Fe^{2+}, Mn^{2+}), DIC concentrations, and DIC $\delta^{13}C_{VPDB}$ values were measured in spring 2017 and are described in the SI; these species are sufficiently concentrated that they are presumed not to change much over timescales of a few years.

POC was high (~1 mM) and increased with depth (Figure 2g). No previous studies have reported POC for comparison, but these concentrations align with Mono Lake's high primary productivity. The $\delta^{13}C_{VPDB}$ values of POC in the hypolimnion were roughly constant at –31.6 ± 0.3‰ (Figure 2h), whereas in the epilimnion, they were variable, with values of –30.2 ± 0.1‰ in fall 2017 and –30.8 ± 0.1‰ in fall 2018. Dissolved organic carbon (DOC) was also very high and ranged from 8.13 to 21.31 mM (Figure 2i). Notably, although inorganic fixed nitrogen was very low (Figure 2d, Table S2), DON was elevated (~0.3 mM; Table S2).

The total hydrolyzable fatty acid (FA) content of cultured *Picocystis* sp. strain ML is shown in Figure 3 and described in detail in the SI. Extractable fatty acids from Mono Lake POM were consistent with *Picocystis* being the main source (Figure 3, Table S3). Saturated FA between C_{14} and C_{20} accounted for a slightly larger normalized abundance than observed in *Picocystis* culture, potentially reflecting significant contributions from bacterial sources and/or degradation of short-lived double bonds (Rontani et al., 2012). Monounsaturated FAs between C_{14} and C_{16} not synthesized by *Picocystis* varied between 2% and 4% in the hypolimnion and reached up to 7% in the epilimnion. Iso and anteiso-C_{15} FAs were uniquely

present in POM and reached up to 5%–6% in hypolimnion samples. Long-chain fatty acids (>C_{20}) were also identified in variable quantities (~1–10 ng/ml); these molecules were likely sourced from terrestrial or littoral vegetation and were removed before normalization (Table S3).

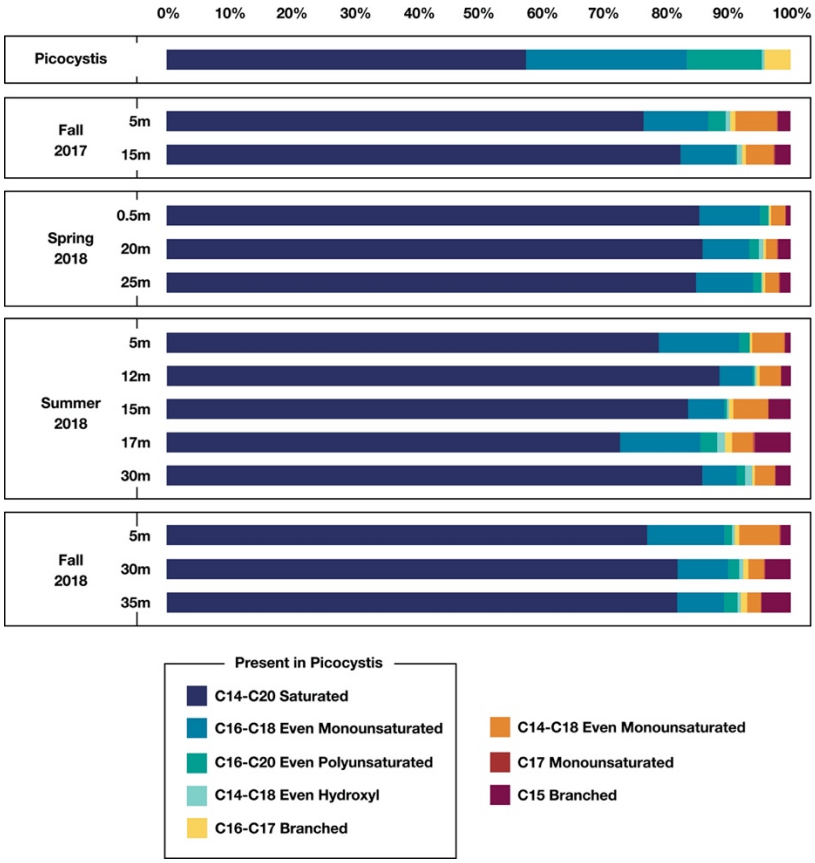

Figure 3 *Relative abundance of fatty acids (FAs) detected in Picocystis cultures and Mono Lake water-column POC, analyzed as fatty acid methyl esters. For the purpose of comparison, FAs are grouped into five categories shared between Picocystis and POC extracts: C_{14}–C_{20} saturated (dark blue), C_{16} and C_{18} monounsaturated (turquoise), C_{16}, C_{18}, and C_{20} polyunsaturated (green), C_{14}, C_{16}, and C_{18} β-hydroxy (light green), and C_{16} and C_{17} branched (yellow). Categories of FAs unique to POC samples included C_{14}, C_{16}, and C_{18} monounsaturated (orange), C_{17} monounsaturated (red), and C_{15} branched (maroon).*

3.2 | Microbial community composition

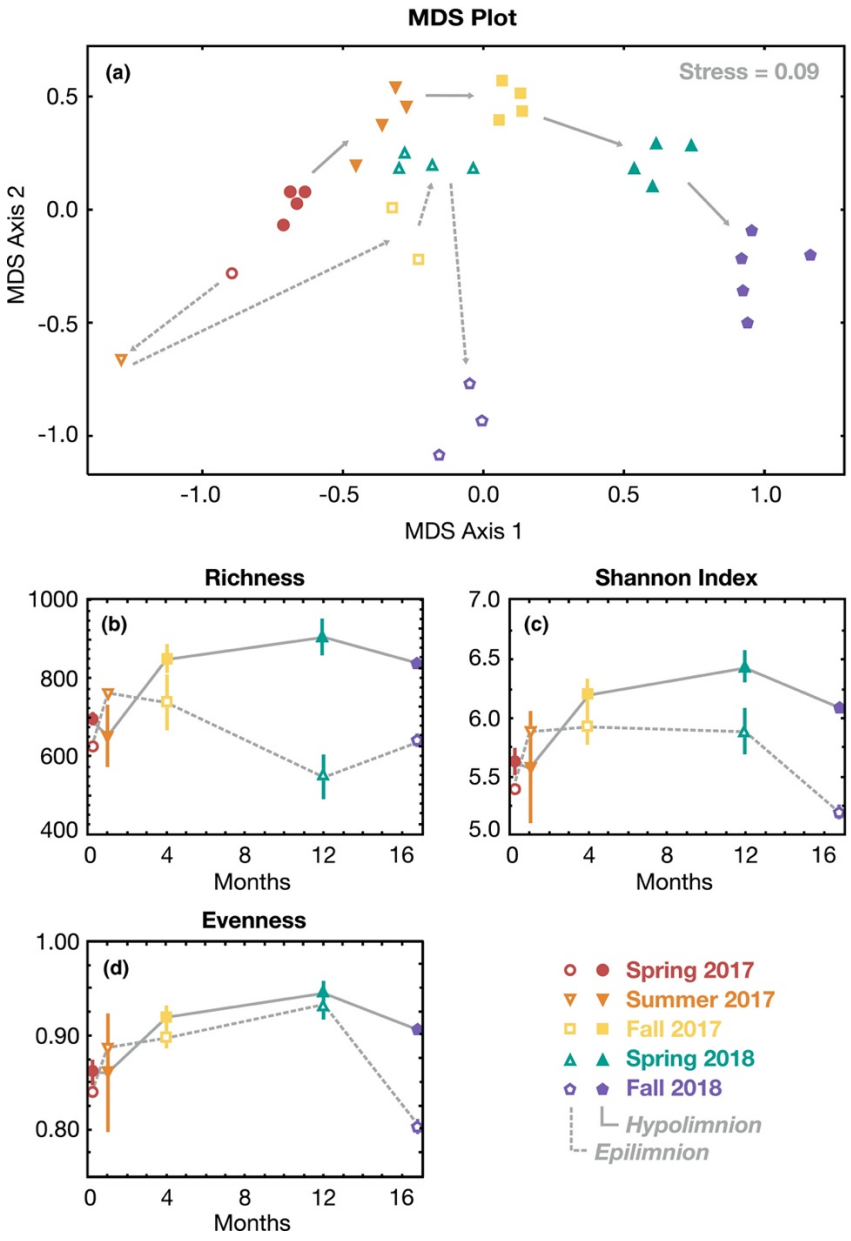

Figure 4 *Visualizations of 16S rRNA gene amplicon data. Epilimnion (surface water) and hypolimnion (deep-water) samples are indicated by open and closed symbols, respectively. Symbols and colors are the same as in Figure 2. Shallow and deep samples from spring 2017 are coded as epilimnion and hypolimnion, respectively, although the thermocline was only weakly developed at that time.*

Dashed arrows indicate the time trajectory of the epilimnion microbial community while solid arrows indicate the hypolimnion. (a) Multidimensional scaling (MDS) plot of all 32 samples across the two-year time series, where distance across either axis represents degree of dissimilarity. (b) Richness (alpha diversity). (c) Shannon diversity index. (d) Species evenness. In panels b–d, values are averaged across all epilimnion or hypolimnion samples for each time point with bars representing standard deviations.

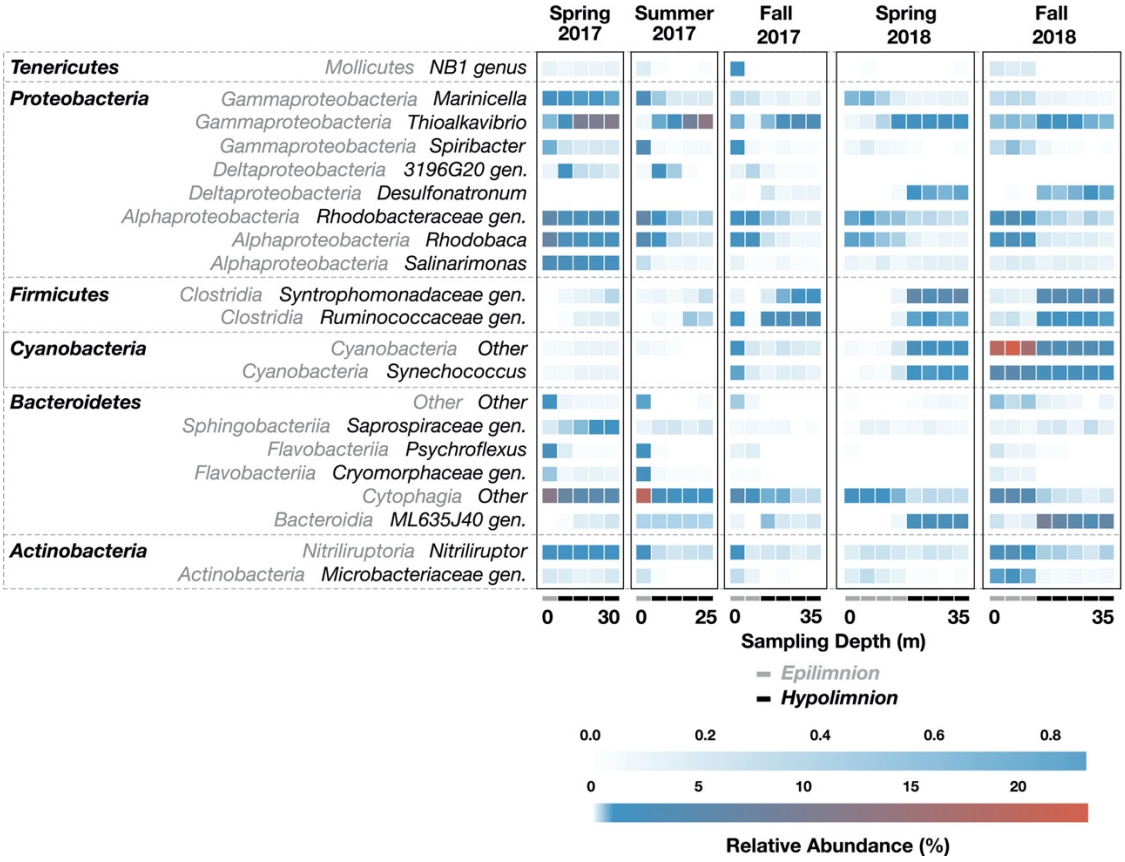

Figure 5 *Heatmap of 16S rRNA sequence relative abundance for genera >1.0% at Station 6. Sampling time points are ordered with increasing depth from left to right within each box, and with increasing time from left to right between boxes. Epilimnion and hypolimnion samples are indicated with gray and black rectangles below each column, respectively. Amplicon sequences are binned at the genus*

level, with phylogenetic classes shown in gray italics to the left of the corresponding genus, and phyla indicated on far left in bold.

The similarity in 16S rRNA gene amplicon diversity for our time-series dataset was visualized using multidimensional scaling (MDS) analyses (Figure 4a). In spring 2017, samples from all depths hosted similar microbial community composition, but with stratification, the communities in the epilimnion and hypolimnion diverged and remained distinct for the rest of the time series. Indeed, when the epilimnion and hypolimnion communities were considered separately, time was the overwhelming driver of variation, with surface water ANOSIM R = 0.9822 (p = .001) and deep-water R = 0.9251 (p = .001; ANOSIM R value is a metric describing the ratio between within-group and between-group ranked Bray–Curtis community dissimilarities, typically ranging from 0 to 1 with increasing correlation). The Pearson correlation of time and dissimilarity was also high in the epilimnion (0.5801, Mantel test p-value = .002) and hypolimnion (0.8508, p = .001). When samples were processed together, time explained less of the variation (R = 0.5316, p = .001), implying that different depths in the water column had independent trajectories. Hypolimnion and epilimnion samples also exhibited distinct patterns in species richness, Shannon diversity, and evenness (Figure 4b-d; Table S4), as described in the SI.

Almost all observed phenotypes belonged to Bacteria (Figure 5, Figure S2). The uncultured lineage DHVEG6 was the only Archaeal group recovered at >0.1%, found in a single sample from fall 2018. Previous studies reported similar bacterial dominance in moderately hypersaline lakes, with Archaea frequently dominating under extremely high salinity (Jiang et al., 2006; Oren, 2008). 98.7% of chloroplast sequences were assigned to the dominant phototrophic alga, *Picocystis*. We therefore used chloroplast relative abundance as a proxy for *Picocystis*, which varied between 17% and 40% relative abundance in the epilimnion (Figure 6a; Figure S1a) and 32%–38% in the hypolimnion (Figure 6b;

Figure S1). *Picocystis* was the only organism consistently abundant throughout the water column at all time points. Abundances of other taxa, described in more detail in the SI, varied strongly between epilimnion and hypolimnion samples (Figures 4-6, Figure S2), with ANOSIM R value = 0.2515 (*p*-value = .002). A one-way ANOSIM with all samples indicated that time was another significant driver of variation in our data (R = 0.5316, *p* = .001); however, seasonality had a smaller effect (R = 0.1553, *p* = .02) implying that ongoing stratification and not necessarily the time of the year influenced the observed changes in microbial community composition.

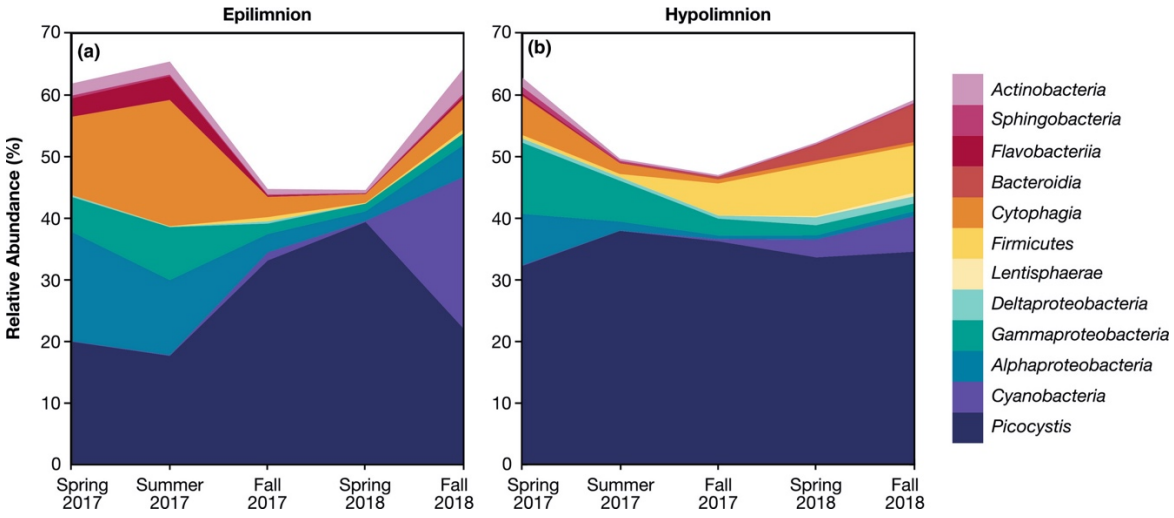

Figure 6 *Relative abundances of bacterial 16S rRNA sequences, grouped by class or phylum, in the (a) epilimnion (b) and hypolimnion. Picocystis (dark blue) abundance was inferred from chloroplast sequences. Some phyla were not included, as their relative abundance was too low to be discernable in this visualization method. These groups included the following: Euryarchaeota, Actinobacteria, Deinococcus–Thermus, Planctomycetes, Spirochaetes, Verrucomicrobia, and Tenericutes.*

3.3 | Sulfate reduction incubations

Sulfide concentrations in the lake water incubations are shown in Figure 7. Incubations with water from 12 m depth (above the chemocline) demonstrated no sulfide production across all conditions and time points. Samples from below the chemocline began with sulfide concentrations at ~0.5 mM. After six weeks, sulfide concentrations were unchanged (~0.5 mM) in all conditions, suggesting that sulfate reduction in situ was very slow at best. After six months, all incubations of samples from below the chemocline, with the exception of killed controls, produced significant sulfide. Additional experiments amended with pyruvate and lactate as the carbon source yielded the highest sulfide concentrations. Extrapolation between the last two time points of the no-addition culture yields a minimum sulfate reduction rate of 0.12 μmol L^{-1} day^{-1}. Given the long lag phase of the incubation, it is unclear how applicable this value is to Mono lake itself, but it nevertheless emphasizes that sulfate reduction rates in the water column are likely very slow.

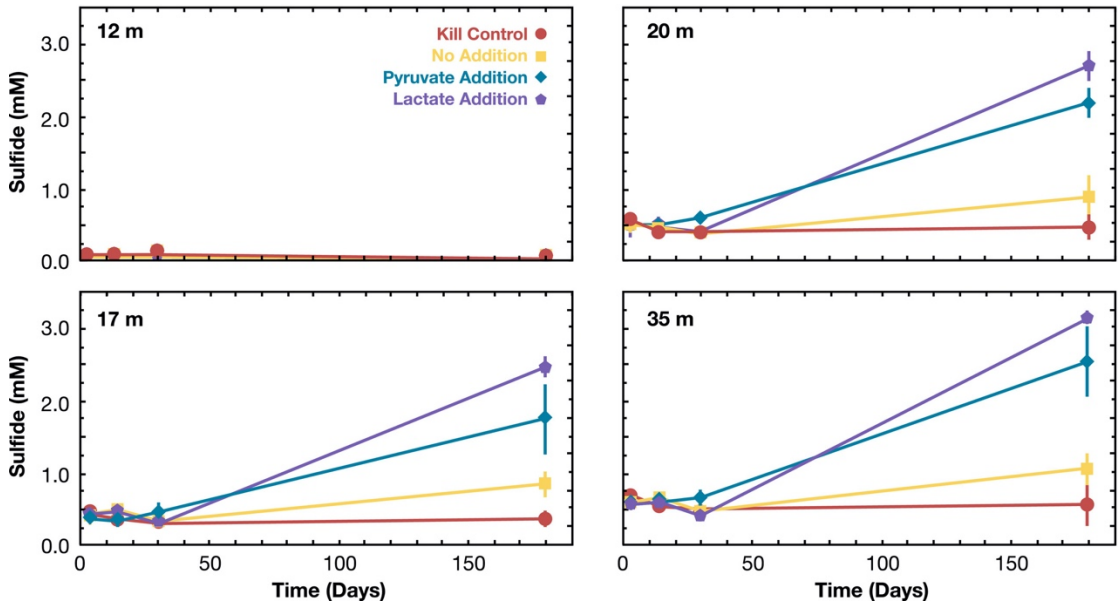

Figure 7 *Measurements of water-column sulfate reduction potential in incubation experiments. Samples were collected in spring 2018 from 12, 17, 20, and 35 m water depths. Each depth was monitored for sulfide production over the course of six months. Values are the average of replicates with vertical error bars displaying*

1σ standard deviations. The 12 m sample was from the epilimnion, while other samples were collected from the hypolimnion and at time zero began with background sulfide concentrations in the lake (0.5 mM). 2 mM lactate addition (purple pentagons), 2 mM pyruvate (blue diamonds), no addition (yellow squares), and the autoclaved killed control (red circles).

4 | DISCUSSION

Our dataset for Mono Lake offers insight into aquatic microbial succession during the onset of meromixis. Within just one month of stratification, community shifts were apparent, and 16 months later, these successional dynamics were still occurring (Figures 4-6). The epilimnion and hypolimnion microbial communities followed distinct paths (Figures 4 and 6), and—with the possible exceptions of *Picocystis* and Cyanobacteria—there appeared to be relatively little biological exchange of these communities across the chemocline. We therefore considered the following four aspects of our data: (a) the dynamic succession in the epilimnion, (b) the more predictable succession patterns in the hypolimnion, (c) the temporal and limnological drivers of sulfur cycling, and (d) the enigmatic ecophysiology of Mono Lake's prolific primary producer, *Picocystis*, and its resistance to stratification.

4.1 | The dynamic surface community

Mono Lake's epilimnion bacterial community experienced drastic changes throughout our two-year time series, demonstrating low resistance and resilience (Figures 4a and 6a). Other surveys of stratified lakes have also found that epilimnion bacteria were more variable over time than hypolimnion populations (Shade et al., 2008), reasoning that surface communities face more variability from climatic interactions. Indeed, seasonal Mono Lake surface water temperatures fluctuated between ~0°C and 20°C and winter storms increased terrestrial organic matter delivery, as inferred from increased long-chain fatty acids (>C_{20}) (Table S3).

Taken together, it was perhaps unsurprising that Mono Lake's surface microbial community shifted as lake stratification stabilized. What was unexpected is the direction of this shift: a reduction in relative numbers of heterotrophs, with concomitant increase in primary producers.

At the start of our time series, during monomixis, the epilimnion microbial community was characterized by the phototrophic alga *Picocystis* (~20% relative abundance) and aerobic or aerotolerant heterotrophic bacteria (~40% relative abundance) within Alphaproteobacteria, Gammaproteobacteria, Cytophagia, Actinobacteria, Bacteroidia, and Flavobacteriia (Figures 5 and 6a, Figure S2; see SI for taxa specific details). This early epilimnion diversity comprised a suite of saline- and alkaline-adapted heterotrophic bacteria likely capable of degrading and remineralizing complex organic matter such as that supplied by the dominant *Picocystis*.

The drastic shoaling of the oxycline in spring–summer 2017 (Figure 2c) reduced the niche for aerobic metabolisms, but the composition of the epilimnion microbial community was only minimally altered (Figures 4-6). By fall 2017, however, putative heterotrophs had fallen drastically to ~10% relative abundance and would remain at that level throughout the remainder of our time series. Simultaneously, from fall 2017 through spring 2018, there was a 15%–20% relative increase in Picocystis. By fall 2018, a bloom of phototrophic, non-diazotrophic, Cyanobacteria appeared, dominated by a genus related to Group 1 species within the marine *Prochlorococcus* and *Synechococcus* clade. This OTU reached ~30% relative abundance, causing epilimnion evenness to drop from 0.93 to 0.80 from spring to fall 2018 (Figure 4d). C_{14}–C_{18} monounsaturated fatty acids also increased in the epilimnion during this phototrophic bloom (orange bars, Figure 3) and were tentatively attributed to the Cyanobacteria. Group 1 cyanobacterial species, like those in the genus *Synechococcus*, are up to 50% C16:1 fatty acid by weight (Murata et al., 1992). As this cyanobacterial bloom is represented in just

one time point, we do not know whether it will be a persistent feature of the meromictic lake. Regardless, we observed a significant shift in the epilimnion microbial population from one dominated by heterotrophs during monomixis to one dominated by primary producers during meromixis.

What mechanisms allowed Cyanobacteria to thrive in fall 2018 when these OTUs were minimally present throughout the rest of the time series? Classically, cyanobacterial blooms following algae have been attributed to nutrient limitation, especially nitrogen. For example, two observed genera of oxygenic phototrophs, *Synechococcus* and *Microcystis*, are highly competitive organisms in post-algal bloom ecosystems, known for their flexibility in utilizing nitrogen sources in low-nutrient environments (Davis et al., 2009; O'Neil et al., 2012). However, bioavailable nitrogen species experienced little change in the epilimnion: Nitrate and nitrite were consistently depleted (Figure 2d; Table S2), while DON concentrations remained high (240–320 μM; Table S2). Further, both *Picocystis* and Cyanobacteria are capable of utilizing ammonium, which appears to be continuously diffusing into surface waters (Figure 2e). Finally, cyanobacterial success post-bloom is often attributed to their high surface area to volume ratios that outcompete larger cells for nutrients. This advantage becomes less relevant when compared to Mono Lake's small (<3 μm) *Picocystis*. Although nitrogen limitation has been favored in other systems for explaining cyanobacterial blooms, it seems unlikely to be the main driver in Mono Lake.

We hypothesize that top-down controls from predation by *Artemia*, rather than bottom-up factors such as nutrients, were responsible for increased phototrophic niche space. Surveys of Mono Lake's algae have documented that net primary production, as measured by chlorophyll *a* abundance, drops by a factor of two or more during meromixis (Melack et al., 2017). The response of *Artemia* is a single population peak in the spring, rather than two smaller generations in the spring and summer (Figure S3b). This pattern is consistent with our PAR data

(Figure S1c), which shows deeper light penetration in spring 2018 compared with spring 2017. Earlier, prolific grazing by *Artemia* would have more efficiently cleared the *Picocystis* bloom, leaving fewer algae for lysis and producing less DOC to support the heterotrophic microbial population. Indeed, our DOC measurements suggest a twofold drop in concentration at 10 m depth from spring 2017 to spring 2018.

It is rare for species competing for the same resources, such as light and nitrogen, to coexist during steady state (Hardin, 1960), although dynamic transitions may create additional niche spaces during succession for organisms to co-occur (Flöder and Sommer, 1999). In our fall 2018 data, Mono Lake's meromictic epilimnion was characterized by two abundant phototrophs. The codominance of algae and Cyanobacteria has been previously reported in another hypersaline system: At Lake Dziani Dzaha, authors found that *Picocystis salinarum* and *Arthrospira fusiformis* spanned the water column of a monomictic lake (Bernard et al., 2019). They hypothesized that this coexistence related to distinct light adaptations. Indeed, *Picocystis* is specifically adapted for low photon flux and blue-green wavelengths (~400–500 nm), allowing survival deeper in the epilimnion (Roesler et al., 2002). The most abundant Cyanobacteria in our study belonged to an uncharacterized genus within the non-diazotrophic marine *Prochlorococcus* and *Synechococcus* clade (Figure 5), but Cyanobacteria in general are often well adapted to high ultraviolet radiation and solar irradiance (Ehling-Schulz and Scherer, 1999), implying greatest success at the top of the photic zone. Future work could increase sampling resolution in the epilimnion to test this possible niche diversification.

Mono Lake's mode of primary productivity shifted drastically as the surface community progressed through microbial succession. If Cyanobacteria continue to populate surface waters, will future bacterial communities respond, switching specialties away from degradation of algal organic matter? Further, some species

of *Artemia* are unable to produce sterols and must acquire them from dietary algal sources (Teshima and Kanazawa, 1971; D'Abramo et al., 1984). As most bacteria, including Cyanobacteria, are also incapable of sterol synthesis, replacement of sterol-producing *Picocystis* in Mono Lake could potentially impact *Artemia* populations, which are critical to the thousands of migratory birds of the Pacific Flyway that flock to Mono Lake annually.

4.2 l Ecological shifts

The water column in spring 2017 was largely oxic to hypoxic (Figure 2c), and the hypolimnion bacterial community resembled that of the epilimnion (Figure 4, Figure S2). With the development of a sharp oxycline, aerobic and aerotolerant populations shoaled. Exceptions included the phototrophic Cyanobacteria and alga *Picocystis*, which maintained substantial abundance in the dark, anoxic hypolimnion throughout the time series (Figure 6b, Figure S1a), an enigma discussed further in Section 4.4. The overall pattern as meromixis developed was a shift from aerobic heterotrophs to anaerobic fermenters and lithotrophic sulfur oxidizers to, eventually, sulfate reducers. In particular, there was a slow rise in obligately anaerobic bacteria, especially the Firmicutes and Bacteroidia. These organisms were likely utilizing ample deep-water DOC and DON (Figure 2i, Table S2) and/or the degradation products of sinking algal debris and fecal pellets. Branched C_{15} fatty acids also increased over time (Figure 3); Firmicutes genera have been documented to contain 45% C_{15} branched FAs by weight (Chan et al., 1971) and were previously implicated in hypersaline environments with the presence of branched compounds (Jiang et al., 2006). These fermenters in turn would have potentially supplied labile organic substrates for sulfate reducers, as implied by our incubation experiments (Figure 7), which only appeared in significant abundance after prolonged stratification. This transition was surprisingly slow, with the first sulfate reducers appearing three months after hypolimnion

anoxia was established, and others appearing after a year of anoxia. We discuss the temporal evolution of sulfur cycling in more detail in Section 4.3.

Interestingly, most of the OTUs observed in the meromictic hypolimnion have been previously identified in Mono Lake sediments (Rojas et al., 2018). To confirm this connection, we characterized the microbial community in sediment core tops in spring 2018 and found persistent symmetry in sediment and hypolimnion bacteria, including genera with fermenting and sulfate-reducing potential (Figure S5). We hypothesize that the bacterial community developing in Mono Lake's meromictic deep water directly reflects sedimentary species colonizing this expanding, anoxic niche. Previous studies support this claim, finding high resistance in sediment bacterial communities while water-column communities are disturbed (Diao et al., 2017). These authors postulated that sediments in stratified lakes act as seed banks for anaerobic bacteria and recent reviews have implicated dormancy in seed banks as a mechanism for species resuscitation following environmental changes (Lennon and Jones, 2011). Indeed, spore-forming Clostridia, which were detected in sediment core tops, were abundant OTUs in the anoxic hypolimnion community of Mono Lake from fall 2017 onward. Taken together, our results for the hypolimnion appear consistent with the idea that sediment seed banks act as a buffer when disturbance alters the chemical composition of a stratified lake.

4.3 | Temporal evolution of sulfur cycling

Mono Lake supports an active microbial sulfur cycle, with ~110 mM sulfate concentration (Table S2) and significant sulfide porewater fluxes (6.3 mmol m^{-2} day^{-1}; Miller et al., 1993). Previous studies have observed different sulfur communities depending on lake stratification: In summer 2016, during the seasonal stratification of a monomictic regime, Stamps et al., (2018) observed abundant sulfide-oxidizing bacteria in the water column, particularly *Thioalkalivibrio*, but found no evidence of sulfate reducers in the anoxic

deep waters. In contrast, multiple studies of the lake under sustained meromictic conditions (>1 year after the onset of stratification) have observed microbial sulfate reduction by diverse deltaproteobacteria at depth (Oremland et al., 2000; Humayoun et al., 2003; Scholten et al., 2005; Edwardson and Hollibaugh, 2018), with sulfide oxidation restricted to the chemocline edge (Edwardson and Hollibaugh, 2017). Our time series provides a detailed view of the ecological transition between these two lake states.

In spring 2017, Mono Lake was monomictic and resembled that described by Stamps et al., (2018), with ~13% of total 16S rRNA reads belonging to *Thioalkalivibrio* (Figure 5). No OTUs representing putative sulfate reducers were observed. By summer 2017, a shallow oxycline had developed, providing a niche with concurrent sulfide and light but minimal oxygen. *Ectothiorhodospira*, an anoxygenic phototroph capable of using reduced sulfur or arsenite as an electron donor, appeared in shallow waters. By fall 2017, Mono Lake had a ~5 m oxycline and hydrogen sulfide was first detected by smell. Thioalkalivibrio remained abundant below the chemocline, *Ectothiorhodospira* disappeared, and 16S rRNA sequences for putative sulfate-reducing organisms appeared for the first time, albeit at low (<1%) relative abundance (Figure S2). The transient appearance of sulfur-based phototrophy has not been previously reported as an intermediate metabolism, although stable communities of *Ectothiorhodospira* in the hot springs around Paoha island may provide a constant inoculum of this organism to the water column (Kulp et al., 2008; Hoeft McCann et al., 2017). By spring 2018 and through fall 2018, with sulfide accumulating below the chemocline to ~400 μM (Figure 2f), the sulfur-cycling community continued to shift. The sulfate reducer *Desulfonatronum* became a dominant organism, with 16S rRNA gene relative abundances of 2%–4% (Figure 5). *Thioalkalivibrio* remained abundant at depth accounting for 2%–4% of reads.

Not until one year after thermal stratification—and at least ten months after anoxia pervaded the hypolimnion—did sulfate reducers reach >1% of the microbial assemblage. This observation of a slow transition from sulfur oxidation to sulfate reduction is in contrast to numerous studies of freshwater lakes, which document rapid expansion of water-column sulfate reduction following seasonal stratification and anoxia, typically within a few weeks to a month (Cappenberg, 1972; Ingvorsen et al., 1981; Cook and Schindler, 1983; Hartland et al., 2015). Mono Lake's more gradual shift has several implications. First, there is a clear need to consider diversity in the context of time since last turnover in these alkaline, seasonally stratified lakes. Single snapshots of diversity are not necessarily comparable even given a similar lake mixing regime because of hysteresis effects. In Mono Lake, for example, we do not know how long meromixis is required to reach a stable microbial ecosystem. Second, under monomixis, it is unlikely that sulfate reduction would ever become strongly established in Mono Lake's water column. One should therefore be cautious in assuming that seasonally stratified soda lakes will harbor significant populations of sulfate reducers. Third, and more generally, it is unknown whether marine populations of sulfate reducers will adjust quickly like those in freshwater lakes, or very slowly like those in Mono Lake. The implications are significant for generation of toxic concentrations of hydrogen sulfide in seasonal ocean anoxic and hypoxic zones (Ulloa et al., 2012; Thrash et al., 2017).

Limited sulfate reduction in hypersaline lakes has previously been attributed to less favorable energetics of sulfate reduction relative to demands of osmoregulation at high salt stress (Oren, 1999; Oremland et al., 2000). We note that sulfate reducers in Mono Lake multiplied only after the appearance of abundant fermenters, particularly Clostridia and Bacteroidia, in fall 2017 (Figures 5 and 6b). Fermenters typically fill an important ecological function of converting polymeric organic molecules into small organic acids that serve as substrates for anaerobic respiration. We hypothesize that the establishment of sulfate reducers in Mono Lake may be limited more by suitable organic substrates than by the metabolic

demands of high salinity. This idea is supported by our microcosm incubations (Figure 7), where sulfide production was significantly enhanced in anoxic Mono Lake water by the addition of lactate and pyruvate—yielding sulfide concentrations up to 3x more than unamended controls. While DOC concentrations in Mono Lake are extremely high (>10 mM), its composition could be highly polymeric and thus largely inaccessible to most sulfate reducers. Future studies could further probe the molecular composition and reactivity of Mono Lake's DOC to study relationships between the available organics and the community of fermenters and sulfur cyclers.

4.4 | Enigmatic ecophysiology of Picocystis

Picocystis sp. strain ML, a close relative of *Picocystis salinarum*, is a small (~3 μm) coccoid green alga that has been an important phytoplankton species in Mono Lake for at least 40 years (Winkler, 1977). While reports through the 1990s list it as subequal in abundance with the diatom *Nitzschia* (Jellison and Melack, 1993; Roesler et al., 2002), recent genetic data suggest a more dominant role for *Picocystis* in Mono Lake, at least during spring through fall (Edwardson and Hollibaugh, 2018; Stamps et al., 2018; this study). For example, in our 16S rRNA data, chloroplast sequences that were not attributable to *Picocystis* comprised <5% relative abundance, over all times and depths. Fatty acid distributions were also extremely similar between lake POC and cultured *Picocystis* (Figure 3). Spring chlorophyll *a* concentrations and turbidity have risen markedly since ~2003 (Collins, 2017) suggesting the shift is relatively recent. The ecological pressures leading to this alga's rise and the subsequent loss of diatoms are unclear but may include the ability of *Picocystis* to thrive in low light at the base of the chemocline throughout extended meromictic events.

Picocystis strain ML was originally isolated from a chlorophyll maximum layer near the base of the chemocline during a meromictic phase of the lake in 1997 by

Roesler et al., 2002). Subsequent characterization revealed that *Picocystis* strain ML exhibits growth across a remarkable range of salinity (0–260 mg/g), pH (4–12), and light (0.6–12 μmol/m^{2}s); this taxon is also resistant to sulfide (100 μM or more), does not require O_2, and exhibits maximal growth rates of 1.5/d. Its low-light adaptations are likely due to a diverse suite of carotenoids and ten times higher cellular chlorophyll *a* concentrations compared with other green algae (Roesler et al., 2002). Its ecological niche was therefore interpreted as being throughout the photic zone but especially suited for the base of the chemocline where some sunlight penetrates, ammonia diffuses from below, and low oxygen limits grazing pressure by *Artemia*.

In the two decades since initial characterization, additional monitoring has raised several new questions about *Picocystis*. Chief among them is the observation from Los Angeles Department of Water and Power (LADWP) monthly surveys that *Picocystis* is consistently abundant throughout the hypolimnion, including down to 35 m depth where there must be essentially no photon flux (Harasick, 2016; Collins, 2017, 2018, 2019). We have compiled monthly LADWP data from 2015 to 2019, creating a time series from discrete measurements of chlorophyll *a* fluorescence in the water column (Figure 8). Given that multiple genetic studies revealed *Picocystis* to be the only significant phototroph in present-day Mono Lake, chlorophyll *a* concentration provides a proxy for *Picocystis* abundance. Our study also found elevated chloroplast reads throughout the hypolimnion (Figure S1; Figure 6b), indicating that *Picocystis* consistently accounted for ~35% of the microbial community at depth. Surprisingly, metatranscriptomics from deep-water samples recovered mRNA for photosynthetic genes in *Picocystis*, suggesting they were being actively transcribed (Stamps et al., 2018). Taken together, these results beg relatively simple questions regarding this enigmatic alga: Is *Picocystis* alive at the bottom of Mono Lake? And if it is alive, how is it metabolizing and possibly growing?

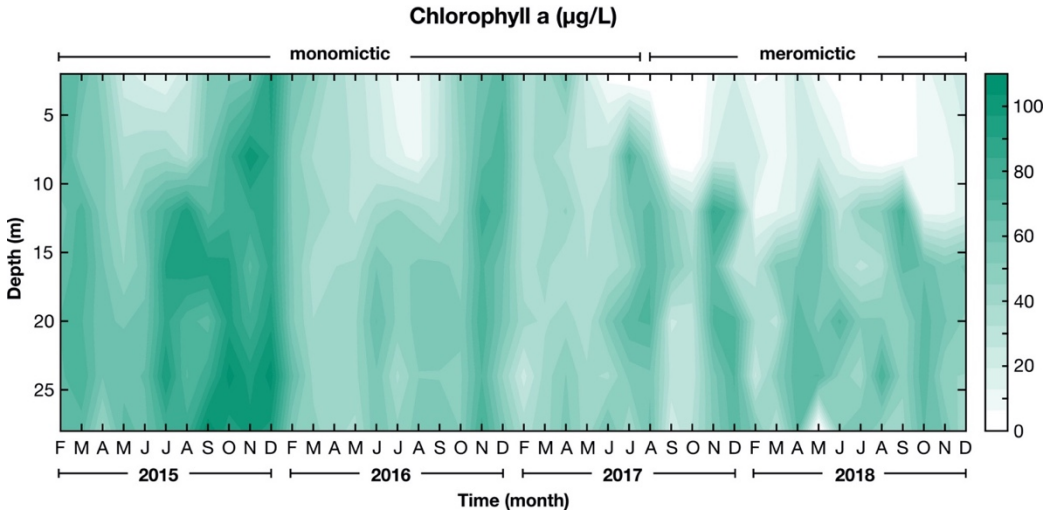

Figure 8 *Chlorophyll a abundance over time and depth in Mono Lake, CA. Data were redrawn from publicly available LADWP reports (from 2016, 2017, 2018, and 2019 (http://www.monobasinresearch.org/onlinereports/). Chlorophyll a concentrations were measured by fluorometry after collection at 2, 8, 16, 20, 24, and 28 m water depth. Note that LADWP did not collect data in January of each year. The approximate transition from monomixis to meromixis is also indicated, but it should be noted that these regime shifts are gradual, not sudden.*

Despite deep chlorophyll *a* maxima, we do not think it plausible that *Picocystis* is photosynthesizing throughout the hypolimnion. Repeated CTD measurements of PAR find <0.01 μmol/m^{2}s photons (the limit of detection by our sensor) at 12–15 m (Figure S1c). Fitting PAR data to an exponential decay, which assumes constant turbidity below the chemocline in accordance with observations during sampling, photon flux would be <10^{-5} μmol/m^{2}s below 17 m. Although adaptations to exceedingly low-light levels are known, for example by an anoxygenic phototrophic *Chlorobium* strain in the Black Sea that survives down to ~10^{-4} μmol/m^{2}s (Manske et al., 2005), *Picocystis* has only been tested as low as 0.6 μmol/m^{2}s. The fact that photosynthesis genes associated with Photosystem I and II (*psaA*, *psaB*, *psbA*, *psbB*, *psbC*) were being actively transcribed at 25 m depth (Stamps et al., 2018) therefore suggests that those cells were recently at a

shallower depth, where photosynthesis was possible, or perhaps that *Picocystis* photosynthetic genes are constitutively expressed. In either case, they appear to be not only alive, but thriving, in the hypolimnion.

We consider two scenarios to explain the depth distribution of *Picocystis*. The first is that *Picocystis* is actively growing at the base of the photic zone and subsequently sinking. Comparison of chlorophyll *a* maxima to our PAR measurements (Figure S1) suggested that these cells are active close to a photon flux of 0.1 μmol/m^{2}s, well below the previously tested minimum of 0.6 μmol/m^{2}s (Roesler et al., 2002). The depth distribution then requires that those cells must sink rapidly, such that CTD profiles and discrete water samplings record high cell densities throughout the hypolimnion. The near-simultaneous appearance of Picocystis maxima throughout the hypolimnion implied settling velocities on the order of ~0.5–1 m/day, faster than the ~5–10 cm/day that have been measured for other, notably larger, green algae such as *Scenedesmus* (Choi et al., 2006). However, flocculation into larger aggregate particles could perhaps achieve such rates. In this scenario, cells isolated (or sequenced) from below ~20 m depth should not be interpreted as growing at those depths, but rather as surviving in sinking particles.

A second scenario is that *Picocystis* growth in the hypolimnion is supported partially or entirely by non-photosynthetic metabolism. In the absence of appreciable exogenous electron acceptors such as oxygen, nitrate, or nitrite, *Picocystis* could perhaps use fermentation to maintain redox homeostasis and conserve energy. The ability to survive transient anoxia via fermentation is widely known in many members of the green algae (Catalanotti et al., 2013). *Chlamydomonas reinhardtii*, the best studied green alga in this regard, has a diverse suite of fermentative pathways and can thrive under anaerobic conditions. When we cross-referenced *Chlamydamonas* fermentation genes against the recently published draft genome of *Picocystis* sp. strain ML (Junkins et al., 2019)

numerous homologous proteins were identified with high confidence (Table S5; Figure S3). However, many of these enzymes also catalyze other cellular functions such as respiration and are alone not evidence of fermentation. Confirmatory laboratory experiments that test the exogenous uptake and subsequent release of carbon compounds by *Picocystis* are required.

Regardless of whether or not *Picocystis* cells are active only at the base of the chemocline or throughout the hypolimnion, it is clear that this ubiquitous alga holds great significance for Mono Lake's biogeochemical cycles and ecology. Numerous questions warrant further investigation, especially in regard to its potential metabolic flexibility, remarkable sulfide tolerance, and transcription of photosynthetic genes in the dark. In addition, our measurements of POC suggested that *Picocystis* strongly fractionates carbon isotopes by up to ~35‰ relative to source DIC, far greater than is expected for algae at such a high pH where [CO_2(aq)] is extremely low. Eukaryotic strategies for survival in extreme environments are less understood than bacteria and archaea (Weber et al., 2007); investigating *Picocystis* may offer novel insights that span environmental applications.

5 I CONCLUSIONS

This study captured the microbial community response of hypersaline, alkaline Mono Lake as it transitioned from monomixis to meromixis following climatic perturbation. Patterns of succession in the epilimnion were less predictable than the hypolimnion, presumably due to greater variability in the epilimnion environment. Notably, the epilimnion community shifted from a dominance of heterotrophic to phototrophic genera, with a significant cyanobacterial bloom in fall 2018. The hypolimnion bacterial population gradually shifted toward the composition of Mono Lake's sediment community, strengthening the ecological role of seed banks and dormancy in steering succession in stratified lakes.

Specifically, hypolimnion bacterial populations, which began in spring 2017 with aerobic heterotrophs and sulfide oxidizers, were replaced by anaerobic metabolisms such as fermentation by fall 2017 and eventually sulfate reduction in spring 2018. Incubation experiments demonstrated that this late appearance of sulfate reducers was likely due to organic substrate limitation. Hypolimnion communities were consistently dominated by *Picocystis*, which survived meromixis either by photosynthesis at the edge of the chemocline or by a metabolic transition to fermentation. Our investigation across this limnological transition highlights the need to move beyond "snapshots" of microbial communities, probing succession over intervals of environmental perturbations and meaningful climatic change.

ACKNOWLEDGEMENTS

We would like to thank Blake Stamps for the use of his code that was modified to generate our 16S OTU heatmaps. We also acknowledge Ronald Oremland for shipping an aliquot of *Picocystis* culture. We thank Sujung Lim and Grayson Chadwick for early conversations on 16S rRNA data, Usha Lingappa for her expertise on Cyanobacteria, and Aaron Martinez for his helpful dialogue on fatty acids. We are grateful to Jared Leadbetter for continuous conversations about the microbial community. We acknowledge Ashley Shade for her helpful dialogue on microbial succession in lakes. We thank Miquela Ingalls for comments and suggestions on the manuscript and her help with sample processing in the field. Additionally, we thank other field assistants: Jodi Blum, Elise Wilkes, Yonaton Goldsmith, and Barbara Ratschbacher. We would like to thank Tim Hollibaugh for use of his Seabird CTD. We thank Melissa Miller from the Oceanographic Data Facility at Scripps Institution of Oceanography for measuring nutrient concentrations and Joshua West at the University of Southern California for measuring trace metals. We acknowledge members of the Agouron International Geobiology Course from 2017 and 2018, especially students who worked directly

with Mono Lake water-column samples: Katherine Fullerton, Rui Bao, Dawson Fairbanks, Michael Wells, Sergio Parra, Qingzeng Zhu, Bridget Conley, and Maria Figueroa. We thank the administrative team for the geobiology courses in 2017 and 2018, including Julie Lee and Ann Close. We also acknowledge course TAs, including Lizzy Trower, John Magyar, Eryn Eitel, and Elise Wilkes. We would like to thank the Agouron Institute and the Simons Foundation for funding the International Geobiology Course and this research. We would also like to acknowledge the Mono Lake Committee and the LA Department of Water and Power for detailed, public records on lake levels and other Mono Lake parameters.

SUPPLEMENTAL INFORMATION

Table S1 *Information regarding which samples were collected for each time point, as well as date of sampling, water depths sampled, and method of water collection.*

	Spring 2017	**Summer 2017**	**Fall 2017**	**Spring 2018**	**Summer 2018**	**Fall 2018**
Date	5/23/17	6/22/17	9/19/17	5/8/18	6/13/18	10/9/18
Sample Depths (m)	0.5, 10, 20, 25, 30	0.5, 10, 15, 20, 27	0.5, 5, 10, 15, 20, 24	0.5, 5, 10, 12, 17, 20, 25, 35	5, 12, 15, 17, 30	0.5, 5, 12, 15, 17, 20, 30, 35
Collection Method	Niskin	Niskin	Pump	Niskin	Niskin	Pump
CTD Cast	✓	✓	✓	✓	✓	✓
DNA	✓	✓	✓	✓		✓
Nutrients	✓		✓	✓	✓	✓
POC			✓	✓	✓	✓
$\delta^{13}C$ POC			✓	✓	✓	✓
DOC	✓	✓	✓	✓	✓	✓
DON			✓		✓	
DIC	✓					
$\delta^{13}C$ DIC	✓					
Sulfate	✓					✓
Sulfide				✓	✓	✓
Incubations						✓
Fatty Acids			✓	✓	✓	✓

Major Elements	✓					

Table S2 *Measured chemical compositions of Mono Lake throughout the time series. N.S. denotes "not sampled" and B.D.L. denotes "below detection limit." Values reported are ranges found within the water column for each time point. When depth trends were apparent, they were plotted and presented in the main text.*

	Spring 2017	**Summer 2017**	**Fall 2017**	**Spring 2018**	**Summer 2018**	**Fall 2018**
K^+ (ppt)	1.18 – 1.24	N.S.	N.S.	N.S.	N.S.	N.S.
Mg^{2+} (ppm)	20.10 – 21.51	N.S.	N.S.	N.S.	N.S.	N.S.
Ca^{2+} (ppm)	11.55 – 12.87	N.S.	N.S.	N.S.	N.S.	N.S.
Si^{4+} (ppm)	9.34 – 9.83	N.S.	N.S.	N.S.	N.S.	N.S.
Sr^{2+} (ppm)	6.54 – 7.46	N.S.	N.S.	N.S.	N.S.	N.S.
Li^{2+} (ppm)	2.08 – 3.64	N.S.	N.S.	N.S.	N.S.	N.S.
Fe^{2+} (ppb)	39.82 – 42.08	N.S.	N.S.	N.S.	N.S.	N.S.
Mn^{2+} (ppb)	11.03 – 13.63	N.S.	N.S.	N.S.	N.S.	N.S.
Nitrite	0.05 –	N.S.	0.10 –	B.D.L.	0.00 –	0.02 –

(μM)	0.10		0.20		0.16	0.29
Nitrate (μM)	0.05 – 1.45	N.S.	0.85 – 1.35	0.05 – 0.12	0.00 – 0.07	0.00 – 0.03
Silica (μM)	514.50 – 535.50	N.S.	455.50 – 559.50	482.00 – 597.00	446.00 – 625.00	489.00 – 708.00
Phosphate (μM)	N.S.	N.S.	643.37 – 779.72	573.00 – 754.00	641.00 – 712.00	618.00 – 774.00
Ammonium (μM)	0.68 – 3.49	N.S.	1.45 – 44.80	0.24 – 103.10	0.18 – 102.00	0.33 – 141.00
Sulfide (μM)	N.S.	N.S.	N.S.	299 – 464	155 – 407	152 – 391
Sulfate (mM)	98.31 – 111.00	N.S.	N.S.	N.S.	N.S.	101.70 – 115.20
DIC (mM)	384 – 396	N.S.	N.S.	N.S.	N.S.	N.S.
δ^{13}C DIC (‰)	2.1 – 2.4	N.S.	N.S.	N.S.	N.S.	N.S.
DOC (mM)	9.79 – 21.00	9.13 – 21.31	8.13 – 10.01	10.81 – 14.13	10.73 – 14.30	10.87 – 14.62
POC (mM)	N.S.	N.S.	1.71 – 1.78	0.92 – 1.60	0.72 – 1.70	0.50 – 2.18
δ^{13}C POC (‰)	N.S.	N.S.	-32.2 – -30.2	-32.1 – -31.5	-31.9 – -31.3	-31.5 – -30.6
DON (mM)	N.S.	N.S.	0.24 – 0.34	N.S.	0.28 – 0.32	N.S.

Table S3 *Fatty acid concentrations per sample, given in ng/mL, organized by time point and depth. Quantification was obtained by use of an internal standard. C21-C30 saturated fatty acids were assumed to be terrestrially sourced and were removed before normalizations for Figure 5.*

		Present in Picocystis Culture					**Not Identified in Picocystis Culture**			
Time Point	Depth (m)	C14-C20 Saturated	C16-C18 Even Mono-unsaturated	C18-C20 Even Poly-unsaturated	C14-C18 Even Hydroxyl	C16 -C17 Branched	C17 Odd Branched	C14-C18 Even Mono-unsaturated	C15 Odd Branched	C21-C30 Saturated
Fall 2017	5	34.36	7.65	2.21	0.35	0.19	0.17	0.88	0.10	1.30
	15	141.54	22.85	13.39	1.43	0.21	0.71	4.26	0.32	10.46
Spring 2018	0.5	133.90	18.83	2.23	0.16	0.14	0.22	1.19	0.12	1.93
	20	91.81	9.92	1.57	0.80	0.19	0.28	2.15	0.14	6.94
	25	91.81	7.90	0.97	0.14	0.08	0.19	1.17	0.18	2.90
Summer 2018	5	20.46	4.66	3.83	0.00	0.00	0.09	0.23	0.05	0.81
	12	41.00	4.04	0.15	0.16	0.07	0.15	0.71	0.01	2.36
	15	53.08	7.24	0.30	0.17	0.20	0.23	2.22	0.03	3.35
	17	14.13	3.17	0.53	0.24	0.08	0.13	1.11	0.05	2.49
	30	12.97	1.33	0.20	0.17	0.03	0.03	0.36	0.02	0.78
Fall 2018	5	29.90	7.26	0.51	0.15	0.09	0.20	0.62	0.07	8.58
	30	49.83	6.42	1.10	0.36	0.29	0.23	2.48	0.13	2.83
	35	39.90	7.24	1.64	0.38	0.42	0.34	3.49	0.14	4.65

Table S4 *Richness, Shannon Diversity, and Evenness for the 32 samples from the Mono Lake water column. The samples were rarified to 1370, the least number of OTUs in any sample after removal of chloroplasts (Picocystis salinarum) and fully unassigned sequences.*

Season and Year	Depth (m)	Richness	Shannon Diversity	Evenness
Spring 2017	0.5	618	5.382	0.837
	10	727	5.807	0.881
	20	689	5.576	0.853
	25	694	5.581	0.853
	30	702	5.609	0.856
Summer 2017	0.5	761	5.890	0.888
	10	770	6.081	0.915
	15	614	5.874	0.915
	20	626	5.218	0.810
	27	596	5.119	0.801
Fall 2017	0.5	790	6.034	0.904
	5	689	5.808	0.889
	10	896	6.348	0.934
	15	862	6.260	0.926
	20	817	6.08	0.91
	24	822	6.096	0.908
Spring 2018	0.5	548	5.839	0.926
	5	472	5.672	0.921
	10	562	5.870	0.927
	12	609	6.141	0.958
	17	839	6.231	0.926
	20	919	6.497	0.952

	25	919	6.479	0.950
	35	948	6.517	0.951
Fall 2018	0.5	658	5.234	0.807
	5	633	5.109	0.792
	12	625	5.137	0.798
	15	825	6.013	0.895
	17	836	6.069	0.902
	20	834	6.091	0.906
	30	829	6.108	0.909

Table S5 *Genes identified in Chlamydomonas for potential fermentation pathways and carbon concentration mechanisms, checked against the draft genome for Picocystis sp. ML. E-value cutoffs of E-6 were used. E values are calculated based on the alignment score and represent the expected number of hits with that alignment score or better. Thus, lower E values indicative of more statistically robust results.*

Function	Gene	Gene Name	Accession Number	In Pico ML?	% Identity	E Value
Fermentation	ACK1	Acetate kinase	XP_001694505.1	No	N.A.	N.A.
	ACK2		XP_001691682.1	No	N.A.	N.A.
	ACS1	Acetyl co-A synthase	XP_001700210.1	Yes	62.25	0
	ACS2		XP_001700230.1	Yes	65.56	0
	ACS3		XP_001702039.1	Yes	55.36	E-28
	ADH1	Alcohol/ acetaldehyde dehydrogenase	XP_001703585.1	Yes	51.82	0

	AAT1	Alanine aminotransferase	XP_001698518.1	Yes	48.34	E-142
	AAT2		XP_001695350.1	Yes	61.59	E-111
	ALD1	Aldehyde dehydrogenase	XP_001696928.1	Yes	58.30	0
	FDX5	Ferredoxin	XP_001690910.1	Yes	38.71	E-7
	FUM1	Fumarase hydratase	XP_001696634.1	No	N.A.	N.A.
	FUM2		XP_001689951.1	Yes	62.23	E-179
	GK	Glycerol kinase	XP_001692205.1	Yes	61.54	E-61
	GPD1	Glycerol-3-phosphate dehydrogenase	XP_001693544.1	Yes	45.65	E-86
	GPP1	Glycerol 3-phosphate phosphatase	XP_001689796.1	Yes	52.13	E-90
	GPP2		XP_001689798.1	Yes	51.56	E-91a
	HYD1	Iron hydrogenase	XP_001693376.1	Yes	28.57	E-39
	HYD2		XP_001694503.1	Yes	31.98	E-25
	LDH	Lactate dehydrogenase	XP_001700756.1	No	N.A.	N.A.
	MDH1	Malate dehydrogenase	XP_001693118.1	Yes	61.86	E-123
	MDH2		XP_001702586.1	Yes	59.34	E-107
	MDH3		XP_001694886.1	Yes	67.55	E-92
	MDH4		XP_001703167.1	Yes	74.60	E-150
	MDH5		XP_001696786.1	Yes	41.57	E-51
	MME1	Malic enzyme	XP_001696240.1	Yes	62.23	E-99
	MME2		XP_001692778.1	Yes	43.44	E-92
	MME3		XP_001692779.1	Yes	41.99	E-94
	MME4		XP_001692684.1	Yes	62.00	E-76
	MME5		XP_001689967.1	Yes	35.53	E-71

	MME6		XP_001696415.1	Yes	34.82	E-81
	PAT1	Phosphate acetyltransferase	XP_001700210.1	No	N.A.	N.A.
	PAT2		XP_001700210.1	No	N.A.	N.A.
	PDC3	Pyruvate decarboxylase	XP_001703530.1	Yes	29.00	E-50
	PEPC	Phosphoenol-pyruvate carboxylase	XP_001695817.1	Yes	54.63	E-128
	PFL1	Pyruvate formate lyase	XP_001689719.1	No	N.A.	N.A.
	PRF1	Pyruvate ferredoxin oxidoreductase	XP_001701208.1	No	N.A.	N.A.
	PYC	Pyruvate carboxylase	XP_001696348.1	Yes	50.30	E-177
	PYK1	Pyruvate kinase	XP_001693008.1	Yes	77.28	0
Carbon Concentration Mechanism	HLA3	ABC transporter	XP_001700040.1	Yes	33.95	E-84
	LCI1	Low CO_2 inducible membrane protein	XP_001703387.1	No	N.A.	N.A.
	LCI2		XP_001695920.1	Yes	42.65	E-11
	LCI3		XP_001697649.1	No	N.A.	N.A.
	LCI5		XP_001690584.1	No	N.A.	N.A.
	LCI6		XP_001694024.1	No	N.A.	N.A.
	LCI9		XP_001694765.1	No	N.A.	N.A.
	LCI11		XP_001697963.1	Yes	43.56	E-13
	LCI13		XP_001698750.1	No	N.A.	N.A.
	LCI21		XP_001692958.1	No	N.A.	N.A.
	LCI22		XP_001702373.1	No	N.A.	N.A.
	LCI23		XP_001695444.1	No	N.A.	N.A.
	LCI24		XP_001703408.1	No	N.A.	N.A.

	LCI30		XP_001690835.1	Yes	78.46	E-136
	LCI31		XP_001691792.1	Yes	33.74	E-7
	LCI33		XP_001701266.1	No	N.A.	N.A.
	LCI34		XP_001691880.1	No	N.A.	N.A.
	LCI36		XP_001696214.1	Yes	35.08	E-33
	LCIB		XP_001698344.1	Yes	48.05	E-90
	LCIC		AB168094.1	Yes	40.00	E-97
	CCP1	Low CO_2 inducible chloroplast envelope protein	XP_001692197.1	Yes	28.57	E-35
	CCP2		XP_001692288.1	Yes	29.55	E-37
	CAG1		XP_001703237.1	Yes	43.79	E-41
	CAG2		XP_001701594.1	Yes	42.97	E-37
	CAG3		XP_001696746.1	Yes	60.82	E-60
	CAH1		XP_001692291.1	No	N.A.	N.A.
	CAH2		XP_001692290.1	No	N.A.	N.A.
	CAH4	Carbonic Anhydrase	XP_001696003.1	No	N.A.	N.A.
	CAH5		XP_001700770.1	No	N.A.	N.A.
	CAH6		XP_001703176.1	No	N.A.	N.A.
	CAH7		XP_001699151.1	No	N.A.	N.A.
	CAH8		XP_001697606.1	No	N.A.	N.A.
	CAH9		XP_001700909.1	No	N.A.	N.A.

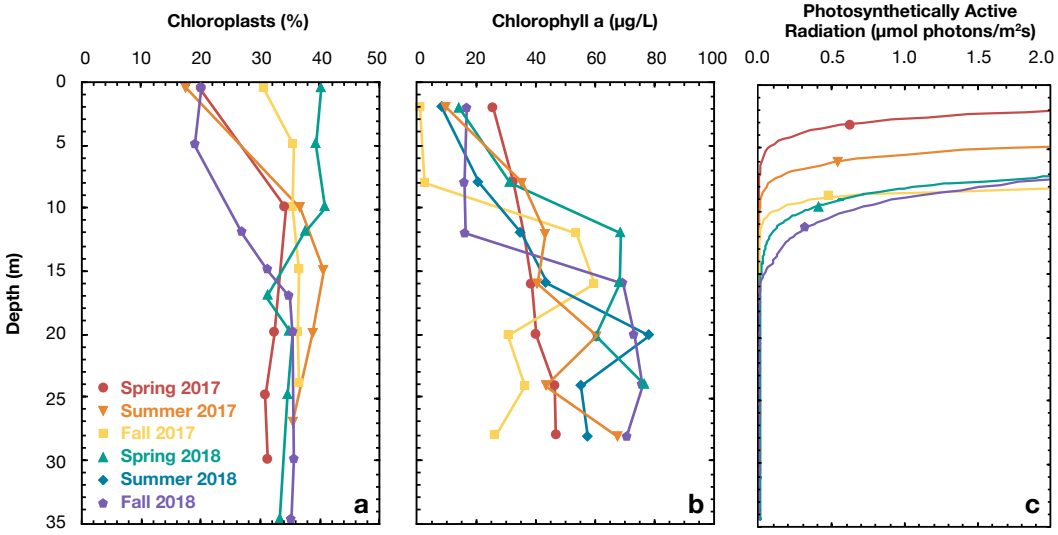

Figure S1 *Parameters relevant to Picocystis: a) 16S rRNA gene amplicons assigned to chloroplasts, interpreted as Picocystis b) chlorophyll a concentrations for the same months as our sampling, redrawn from 2018 and 2019 LADWP Compliance Reports and c) PAR (photosynthetically active radiation, which can be interpreted as photon flux, as measured by CTD. For each panel data is plotted as Spring 2017 (red circles), Summer 2017 (orange inverted triangles), Fall 2017 (yellow squares), Spring 2018 (green triangles), Summer 2018 (blue diamonds) and Fall 2018 (purple pentagons).*

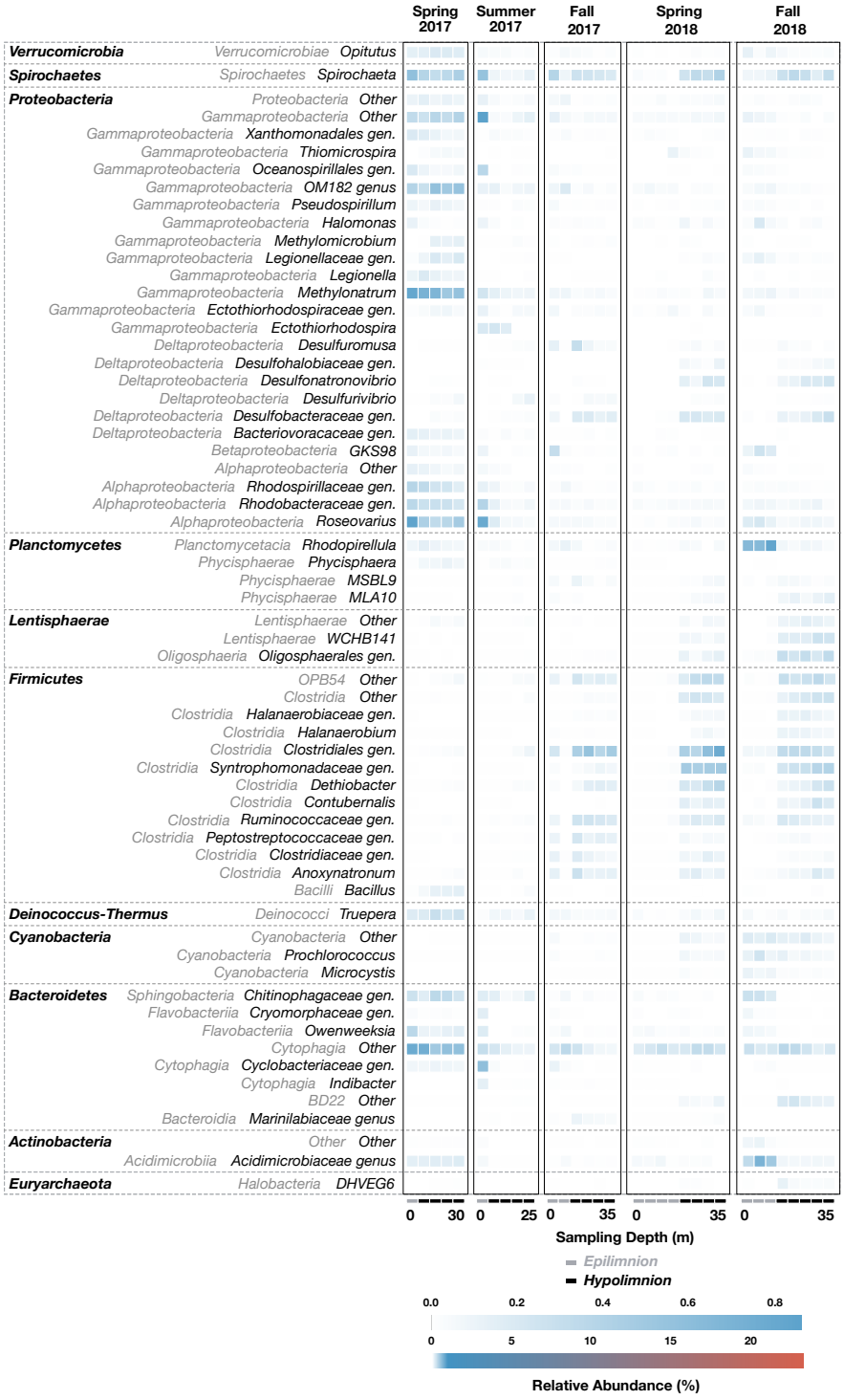

Figure S2 *Heatmap of 16S rRNA relative abundance for genera between 0.1 – 1.0% at Station 6. This figure uses the same color scale and ordering of time and depth points as in Figure 7.*

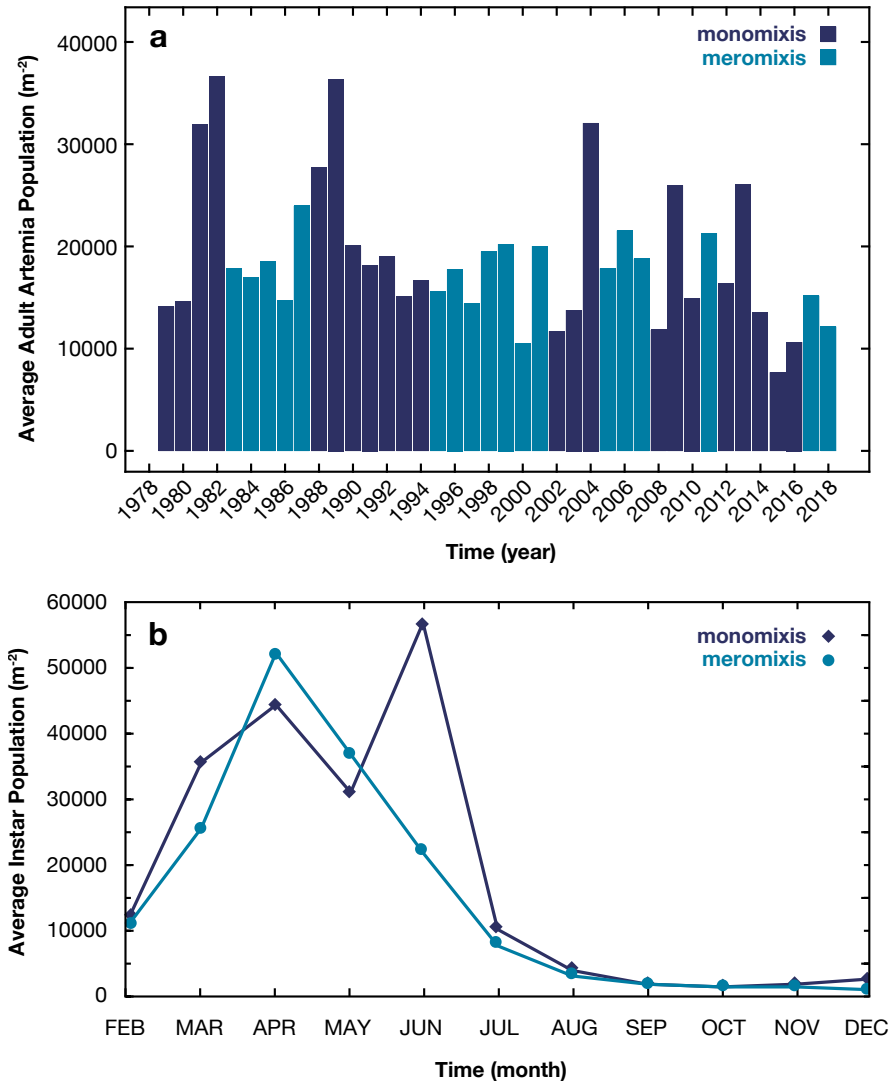

Figure S3 *Artemia population data for a) adults and b) nauplii and juveniles, redrawn from publicly available LADWP reports from 2018 and 2019 (http://www.monobasinresearch.org/onlinereports/). Average population is seen per meter squared across the lake's 12 monitored stations in seen in panel. Instar abundance, spanning nauplii and juveniles, was averaged for each month for meromictic and monomictic years when such monthly data was available (1987-present).*

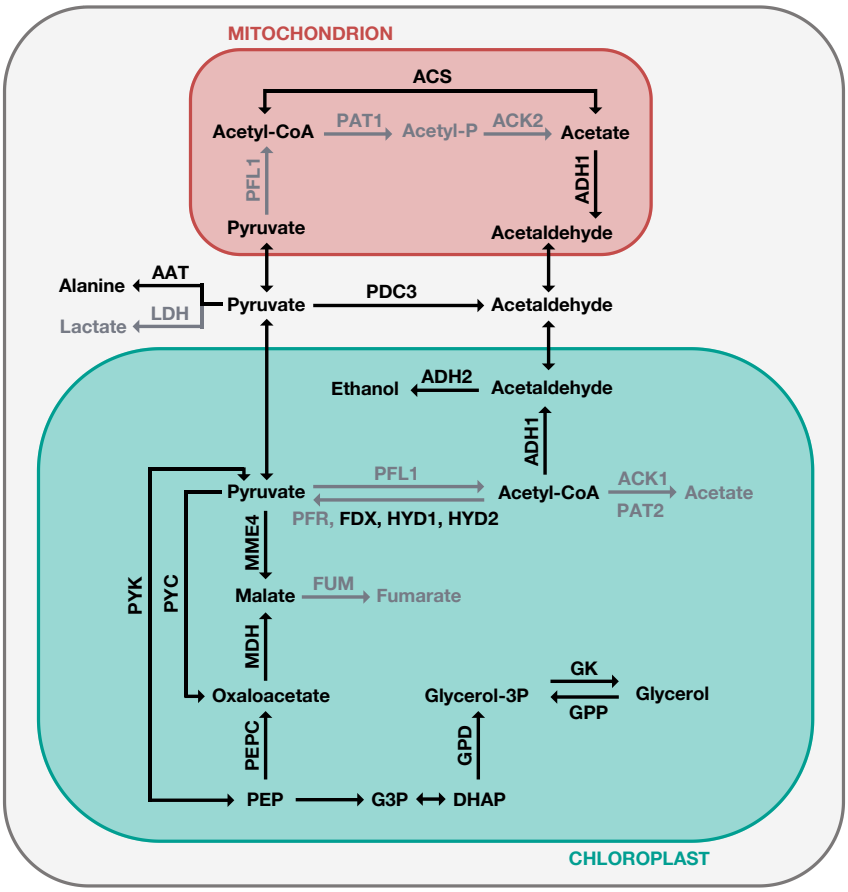

Figure S4 *Potential algal fermentation pathways in the model green alga Chlamydomonas reinhardtii, redrawn from Catalanotti et al. 2013. Genes colored in black are those with homologous proteins (E value < E-6, Table S5) observed in the Picocystis sp. ML draft genome. In gray are genes present in Chlamydomonas but not Picocystis.*

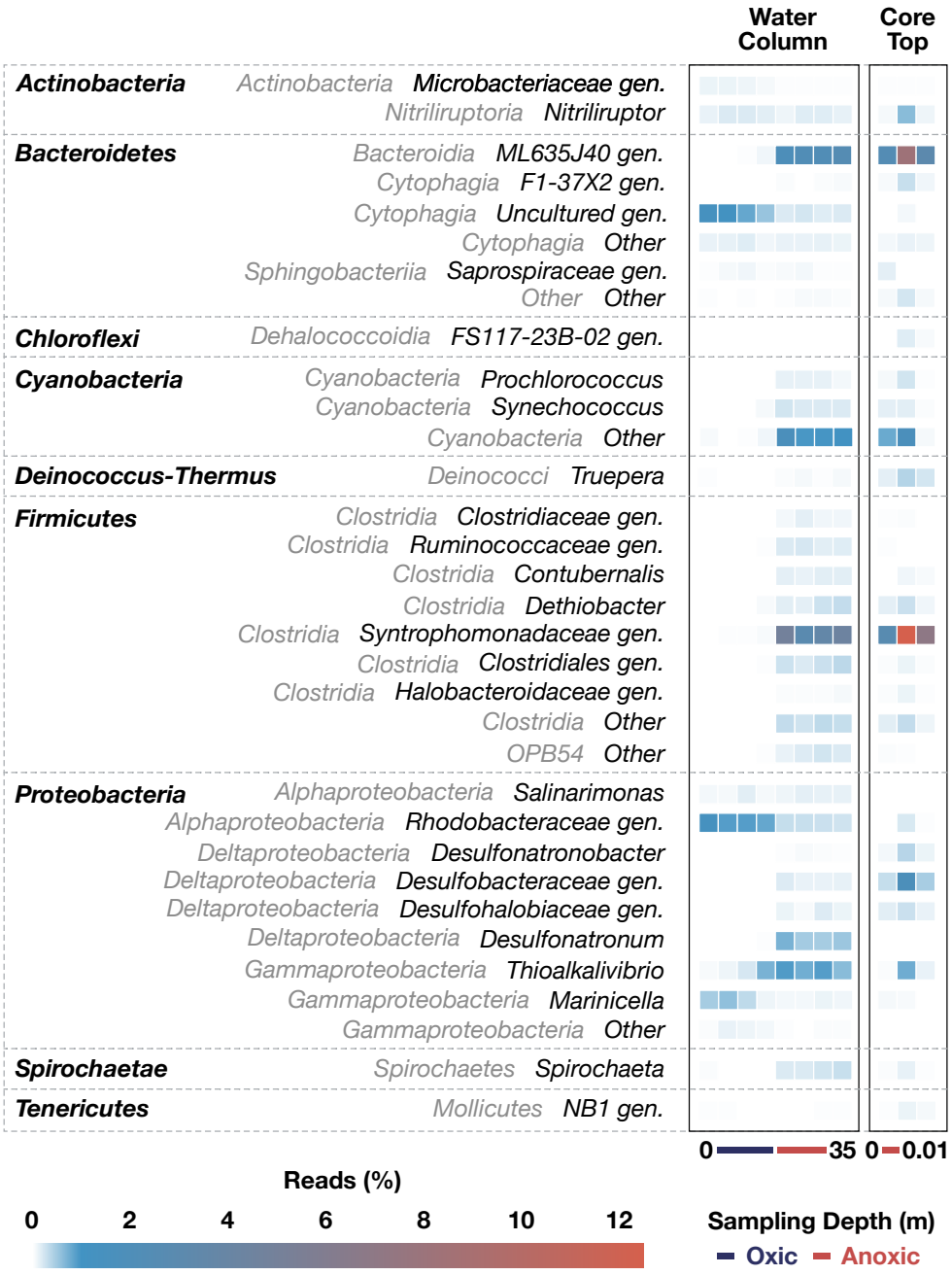

Figure S5 *Heatmap of 16S rRNA gene amplicons (that at one point reached >0.1% relative abundance) of water column samples and core top sediment samples from Spring 2018.*

Sediment sampling

A sediment core ~80cm in length was collected via a hand-held Aquatic Research Instruments universal core head, with 10kg weight and slide hammer. The recovered core had a visible sediment/water interface, and was capped and stored on ice until return to shore (1-3 hours). Overlying water was then removed by siphon, and the core extruded and sectioned in 5cm lengths. The core top used for this study consisted of soupy, dark green mud smelling strongly of sulfide. Sediment sample for sequencing was scooped from the middle of the core and frozen at -20°C until return to Caltech (2 days).

DNA extraction

Cell pellets were resuspended in 675 μL 1% CTAB (cetyltrimethylammonium bromide) extraction buffer (100 mM TRIS, 100 mM EDTA, 100 mM Na_2HPO_4, 1.5 M NaCl, 1% w/v CTAB) and incubated (37˚C, 30 min) with 50 μL Lysozyme (10 mg/mL). This was followed by incubation (37˚C, 30 min) with 50 μL proteinase K (10mg/mL). Lysis was achieved by incubation (65˚C, 120 min) with 150 μL 10% SDS buffer. Incubation (65˚C, 20 min) with 900 μL phenol/ chloroform/ isoamyl alcohol (25:24:1) was used to separate DNA from cell debris. After benchtop centrifugation (16,000 $\times$ *g*, 10 min), the upper aqueous phase was transferred, and trace phenol was removed with 900 μL chloroform/ isoamylalcohol (24:1). DNA was incubated (23˚C, 60 min) with 500 μL isopropanol and precipitated by centrifugation (16,000 $\times$ *g*, 15 min). Pellets were washed with ice cold ethanol (70%), centrifuged, decanted, air dried, and stored at -20˚C. 16S amplicons of the V4-V5 region of the 16S rRNA gene were obtained using PCR amplification with 515f and 926r primers (Goffredi et al., 2020). The protocol followed a 2 min initial denaturation at 98˚C, 28 cycles of 10 s at 98˚C, 20 s at 54˚C, 20 s at 72˚C, and a final elongation for 2 min at 72˚C. Product size was verified using a 1.5% agarose gel and 100 bp ladder (Fisher Scientific).

Modified Cline assay for sulfide analysis

The Cline assay for hydrogen sulfide had to be modified for Mono Lake water because the high DIC content causes precipitation of large amounts of zinc carbonate when samples are 'fixed' using zinc acetate. Precipitated zinc sulfide samples were first rinsed with ultrapure water three times, after which water was added to reach a final volume of 10 mL. Samples were shaken vigorously to resuspend the precipitate and 100 μL aliquots were taken and added into 20 μL of a 1:1 mixture of 11.5 mM N,N-dimethyl-p-phenylenediamine dihydrochloride (DPDD) in 6 N HCl and 30 mM $FeCl_3$. The resulting blue solution was measured for absorbance at 670 nm with a Tecan Sunrise-Basic microplate reader with Magellan software (version 5.0.3.5) at Caltech. Standard curves were generated with 50 μM to 2 mM solutions of zinc sulfide (10 μm) prepared with sulfide-free Mono Lake water. Samples were diluted to be measured within the standard curve's range.

DON measurements

In a pre-combusted 4 mL glass vial, 0.1 mL of Mono Lake water was combined with 1 mL persulfate oxidizing reagent (1 g recrystallized low-N $K_2S_2O_8$ and ACS grade 1.5 g NaOH in 100 mL ultrapure water) and autoclaved for 1 hr. DON concentration was calculated by subtracting the concentrations of nitrate and ammonium/ammonia from the concentration of TDN. The nitrogen concentration of blanks (persulfate oxidizing reagent) were <0.3 µM.

Fatty acid extractions and measurements

POC filters were placed in Teflon tubes with 20 mL dichloromethane (DCM) and methanol (9:1) in a Microwave Accelerated Reaction System 5 (CEM Instruments; 8 min ramp to 100˚C, hold for 15 min with stirring). Extracts were saponified in 0.5 M NaOH (70˚C, 4 hrs), adjusted to pH 1.5 then extracted into methyl tert-butyl

ether (MTBE). Fatty acids were purified via solid phase extraction using 0.5 g of Sepra NH2 stationary phase (Phenomenex; 50 μm, 65 Å) and eluted in 2.5% formic acid in DCM (8 mL), Collected fatty acids were then converted to fatty acid methyl esters (FAMEs) by reaction (70°C, 10 min) in DCM (3 mL) and 14% BF_3 in methanol (100 μL). FAMEs were separated on a Thermo Scientific Trace GC equipped with a 30 m x 0.25 mm ZB-5MS capillary column (Phenomenex Zebron; 0.25 μm film thickness) using helium as the carrier gas (0.8 mL/min). Detection was with a Thermo Scientific DSQII mass spectrometer, with electron-impact ionization source operated at 70 eV and 250˚C and 50-800 Da full scan. Samples were injected in splitless mode with a PTV injector. The GC oven was programmed at 100˚C (1 min), heated to 140˚C (20˚C/min), to 250˚C (3˚C/min), to 310˚C (20˚C/min) and held at 310˚C (10 min). Samples were identified using mass spectral comparisons with the NIST 200x database and laboratory standards. Compounds were quantified by comparing TIC peak areas to an internal standard (palmitic acid isobutyl ester) assuming equal response factors.

DIC and major cations

Major element abundances were measured only in spring 2017: concentrations of K^+ (1.18 – 1.24 ppt), Mg^{2+} (20.10 – 21.51 ppm), Ca^{2+} (11.55 – 12.87 ppm), Si^{4+} (9.34 – 9.83 ppm), Sr^{2+} (6.54 – 7.46 ppm), Li^{2+} (2.08 – 3.64 ppm), Fe^{2+} (39.82 – 42.08 ppb) and Mn^{2+} (11.03 – 13.63 ppb) were consistent with previous reports (Garrels and Mackenzie, 1967; Gray et al., 2008). DIC concentrations, also measured only in spring 2017, spanned 384 – 396 mM, agreeing with published values for Mono Lake at the same approximate lake level (Oremland et al., 2004). The $\delta^{13}C_{VPDB}$ values of DIC were also measured, averaging 2.2 ± 0.2‰, matching previous studies by (Li and Ku, 1997) who reported the $\delta^{13}C_{PDB}$ as 2‰ for Mono Lake.

Picocystis fatty acid composition

The FA composition of *Picocystis* has not been previously described. *Picocystis* synthesized a variety of FAs. Palmitic acid (C_{16}) was the most abundant—53% of the total signal. Monounsaturated, even-numbered FAs, including one isomer of hexadecenoic acid (16:1) and three isomers of octadecenoic acid (18:1) were also significant, accounting for a further 26% of the FA profile. Of the monounsaturated FAs, 16:1 was most abundant. Polyunsaturated fatty acids, with two or more double bonds, were 12% of normalized FA abundance and comprised 16:3, 18:2, 20:4, 20:3, and 20:2. Anteiso 16:0 was also detected in significant quantities, accounting for 4% of *Picocystis* fatty acids. Interestingly, iso and anteiso C_{17} FA were also identified, but at much lower levels (<1%). A series of even fatty acids ranging from C_{14} to C_{18} with a hydroxyl group at C-3 were also found in low abundance (<1%). Similar β-hydroxy FA's have been previously reported in green algae (Matsumoto and Nagashima, 1984).

Species richness, evenness, and Shannon diversity

Species richness—a measure of the number of OTUs—was higher in the hypolimnion, where OTUs increased after prolonged stratification. Epilimnion species richness was more variable, peaking with summer stratification and stabilizing under meromictic conditions. Shannon diversity ranged from 5.10 to 6.52, values similar to other freshwater stratified lakes (Roger et al., 2016). Like species richness, Shannon diversity was higher in the hypolimnion than the epilimnion. Evenness, however, was similar across these two depth regimes until spring 2018, when evenness dropped to a low of 0.80 in the epilimnion.

16S rRNA gene amplicon taxa abundances

Eukaryotes

98.7% of chloroplast sequences were assigned to the dominant phototrophic alga, *Picocystis*, while 0.9% belonged to a *Dictyochophyceae* genus and 0.2% to a

Chrysophyceae genus. Only trace (<0.1%) chloroplast reads were assigned to Bacillariophyceae (diatoms).

Epilimnion bacteria

In spring 2017, Mono Lake was monomictic and the epilimnion microbial community was characterized by the phototrophic alga *Picocystis* (~20% relative abundance) and aerobic or aerotolerant heterotrophic bacteria (~40% relative abundance) within Alphaproteobacteria, Gammaproteobacteria, Cytophagia, Actinobacteria, Bacteroidia, and Flavobacteriia. Notable Alphaproteobacteria detected included members of the photoheterotrophic genera *Roseovarius* and *Rhodobaca*, which were first isolated from hypersaline lakes (Labrenz et al., 1999; Milford et al., 2000). Heterotrophic genera of the Gammaproteobacteria, including *Methylonatrum* and *Spiribacter*, were also abundant. Characterized members of the *Spiribacter* genus degrade osmolytes like glycerol, secreted in abundance by algae under salt stress (López-Pérez et al., 2013) while *Methylonatrum* isolates oxidize numerous C_1 and C_2 compounds like formate, ethanol, methanol, and dimethylamine (Rua and Thompson, 2014). Notable Bacteroidetes genera included the cryophilic heterotrophs *Psychroflexus*, and the potential polysaccharide degraders Cyclobacteriaceae. The type species of the abundant Actinobacteria, *Nitriliruptor*, was originally isolated from a soda lake (Sorokin et al., 2009). Finally, *Spirochaeta*, a genus of facultatively anaerobic chemoheterotrophs and the Verrucomicrobia (genus *Opitutus*) known to degrade complex polysaccharides such as xylan and pectin (Rodrigues and Isanapong, 2014) were also identified. In fall 2017 there was an increase in unclassified sequences. We can say little about this unknown community, but due to coincident changes in hydrology, these OTUs may in part reflect organisms delivered directly from fresh water. This abundance of unknown taxa remained throughout spring 2018 as *Picocystis* bloomed.

Hypolimnion bacteria

Other likely heterotrophic bacteria were identified in the hypolimnion, including *Methylomicrobium*—an obligate methane or methanol oxidizer (Kalyuzhnaya et al., 2008). Bacteroidia were dominated by an unknown genus in the ML635J-40 order, previously identified in a clone library of Mono Lake deep water. The majority of Firmicute OTUs belonged to Clostridia, a class of predominantly spore-forming anaerobic fermenters. *Syntrophomonadaceae*, short-chain (C_4+) carboxylic acid degraders (Sobieraj and Boone, 2006) and *Ruminococcus*, carbohydrate fermenters, were the most abundant Firmicutes (Figure 5). Bacteroidia were dominated by an unknown genus in the ML635J-40 order, previously identified in a clone library of Mono Lake deep water. The majority of Firmicute OTUs belonged to Clostridia, a class of predominantly spore-forming anaerobic fermenters. *Syntrophomonadaceae*, short-chain (C_4+) carboxylic acid degraders (Sobieraj and Boone, 2006) and *Ruminococcus*, carbohydrate fermenters, were the most abundant Firmicutes (Figure 7). Many other genera also increased in the hypolimnion at this time, with concurrent rises in both species richness and Shannon diversity (Table S4, Figure 6). While no single taxon dominated, the relative abundance of all Firmicutes was significant, accounting for almost 10% of the microbial community (Figures 8b, S2). Detected (> 0.1% relative abundance) members of Deltaproteobacteria included the sulfate reducing bacteria *Desulfonatronum, Desulfonatronovibrio,* and two uncharacterized genera from *Desulfobacteraceae* and *Desulfohalobiaceae* families. Notably, the *Contubernalis* genus, containing known syntrophic partners to *Desulfobacteraceae* and *Desulfohalobiaceae* was also detected. This anaerobic alkaliphile was previously isolated from soda lakes (Zhilina et al., 2005; Sorokin et al., 2014). Sulfur reducers capable of using electron acceptors other than sulfate, such as thiosulfate or elemental sulfur, were also detected, including the spore-forming firmicute *Dethiobacter* as well as the Deltaproteobacteria *Desulfuromusa.* Several lithotrophic organisms with sulfur-oxidizing potential were identified. The most

abundant sulfur oxidizer, *Thioalkalivibrio*, a chemolithoautotrophic halophile previously isolated from Mono Lake (Sorokin et al., 2002), accounted for up to ~10% of the microbial community at depth (Figures 4, 5). Other sulfur oxidizers were detected including *Thiomicrospira* and *Ectothiorhodospira*, also in the Gammaproteobacteria. Many of these sulfur cyclers persisted in the hypolimnion into summer 2017 as Mono Lake entered thermal stratification. Cyanobacteria that bloomed in the last time point were also surprisingly abundant in hypolimnion samples, although reasons for their appearance are unclear and could be due to sinking particles following their bloom or their transient survival at the edge of the chemocline.

Picocystis' enigmatic carbon isotope fractionation

We observed remarkably large carbon isotope offsets between particulate organic matter and lake DIC. Mono Lake POM, which is dominantly algal biomass in deep waters (Figure 3), yielded an average $\delta^{13}C$ value of -31.6 ± 0.3‰ in the hypolimnion, which we interpret as Picocystis' bulk biomass value. $\delta^{13}C$ measurements of DIC yielded an average value of 2.2 ± 0.2‰ across depths. These offsets imply a large carbon isotope fractionation associated with photosynthesis, on the order of ~34‰ relative to source DIC and ~27-29‰ relative to dissolved CO_2. This is unexpected because larger isotope fractionations (up to ~25‰ relative to dissolved CO_2) are typically correlated with high concentrations of dissolved CO_2, which is negligible in alkaline Mono Lake (Popp et al., 1998; Wilkes and Pearson, 2019). Further, if Picocystis is instead using bicarbonate as its primary inorganic carbon source, we would expect smaller net fractionations because bicarbonate is enriched in ^{13}C compared to CO_2 and the carbon isotope fractionation of RuBisCO (Ribulose-1,5-bisphosphate carboxylase/oxygenase) is minimized due to closed-system behavior (Zeebe and Wolf-Gladrow, 2001). From investigating the Picocystis sp. strain ML genome against known genes in Chlamydamonas reinhardtii, Picocystis indeed appears to have machinery to take

up bicarbonate, including putative transporters and carbonic anhydrases that comprise a carbon concentrating mechanism (Atkinson et al., 2016; Table S5). However, the detailed pathways of carbon acquisition and fixation in Picocystis and their associated isotopic consequences are unknown and – like much about this alga – beg further investigation.

BIBLIOGRAPHY

Armstrong, F.A.J., Stearns, C.R., Strickland, J.D.H., 1967. The measurement of upwelling and subsequent biological process by means of the Technicon Autoanalyzer® and associated equipment. Deep Sea Research and Oceanographic Abstracts 14, 381–389.

Arvola, L., George, G., Livingstone, D., Järvinen, M., Blenckner, T., Dokulil, M., Jennings, E., Aonghusa, C., Nõges, P., Noges, T., Weyhenmeyer, G., 2009. The Impact of the Changing Climate on the Thermal Characteristics of Lakes. pp. 85–101.

Atkinson, N., Feike, D., Mackinder, L.C.M., Meyer, M.T., Griffiths, H., Jonikas, M.C., Smith, A.M., McCormick, A.J., 2016. Introducing an algal carbon-concentrating mechanism into higher plants: location and incorporation of key components. Plant Biotechnology Journal 14, 1302–1315.

Benson, L.V., Lund, S.P., Burdett, J.W., Kashgarian, M., Rose, T.P., Smoot, J.P., Schwartz, M., 1998. Correlation of Late-Pleistocene Lake-Level Oscillations in Mono Lake, California, with North Atlantic Climate Events. Quaternary Research 49, 1–10.

Bernard, C., Escalas, A., Villeriot, N., Agogué, H., Hugoni, M., Duval, C., Carré, C., Got, P., Sarazin, G., Jézéquel, D., Leboulanger, C., Grossi, V., Ader, M., Troussellier, M., 2019. Very Low Phytoplankton Diversity in a Tropical Saline-Alkaline Lake, with Co-dominance of Arthrospira fusiformis (Cyanobacteria) and Picocystis salinarum (Chlorophyta). Microbial Ecology 78, 603–617.

Bernhardt, H., Wilhelms, A., 1967. The continuous determination of low level iron, soluble phosphate and total phosphate with the AutoAnalyzer. Automation in Analytical Chemistry 385–389.

Braman, R.S., Hendrix, S.A., 1989. Nanogram nitrite and nitrate determination in environmental and biological materials by vanadium(III) reduction with chemiluminescence detection. Analytical Chemistry 61, 2715–2718.

Bruce, L.C., Jellison, R., Imberger, J., Melack, J.M., 2008. Effect of benthic boundary layer transport on the productivity of Mono Lake, California. Saline Systems 4, 11.

Caporaso, J.G., Kuczynski, J., Stombaugh, J., Bittinger, K., Bushman, F.D., Costello, E.K., Fierer, N., Peña, A.G., Goodrich, J.K., Gordon, J.I., Huttley, G.A., Kelley, S.T., Knights, D., Koenig, J.E., Ley, R.E., Lozupone, C.A.,

McDonald, D., Muegge, B.D., Pirrung, M., Reeder, J., Sevinsky, J.R., Turnbaugh, P.J., Walters, W.A., Widmann, J., Yatsunenko, T., Zaneveld, J., Knight, R., 2010. QIIME allows analysis of high-throughput community sequencing data. Nature Methods 7, 335–336.

Cappenberg, Th.E., 1972. Ecological observations on Heterotrophic, methane oxidizing and sulfate reducing bacteria in Pond. Hydrobiologia 40, 471–485.

Carini, S., Bano, N., LeCleir, G., Joye, S.B., 2005. Aerobic methane oxidation and methanotroph community composition during seasonal stratification in Mono Lake, California (USA). Environmental Microbiology 7, 1127–1138.

Carini, S.A., Joye, S.B., 2008. Nitrification in Mono Lake, California: Activity and community composition during contrasting hydrological regimes. Limnology and Oceanography 53, 2546–2557.

Catalanotti, C.P., Yang, W., Posewitz, M.C., Grossman, A.R., 2013. Fermentation metabolism and its evolution in algae. Frontiers in Plant Science 4.

Chan, M., Himes, R.H., Akagi, J.M., 1971. Fatty Acid Composition of Thermophilic, Mesophilic, and Psychrophilic Clostridia. Journal of Bacteriology 106, 876–881.

Choi, S.K., Lee, J.Y., Kwon, D.Y., Cho, K.J., 2006. Settling characteristics of problem algae in the water treatment process. Water Science and Technology 53, 113–119.

Cline, J.D., 1969. Spectrophotometric Determination of Hydrogen Sulfide in Natural Waters. Limnology and Oceanography 14, 454–458.

Collins, A.G., 2017. Compliance with State Water Resources Control Board decision 1631 order nos. 98–05 and 98–07.

Collins, A.G., 2018. Compliance with State Water Resources Control Board decision 1631 order nos. 98–05 and 98–07.

Collins, A.G., 2019. Compliance with State Water Resources Control Board decision 1631 order nos. 98–05 and 98–07.

Cook, R.B., Schindler, D.W., 1983. The Biogeochemistry of Sulfur in an Experimentally Acidified Lake. Ecological Bulletins 115–127.

Cooper, S.D., Winkler, D.W., Lenz, P.H., 1984. The Effect of Grebe Predation on a Brine Shrimp Population. Journal of Animal Ecology 53, 51–64.

D'Abramo, L.R., Bordner, C.E., Conklin, D.E., Baum, N.A., 1984. Sterol requirement of juvenile lobsters, Homarus sp. Aquaculture 42, 13–25.

Davis, T.W., Berry, D.L., Boyer, G.L., Gobler, C.J., 2009. The effects of temperature and nutrients on the growth and dynamics of toxic and non-toxic strains of Microcystis during cyanobacteria blooms. Harmful Algae, This issue contains the special section on "Strains" 8, 715–725.

Diao, M., Sinnige, R., Kalbitz, K., Huisman, J., Muyzer, G., 2017. Succession of Bacterial Communities in a Seasonally Stratified Lake with an Anoxic and Sulfidic Hypolimnion. Frontiers in Microbiology 8, 2511.

Edwardson, C.F., Hollibaugh, J.T., 2017. Metatranscriptomic analysis of prokaryotic communities active in sulfur and arsenic cycling in Mono Lake, California, USA. The ISME Journal 11, 2195–2208.

Edwardson, C.F., Hollibaugh, J.T., 2018. Composition and Activity of Microbial Communities along the Redox Gradient of an Alkaline, Hypersaline, Lake. Frontiers in Microbiology 9.

Ehling-Schulz, M., Scherer, S., 1999. UV protection in cyanobacteria. European Journal of Phycology 34, 329–338.

Flöder, S., Sommer, U., 1999. Diversity in planktonic communities: An experimental test of the intermediate disturbance hypothesis. Limnology and Oceanography 44, 1114–1119.

Garrels, R.M., Mackenzie, F.T., 1967. Origin of the Chemical Compositions of Some Springs and Lakes, in: Equilibrium Concepts in Natural Water Systems, Advances in Chemistry. American Chemical Society , pp. 222–242.

Goffredi, S.K., Tilic, E., Mullin, S.W., Dawson, K.S., Keller, A., Lee, R.W., Wu, F., Levin, L.A., Rouse, G.W., Cordes, E.E., Orphan, V.J., 2020. Methanotrophic bacterial symbionts fuel dense populations of deep-sea feather duster worms (Sabellida, Annelida) and extend the spatial influence of methane seepage. Science Advances 6, eaay8562.

Gray, W., Glazner, A.F., Coleman, D.S., Bartley, J.M., 2008. Long-term geochemical variability of the Late Cretaceous Tuolumne Intrusive Suite, central Sierra Nevada, California.

Guillard, R.R.L., Hargraves, P.E., 1993. Stichochrysis immobilis is a diatom, not a chrysophyte. Phycologia 32, 234–236.

Hansell, D.A., 2005. Dissolved Organic Carbon Reference Material Program. Eos, Transactions American Geophysical Union 86, 318–318.

Harasick, R.F., 2016. Compliance with State Water Resources Control Board decision 1631 order nos. 98–05 and 98–07.

Hardin, G., 1960. The Competitive Exclusion Principle. Science 131, 1292–1297.

Hartland, A., Andersen, M., Hamilton, D., 2015. Phosphorus and arsenic distributions in a seasonally-stratified, iron-and manganese-rich lake: microbiological and geochemical controls. Environmental Chemistry 12.

Hoeft McCann, S., Boren, A., Hernandez-Maldonado, J., Stoneburner, B., Saltikov, C.W., Stolz, J.F., Oremland, R.S., 2017. Arsenite as an Electron Donor for Anoxygenic Photosynthesis: Description of Three Strains of Ectothiorhodospira from Mono Lake, California and Big Soda Lake, Nevada. Life 7, 1.

Hollibaugh, J.T., Wong, P.S., Bano, N., Pak, S.K., Prager, E.M., Orrego, C., 2001. Stratification of microbial assemblages in Mono Lake, California, and response to a mixing event, in: Melack, J.M., Jellison, R., Herbst, D.B. (Eds.), Saline Lakes: Publications from the 7th International Conference on Salt Lakes, Held in Death Valley National Park, California, U.S.A., September 1999, Developments in Hydrobiology. Springer Netherlands, Dordrecht, pp. 45–60.

Humayoun, S.B., Bano, N., Hollibaugh, J.T., 2003. Depth Distribution of Microbial Diversity in Mono Lake, a Meromictic Soda Lake in California. Applied and Environmental Microbiology 69, 1030–1042.

Ingvorsen, K., Zeikus, J.G., Brock, T.D., 1981. Dynamics of bacterial sulfate reduction in a eutrophic lake. Applied and Environmental Microbiology 42, 1029–1036.

Jellison, R., Macintyre, S., Millero, F.J., 1999. Density and conductivity properties of Na-CO3-Cl-SO4 brine from Mono Lake, California, USA. International Journal of Salt Lake Research 8, 41–54.

Jellison, R., Melack, J.M., 1993. Algal photosynthetic activity and its response to meromixis in hypersaline Mono Lake, California. Limnology and Oceanography 38, 818–837.

Jiang, H., Dong, H., Zhang, G., Yu, B., Chapman, L.R., Fields, M.W., 2006. Microbial Diversity in Water and Sediment of Lake Chaka, an Athalassohaline Lake in Northwestern China. Applied and Environmental Microbiology 72, 3832–3845.

Jones, S.E., Chiu, C.-Y., Kratz, T.K., Wu, J.-T., Shade, A., McMahon, K.D., 2008. Typhoons initiate predictable change in aquatic bacterial communities. Limnology and Oceanography 53, 1319–1326.

Junkins, E.N., Stamps, B.W., Corsetti, F.A., Oremland, R.S., Spear, J.R., Stevenson, B.S., 2019. Draft Genome Sequence of Picocystis sp. Strain ML, Cultivated from Mono Lake, California. Microbiology Resource Announcements 8.

Kalyuzhnaya, M.G., Khmelenina, V., Eshinimaev, B., Sorokin, D., Fuse, H., Lidstrom, M., Trotsenko, Y., 2008. Classification of halo(alkali)philic and halo(alkali)tolerant methanotrophs provisionally assigned to the genera Methylomicrobium and Methylobacter and emended description of the genus Methylomicrobium. International Journal of Systematic and Evolutionary Microbiology 58, 591–596.

Kulp, T.R., Hoeft, S.E., Asao, M., Madigan, M.T., Hollibaugh, J.T., Fisher, J.C., Stolz, J.F., Culbertson, C.W., Miller, L.G., Oremland, R.S., 2008. Arsenic(III) Fuels Anoxygenic Photosynthesis in Hot Spring Biofilms from Mono Lake, California. Science 321, 967–970.

Labrenz, M., Collins, M.D., Lawson, P.A., Tindall, B.J., Schumann, P., Hirsch, P., 1999. Roseovarius tolerans gen. nov., sp. nov., a budding bacterium with variable bacteriochlorophyll a production from hypersaline Ekho Lake. International Journal of Systematic and Evolutionary Microbiology, 49, 137–147.

Lennon, J.T., Jones, S.E., 2011. Microbial seed banks: the ecological and evolutionary implications of dormancy. Nature Reviews Microbiology 9, 119–130.

Li, H.C., Ku, T.L., 1997. δ13C–δ18C covariance as a paleohydrological indicator for closed-basin lakes. Palaeogeography, Palaeoclimatology, Palaeoecology 133, 69–80.

López-Pérez, M., Ghai, R., Leon, M.J., Rodríguez-Olmos, Á., Copa-Patiño, J.L., Soliveri, J., Sanchez-Porro, C., Ventosa, A., Rodriguez-Valera, F., 2013. Genomes of “Spiribacter”, a streamlined, successful halophilic bacterium. BMC Genomics 14, 787.

Manske, A.K., Glaeser, J., Kuypers, M.M.M., Overmann, J., 2005. Physiology and Phylogeny of Green Sulfur Bacteria Forming a Monospecific Phototrophic Assemblage at a Depth of 100 Meters in the Black Sea. Applied and Environmental Microbiology 71, 8049–8060.

Matsumoto, G., Nagashima, H., 1984. Occurrence of 3-hydroxy acids in microalgae and cyanobacteria and their geochemical significance. Geochimica et Cosmochimica Acta 48, 1683–1687.

Melack, J.M., Jellison, R., MacIntyre, S., Hollibaugh, J.T., 2017. Mono Lake: Plankton Dynamics over Three Decades of Meromixis or Monomixis, in: Gulati, R.D., Zadereev, E.S., Degermendzhi, A.G. (Eds.), Ecology of Meromictic Lakes, Ecological Studies. Springer International Publishing, Cham, pp. 325–351.

Milford, A.D., Achenbach, L.A., Jung, D.O., Madigan, M.T., 2000. Rhodobaca bogoriensis gen. nov. and sp. nov., an alkaliphilic purple nonsulfur bacterium from African Rift Valley soda lakes. Archives of Microbiology 174, 18–27.

Miller, L.G., Jellison, R., Oremland, R.S., Culbertson, C.W., 1993. Meromixis in hypersaline Mono Lake, California. 3. Biogeochemical response to stratification and overturn. Limnology and Oceanography 38, 1040–1051.

Murata, N., Wada, H., Gombos, Z., 1992. Modes of Fatty-Acid Desaturation in Cyanobacteria. Plant and Cell Physiology 33, 933–941.

Nercessian, O., Kalyuzhnaya, M.G., Joye, S.B., Lidstrom, M.E., Chistoserdova, L., 2005. Analysis of fae and fhcD Genes in Mono Lake, California. Applied and Environmental Microbiology 71, 8949–8953.

Nydahl, F., 1978. On the peroxodisulphate oxidation of total nitrogen in waters to nitrate. Water Research 12, 1123–1130.

Oksanen, J., Blanchet, F.G., Friendly, M., Kindt, R., Legendre, P., McGlinn, D., Minchin, P.R., O'Hara, R.B., Simpson, G.L., Solymos, P., Stevens, M.H.H., Szoecs, E., Wagner, H., 2020. vegan: Community Ecology Package.

O'Neil, J.M., Davis, T.W., Burford, M.A., Gobler, C.J., 2012. The rise of harmful cyanobacteria blooms: The potential roles of eutrophication and climate change. Harmful Algae, Harmful Algae--The requirement for species-specific information 14, 313–334.

Oremland, R.S., Dowdle, P.R., Hoeft, S., Sharp, J.O., Schaefer, J.K., Miller, L.G., Switzer Blum, J., Smith, R.L., Bloom, N.S., Wallschlaeger, D., 2000. Bacterial dissimilatory reduction of arsenate and sulfate in meromictic Mono Lake, California. Geochimica et Cosmochimica Acta 64, 3073–3084.

Oremland, R.S., Stolz, J.F., Hollibaugh, J.T., 2004. The microbial arsenic cycle in Mono Lake, California. FEMS Microbiology Ecology 48, 15–27.

Oren, A., 1999. Bioenergetic aspects of halophilism. Microbiology and molecular biology reviews: MMBR 63, 334–348.

Oren, A., 2008. Microbial life at high salt concentrations: phylogenetic and metabolic diversity. Saline Systems 4, 2.

Peeters, F., Livingstone, D.M., Goudsmit, G.-H., Kipfer, R., Forster, R., 2002. Modeling 50 years of historical temperature profiles in a large central European lake. Limnology and Oceanography 47, 186–197.

Popp, B.N., Laws, E.A., Bidigare, R.R., Dore, J.E., Hanson, K.L., Wakeham, S.G., 1998. Effect of Phytoplankton Cell Geometry on Carbon Isotopic Fractionation. Geochimica et Cosmochimica Acta 62, 69–77.

Quast, C., Pruesse, E., Yilmaz, P., Gerken, J., Schweer, T., Yarza, P., Peplies, J., Glöckner, F.O., 2013. The SILVA ribosomal RNA gene database project: improved data processing and web-based tools. Nucleic Acids Research 41, D590–D596.

Rodrigues, J.L.M., Isanapong, J., 2014. The Family Opitutaceae, in: Rosenberg, E., DeLong, E.F., Lory, S., Stackebrandt, E., Thompson, F. (Eds.), The Prokaryotes. Springer Berlin Heidelberg, Berlin, Heidelberg, pp. 751–756.

Roesler, C.S., Culbertson, C.W., Etheridge, S.M., Goericke, R., Kiene, R.P., Miller, L.G., Oremland, R.S., 2002. Distribution, production, and ecophysiology of Picocystis strain ML in Mono Lake, California. Limnology and Oceanography 47, 440–452.

Roger, F., Bertilsson, S., Langenheder, S., Osman, O.A., Gamfeldt, L., 2016. Effects of multiple dimensions of bacterial diversity on functioning, stability and multifunctionality. Ecology 97, 2716–2728.

Rojas, P., Rodríguez, N., de la Fuente, V., Sánchez-Mata, D., Amils, R., Sanz, J.L., 2018. Microbial diversity associated with the anaerobic sediments of a soda lake (Mono Lake, California, USA). Canadian Journal of Microbiology 64, 385–392.

Rontani, J.-F., Charriere, B., Petit, M., Vaultier, F., Heipieper, H.J., Link, H., Chaillou, G., Sempéré, R., 2012. Degradation state of organic matter in surface sediments from the Southern Beaufort Sea: a lipid approach. Biogeosciences 9, 3513–3530.

Rua, C.P.J., Thompson, F., 2014. The Unclassified Genera of Gammaproteobacteria: Alkalimonas, Arenicella, Chromatocurvus, Congregibacter, Gallaecimonas, Halioglobus, Marinicella, Methylohalomonas, Methylonatrum, Orbus, Plasticicumulans, Porticoccus, Sedimenticola, Simiduia, Solimonas, in: Rosenberg, E., DeLong, E.F., Lory, S., Stackebrandt, E., Thompson, F. (Eds.), The Prokaryotes. Springer Berlin Heidelberg, Berlin, Heidelberg, pp. 749–768.

Scholten, J.C.M., Joye, S.B., Hollibaugh, J.T., Murrell, J.C., 2005. Molecular Analysis of the Sulfate Reducing and ArchaealCommunity in a Meromictic Soda Lake (Mono Lake, California) by Targeting 16S rRNA, mcrA, apsA, and dsrAB Genes. Microbial Ecology 50, 29–39.

Shade, A., Jones, S.E., McMahon, K.D., 2008. The influence of habitat heterogeneity on freshwater bacterial community composition and dynamics. Environmental Microbiology 10, 1057–1067.

Shade, A., Read, J.S., Welkie, D.G., Kratz, T.K., Wu, C.H., McMahon, K.D., 2011. Resistance, resilience and recovery: aquatic bacterial dynamics after water column disturbance. Environmental Microbiology 13, 2752–2767.

Shade, A., Read, J.S., Youngblut, N.D., Fierer, N., Knight, R., Kratz, T.K., Lottig, N.R., Roden, E.E., Stanley, E.H., Stombaugh, J., Whitaker, R.J., Wu, C.H., McMahon, K.D., 2012. Lake microbial communities are resilient after a whole-ecosystem disturbance. The ISME Journal 6, 2153–2167.

Shannon, C., Weaver, W., n.d. The Mathematical Theory of Communication 131.

Sobieraj, M., Boone, D.R., 2006. Syntrophomonadaceae, in: Dworkin, M., Falkow, S., Rosenberg, E., Schleifer, K.-H., Stackebrandt, E. (Eds.), The Prokaryotes. Springer US, New York, NY, pp. 1041–1049.

Sorokin, D.Y., Abbas, B., Tourova, T.P., Bumazhkin, B.K., Kolganova, T.V., Muyzer, G., 2014. Sulfate-dependent acetate oxidation under extremely natron-alkaline conditions by syntrophic associations from hypersaline soda lakes. Microbiology, 160, 723–732.

Sorokin, D.Y., Gorlenko, V.M., Tourova, T.P., Tsapin, A.I., Nealson, K.H., Kuenen, G.J., 2002. Thioalkalimicrobium cyclicum sp. nov. and Thioalkalivibrio jannaschii sp. nov., novel species of haloalkaliphilic, obligately chemolithoautotrophic sulfur-oxidizing bacteria from hypersaline alkaline Mono Lake (California). International Journal of Systematic and Evolutionary Microbiology 52, 913–920.

Sorokin, D.Y., van Pelt, S., Tourova, T.P., Evtushenko, L.I., 2009. Nitriliruptor alkaliphilus gen. nov., sp. nov., a deep-lineage haloalkaliphilic actinobacterium from soda lakes capable of growth on aliphatic nitriles, and proposal of Nitriliruptoraceae fam. nov. and Nitriliruptorales ord. nov. International Journal of Systematic and Evolutionary Microbiology 59, 248–253.

Stamps, B.W., Nunn, H.S., Petryshyn, V.A., Oremland, R.S., Miller, L.G., Rosen, M.R., Bauer, K.W., Thompson, K.J., Tookmanian, E.M., Waldeck, A.R., Loyd, S.J., Johnson, H.A., Stevenson, B.S., Berelson, W.M., Corsetti, F.A., Spear, J.R., 2018. Metabolic Capability and Phylogenetic Diversity of Mono Lake during a Bloom of the Eukaryotic Phototroph Picocystis sp. Strain ML. Applied and Environmental Microbiology 84.

Subhas, A.V., Rollins, N.E., Berelson, W.M., Dong, S., Erez, J., Adkins, J.F., 2015. A novel determination of calcite dissolution kinetics in seawater. Geochimica et Cosmochimica Acta 170, 51–68.

Teshima, S., Kanazawa, A., 1971. Utilization and Biosynthesis of Sterols in Artemia saina. Nippon Suisan Gakkaishi 37, 720–723.

Thrash, J.C., Seitz, K.W., Baker, B.J., Temperton, B., Gillies, L.E., Rabalais, N.N., Henrissat, B., Mason, O.U., 2017. Metabolic Roles of Uncultivated Bacterioplankton Lineages in the Northern Gulf of Mexico “Dead Zone.” mBio 8.

Ulloa, O., Canfield, D.E., DeLong, E.F., Letelier, R.M., Stewart, F.J., 2012. Microbial oceanography of anoxic oxygen minimum zones. Proceedings of the National Academy of Sciences 109, 15996–16003.

Wang, X.T., Sigman, D.M., Cohen, A.L., Sinclair, D.J., Sherrell, R.M., Weigand, M.A., Erler, D.V., Ren, H., 2015. Isotopic composition of skeleton-bound organic nitrogen in reef-building symbiotic corals: A new method and proxy evaluation at Bermuda. Geochimica et Cosmochimica Acta 148, 179–190.

Weber, A.P.M., Horst, R.J., Barbier, G.G., Oesterhelt, C., 2007. Metabolism and Metabolomics of Eukaryotes Living Under Extreme Conditions, in: International Review of Cytology. Academic Press, pp. 1–34.

Wiens, J.A., Patten, D.T., Botkin, D.B., 1993. Assessing Ecological Impact Assessment: Lessons from Mono Lake, California. Ecological Applications: A Publication of the Ecological Society of America 3, 595–609.

Wilkes, E.B., Pearson, A., 2019. A general model for carbon isotopes in red-lineage phytoplankton: Interplay between unidirectional processes and fractionation by RubisCO. Geochimica et Cosmochimica Acta 265, 163–181.

Winkler, D.W., 1977. An Ecological Study of Mono Lake, California.

Zeebe, R.E., Wolf-Gladrow, D., 2001. CO2 in Seawater: Equilibrium, Kinetics, Isotopes. Elsevier.

Zhilina, T.N., Zavarzina, D.G., Kolganova, T.V., Turova, T.P., Zavarzin, G.A., 2005. “Candidatus contubernalis alkalaceticum,” an obligately syntrophic alkaliphilic bacterium capable of anaerobic acetate oxidation in a coculture with Desulfonatronum cooperativum. Mikrobiologiia 74, 800–809.

Zhou, J., Bruns, M.A., Tiedje, J.M., 1996. DNA recovery from soils of diverse composition. Applied and Environmental Microbiology 62, 316–322.

Chapter 2

SULFUR ISOTOPE ANALYSIS OF CYSTEINE AND METHIONINE VIA PREPARATORY LIQUID CHROMATOGRAPHY AND ELEMENTAL ANALYZER ISOTOPE RATIO MASS SPECTROMETRY

Phillips, A.A., Wu, F., Sessions, A.L., 2021. Sulfur isotope analysis of cysteine and methionine via preparatory liquid chromatography and elemental analyzer isotope ratio mass spectrometry. Rapid Communications in Mass Spectrometry 35, e9007. https://doi.org/10.1002/rcm.9007.

ABSTRACT

Rationale: Sulfur isotope analysis of organic sulfur-containing molecules has previously been hindered by challenging preparatory chemistry and analytical requirements for large sample sizes. The natural-abundance sulfur isotopic compositions of the sulfur-containing amino acids, cysteine and methionine, have therefore not yet been investigated despite potential utility in biomedicine, ecology, oceanography, biogeochemistry, and other fields.

Methods: Cysteine and methionine were subjected to hot acid hydrolysis followed by quantitative oxidation in performic acid to yield cysteic acid and methionine sulfone. These stable, oxidized products were then separated by reversed-phase high-performance liquid chromatography (HPLC) and verified via offline liquid chromatography/mass spectrometry (LC/MS). The sulfur isotope ratios ($\delta^{34}S$ values) of purified analytes were then measured via combustion elemental analyzer coupled to isotope ratio mass spectrometry (EA/IRMS). The EA was equipped with a temperature-ramped chromatographic column and programmable helium carrier flow rates.

Results: On-column focusing of SO_2 in the EA/IRMS system, combined with reduced He carrier flow during elution, greatly improved sensitivity, allowing precise (0.1–0.3‰ 1 s.d.) $\delta^{34}S$ measurements of 1 to 10 µg sulfur. We validated that our method for purification of cysteine and methionine was negligibly fractionating using amino acid and protein standards. Proof-of-concept measurements of fish muscle tissue and bacteria demonstrated differences up to 4‰ between the $\delta^{34}S$ values of cysteine and methionine that can be connected to biosynthetic pathways.

Conclusions: We have developed a sensitive, precise method for measuring the natural-abundance sulfur isotopic compositions of cysteine and methionine isolated from biological samples. This capability opens up diverse applications of sulfur isotopes in amino acids and proteins, from use as a tracer in organisms and the environment, to fundamental aspects of metabolism and biosynthesis.

1 | INTRODUCTION

The sulfur isotopic compositions of amino acids (AAs) are virtually unexplored but may hold significant utility across diverse scientific disciplines. In biomedicine, pilot studies have suggested that cysteine and methionine $\delta^{34}S$ values could indicate disease progression as sulfur metabolism is dysregulated at the onset of liver cancer (Albalat et al., 2016). In archeology, bulk protein $\delta^{34}S$ values of mummy hair (Fourel et al., 2015) and mammalian collagen (Richards et al., 2001) have been used to reconstruct ancestral migration and reliance on fish protein, indicating this as a promising direction for targeted paleodiet reconstruction. Mass-balance isotopic models in plants suggest that differences related to metabolism could exist between cysteine and methionine $\delta^{34}S$ values, which in turn could inform agricultural sectors on the efficiency of sulfur uptake in soils (Tcherkez and Tea, 2013). Cysteine and methionine also have potential in biogeochemical studies to record redox conditions; for example, direct incorporation of ^{34}S-depleted sulfide

in anoxic sediments has been demonstrated in deep-reaching mangrove roots (Brunold and Erismann, 1975). Measuring the compound-specific S isotope ratios of cysteine and methionine offers more powerful insights than would bulk protein analyses, disentangling the effects of metabolism versus environmental change. Here, we present the first method for natural-abundance sulfur isotope characterization of these amino acids, with successful measurements of 1–10 µg sulfur (~ 4–40 µg analyte).

Table 1 *Summary of mass spectrometric methods for the determination of natural-abundance sulfur isotope ratios, with reported sensitivity and precision. Asterisks indicate work in this study.*

Measured Species	Analytical Technique	Minimum Sample (µg S)	$\delta^{34}S$ precision (‰, 1 s.d.)	Parameters Measured	Reference
S^+	MC/ICPMS	0.2	0.05-0.10	$\delta^{34}S$, $\Delta^{33}S$	Mayer and Krouse, 2004
	GC/MCICPMS	0.001	0.1	$\delta^{34}S$	Amrani et al., 2009
SF_6^+	IRMS (dual-inlet)	440	0.05	$\delta^{34}S$, $\Delta^{33}S$, $\Delta^{36}S$	Thode and Rees, 1971
	IRMS (microvolume)	0.6	0.04-0.15	$\delta^{34}S$, $\Delta^{33}S$, $\Delta^{36}S$	Au Yang et al., 2016
SO_2^+	IRMS (dual-inlet)	640	<0.2	$\delta^{34}S$	Ueda and Krouse, 1986
	EA/IRMS (conventional)	70	0.3	$\delta^{34}S$	Giesemann et al., 1994
	EA/IRMS (purge and trap)	35	0.4	$\delta^{34}S$	Fourel et al., 2014
	EA/IRMS (dual GC column)	30	<0.2	$\delta^{34}S$	Fry, 2007
	EA/IRMS (ramped GC column)	2.0 1.0*	0.3 0.2*	$\delta^{34}S$	Sayle et al., 2019

Progress towards the compound-specific isotopic analysis of organic sulfur-containing compounds has historically been hindered by mass spectrometric limitations (Table 1). Sulfur isotope measurements typically relied on analyte

combustion to SO_2, a highly polar, toxic, corrosive, and hygroscopic gas, before online measurement via isotope ratio mass spectrometry (IRMS). To compensate for a host of analytical difficulties resulting from these properties of SO_2, analyses required relatively large sample sizes ranging from 70 to 100 µg S even when using a specialized elemental analyzer (EA) with online combustion that improved on traditional dual-inlet designs (Ueda and Krouse, 1986; Giesemann et al., 1994). Moreover, because the EA does not inherently separate different analyte compounds, offline preparative purification is needed prior to analysis. The combination of these two requirements presented a substantial barrier to measurements of analytes such as amino acids that exist in the environment in low concentrations. An alternative strategy for sulfur isotope determination used fluorination of analytes to sulfur hexafluoride (SF_6), which required large sample sizes but improved analytical precision due to the favorable properties of SF_6 (Thode and Rees, 1971). When measurements of this inert gas were combined with a microvolume and tenfold-increased signal amplification, detection limits were lowered to 0.6–3.2 µg S (Au Yang et al., 2016). However, the preparation of SF_6 requires specialized vacuum lines and dangerous reagents and has not yet been demonstrated for organic analytes (Hulston and Thode, 1965; Mayer and Krouse, 2004; Au Yang et al., 2016). Multi-collector inductively coupled plasma mass spectrometry (MC/ICPMS) has also recently demonstrated remarkably low sensitivity for measuring sulfur isotopes in sulfate and sulfur-bearing minerals (Craddock et al., 2008; Paris et al., 2013), but thus far requires conversion of analytes into sulfate. Direct coupling of gas chromatography (GC) to MC/ICPMS was first reported in 2009 (Amrani et al., 2009), and has enabled highly sensitive, compound-specific measurements of organic sulfur compounds, including volatile species from crude oils (Amrani et al., 2009) and mature sediments (Raven et al., 2015), as well as marine dimethylsulfonopropionate (DMSP; (Oduro et al., 2012). Unfortunately, for our application GC separation of cysteine and methionine is not

a viable option because existing derivatization strategies are not reliably quantitative and may fractionate sulfur isotopes.

Simultaneous with ICPMS development, there has been a parallel renaissance in EA/IRMS technology leading to significantly reduced sample sizes: online ‘purge and trap’ configurations have measured 35–350 µg sulfur (Fourel et al., 2014) and dual-column GC systems have reached 30–70 µg sulfur (Fry, 2007). Most recently, the Thermo Scientific Flash EA-Isolink equipped with a temperature-ramped chromatographic column was used to measure $\delta^{34}S$ in bone collagen samples containing just 2–3 µg sulfur (Sayle et al., 2019). This system, which we improved upon in the current study, provides sufficient sensitivity to make offline preparative isolation of the sulfur AAs much less tedious.

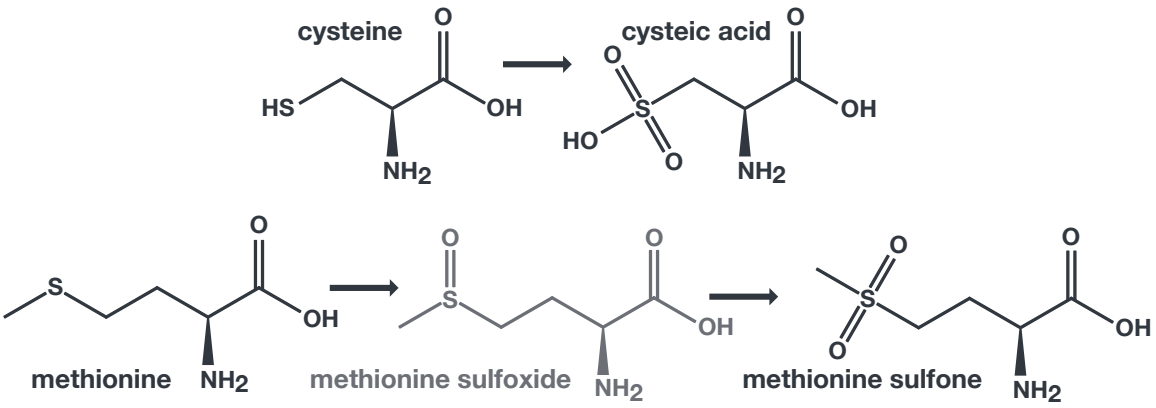

Figure 1 *Progressive oxidation of the amino acids cysteine and methionine. Although cysteine has intermediate oxidation states, the sulfonic acid endmember (cysteic acid) is most stable and is therefore the common oxidation product. In contrast, methionine oxidation often yields several products including methionine sulfoxide and methionine sulfone. Such uncontrolled oxidation reactions have hampered many previous efforts at quantification and/or isolation of the sulfur amino acids.*

Analyses of cysteine and methionine have also faced significant difficulties in their chemical separation. Isolation methods have typically employed hot acid hydrolysis to release amino acid residues from proteins (Steine and Moore, 1949). However, this approach led to partial or complete oxidation of cysteine and methionine to cysteic acid and methionine sulfone (Figure 1), even when the headspace was flushed with argon or nitrogen gas (Keutmann and Potts, 1969; Hunt, 1985). To avoid such problems, amino acid residues were often oxidized (Macdonald et al., 1985; Manneberg et al., 1995; Abadie and Tcherkez, 2019), reduced (Keutmann and Potts, 1969; Inglis and Liu, 1970; Yano et al., 1990), or alkylated (Smyth et al., 1963; Guidotti and Konigsberg, 1964; Friedman et al., 1970; Grant, 2017). However, alkylation only effectively targets cysteine, and reduction only methionine (Table S1). Recent studies have thus converged on oxidation with performic acid (CH_2O_3) to quantitatively yield cysteic acid and methionine sulfone prior to LC/MS separation and quantification (Albert et al., 2008; Rampler et al., 2012).

Here we employed a modified version of this oxidation strategy. We validated the method as non-fractionating using commercial standards of cysteine, methionine, and bovine serum albumin (a well-characterized, sulfur-rich protein), and established the performance characteristics of the methodology. We then applied our novel approach to biomass from two ubiquitous microbes, *Escherichia coli* and *Pseudomonas fluorescens*, and to muscle tissue from two ecologically important fish species, *Oncorhynchus nerka* (salmon) and *Thunnus albacares* (tuna). These analyses revealed offsets of up to 4‰ in the cysteine and methionine $\delta^{34}S$ values that can probably be traced to metabolism. We expect that this new methodology will augment the growing stable isotope toolkit, with applications in biomedicine, ecology, agriculture, oceanography, biogeochemistry, and other diverse scientific fields.

2 I EXPERIMENTAL

2.1 I Method overview

Samples were freeze-dried then homogenized with a mortar and pestle prior to acid hydrolysis (Figure 2). An aliquot was taken for bulk $\delta^{34}S$ analysis via EA/IRMS. Filtered, hydrolyzed AAs were then heated in performic acid, where cysteine and methionine were quantitatively oxidized to cysteic acid and methionine sulfone. Reversed-phase preparatory HPLC/UV was used to separate and purify the two sulfur AAs. Aliquots were assayed for purity via a separate LC/MS analysis. Further aliquots of the purified AAs were analyzed via EA/IRMS to measure $\delta^{34}S$ values.

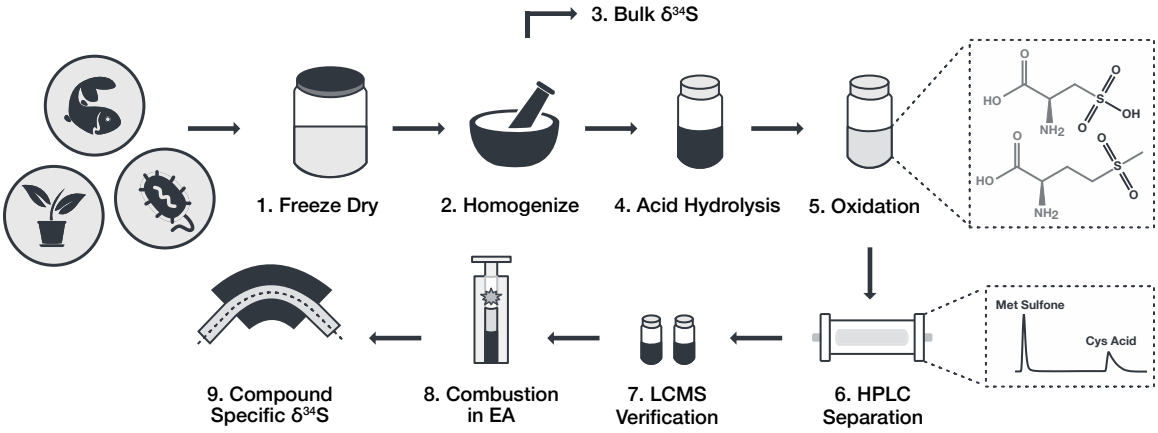

Figure 2 *A flowchart of the overall approach to sulfur isotope analysis of cysteine and methionine from biological samples*.

2.2 I Reagents

Standards of cysteine, methionine, cysteic acid, methionine sulfone, and bovine serum albumin (BSA) were purchased from Sigma Aldrich (St Louis, MO, USA; all >99% purity). All solvents used were ACS reagent grade, with the exception of ammonium hydroxide and ammonium acetate, which were HPLC grade. All water used was ultrapure (>18.2 MΩ). All glassware was combusted at 460 ˚C for 7 h to

remove organic carbon contamination. Vials and syringes were additionally washed with solvent before use (methanol, dichloromethane).

2.3 l Sample preparation

Fillets of wild-caught *O. nerka* (sockeye salmon) and *T. albacares* (yellowfin tuna) were purchased at a grocery store in Pasadena, CA, USA. Bacterial cultures (E. coli, P. fluorescens) were grown in our laboratory (details below). Biomass from all four was rinsed with water five times, then freeze-dried with a VirTis lyophilizer (SP Scientific, Stone Ridge, NY, USA) for 1–3 days until dry (Figure 2, Step 1). Samples were transferred to a solvent-washed ceramic mortar and pestle and ground under liquid N_2 until homogenized (Figure 2, Step 2). Homogenized samples were then transferred to glass jars and 3 × 1 mg aliquots were taken for bulk $\delta^{34}S$ analysis via EA/IRMS (Figure 2, Step 3).

2.4 l Acid hydrolysis

Each AA standard, BSA protein, and microbial biomass (30 mg), and 100 mg of fish tissue, were weighed directly into 60-mL vials. Then 10 mL of water was added and samples were sonicated for 15 min before the addition of 10 mL 12 N HCl. Vials were placed on a hot plate in the fume hood (100 ˚C, 24 h; Figure 2, Step 4). Following hydrolysis, samples were vacuum-filtered through baked Whatman GF/F glass fiber filters (0.7 µm equivalent pore size) and rinsed with water into new 60-mL vials. Filtered samples were dried to completion under a stream of N_2 in an acid-grade fume hood.

2.5 l Performic acid oxidation

Performic acid was prepared immediately prior to use by mixing hydrogen peroxide and formic acid in a 9:1 (v/v) ratio and incubating (30 min, 23 ˚C). Performic acid (5–10 mL) was added to dried samples, which were placed on a hot plate (70 ˚C,

60 min) in the fume hood, with occasional stirring throughout the reaction before quenching on ice (Figure 2, Step 5). Oxidized samples were dried under a stream of N_2. Samples were then resuspended via vortexing in 1.5 mL ultrapure water and filtered through a 13-mm 0.22-µm PVDF (polyvinylidene fluoride) syringe filter (Millex) into a 2-mL vial for HPLC separation.

2.6 I HPLC/UV separation

Methionine sulfone and cysteic acid were separated (Figure 2, Step 6) with a model 1100 HPLC/UV system (Agilent, Santa Clara, CA, USA) coupled to a FC203B fraction collector (Gilson, Middleton, WI, USA) adapted from a previously described method (Rampler et al., 2012). Briefly, samples (100 µL) were separated on a PRP-X100 strong anion- exchange column (250mm × 4.6 mm × 5 µm, 30 ˚C; Hamilton, Reno, NV, USA) with isocratic 50 mM ammonium acetate, buffered to pH 8 with 25% ammonia solution, at a flow rate of 1.0 mL/min. Hydrolyzed samples produced a high and continuous background UV absorption signal, obscuring the peaks for cysteic acid and methionine. Fraction collection of samples was therefore based solely on time windows derived from separate analyses of methionine sulfone and cysteic acid standards monitored at 254 nm.

2.7 I LC/MS verification

LC/MS analysis of all samples and standards was used to ensure that the collected analytes were pure. Fractions collected from HPLC/UV separation were derivatized with FDAA (1-fluoro-2-4-dinitrophenyl-5-L-alanine amide) and separated (Figure 2, Step 7) following a previously published procedure ((Hess et al., 2002). Briefly, 100 µL of aqueous sample was reacted with 10 µL of 6% triethylamine and 10 µL of 1% (w/v) FDAA in acetone at 50 ˚C for 60 min then quenched with 10 µL of 5% acetic acid. Aliquots (20 µL) were introduced into a 1100 Series LC/MSD system (Agilent) with a Zorbax 300SB-CS column (2.1 mm × 150mm × 5 µm; Agilent), housed in the Caltech Proteomics Laboratory, for a 45

min gradient between 5% acetic acid and acetonitrile at a flow rate of 0.25mL/min. Mass spectra were obtained in positive ion mode, scanning between *m/z* 300 and 450. The electrospray voltage was 4 kV at 350 ˚C. The diode-array detector measured the UV absorption at 340 nm.

2.8 I EA/IRMS measurements

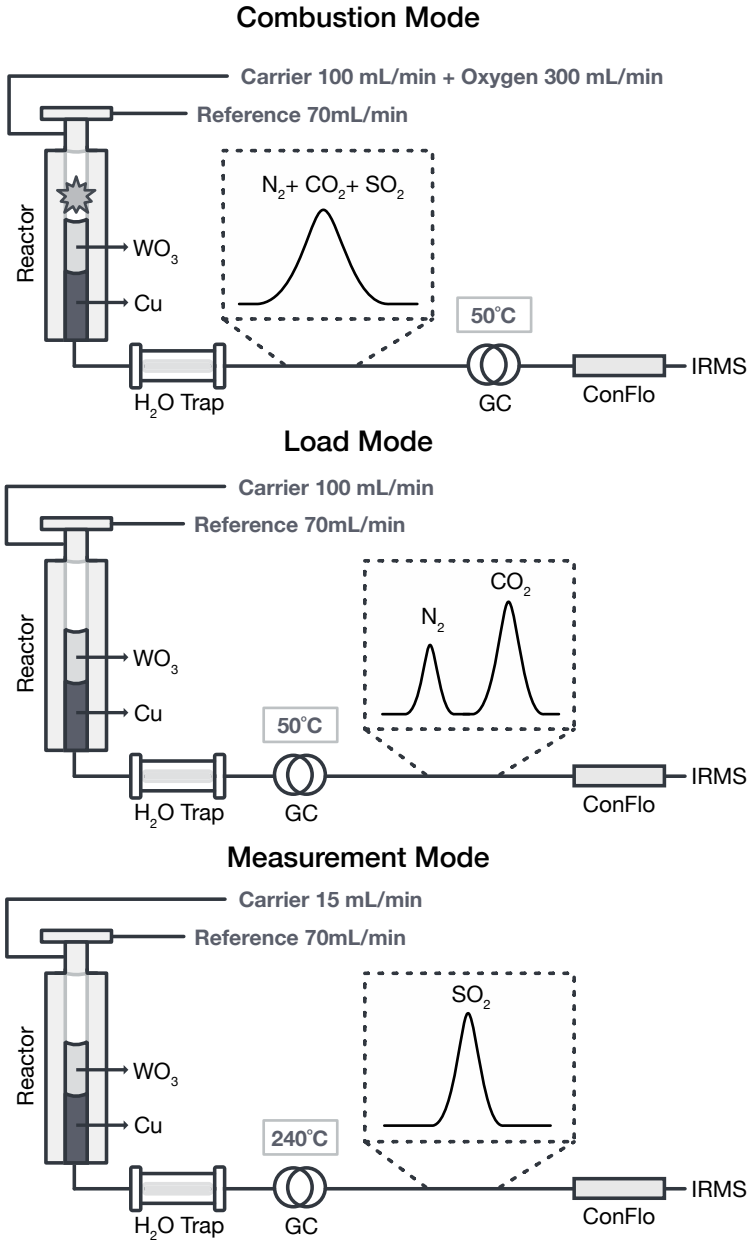

Figure 3 *Schematic illustration of sulfur isotope measurement using a Thermo Fisher™ Scientific Flash IsoLink™ CN elemental analyzer connected to an isotope ratio mass spectrometer. In load mode, SO_2 remains on the GC column, while N_2 and CO_2 elute. SO_2 is released in measurement mode, when the GC temperature ramps to 240 ˚C and carrier gas flow rate drops to 15 mL/min.*

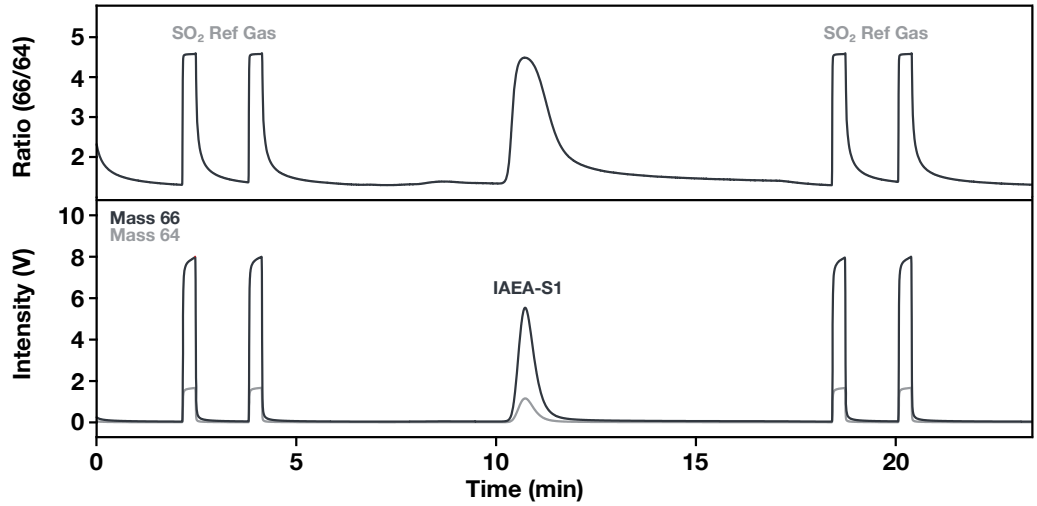

Figure 4 *Representative chromatogram for an EA/IRMS acquisition. Total run time is 24 min. Here, the sample is 37 µg of the silver sulfide standard IAEA-S1 (4.8 µg S). 1 V intensity for m/z 64 corresponds to a 3.3 nA ion current*.

Fractions collected from the HPLC/UV separation were transferred to tin capsules (OEA Labs, Exeter, UK; 9 mm × 5 mm, pressed, ultra- clean) and dried overnight in an oven at 50 ˚C. Samples were analyzed with an EA IsoLink™ combustion elemental analyzer system coupled to a Delta V Plus isotope ratio mass spectrometer (both from Thermo Scientific, Bremen, Germany) via a ConFlo IV Universal interface (Thermo Scientific, Figure 2, Step 8; Figure 3). The EA utilized a single-reactor configuration with a user-packed column comprising 3 cm of quartz wool, 14 cm wireform copper (5 mm size), 2 cm quartz wool, 6 cm granular tungsten(III) oxide, 1 cm quartz wool, and 0.5 cm additional tungsten(III) oxide. Sample combustion was accompanied by a pulse (4 s) of O_2 and carried in a high

(100 mL/min) He carrier gas flow rate. SO_2 is trapped on the GC column at 50 ˚C, helping to sharpen the SO_2 peak while allowing CO_2 and N_2 to elute. The He carrier flow rate is then reduced to 15 mL/min to improve the split ratios, and SO_2 is eluted as a sharp peak (<30 s full width at half maximum (FWHM)) by ramping the GC column temperature to 240 ˚C at 100 ˚C/s. A typical IRMS measurement (24 min) brackets the sample SO2 peak between four SO2 reference gas peaks, with no magnet jump (Figure 4).

2.9 l Data processing

The S contents (typically <0.25 μg S) and $\delta^{34}S$ values (typically 1–10‰) of empty tin capsules were measured by EA/IRMS and used to correct all subsequent analyses for the blank contribution (Hayes, 2004). Different batches of capsules varied in their S isotope composition by up to ~5‰ and therefore the same batch was used for all samples and standards within a day's run. In the current study this blank adjustment was minimal (<5%) as sample peaks were sufficiently large (~30 Vs, 5 µg S); however, for smaller sample sizes, the blank correction can become precision-limiting. A previous report concluded that oxygen isotope correction, i.e. for $^{32}S^{16}O^{18}O$, had a negligible effect on $\delta^{34}S$ values and therefore they performed no explicit $\delta^{18}O$ correction (Sayle et al., 2019). In our data processing, any ^{18}O effects are corrected for during calibration with external reference materials: δ34S values were measured relative to a lab SO_2 reference gas that was itself calibrated against IAEA reference materials S1, S2, and S3 using the same EA/IRMS system. IAEA-S1 and IAEA-S2 standards were also analyzed in triplicate at the beginning, middle, and end of daily sequences to further calibrate sample $\delta^{34}S$ values, which were reported as permil (‰) variations relative to the Vienna Canyon Diablo Troilite (VCDT) reference frame.

(Sayle et al., 2019)) observed large (0.6‰ per V) size-related errors for aliquots of bone collagen analyzed for $\delta^{34}S$ with the same model of EA/IRMS system. In our

tests with SO_2 reference gas, performed daily prior to analyses, linearity effects were consistently low (<0.1‰ per V). We observed no significant size-related effects for organic sulfur across a 3 V range of signal intensities, except at very low sample sizes where blank contributions exceed 15%. This ~6× lower linearity dependence was potentially due to the less complicated sample matrices of purified AAs versus bone collagen. Low concentrations of cysteine and methionine in tissues precluded triplicate analyses of our proof-of-concept samples. The uncertainties for these analyses are therefore conservatively reported as <0.3‰, representing the poorest 1σ precision encountered for any of the sulfur standard measurements, at the smallest concentration of 1 µg sulfur (see section 3.2 for further details).

2.10 l Culturing conditions

E. coli MG1655 and *P. fluorescens* WCS365 were grown in batch cultures on glucose in 1 L M9 minimal media that was modified to use ammonium sulfate as the sole sulfur source. The recipe was as follows: in 1 L add 7.52 g $Na_2HPO_4 \cdot 2H_2O$, 3.0 g KH_2PO_4, 0.5 g NaCl, 2.5 g $(NH_4)_2SO_4$, 1 mL 0.1 M $CaCl_2$, 1 mL 1.0 M $MgCl_2$, 4 g glucose, and 1mL 1000x vitamins mix (DSM141 recipe). Initial inoculation occurred in 10-mL culture tubes before transfer to a 1-L Erlenmeyer flask. Cultures were kept at 37 ˚C on an Excella E24 incubator (Shaker Series; New Brunswick Scientific, Edison, NJ, USA) and grown overnight at 250 rpm. Cell growth was monitored by measuring OD600 on a DU 800 UV/VIS spectrophotometer (Beckman Coulter, Brea, CA, USA). Cells were harvested in mid-log phase, at OD_{600} ~1, and washed twice with 0.9% NaCl at 4 ˚C. Pellets were stored at –20 ˚C until analysis.

2.11 l Proton NMR

^1H NMR scans were performed on an Avance III HD spectrometer (Bruker BioSpin, Rheinstetten, Germany) with a Prodigy broadband cryoprobe (at 400 MHz) at

Caltech. Approximately 1 mg of sample was dissolved in D_2O in a Wilmad (Buena, NJ, USA) thin-walled high- throughput NMR tube (Fisher Scientific, Hampton, NH, USA). One- dimensional (1D) experiments were conducted with 64 scans (~5 min acquisitions) to increase signal-to-noise (S/N) ratios.

3 I RESULTS AND DISCUSSION

3.1 I Method development

3.1.1 I Acid hydrolysis

In early versions of method development, we first attempted to recover intact cysteine and methionine following acid hydrolysis, but were unable to achieve quantitative yields. Reported loss mechanisms for cysteine and methionine in typical acid hydrolysis conditions (100–110 ˚C, 6 N HCl, 24 h) point to oxidation of the sulfur atom as the key process (Hunt, 1985), Figure 1). To minimize such reactions, we carried out hydrolysis in closed ampules flushed with argon gas. While this successfully prevented any significant oxidation of methionine, ^{1}H NMR revealed ~5–10% conversion of cysteine into cysteic acid that presumably occurred during sample transfers and transient exposure to atmospheric O_2 (Figure S1, supporting information). Isotope fractionation (change in $\delta^{34}S$ of ~1.6‰) of cysteine following anoxic hydrolysis was also observed, implying a kinetic isotope effect (KIE) for oxidation of roughly 15‰, assuming irreversible, closed-system behavior (Hayes, 2004). Previous reports of acid hydrolysis under anoxic conditions echo these results, with up to 25% loss of cysteine (Keutmann and Potts, 1969). Furthermore, although we did not observe methionine oxidation, others have noted significant conversion into methionine sulfoxide during sample storage and anoxic hydrolysis (Keutmann and Potts, 1969). Given these problematic yields and apparent isotopic fractionation, this strategy was abandoned in favor of quantitative oxidation of the AAs to more stable products prior to separation, as discussed next.

3.1.2 | Performic acid oxidation

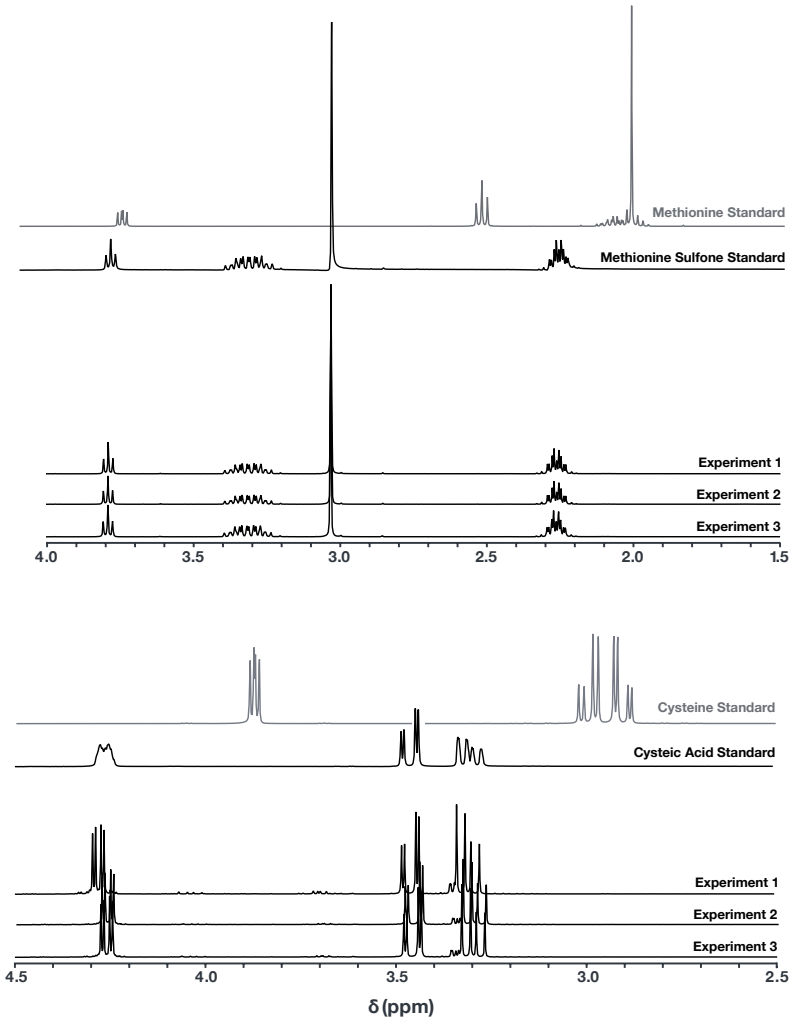

Figure 5 *^{1}H NMR spectra of the performic acid oxidation of cysteine to cysteic acid (top) and methionine to methionine sulfone (bottom). Experiments were conducted in triplicate (displayed here as stacked spectra). Reference spectra are seen above. In each case, NMR profiles were unambiguously assigned to the oxidized species, with no detectable cysteine, methionine, or methionine sulfoxide.*

Oxidation of the sulfur atoms in cysteine and methionine – whether intentional or accidental – is liable to be fractionating, a fact reinforced by our acid hydrolysis experiments with cysteine. In pursuing a strategy of intentional oxidation, it was

therefore critical to ensure quantitative conversion. Sodium azide (NaN_3) has been suggested as a useful reagent because it can be added directly to the hydrolysis mixture with little additional workup. However, yields of cysteic acid only reached 87%, which is insufficient to mitigate isotope fractionation (Manneberg et al., 1995). Success in rapid oxidation of disulfides with hydrogen peroxide catalyzed by methyl trioxorhenium (MTO; CH_3ReO_3) has been demonstrated previously (Wang and Espenson, 2000), but in our experiments methionine oxidation yields were incomplete and inconsistent, with a mixture of sulfoxide and sulfone products despite attempts to optimize reaction conditions (Figure S2). MTO did yield quantitative oxidation of cysteine to cysteic acid, however. Performic acid oxidation, which has previously been reported to give near-quantitative yields for both cysteine and methionine (Macdonald et al., 1985), proved to be the most suitable for our needs. Increasing the reaction time and temperature from the previously described 15 min incubation at 50 ˚C, to 60 min at 70 ˚C, resulted in quantitative yields within the limits of detection of ^1H NMR. Under these conditions, no cysteine, methionine, or methionine sulfoxide was detected in a triplicate experiment conducted on standards (Figure 5).

3.1.3 I Ion-exchange chromatography

Cation-exchange techniques are frequently employed in the isolation of AAs from environmental samples (Cheng, 1975; Amelung and Zhang, 2001; Takano et al., 2010) and could be beneficial to our application as a clean-up step. Unfortunately, the conventional strong cation-exchange resin, Dowex 50WX8, employs a sulfonic acid functional group. Previous studies have concluded that significant column bleed probably results in the largest contribution to analytical blanks for isotope analysis of AAs (Epstein et al., 1987). Given that no other commercial strong cation-exchange resins are available, we were forced to omit this typical step from our procedure, and instead limited clean-up to filtration through non-sulfur-containing materials such as glass fiber filters and PVDF syringe filters. This does

not present a significant limitation for analyses of pure biomass, as are presented here. However, for future work on more complex samples such as soils or sediments, this procedure should be revisited. In particular, sulfonic-acid stationary phase bleed may be resolved from the target analytes in the subsequent HPLC separation.

3.1.4 l HPLC separation

With cysteine and methionine in their native (unoxidized) form, we initially employed a reversed-phase Primesep A column (SIELC, Wheeling, IL, USA) to separate those analytes, following previously published methods specific to AA CSIA with hydrochloric acid substituted for sulfuric acid (McCullagh et al., 2008). However, after the decision to oxidize cysteine and methionine, two problems precluded further use of the Primesep A column. First, cysteic acid standards partially co-eluted with the void peak, despite method adjustments. Second, methionine sulfone standards co-eluted with cysteine, preventing the possibility of monitoring completion of the oxidation reaction via HPLC.

Cysteic acid and methionine sulfone were instead separated on a PRP-X100 anion-exchange column (Hamilton). Previous methods with this column used ICPMS for sulfur-specific detection (Rampler et al., 2012), but such instrumentation was not available for our application, and is more complicated than necessary. We instead adapted the published separation to our HPLC/UV–Vis system, minimizing eluent ammonium acetate concentration due to UV absorption: the published 10 min gradient method between 25 and 250 mM ammonium acetate became a 20 min 50 mM isocratic run (Figure 6). One drawback to this isocratic method was the significant peak tailing of cysteic acid. Despite adjustments to flow rate and eluent concentration, suboptimal peak shapes remained but – as the compounds of interest were well resolved – we did not revisit this potential optimization. Further

tests with cysteine, methionine, and sulfate confirmed that other sulfur-containing compounds did not co- elute with cysteic acid or methionine sulfone.

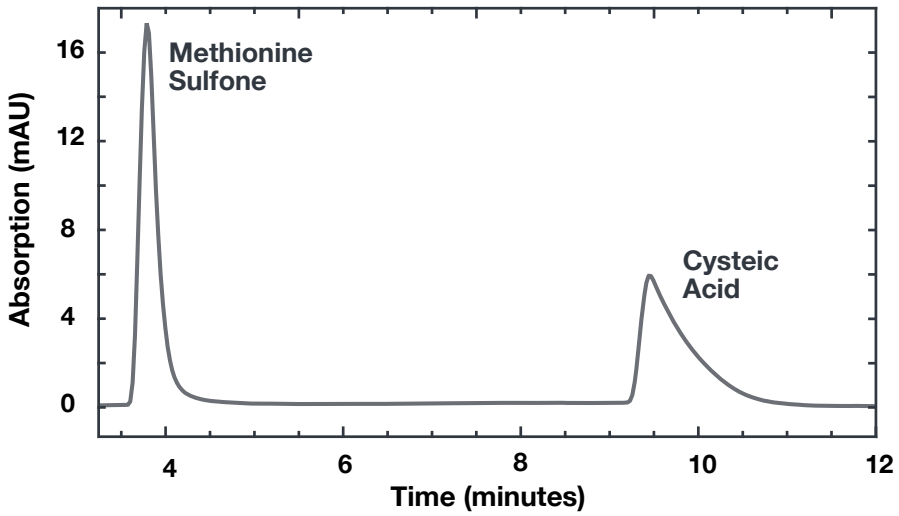

Figure 6 *HPLC/UV chromatogram showing separation of cysteic acid and methionine sulfone standards on the PRP-X100 column. The 20 min isocratic method uses 50 mM ammonium acetate buffered to pH 8 as the mobile phase, with UV absorption measured at 254 nm.*

3.1.5 l LC/MS verification

Due to the high absorption of protein components, the UV detector was saturated during sample runs and fractions were collected solely based on elution time. To verify that the correct analytes were collected, aliquots of each fraction were measured as their FDAA derivatives via electrospray ionization LC/MS. Selected-ion chromatograms were used to confirm the presence of derivatized cysteic acid (*m/z* 422) at 15.7 min or methionine sulfone (*m/z* 434) at 22.8 min (Figure 7). We used this procedure as a screening tool prior to EA/IRMS, only analyzing samples that had positive identification of the analyte and negative presence of the other AA residues. The procedure could also be used for quantification of the AAs, for example by using a heavy isotope labeled internal standard for calibration (Hess

et al., 2002). FDAA has also been successfully used to determine the stereochemistry of AAs, even at trace concentrations (50 pmol; (Kochhar and Christen, 1989; Fujii et al., 1997).

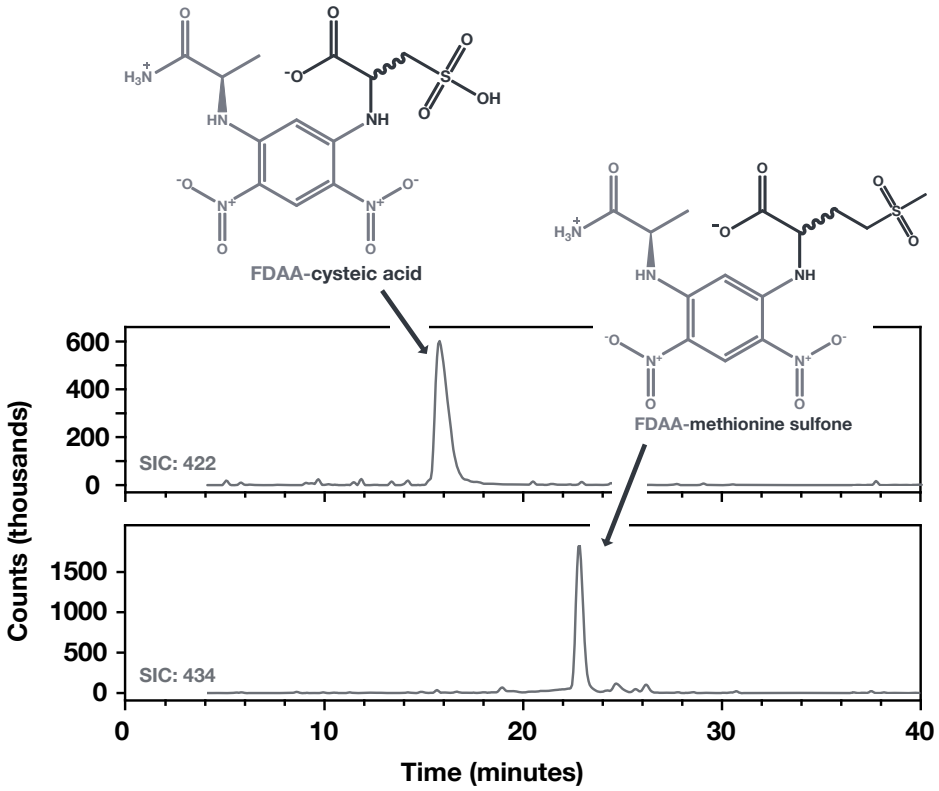

Figure 7 *LC/MS selected-ion chromatograms of cysteic acid (top) and methionine sulfone (bottom) from collected fractions of the HPLC separation. Aliquots were derivatized with FDAA (1-fluoro-2-4-dinitrophenyl-5-L-alanine amide). Derivatized cysteic acid and methionine sulfone were identified via selected ion chromatograms at m/z 422 and 434, respectively*.

3.1.6 l Sulfur isotopic analysis by EA/IRMS

We made several attempts to measure cysteine and methionine $\delta^{34}S$ values by MC/ICPMS, as this approach would offer better sensitivity and higher precision than EA/IRMS, and concurrent measurement of $\delta^{33}S$ values. Given that matrix-matching of samples and standards is an important component of this analytical

method, and that matrix effects have only been characterized for sulfate, we attempted to oxidize the sulfur AAs to sulfate using hydrogen peroxide and UV light (Huston and Pignatello, 1999; Raven et al., 2016). However, sulfate yields were low and variable when tested for cysteine (43.5 ± 10.1%, n = 6) and methionine (21.5 ± 3.5%, n = 2). Direct injection of sulfur AAs into the ICPMS system is theoretically possible but would require significant effort to matrix-match standards and was not pursued. Use of GC/MC/ICPMS was precluded by the lack of a suitable derivatization strategy for cysteic acid (White, 1981), probably related to its negligible solubility in organic solvents. Indeed, our numerous attempts with various methylating and silylating agents produced no successful derivatives.

Ultimately, we decided to measure the sulfur AAs by EA/IRMS, taking advantage of a new instrument with improved sensitivity. Two key improvements of this system were (i) a temperature-ramped GC oven and (ii) computer-controlled He flow rates (Figure 3). These modifications allowed SO_2 from combustion to have sharpened peak shapes and improved split ratios, as follows: during combustion mode, samples are burned (>1020 ˚C) with a pulse (4 s) of O2 carried by a high He carrier gas flow rate of 100 mL/min. The combustion reactor contains tungsten(III) oxide acting as oxidant and catalyst, and metallic copper which reduces combustion gases to NO_x, SO_2, CO_2, and H_2O. A water trap removes H_2O to prevent formation of sulfuric acid. The copper scrubs extra oxygen from combustion and reduces NO_x species to N_2, and SO_3 to SO_2. In sulfur load mode, with the GC oven at 50 ˚C, N_2 and CO_2 are eluted (and can be measured) while SO_2 is trapped in a narrow band on the column. Next, in sulfur measurement mode, the carrier gas flow rate is lowered to 15 mL/min to improve split ratios, while the GC temperature ramps to 240 ˚C releasing SO_2 as a sharp peak (<30 s FWHM), boosting S/N ratios. This flow rate of 15 mL/min represented the optimum choice for peak shape and sensitivity. Lower flow rates would improve split ratios further, but at the expense of increased peak width and lower S/N ratios. Other explored parameters included timing of the GC heating cycle and sample combustion.

The factory default configuration for combined $\delta^{15}N$, $\delta^{13}C$, and $\delta^{34}S$ measurements by EA/IRMS includes a second reducing reactor, filled with copper shavings, to ensure complete reduction of NO_x species into N_2. In practice, the presence of this additional reactor broadened SO_2 peaks significantly, and we therefore opted for the single-reactor configuration. A previous characterization of this EA/IRMS system measured concurrent $\delta^{15}N$, $\delta^{13}C$, and $\delta^{34}S$ values of bone collagen also using a single reactor (Sayle et al., 2019). Without additional copper in the second reactor, however, there is potential for incomplete NO_x conversion into N_2, which was not explicitly tested for in their study. Although it is appealing to simultaneously measure all three isotope systems, to save time and expenses, we obtained the best precision for $\delta^{34}S$ values when only sulfur was analyzed. As our method focused on sulfur, we did not revisit combined analyses.

3.2 | Method Verification

3.2.1 | Sensitivity and precision of isotopic analyses

To characterize the sensitivity and precision of our improved EA/IRMS methodology, we measured in triplicate two inorganic and two organic sulfur standards (1–10 µg sulfur per aliquot): the silver sulfide standard IAEA-S1, seawater sulfate, cysteic acid, and methionine sulfone (Figure 8). Weighing standards at such low levels is challenging, so all but IAEA-S1 were dispensed volumetrically in aqueous solution, then dried in air at 50 ˚C. The replicate precision (1 s.d.) for $\delta^{34}S$ values was <0.20‰ for virtually all standards across this concentration range, rising to 0.30‰ only for the lowest level (1 µg S) of methionine sulfone. This result represents a decrease in sample size over a previous report focused on bone collagen, which reported analyses requiring 2–3 µg S, while at the same time improving on their average standard deviation of 0.3‰ (Sayle et al., 2019). We believe that sensitivity and precision improvements are largely attributable to our advantages in running purified samples rather than

archeological material and analyzing only sulfur rather than carbon and nitrogen simultaneously.

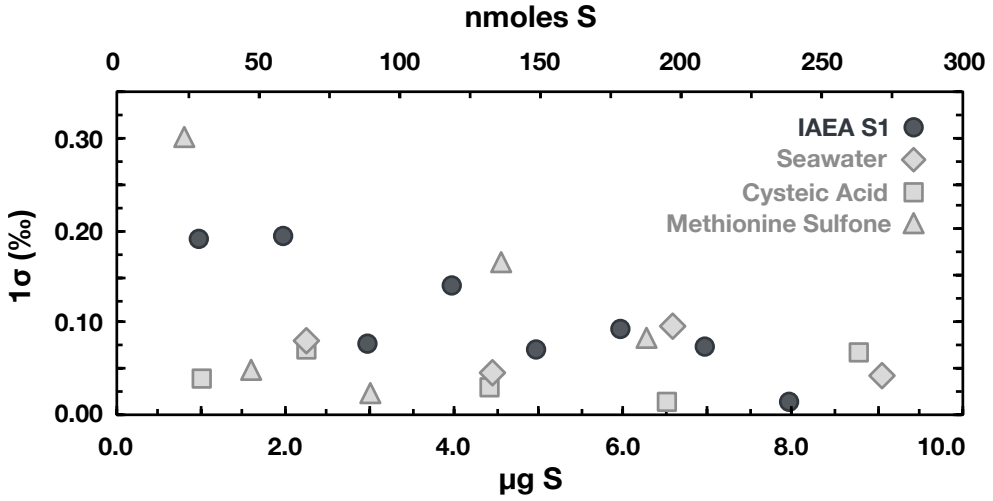

Figure 8 *Precision (1 s.d.) of triplicate analyses of δ34S for pure standards of cysteic acid, methionine sulfone, silver sulfide (IAEA-S1), and seawater sulfate analyzed by EA/IRMS. Sulfur in seawater is present almost entirely as dissolved sulfate.*

3.2.1 I $\delta^{34}S$ accuracy

Pure standards of cysteine and methionine were subjected to the entire amino acid separation procedure, with $\delta^{34}S$ measurements before and after, to examine the possibility of artifacts leading to sulfur isotope fractionations (Table 2). The initial $\delta^{34}S$ value of cysteine was 5.8 ± 0.3‰ and after acid hydrolysis, oxidation, and HPLC-UV separation, the value for the resultant cysteic acid was within uncertainty, 5.6 ± 0.3‰. Similarly, methionine had an initial $\delta^{34}S$ value of 7.4 ± 0.3‰ and a final methionine sulfone $\delta^{34}S$ value of 7.6 ± 0.3‰. Further verification using a pure protein, bovine serum albumin (BSA), largely confirmed these results but with a slight offset (0.4‰) between the reactant BSA protein and the product AAs that falls within the 2σ limit (0.6‰) of analytical uncertainty (Table 2). Whether this offset represents random error, slight fractionation, or contamination of the

parent BSA material (with, for example, trace amounts of sulfate) is unclear; regardless, any fractionation induced is very small relative to the ~50‰ range of $\delta^{34}S$ values encountered in nature (Canfield, 2001; Habicht and Canfield, 2001).

Table 2 *$\delta^{34}S$ values of amino acid and protein standards measured before and after sample workup.*

Sample	Before (± 0.3‰)	After (± 0.3‰)
Cysteine	5.8	5.6
Methionine	7.4	7.6
Bovine serum albumin	1.5	Cysteic acid: 1.9 Methionine sulfone: 1.9

3.3 | Pilot samples

Biomass samples from the bacteria *E. coli* and *P. fluorescens*, and muscle tissue from the fish *O. nerka* and *T. albacares*, were analyzed for their compound-specific cysteine and methionine sulfur isotope ratios using the newly developed methodology (Figure 9).

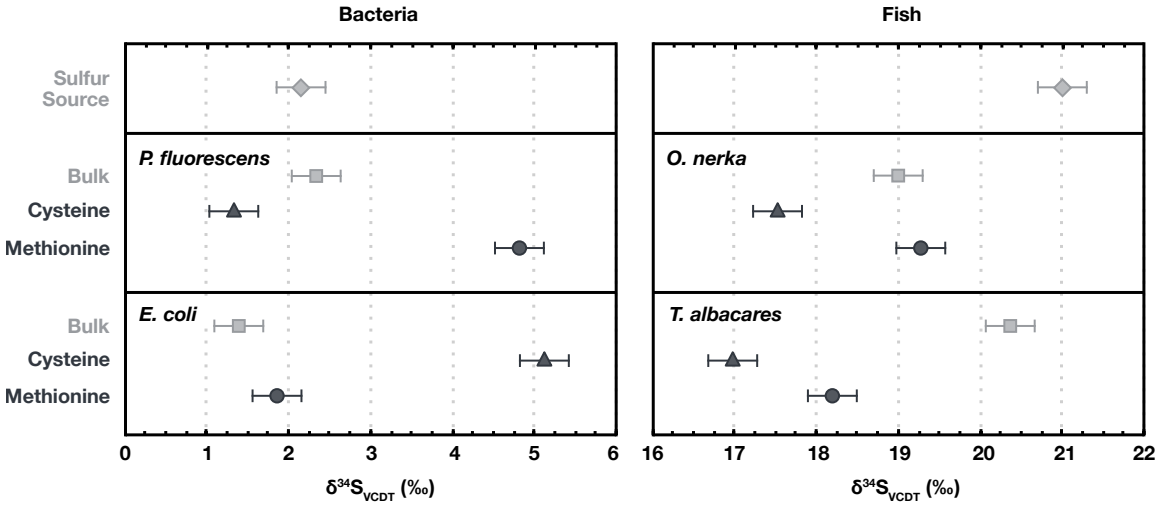

Figure 9 *$\delta^{34}S$ values of cysteine (measured as cysteic acid), methionine (measured as methionine sulfone), bulk bacterial/fish muscle biomass, and sulfur source for bacteria and fish. For bacteria, the sulfur source was ammonium sulfate added to the culture medium, which was measured directly by EA/IRMS. The indirect sulfur source for fish was inferred to be marine sulfate ($\delta^{34}S$ = 21‰) for both species*.

3.3.1 l Bulk tissue isotopic compositions

P. fluorescens biomass δ34S (2.3‰) was within error of its sulfur source, NH4SO4, which was added to the culture medium (2.1‰), while E. coli biomass was slightly ^{34}S-depleted (1.4‰). These minimal fractionations are consistent with previous reports that suggest offsets ranging from +0.5 to –4.4‰ between biomass and supplied sulfate for aquatic plants due to assimilatory sulfate reduction (Kaplan et al., 1963; Mekhtieva and Pankina, 1968). More recent studies measuring the $\delta^{34}S$ values of DMSP in phytoplankton and macroalgae suggest a smaller offset between sulfate and metabolites, between –1.4 and –2.8‰ (Oduro et al., 2012). Our results, and future measurements of cysteine and methionine $\delta^{34}S$, add to these limited examples, expanding our understanding of the isotopic consequences of the understudied assimilatory pathway.

The $\delta^{13}C$ and $\delta^{15}N$ values of fish biomass are often related to food-chain position, with trophic effects expressed in consumers such as *O. nerka* and *T. albacares*. However, previous studies of trout suggest that $\delta^{34}S$ values do not track trophic levels, instead preserving the isotopic composition of local sulfate to within ~2‰ (Peterson et al., 1985; Peterson and Fry, 1987; Richards et al., 2001). Indeed, observed values for both O. nerka (19‰) and *T. albacares* (20‰) reflect those for marine sulfate (21‰; Paris et al., 2013).

3.3.2 l Cysteine and methionine isotopic compositions

Compound-specific AA measurements were significantly more variable than the bulk biomass or muscle tissue measurements. For *E. coli*, the cysteine $\delta^{34}S$ value was 5.1‰ while the methionine value was 1.9‰. *P. fluorescens* exhibited the opposite pattern, with methionine ^{34}S-enriched with a $\delta^{34}S$ value at 4.8‰ relative to cysteine at 1.3‰. *O. nerka* and *T. albacares* had smaller differences between cysteine and methionine, although methionine was ^{34}S-enriched relative to cysteine in both species: the $\delta^{34}S$ values of *O. nerka* cysteine and methionine were 17.5‰ and 19.3‰, respectively, while in *T. albacares* cysteine was 17.0‰ and methionine was 18.2‰. Furthermore, although cysteine and methionine account for a large portion of cellular sulfur, the average isotope ratios of the two AAs (cysteine, methionine) do not necessarily reflect bulk tissue values: for example, in T. albacares, both cysteine and methionine are ^{34}S-depleted compared with muscle tissue. As our analytical method minimally or negligibly fractionates, these results imply the presence of other components of cellular sulfur with divergent $\delta^{34}S$ values, such as taurine, glutathione, sulfate esters, or inorganic sulfate stored in cells.

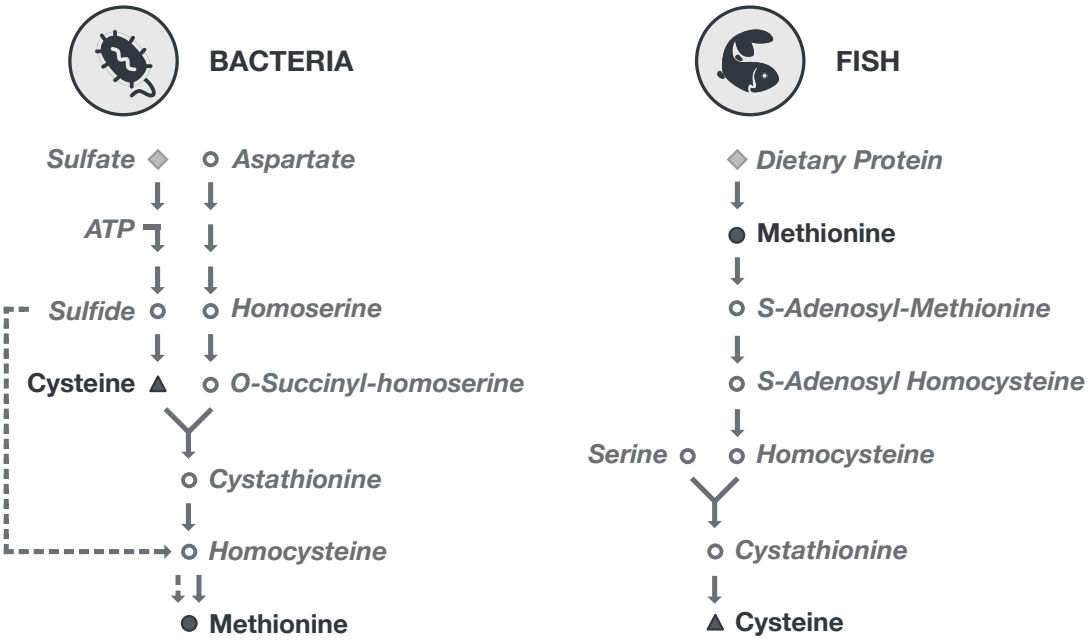

Figure 10 *Known sulfur assimilation pathways in bacteria and fish. Note that the fish metabolism shown is from the closest living organism for which the pathway is well studied, Danio rerio (zebrafish). Solid arrows in the bacterial pathway are taken from the E. coli MetaCyc database and show the ubiquitous methionine synthesis pathway via transsulfuration. The dashed arrow represents an alternative route via sulfhydrylation where methionine is synthesized directly from sulfide via homocysteine. Sulfhydrylation is not present in E. coli but has been found in diverse bacteria including P. putida and B. subtilis.*

Heterogeneity in the cysteine and methionine $\delta^{34}S$ values implies further metabolic fractionations beyond the exogenous sulfur source (Figure 10). In fish, methionine is an essential amino acid that cannot be synthesized directly and must be acquired through dietary sources ((Wu et al., 2017), which are only minimally fractionating. Cysteine is produced from this methionine pool, through the intermediates cystathionine and homocysteine (Howe et al., 2013). Given that methionine is not entirely converted into cysteine, this synthesis represents a branch point in metabolism that could express intrinsic isotope effects. We predict that a normal kinetic isotope effect (KIE) accompanies these reactions at the sulfur atom, which should leave the reactant, methionine, enriched relative to the product, cysteine, potentially explaining the patterns of enrichment which we observed in *O. nerka* and *T. albacares*. While this reaction has not explicitly been studied for the existence of isotope effects, early experiments using Raman spectroscopy suggest a 4–12‰ fractionation accompanying the nucleophilic addition of $R\text{-}S^-$ groups (Kwart and Stanulonis, 1976; Tcherkez and Tea, 2013) compatible with the observed offsets.

Unlike fish, E. coli, P. fluorescens, and most bacteria can synthesize de novo all 20 proteinogenic AAs, including cysteine and methionine (Price et al., 2018). However, bacterial sulfur AA synthesis is inherently more diverse, involving multiple potential pathways with distinct enzymes. In *E. coli*, cysteine biosynthesis

proceeds by combining an activated homoserine intermediate with sulfide, the product of assimilatory sulfate reduction (Caspi et al., 2018). Cysteine is then used as a substrate for methionine synthesis, through the trans-sulfuration pathway catalyzed by cystathionine γ-synthase and cystathionine β-lyase (Hwang et al., 2002); Figure 10, solid arrows). Alternatively, other bacteria, including multiple species of *Pseudomonas*, employ the sulfhydrylation pathway, which utilizes inorganic sulfide directly as the sulfur donor and the enzyme acylhomoserine sulfhydrylase (Hwang et al., 2002; Figure 10, dashed arrows). These different sulfur metabolisms offer a potential explanation for the contrasting patterns of *E. coli* and *P. fluorescens* cysteine and methionine $\delta^{34}S$ values. More specifically, the pattern of ^{34}S-enriched cysteine relative to methionine in *E. coli* can be understood as a result of the normal ^{34}S kinetic isotope effect of the trans-sulfuration pathway. Indeed, protein sulfur isotope studies and numerical models of higher plant biosynthesis, which uses similar trans-sulfuration pathways, suggest that methionine is naturally ^{34}S depleted relative to cysteine (Tcherkez and Tea, 2013), as we observed in *E. coli*. In contrast, *P. fluorescens* must be enriching methionine in ^{34}S relative to cysteine. This is possibly occurring through the sulfhydrylation pathway, although details require further study. A third methionine synthesis pathway was recently discovered in freshwater and soil bacteria, although it is unlikely that this nitrogenase-like enzyme is relevant here, as it is used only in sulfate-limiting conditions (North et al., 2020).

4.0 I CONCLUSIONS

We have developed a novel approach to determining the natural- abundance $\delta^{34}S$ values of cysteine and methionine from biological samples. Acid hydrolysis, followed by quantitative oxidation of the sulfur amino acids to their sulfone and sulfonic acid products with performic acid, results in air-stable analytes that can be further handled and purified. Separation was achieved via rapid (20 min) isocratic elution on a PRP-X100 column and fraction purity was verified using derivatization

with FDAA and characterization on an LC/MS system. Modifications to the operation of a Thermo Flash EA/IRMS system yielded substantially increased sensitivity (1–10 µg sulfur) while maintaining precision (<0.3‰), enabling separation of measurable aliquots via HPLC separation. Comparison of standard amino acids and the BSA protein before and after sample processing indicates no significant methodological sulfur isotope fractionation. Proof-of-principle analyses of muscle tissue from two fish (*O. nerka* and *T. albacares*) found ^{34}S-enrichment of methionine by ~1–2‰ relative to cysteine, in rough agreement with known metabolic KIEs. We found the opposite pattern in E. coli, with ~3‰ cysteine ^{34}S-enrichment relative to methionine, probably due to fractionations in the trans-sulfuration synthesis pathway. The isotope patterns of *P. fluorescens* remained enigmatic, with methionine ~4‰ 34S-enriched relative to cysteine, a potential signature of the alternative synthesis via sulfhydrylation. Such heterogeneity in cysteine and methionine δ^{34}S values across diverse organisms holds much potential for further understanding of sulfur metabolism.

ACKNOWLEDGEMENTS

The authors would like to thank the technicians and directors of the Proteomics Exploration Lab at Caltech: Sonja Hess and Anne Radimin for assistance with LC/MS operation and FDAA derivatization. This project benefited from the use of instrumentation made available by the Caltech Environmental Analysis Center and the authors acknowledge its director Nathan Dalleska for assistance with the HPLC/UV system. Caltech professors Victoria Orphan and Jess Adkins volunteered lab space for this project and the authors thank them and their lab technicians Stephanie Connon, Jared Markse, Grecia Lopez, and Guillaume Paris. Thanks are also extended to high school interns Zekaria Beshir, Brenna Bowlen, and Hannah Betts for their valuable assistance on the project and Reto Wijker for providing cultures, media recipes, and assistance with microbial culturing. The following colleagues are thanked for their valuable insight and review of early

manuscripts: Ted Present, Preston Kemeny, Eryn Eitel, Hannah Dion-Kirschner, Frank Pavia, and Makayla Betts. Thanks are also due to Guillaume Tcherkez for procedures and advice on oxidation via MTO as well as Emilia Hernandez and Tony Wang for assistance testing oxidation of organics to sulfate. Tony Wang is also acknowledged for his help with optimizing initial EA/IRMS parameters. Two anonymous reviewers are thanked for feedback during peer-review. Funding for this project was provided by the NSF (Grant 1436566) and NASA Astrobiology Institute (Grant No. 80NSSC18M094).

SUPPLEMENTAL INFORMATION

Table S1 *Common protection strategies for cysteine and methionine.*

Strategy	Additive	Product	Yield	Pros	Cons	References
Oxidation	Performic acid	Cysteic acid	95%	Reliable, quantitative, products are stable during hydrolysis	Tyrosine, tryptophan, and histidine yields altered, adds steps	Macdonald et al., 1985
		Methionine sulfone	100%			
	Sodium azide	Cysteic acid	87%	No effect on tyrosine, can be added directly to acid hydrolysis	Partially oxidizes methionine, concentrated acidic azides are explosive	Manneberg et al., 1995
Reduction	Dithiothreitol and sodium tetrathionate	S-sulfo-cysteine	98%	Other amino acids are unaffected except tyrosine	Methionine oxidation yield was not explicitly tested	Inglis and Liu, 1970
	β-mercaptoethanol	Methionine	98%	Improves serine and tyrosine yield, added directly to hydrolysis	Cysteine was not tested, recoveries only reported for alkylated cysteine	Keutmann and Potts, 1969
		S-carboxyl-methylcysteine	89%			
	Thioglycolic acid	Methionine	100%	Requires short 30 min vapor hydrolysis, good tyrosine yields	Added step to procedures, serine loss, cysteine yield not reported	Inglis and Liu, 1970
Alkylation	Iodoacetic acid or iodoacetamide	S-carboxyl-methylcysteine	98%	Quantitative cysteine conversion in a 40 min reaction	Carboxy-methyl groups are unstable during hydrolysis	Yano et al., 1990
	N-ethyl-maleimide	S-succinyl-cysteine	88%	Membrane permeable, can be purchased with radioactive labels	Unstable above pH 7, can react with histidine and other amine groups	Smyth et al., 1963; Guidotti and Konigsberg, 1964
	4-vinylpyridine	S-4-pyridyl-ethylcysteine	94%	Product is stable during hydrolysis, reagent does not react with other amino acids	Requires reduction of cystine to cysteine with *β*-mercaptoethanol, adds multiple steps	Grant, 2017

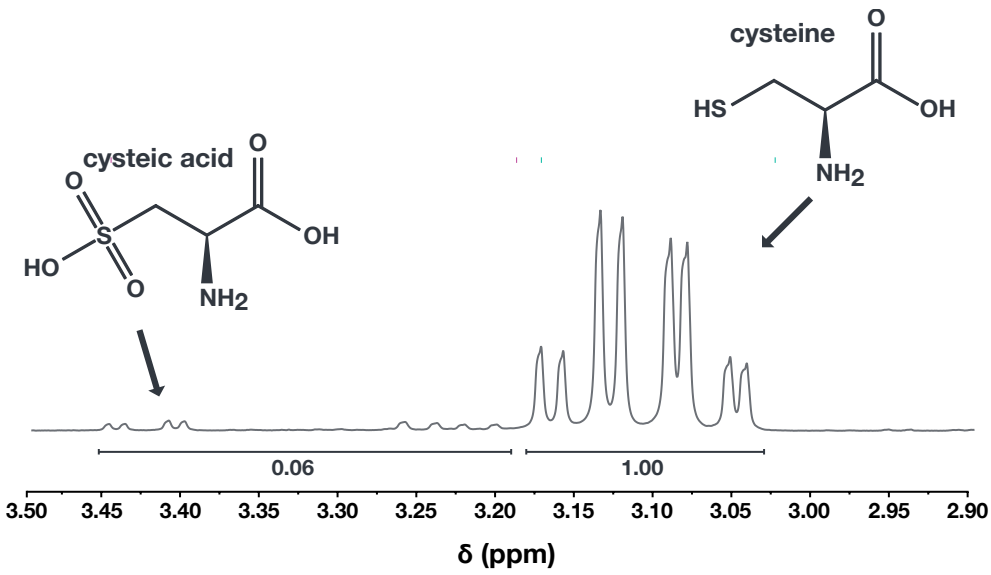

Figure S1 *[1]H NMR spectrum of cysteine standard following hydrolysis in a sealed ampule with Ar-flushed headspace. Peak area quantitation indicates between 5-10% oxidative conversion of cysteine to cysteic acid across replicates.*

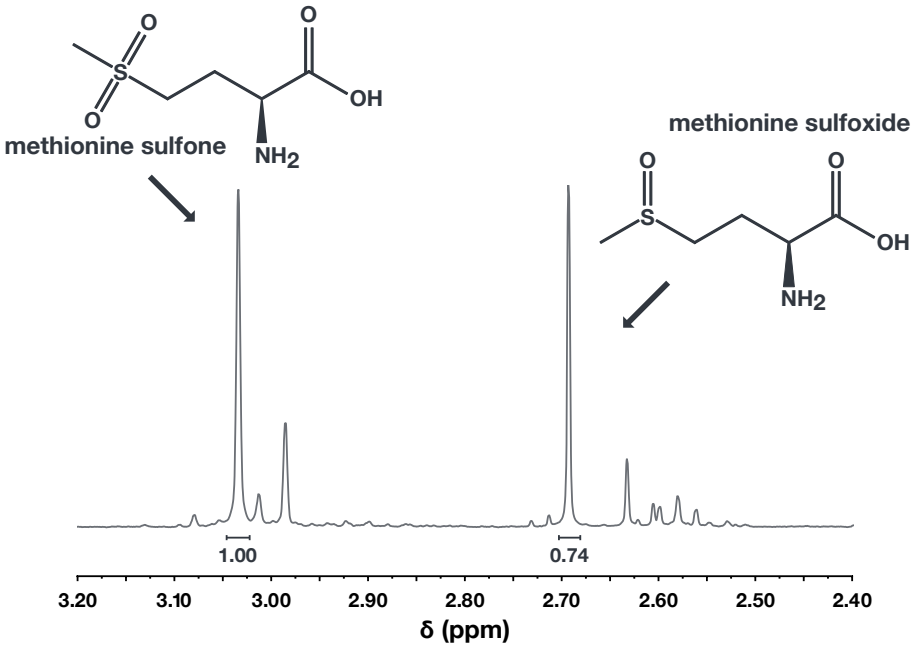

Figure S2 *[1]H NMR spectrum of methionine standard following oxidation in hydrogen peroxide and MTO. Methionine's singlet occurs further upfield at 2.0 ppm, but it was not detected in any experiments with these reagents.*

BIBLIOGRAPHY

Abadie, C., Tcherkez, G., 2019. Plant sulphur metabolism is stimulated by photorespiration. Communications Biology 2, 1–7.

Albalat, E., Telouk, P., Balter, V., Fujii, T., Bondanese, V.P., Plissonnier, M.-L., Vlaeminck-Guillem, V., Baccheta, J., Thiam, N., Miossec, P., Zoulim, F., Puisieux, A., Albarède, F., 2016. Sulfur isotope analysis by MC-ICP-MS and application to small medical samples. Journal of Analytical Atomic Spectrometry 31, 1002–1011.

Albert, C., Lóki, K., Pohn, G., Varga-Visi, É., Csapó, J., 2008. Investigation of performic acid oxidation in case of thiol-containing amino acid enantiomers. undefined 1, 73–80.

Amelung, W., Zhang, X., 2001. Determination of amino acid enantiomers in soils. Soil Biology and Biochemistry 33, 553–562.

Amrani, A., Sessions, A.L., Adkins, J.F., 2009. Compound-Specific δ34S Analysis of Volatile Organics by Coupled GC/Multicollector-ICPMS. Analytical Chemistry 81, 9027–9034.

Au Yang, D., Landais, G., Assayag, N., Widory, D., Cartigny, P., 2016. Improved analysis of micro- and nanomole-scale sulfur multi-isotope compositions by gas source isotope ratio mass spectrometry. Rapid communications in mass spectrometry: RCM 30, 897–907.

Brunold, C., Erismann, K.H., 1975. H2S as sulfur source in Lemna minor L.: II. Direct incorporation into cysteine and inhibition of sulfate assimilation. Experientia 31, 508–510.

Canfield, D.E., 2001. Biogeochemistry of Sulfur Isotopes. Reviews in Mineralogy and Geochemistry 43, 607–636.

Caspi, R., Billington, R., Fulcher, C.A., Keseler, I.M., Kothari, A., Krummenacker, M., Latendresse, M., Midford, P.E., Ong, Q., Ong, W.K., Paley, S., Subhraveti, P., Karp, P.D., 2018. The MetaCyc database of metabolic pathways and enzymes. Nucleic Acids Research 46, D633–D639.

Cheng, C.N., 1975. Extracting and desalting amino acids from soils and sediments: Evaluation of methods. Soil Biology and Biochemistry 7, 319–322.

Craddock, P.R., Rouxel, O.J., Ball, L.A., Bach, W., 2008. Sulfur isotope measurement of sulfate and sulfide by high-resolution MC-ICP-MS. Chemical Geology 253, 102–113.

Epstein, S., Krishnamurthy, R.V., Cronin, J.R., Pizzarello, S., Yuen, G.U., 1987. Unusual stable isotope ratios in amino acid and carboxylic acid extracts from the Murchison meteorite. Nature 326, 477–479.

Fourel, F., Lécuyer, C., Balter, V., 2015. New Frontiers for Sulfur Isotopic Analyses. Procedia Earth and Planetary Science, 11th Applied Isotope Geochemistery Conference AIG-11 13, 232–239.

Fourel, F., Martineau, F., Seris, M., Lécuyer, C., 2014. Simultaneous N, C, S stable isotope analyses using a new purge and trap elemental analyzer and an isotope ratio mass spectrometer. Rapid Commun. Mass Spectrom. 8.

Friedman, M., Krull, L.H., Cavins, J.F., 1970. The Chromatographic Determination of Cystine and Cysteine Residues in Proteins as S-β-(4-Pyridylethyl)cysteine. Journal of Biological Chemistry 245, 3868–3871.

Fry, B., 2007. Coupled N, C and S stable isotope measurements using a dual-column gas chromatography system. Rapid Communications in Mass Spectrometry 21, 750–756.

Fujii, K., Ikai, Y., Mayumi, T., Oka, H., Suzuki, M., Harada, K., 1997. A Nonempirical Method Using LC/MS for Determination of the Absolute Configuration of Constituent Amino Acids in a Peptide: Elucidation of Limitations of Marfey's Method and of Its Separation Mechanism. Analytical Chemistry 69, 3346–3352.

Giesemann, A., Jaeger, H.-J., Norman, A.L., Krouse, H.R., Brand, W.A., 1994. Online Sulfur-Isotope Determination Using an Elemental Analyzer Coupled to a Mass Spectrometer. Analytical Chemistry 66, 2816–2819.

Grant, G.A., 2017. Modification of Cysteine. Current Protocols in Protein Science 87, 15.1.1-15.1.23.

Guidotti, G., Konigsberg, W., 1964. The Characterization of Modified Human Hemoglobin I: Reaction with iodoacetamide and n-ethylmaleimide. Journal of Biological Chemistry 239, 1474–1484.

Habicht, K.S., Canfield, D.E., 2001. Isotope fractionation by sulfate-reducing natural populations and the isotopic composition of sulfide in marine sediments. Geology 29, 555–558.

Hayes, J.M., 2004. An Introduction to Isotopic Calculations 1–10.

Hess, S., van Beek, J., Pannell, L.K., 2002. Acid hydrolysis of silk fibroins and determination of the enrichment of isotopically labeled amino acids using precolumn derivatization and high-performance liquid chromatography–electrospray ionization–mass spectrometry. Analytical Biochemistry 311, 19–26.

Howe, K., Clark, M.D., Torroja, C.F., et al., 2013. The zebrafish reference genome sequence and its relationship to the human genome. Nature 496, 498–503.

Hulston, J.R., Thode, H.G., 1965. Variations in the S33, S34, and S36 contents of meteorites and their relation to chemical and nuclear effects. Journal of Geophysical Research (1896-1977) 70, 3475–3484.

Hunt, S., 1985. Degradation of Amino Acids Accompanying in vitro Protein Hydrolysis, in: Barrett, G.C. (Ed.), Chemistry and Biochemistry of the Amino Acids. Springer Netherlands, Dordrecht, pp. 376–398.

Huston, P.L., Pignatello, J.J., 1999. Degradation of selected pesticide active ingredients and commercial formulations in water by the photo-assisted Fenton reaction. Water Research 33, 1238–1246.

Hwang, B.-J., Yeom, H.-J., Kim, Y., Lee, H.-S., 2002. Corynebacterium glutamicum utilizes both transsulfuration and direct sulfhydrylation pathways for methionine biosynthesis. Journal of Bacteriology 184, 1277–1286.

Inglis, A.S., Liu, T.-Y., 1970. The Stability of Cysteine and Cystine during Acid Hydrolysis of Proteins and Peptides 245, 6.

Kaplan, I.R., Emery, K.O., Rittenberg, S.C., 1963. The distribution and isotopic abundance of sulphur in recent marine sediments off southern California. Geochimica et Cosmochimica Acta 27, 297–331.

Keutmann, H.T., Potts, J.T., 1969. Improved recovery of methionine after acid hydrolysis using mercaptoethanol. Analytical Biochemistry 29, 175–185.

Kochhar, S., Christen, P., 1989. Amino acid analysis by high-performance liquid chromatography after derivatization with 1-fluoro-2,4-dinitrophenyl-5-L-alanine amide. Analytical Biochemistry 178, 17–21.

Kwart, H., Stanulonis, J., 1976. Assessment of the thioallylic rearrangement by a simplified technique for high-precision measurement of isotope effects. Journal of the American Chemical Society 98, 4009–4010.

Macdonald, J.L., Krueger, M.W., Keller, J.H., 1985. Oxidation and Hydrolysis Determination of Sulfur Amino Acids in Food and Feed Ingredients: Collaborative Study. Journal of Association of Official Analytical Chemists 68, 826–829.

Manneberg, M., Lahm, H.-W., Fountoulakis, M., 1995. Quantification of Cysteine Residues Following Oxidation to Cysteic Acid in the Presence of Sodium Azide. Analytical Biochemistry 231, 349–353.

Mayer, B., Krouse, H.R., 2004. Chapter 26 - Procedures for Sulfur Isotope Abundance Studies, in: de Groot, P.A. (Ed.), Handbook of Stable Isotope Analytical Techniques. Elsevier, Amsterdam, pp. 538–596.

McCullagh, J., Gaye-Siessegger, J., Focken, U., 2008. Determination of underivatized amino acid δ13C by liquid chromatography/isotope ratio mass spectrometry for nutritional studies: the effect of dietary non-essential amino acid profile on the isotopic signature of individual amino acids in fish. Rapid Communications in Mass Spectrometry 22, 1817–1822.

Mekhtieva, V.L., Pankina, R.G., 1968. Isotopic composition of sulfur in aquatic plants and dissolved sulfates. Geochemistry International 5, 624–627.

North, J.A., Narrowe, A.B., Xiong, W., Byerly, K.M., Zhao, G., Young, S.J., Murali, S., Wildenthal, J.A., Cannon, W.R., Wrighton, K.C., Hettich, R.L., Tabita, F.R., 2020. A nitrogenase-like enzyme system catalyzes methionine, ethylene, and methane biogenesis. Science 369, 1094–1098.

Oduro, H., Alstyne, K.L.V., Farquhar, J., 2012. Sulfur isotope variability of oceanic DMSP generation and its contributions to marine biogenic sulfur emissions. Proceedings of the National Academy of Sciences 109, 9012–9016.

Paris, G., Sessions, A.L., Subhas, A.V., Adkins, J.F., 2013. MC-ICP-MS measurement of $\delta^{34}S$ and $\Delta^{33}S$ in small amounts of dissolved sulfate. Chemical Geology 345, 50–61.

Peterson, B.J., Fry, B., 1987. Stable Isotopes in Ecosystem Studies. Annual Review of Ecology and Systematics 18, 293–320.

Peterson, B.J., Howarth, R.W., Garritt, R.H., 1985. Multiple Stable Isotopes Used to Trace the Flow of Organic Matter in Estuarine Food Webs. Science 227, 1361–1363.

Price, M.N., Zane, G.M., Kuehl, J.V., Melnyk, R.A., Wall, J.D., Deutschbauer, A.M., Arkin, A.P., 2018. Filling gaps in bacterial amino acid biosynthesis pathways with high-throughput genetics. PLOS Genetics 14, e1007147.

Rampler, E., Dalik, T., Stingeder, G., Hann, S., Koellensperger, G., 2012. Sulfur containing amino acids – challenge of accurate quantification. Journal of Analytical Atomic Spectrometry 27, 1018–1023.

Raven, M.R., Adkins, J.F., Werne, J.P., Lyons, T.W., Sessions, A.L., 2015. Sulfur isotopic composition of individual organic compounds from Cariaco Basin sediments. Organic Geochemistry 80, 53–59.

Raven, M.R., Sessions, A.L., Adkins, J.F., Thunell, R.C., 2016. Rapid organic matter sulfurization in sinking particles from the Cariaco Basin water column. Geochimica et Cosmochimica Acta 190, 175–190.

Richards, M.P., Fuller, B.T., Hedges, R.E.M., 2001. Sulphur isotopic variation in ancient bone collagen from Europe: implications for human palaeodiet, residence mobility, and modern pollutant studies. Earth and Planetary Science Letters 191, 185–190.

Sayle, K.L., Brodie, C.R., Cook, G.T., Hamilton, W.D., 2019. Sequential measurement of $\delta^{15}N$, $\delta^{13}C$ and $\delta^{34}S$ values in archaeological bone collagen at the Scottish Universities Environmental Research Centre (SUERC): A new analytical frontier. Rapid Communications in Mass Spectrometry 33, 1258–1266.

Smyth, D.G., Stein, H., Moore, S., 1963. The Sequence of Amino Acid Residues in Bovine Ribonuclease: Revisions and Confirmations 238, 9.

Steine, W., Moore, S., 1949. Amino acid composition of beta-lactoglobulin and bovine serum albumin. The Journal of Biological Chemistry 178, 79–91.

Takano, Y., Kashiyama, Y., Ogawa, N.O., Chikaraishi, Y., Ohkouchi, N., 2010. Isolation and desalting with cation-exchange chromatography for compound-specific nitrogen isotope analysis of amino acids: application to biogeochemical samples. Rapid Communications in Mass Spectrometry 24, 2317–2323.

Tcherkez, G., Tea, I., 2013. $^{32}S/^{34}S$ isotope fractionation in plant sulphur metabolism. New Phytologist 200, 44–53.

Thode, H.G., Rees, C.E., 1971. Measurement of sulphur concentrations and the isotope ratios $^{33}S/^{32}S$, $^{34}S/^{32}S$ and $^{36}S/^{32}S$ in Apollo 12 samples. Earth and Planetary Science Letters 12, 434–438.

Ueda, A., Krouse, H.R., 1986. Direct conversion of sulphide and sulphate minerals to SO2 for isotope analyses. Geochemical Journal 20, 209–212.

Wang, Y., Espenson, J.H., 2000. Oxidation of Symmetric Disulfides with Hydrogen Peroxide Catalyzed by Methyltrioxorhenium(VII). The Journal of Organic Chemistry 65, 104–107.

White, R.H., 1981. A method for the measurement of sulfur-34 abundance in bound cysteine and methionine. Analytical Biochemistry 114, 349–354.

Wu, P., Tang, L., Jiang, W., Hu, K., Liu, Y., Jiang, J., Kuang, S., Tang, L., Tang, W., Zhang, Y., Zhou, X., Feng, L., 2017. The relationship between dietary methionine and growth, digestion, absorption, and antioxidant status in intestinal and hepatopancreatic tissues of sub-adult grass carp (Ctenopharyngodon idella). Journal of Animal Science and Biotechnology 8.

Yano, H., Aso, K., Tsugita, A., 1990. Further study on gas phase acid hydrolysis of protein: improvement of recoveries for tryptophan, tyrosine, and methionine. Journal of Biochemistry 108, 579–582.

Chapter 3

RESOLVING SOURCES AND SINKS OF MARINE DISSOLVED ORGANIC MATTER VIA NOVEL SULFUR ISOTOPE ANALYSIS

Phillips, A.A., White, M.E., Seidel, M., Wu, F., Pavia, F.J., Kemeny, P.C., Ma, A.C., Aluwihare, L.I., Dittmar, T., Sessions, A.L. Resolving sources and sinks of marine dissolved organic matter via novel sulfur isotope analysis. *In Prep.*

ABSTRACT

Marine dissolved organic matter (DOM) is a dynamic reservoir relevant to the global carbon, nitrogen, and phosphorus cycles. Recent work demonstrated that DOM also is significant for sulfur biogeochemistry, with revelations that dissolved organic sulfur (DOS) is the largest inventory of marine organic sulfur. Fundamental questions remain about DOS dynamics, including its sources and connections to carbon cycling. DOS may originate from phytoplankton-derived organic sulfur in the surface ocean or from anoxic sediments of abiotically "sulfurized" organic matter. To determine the relative importance of these hypothesized sources, we conducted the first measurements of $^{34}S/^{32}S$ ratios ($\delta^{34}S$ values) of solid phase extracted (SPE) marine DOM_{SPE} on profiles from seven stations throughout the Pacific and Atlantic, including from oxygen minimum zones, productive shelves, and hypoxic basins. We also report $\delta^{34}S$ values of porewater from sulfidic sediments to constrain this abiotic endmember. DOM_{SPE} $\delta^{34}S$ values ranged from 14.7‰ to 19.7‰, with C:S ratios between 153 and 303 with lower $\delta^{34}S$ values corresponding to higher C:S ratios. Marine samples also showed consistent trends with depth: $\delta^{34}S$ values decreased, C:S ratios increased, and $\delta^{13}C$ values were constant. Porewater samples were significantly ^{34}S-depleted and sulfur-rich compared to marine samples, with average $\delta^{34}S$ values and C:S ratios of -0.4‰ and 37, respectively. We interpret these trends as reflecting <10% contribution of

abiotically sulfurized sources to marine DOS and conclude that porewater fluxes do not meaningfully contribute to oceanic DOM budgets. We hypothesize that observed heterogeneity in $\delta^{34}S$ values and C:S ratios with depth instead reflects efficient heterotrophic recycling of phytoplankton-derived DOS metabolites. Our findings strengthen links between sulfur and carbon cycling in the pelagic ocean and support a paradigm shift that recognizes the central role of organic sulfur, not just inorganic sulfate, in marine biogeochemistry.

1 | INTRODUCTION

Dissolved organic matter (DOM) is the largest inventory of fixed carbon in the ocean (~662 Pg C) and is a critical component in marine food webs, nutrient cycling, and climate over geological time scales (Hansell et al., 2009). Despite decades of intensive study, fundamental questions remain regarding DOM sources and sinks in the modern ocean. In recent work, Ksionzek *et al.* (2016) demonstrated that DOM contains a substantial quantity of organic sulfur. The marine dissolved organic sulfur (DOS) pool is estimated to contain ~7 Pg S, more than ten times the sulfur in phytoplankton, bacteria, and particulate organic sulfur (POS) combined (Figure 1). Although estimates of DOS concentration vary (Ksionzek et al., 2016; Longnecker et al., 2020), it is clear that DOS is central to marine sulfur cycling, with growing evidence for important links to carbon cycling (Moran and Durham, 2019). For example, reduced sulfur compounds within DOS lower trace metal availability by tightly binding free zinc and copper and potentially limiting primary production (Smith et al., 2002). Concentration of alkyl thiols, such as the amino acid cysteine, have been correlated to chlorophyll concentrations, implying further connections to phytoplankton growth (Matrai and Vetter, 1988; Al-Farawati and Van Den Berg, 2001). DOS metabolites may also limit heterotrophic organic carbon oxidation, as clades of the ubiquitous SAR11 and SAR86 bacteria are unable to assimilate sulfate and must rely on scavenging reduced OS from the water column. It remains unknown whether this important subset of S-containing

molecules within DOM (i.e., DOS) behaves similarly to the larger DOC pool or has unique origins and/or dynamics.

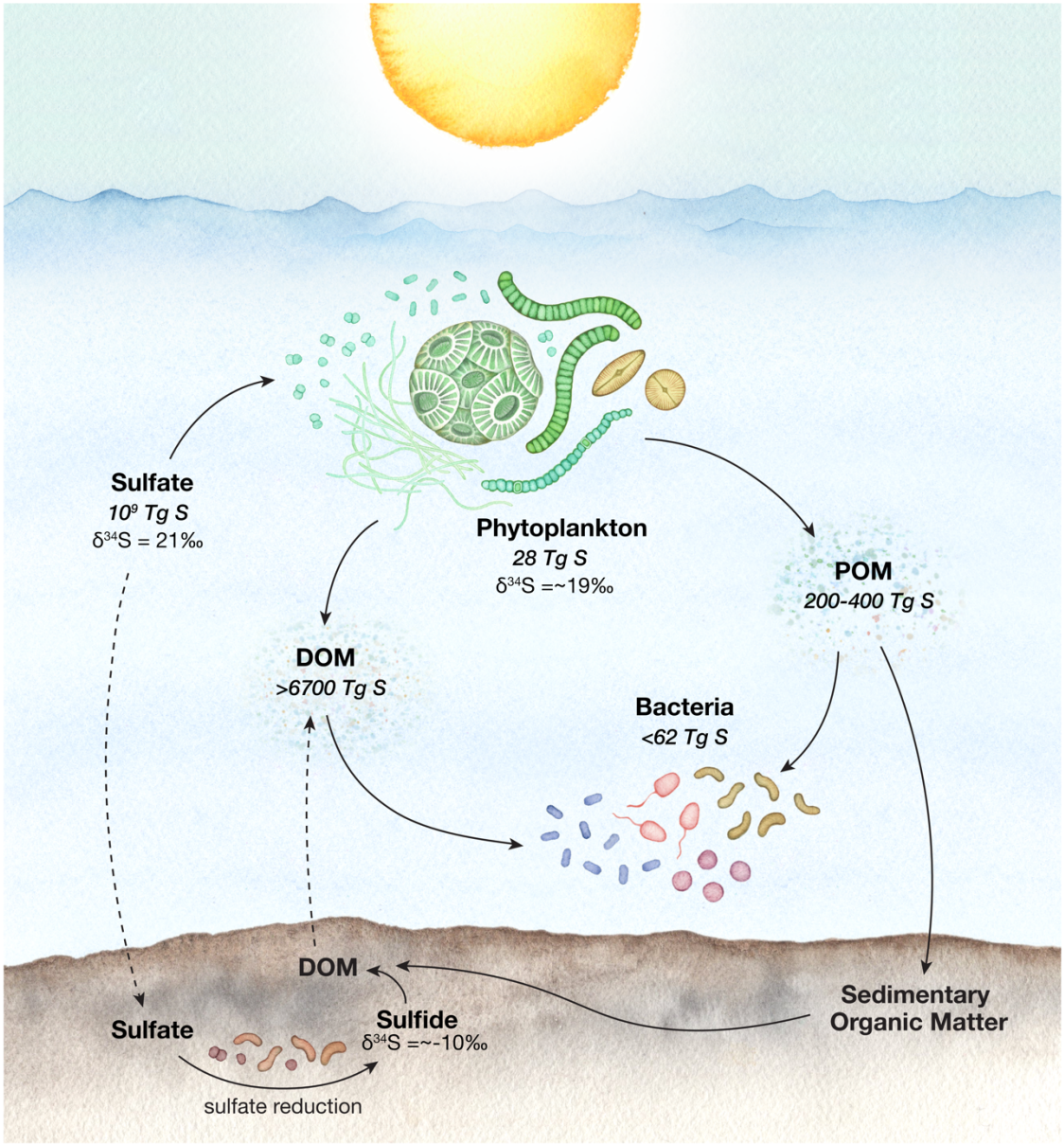

Figure 1 *A simplified marine organic sulfur cycle. Sulfate is the largest reservoir of sulfur in the ocean (Newton and Bottrell, 2007; Paris et al., 2013). Phytoplankton in the sunlit ocean use this sulfate to build biomass. Through lysis, exudation, and senescence, phytoplankton biomass enters the dissolved organic sulfur (DOS)*

pool, which is the second largest marine OS reservoir (Ksionzek et al., 2016). DOS may also originate from sediments, where sulfide is incorporated into sedimentary organic matter (POM) and porewater DOM to form sulfurized DOS (Pohlabeln et al., 2017). The sulfur isotopic composition of DOS indicates the relative balance of these two sources.

A first order question regarding DOS dynamics is the origin of OS compounds. Ksionzek *et al.* (2016) proposed a DOS cycle that mirrors DOC, with DOS produced by phytoplankton in the sunlit ocean. Under this hypothesis, microbial reworking during the aging of DOS, such as heterotrophic uptake for growth or remineralization back to sulfate, leaves remaining DOS increasingly recalcitrant. If correct, then DOS is a potentially representative subset of DOM; studying DOS may then offer a unique lens to DOM cycling more broadly. A second hypothesis, proposed by Pohlabeln *et al.* (2017) argues that a significant portion of DOS originates not in the surface ocean, but from anoxic sediments. Here, sulfide produced via microbial sulfate reduction (MSR) reacts with organic molecules to "sulfurize" organic matter. The resulting covalent C-S bonds are thought to be resistant to microbial degradation via inducing stable S-S cross-linked structures and replacing otherwise more labile functional groups (Boussafir et al., 1995; Boussafir and Lallier-Verges, 1997; Sinninghe Damsté et al., 1998). As such, sulfurization reactions have been recognized as an important pathway for sedimentary organic matter preservation (de Leeuw and Sinninghe-Damste, 1990; Grice et al., 2003). In anoxic sediments, these reactions are a major process: in a study of the Santa Barbara Basin, 70% of detected DOS formulas were products of sulfide and polysulfide sulfurization reactions (Abdulla et al., 2020). Pohlabeln *et al.* (2017) calculated that the flux of these highly recalcitrant DOS species could be a significant source to benthic DOS, and by extension to water column DOM: while the proportion of DOM molecules that contain S is not known precisely, estimates from molecular formulas suggest it could be on the order of ~5-10% (Longnecker et al., 2020). If true, then DOS also represents a unique sub-cycle within DOM.

This overlooked source could also help explain why some components of DOM have paradoxically long lifetimes, strengthening connections between C and S cycles in the ocean (Dittmar, 2015).

Although marine DOM has been studied for decades via isotopic measurements (i.e., $^{14}C/^{12}C$, $^{13}C/^{12}C$, and $^{15}N/^{14}N$; Druffel and Williams, 1992), no complementary measurements have been made for sulfur. Measurements of DOS have been hindered by two significant roadblocks: salt concentration and sample size. Dissolved inorganic sulfate, at 28 mM, is 4-5 orders of magnitude higher in concentration than DOS (~100 nM). To resolve OS metabolites from this high salt background, studies rely on solid phase extraction (SPE) on a styrene-divinylbenzene stationary phase (Bond Elute PPL; Dittmar et al., 2008). These hydrophobic resins isolate DOM that is largely representative, although with slight biases towards older material and lower molecular weight compounds (Green et al., 2014; Coppola et al., 2015; Dittmar, 2015). Yields are high, but variable for DOC (35-65%), very low (~21%) for DON, and unknown for DOS (Broek et al., 2017). Salt removal is crucial for most analyses of DOM, including isotopic measurements by isotope ratio mass spectrometry (IRMS). However, traditional combustion IRMS methods require much more S (~70 μg) than C (~20 μg). Further, DOM has high C:S ratios (~150 to 300), especially after extraction by SPE methods. Sample sizes were therefore prohibitively large, requiring many mg of material per measurement. Recent developments in EA-IRMS technology have enabled lower sample sizes (1-10 μg S; Phillips et al., 2021) for OS compounds. Here, we used the SPE extraction method and adapted our sulfur isotope measurement to allow simultaneous determination of $\delta^{13}C$ values, $\delta^{34}S$ values, and C:S molar ratios on samples of ~350 μg DOM_{SPE}. We applied this novel method to over 100 SPE extracts across ocean basins, generating the first profiles of $\delta^{34}S$ values of marine DOM_{SPE}. Our data indicate that sulfurization reactions contribute minimal global DOS, and by extension, DOM.

2 | MATERIALS AND METHODS

2.1 | Sample collection

DOM samples were collected between 2016 and 2021 on ten cruises (see supporting information for details), including the Bermuda Atlantic Time Series (BATS) and the Hawaii Ocean Time-series (HOT), that covered the following regions: N Pacific Gyre, N Atlantic Gyre, S Pacific Gyre, NE Pacific, NE Pacific Shelf, NE Pacific OMZ, San Pedro Basin, and the Caeté Estuary (in the Brazilian Amazon). Porewater DOM samples were collected from the intertidal sediments of the mangrove-fringed Caeté Estuary and a North Sea intertidal flat. For marine samples, CTD casts for physical parameters (i.e., oxygen, salinity, fluorescence, temperature) were taken at each station and can be found in the supporting information. Seawater (~5-20 L samples) was collected from niskin bottles into acid-washed containers and filtered through a 0.80/0.45 μm capsule filter (AcroPak™ 500) prior to acidification to pH 2 with reagent grade 12 N hydrochloric acid.

2.2 | DOM isolation

DOM was concentrated using solid phase extraction (SPE) with Bond Elute PPL cartridges (Agilent; 1 g, 6 mL size) following Dittmar *et al.* (2008). DOM_{SPE} samples were eluted in GC grade methanol. Extracts were dried under a stream of N_2 gas and transferred to 2mL GC vials and then to 150 μL glass inserts. Aliquots corresponding to ~4.5 μg S (~350 μg DOC_{SPE}) were transferred in methanol from 2 mL GC vials into smooth walled tin capsules (6 x 2.9 mm, OEA labs). Methanol was evaporated at room temperature (~2 hrs). SPE cartridges were also tested to confirm quantitative sulfate removal by extracting a 10L 28 mM sodium sulfate solution in deionized water. Sulfate in methanol extracts were below detection limits following analysis with a Dionex Ion Chromatography System 2000 and an AS29-Fast (4 μm diameter column) at Caltech's Environmental Analysis Center.

2.3 | Isotope measurement

Dried capsules were closed, folded, loaded into an autosampler, and then combusted and analyzed in a Thermo Scientific (Bremen, Germany) EA IsoLink™ IRMS system. The system included an elemental analyzer (EA) coupled to a Delta V Plus Isotope Ratio Mass Spectrometer (IRMS) via a ConFlo IV Universal interface. Carbon and sulfur isotope determination and data processing followed a previously published method (Phillips et al., 2021). Due to high C:S molar ratios of DOM_{SPE}, CO_2 was diluted by the highest setting, 88.4%, following combustion. Urea standards were run at the same settings to account for any possible fractionation during dilution. Sulfur isotope and concentration standards included an in-house calibrated methionine, seawater sulfate, and silver sulfides (IAEA S1, S2, S3). Additionally, a working standard of DOM_{SPE} extracted from the Scripps Institution of Oceanography (SIO) pier was run in at least triplicate with each sample set. Extracts supplied by collaborators were often limited to single or duplicate analysis, while other DOM_{SPE} samples allowed up to five measurements. Uncertainties in isotopic compositions and C:S ratios are therefore reported using standard deviations of our DOM_{SPE} SIO pier standard, divided by the square root of sample replicates analyzed. DOM samples with peak sizes that corresponded to < 1 μg S were not reported. $\delta^{34}S$ values are reported as permil (‰) variations relative to the Vienna Canyon Diablo Troilite (VCDT) reference frame while $\delta^{13}C$ values are reported relative to Vienna Pee Dee Belemnite (VPDB). Typical precision (1σ std. dev.) on replicates of DOM samples and consistency standards were ≤ 0.2‰ for $\delta^{34}S$ values and $\delta^{13}C$ values and ≤ 6 for C:S ratios.

3 | RESULTS

A global dataset of 90 marine, 5 estuarine, and 5 porewater samples were analyzed for $\delta^{13}C$ values, $\delta^{34}S$ values, and C:S molar ratios in DOM_{SPE} (Figure

2a). Marine samples spanned gyres, shelves, restricted basins, oxygen minimum zones (OMZs), and coastal oceans (Figure 2a).

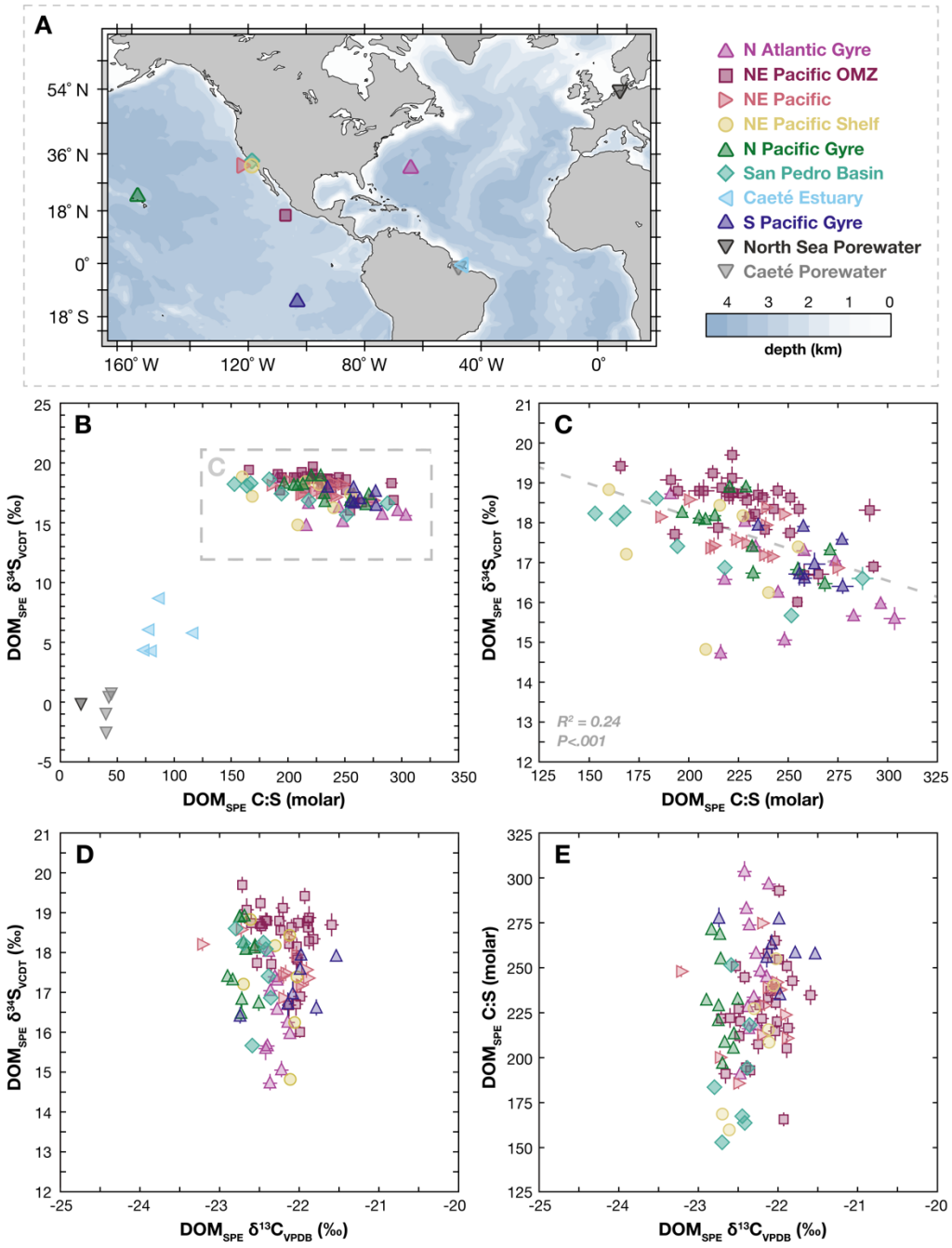

Figure 2 *(A) Map of sample locations for the study, which spanned oceanographic regimes including gyres (N Atlantic: pink triangles, N Pacific: green triangles, S*

Pacific: dark blue triangles), shelves (NE Pacific Shelf: yellow circles), mangrove-fringed estuaries (Caeté Estuary: light blue left-facing triangles), restricted hypoxic basins (San Pedro Basin: turquoise diamonds), oxygen minimum zones (NE Pacific OMZ: magenta squares), coastal settings (NE Pacific: light pink right-facing triangles), and sulfidic porewater (North Sea: dark grey down-facing triangles). (B) C:S ratios versus $\delta^{34}S$ values of all analyzed DOM_{SPE} samples (n=100) (C) Expanded view of marine DOM_{SPE} samples (indicated by the dashed gray box in panel B), showing a negative correlation between DOM_{SPE} $\delta^{34}S$ values and C:S ratios (R^2 = 0.24, P<.001). (D) DOM_{SPE} $\delta^{13}C$ values versus $\delta^{34}S$ values and (E) C:S ratios, showing no significant correlations.

3.1 | Porewater and estuary samples

Porewater DOM_{SPE} samples from sulfidic sediments in the mangrove tidal creek within the Caeté Estuary ranged in $\delta^{34}S$ values from -2.6 to 0.8‰, with C:S molar ratios between 40 and 45 (Figure 2b) and $\delta^{13}C$ values between -27.1 and -26.8‰. Porewater DOM_{SPE} was also analyzed from sulfidic sediments in the back barrier tidal flats of the North Sea, yielding a $\delta^{34}S$ value of -0.2‰, C:S molar ratio of 18, and $\delta^{13}C$ value of -23.3‰. DOM_{SPE} surface water samples from the Caeté river estuary were analyzed across a transect from the coastal ocean to the mangrove-fringed estuary. C:S ratios ranged from 74 to 117 with $\delta^{34}S$ values between 4.3 to 8.7‰. $\delta^{13}C$ values spanned -28.6 to -24.2‰ across the transect.

3.2 | Marine samples

Marine DOM_{SPE} had $\delta^{34}S$ values and C:S ratios ranging from 14.7 to 19.7‰ and 160 to 303, respectively (Figure 2-3). Lower $\delta^{34}S$ values correlated with higher C:S ratios (R^2 = 0.24; *P*<.001) and deeper depths (R^2 = 0.24; *P*<.001). Depth was a more robust driver of lower $\delta^{34}S$ values within the upper 1500m of the water column (R^2 = 0.42; *P*<.001; Figure 3b). DOM_{SPE} $\delta^{34}S$ values also had statistically significant positive correlations with DOC concentration (R^2 = 0.23; *P*<.001), but

not other measured nutrients (Figure S8). DOM_{SPE} C:S ratios showed statistically significant increases with depth (R^2 = 0.20; *P*<.001) – with a similar trend in the upper 1500m (R^2 = 0.14; *P*<.001). Generally, DOM_{SPE} $\delta^{34}S$ values decreased from an average of 18.4 ± 0.5‰ in the surface ocean (<50 m; *n*=16) to 16.7 ± 0.8‰ in the deep ocean (>2000 m; *n*=14), while C:S ratios increased from 192 ± 25 to 259 ± 26. Meanwhile, DOM_{SPE} $\delta^{13}C$ values were constant throughout the water column with an average of -22.3 ± 0.3‰ (1σ; Figures 2-3). See supporting information for details on average measurements for each station.

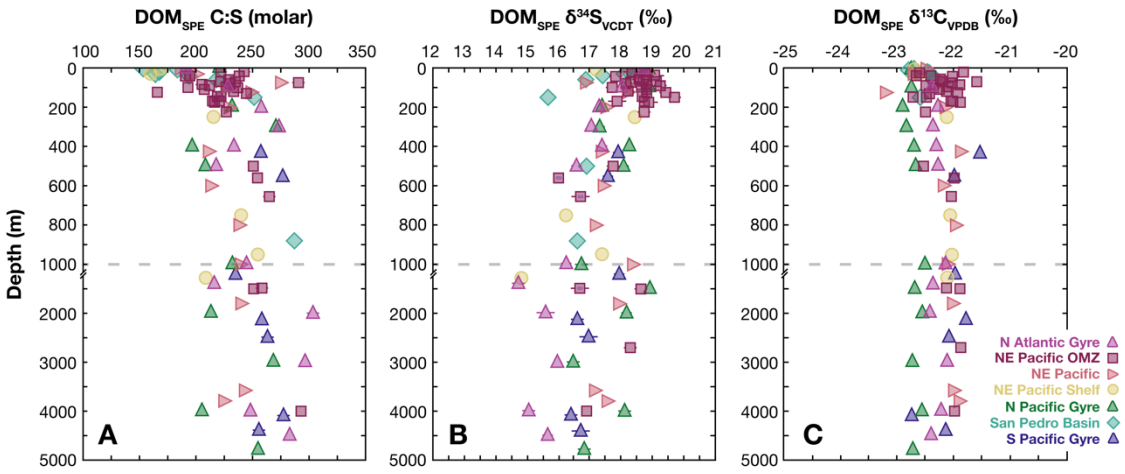

Figure 3 *DOM_{SPE} samples plotted by location against depth for (A) C:S ratios, (B) $\delta^{34}S$ values and (C) $\delta^{13}C$ values. Note the scale break at 1000 m on the y-axis. Colors and symbols for stations are the same as Figure 2. DOM_{SPE} C:S ratios slightly increased with depth (R^2 = 0.20, P<.001), while $\delta^{34}S$ values generally decreased from the surface to deep ocean (R^2 = 0.24, P<.001), especially in the upper 1500m (R^2 = 0.42, P<.001). DOM_{SPE} $\delta^{13}C$ values were constant.*

4 I DISCUSSION

We evaluated a global dataset of DOM_{SPE} to test the relative contribution from two potential sources of marine DOS: phytoplankton-derived organic molecules in the surface ocean versus abiotic sulfurized organic matter from anoxic sediments.

First, we constrain (1) the composition of biotic DOS in the surface ocean, which we define as <50 m water depth, and (2) the composition of abiotic DOS in sulfidic porewaters. This allows us to determine the relative contribution of each of these hypothesized endmembers to overall marine DOS, where we conclude that (3) there is limited evidence for porewater sources to DOS and more broadly, to DOM. Finally, we discuss (4) alternative potential drivers for observed sulfur isotope heterogeneity with depth.

4.1 | Composition of biotic DOS in the surface ocean

Primary producers in the photic zone invest energy to transform inorganic sulfate into biomass in a process called assimilatory sulfate reduction. Sulfate is reduced first to adenosine 5'-phosphosulfate, then to sulfite, and finally to bisulfide, which reacts with activated organic carbon compounds to form the amino acid cysteine (Moran and Durham, 2019). Further metabolic reactions downstream of cysteine create a suite of organic sulfur metabolites that range in S oxidation state from +6 to -2. Very few studies have examined the consequences of these reactions for the sulfur isotope composition of organic matter in phytoplankton. Early work on aquatic plants implied mostly negligible fractionation during assimilatory sulfate reduction (Mekhtieva and Pankina, 1968), with organic $\delta^{34}S$ values closely tracking those of marine sulfate, which is a nearly constant 21.0‰ (Paris et al., 2013). Compound-specific sulfur isotope analysis found that that phytoplankton DMSP (dimethylsulfoniopropionate) was ^{34}S-depleted from marine sulfate by 1.4 to 2.8‰, suggesting measurable fractionations during sulfate assimilation (Oduro et al., 2012). Analysis of cysteine and methionine $\delta^{34}S$ values from marine fish were similarly ^{34}S-depleted relative to sulfate by ~2-3‰ (Phillips et al., 2021). It has remained unclear whether these fractionations observed in a few metabolites are translatable to bulk organic sulfur. However, our data set of surface (<50 m) DOM_{SPE} $\delta^{34}S$ values, which averaged 18.4 ± 0.5‰, aligns with compound-specific

studies and supports the idea that assimilatory sulfate assimilation does result in fractionation of sulfur isotopes.

Similar to phytoplankton $\delta^{34}S$ values, there are few studies that have investigated primary producer C:S ratios. Laboratory experiments found cultures of *Synechococcus* incorporating C, N, and S at a ratio of 95:16:1 (Cuhel and Waterbury, 1984). Meanwhile, marine particulate organic sulfur (POS), which is assumed to derive from phytoplankton, has C:N:S ratios of ~187:27:1 in the North Pacific (Matrai and Eppley, 1989; Bates et al., 1994). Euphotic zone DOM_{SPE} (<50 m depth) C:S ratios in this study were similar, averaging 192 ± 25 and ranging between 153 to 243. This aligns with previous studies of DOM_{SPE} C:S ratios, which ranged between 188 and 290 in the upper 100 m of the Eastern Atlantic and Southern Ocean (Ksionzek et al., 2016). Higher C:S ratios in DOM/POM versus phytoplankton suggest rapid and substantial losses of relatively sulfur-rich compounds. This could include volatile species like DMS (Dimethyl sulfide, $(CH_3)_2S$; C:S = 2:1), which accounts for 40% of the atmospheric sulfur flux from the ocean (Lana et al., 2011). Loss of DMS and other volatile compounds could therefore bridge the gap between phytoplankton cultures and surface DOM_{SPE} C:S ratios.

Euphotic zone (<50 m) DOM_{SPE} $\delta^{34}S$ values (~17 to 19‰) and C:S ratios (~150 to 250) observed in our study offer constrains for the phytoplankton-derived DOS endmember. Further, the observed variability hints at dynamics in local phytoplankton community structure that can alter the initial composition of organic sulfur produced in the surface ocean. Additional global surveys of marine primary producers and their elemental and isotopic compositions would help to further our understanding of assimilatory sulfate reduction.

4.2 | Composition of abiotic DOS in sulfidic porewater

Dissimilatory sulfate reduction, unlike the assimilatory pathway, strongly fractionates sulfur isotopes, with resulting porewater sulfide $\delta^{34}S$ values as low as -45‰ (Thode et al., 1953; Habicht and Canfield, 1997; Sim et al., 2011). The magnitude of this fractionation is generally inversely correlated with sulfate reduction rate (Bradley et al., 2011; Wing and Halevy, 2014). For example, high rates minimize expressed isotope effects, leading to smaller isotopic offsets between sulfide and sulfate, and higher sulfide $\delta^{34}S$ values. We analyzed porewater samples from tidal flats with high rates of sulfate reduction and organic matter sulfurization: the mangrove fringed Caeté Estuary and the North Sea (Kamyshny and Ferdelman, 2010; Seidel et al., 2014; Jørgensen et al., 2019; Raven et al., 2019). These samples should therefore reflect an upper bound on porewater sulfide $\delta^{34}S$ values.

Porewater sulfide and polysulfides attack organic carbon functional groups to form new C-S bonds in a process called sulfurization. The sulfur isotopic consequences of these reactions are much less studied than dissimilatory sulfate reduction, but generally suggest that sulfurized organic matter has higher $\delta^{34}S$ values than coexisting sulfide. Most convincingly, compound specific isotope analysis suggest that sulfide incorporation into carbonyls leads to organics that are 4-5‰ ^{34}S-enriched relative to reactants (Amrani and Aizenshtat, 2004). Sulfurized organic matter in the rock record corroborates this trend, with preserved kerogen consistently ^{34}S-enriched compared to pyrite, which is taken to represent sulfide (Anderson and Pratt, 1995; Bottrell and Raiswell, 2000). Other investigations of bulk organic sulfur in modern marine sediments agree, finding higher $\delta^{34}S$ values in kerogen versus sulfide (Werne et al., 2004; Dale et al., 2009) However, individual organics in Cariaco Basin sediments had lower $\delta^{34}S$ values than sulfide, hinting that kinetic isotope effects may be expressed over equilibrium fractionations during certain sulfurization reactions. This research highlights the utility of expanding sulfur measurements to other phases, such as porewater DOM_{SPE} $\delta^{34}S$ values, which to our knowledge, have not yet been investigated.

Our data from the mangrove fringed Caeté Estuary and the North Sea provide the first direct constraints on porewater DOS sulfur isotope compositions. The $\delta^{34}S$ values of DOM_{SPE} in these porewaters ranged from to -2.5 to 0.8‰, unsurprisingly ^{34}S-enriched given the (a) high sulfate reduction rates in these environments and (b) potential equilibrium fractionation during sulfurization. DOM_{SPE} C:S ratios ranged between 18 and 45, with much higher sulfur content than phytoplankton-derived DOS in the surface ocean. These values align with both laboratory studies that incubated DOM in sulfidic water, finding post-sulfurization C:S ratios ~15, and previous measurements of North Sea porewaters with a C:S ratio of ~27 (Pohlabeln et al., 2017). Porewater DOM_{SPE} $\delta^{13}C$ values differed in the Caeté Estuary (-26.9 ± 0.1‰) and the North Sea (-23.3 ± 0.2‰), likely reflecting higher terrestrial influences in the mangrove-fringed estuary.

4.3 l Limited global evidence for porewater sources to DOS

Analysis of euphotic zone (<50 m depth) allowed us to constrain the isotopic and elemental composition of phytoplankton-derived DOS (see section 4.1). Porewater samples provided C:S ratios and upper bounds on the $\delta^{34}S$ values of abiotic, sulfurized DOS that may flux from sediments (section 4.2). These endmembers allow us to calculate the influence of each source, revealing <10% contributions of porewater-derived DOS to marine samples (Figure 4). Only samples from the mangrove-fringed Caeté Estuary were within a range of significant contributions (~50-80%) from sulfurized organic matter (see supporting information for further discussion). As our Caeté Estuary and North Sea porewater samples are, if anything, more ^{34}S-enriched than porewater from marine sediments, this calculation represents a conservative maximum estimate. Thus, we can conclude that DOS has a dominantly (>90%) biotic origin, produced by phytoplankton in the sunlit, surface ocean.

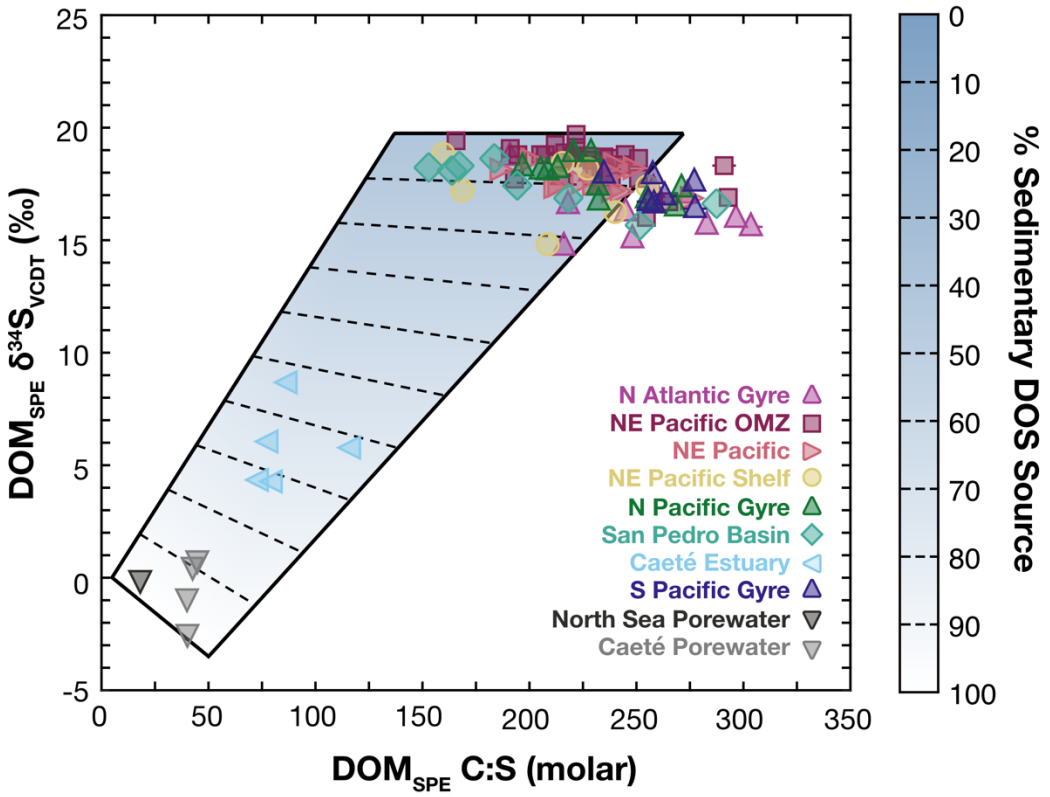

Figure 4 *DOM$_{SPE}$ samples plotted in the same coordinate space and color scheme as Figure 1b, with C:S molar ratios on the x-axis and δ^{34}S values on the y-axis. A linear mixing space is seen in the white to blue colored polygon, with dashed lines for 10% intervals. Caeté Estuary water samples plot within a 50-80% range for sediment porewater contributions, while ocean samples that fall within the mixing space largely fall as > 90% surface production. See discussion 4.1 and 4.2 for determination of end-member constraints.*

Sulfurization reactions have also been documented to occur within anoxic micro-environments in the pelagic ocean, such as sinking particles in OMZs: Genomic studies found active transcription of genes for sulfate reduction (Smith et al., 2013; Carolan et al., 2015) and incubation studies with radioactively labeled sulfur confirmed that particulate organic matter sulfurization was occurring (Raven et al., 2020). It remains uncertain if this process translates from the particulate to the

dissolved sulfur pool. Our data from the NE Pacific OMZ (*n*=31; magenta squares, Figures 2-4) were collected from adjacent stations to Raven et al. (2020) and spanned dissolved oxygen concentrations from 0 to 250 μM. Yet, we observed no significant changes to either C:S ratios or $\delta^{34}S$ values with oxygen (Figure S3). This hints that sulfurization reactions in water columns, in addition to those in sediments, minimally or negligibly contribute to marine DOS.

The conclusion that sedimentary fluxes of sulfurized organic matter do not impact global marine DOS is somewhat unexpected given previous estimates of large benthic fluxes (30-200 Tg S yr^{-1}; Pohlabeln et al., 2017), calculated by dividing DOC fluxes by DOM_{SPE} C:S ratios. The simplest explanation is that the calculated fluxes do not represent the environmental reality. Our data offer an independent approximate constraint of sedimentary DOS flux for comparison. Given that a maximum of 10% (Figure 4) of the 6700 Tg S DOS inventory (Ksionzek et al., 2016) comes from porewater sources and that the average lifetime of DOS is ~4,000 years (Moran and Durham, 2019), the sedimentary flux of DOS is to the global ocean is ~0.2 Tg S yr^{-1}. Porewater C:S ratios (~10 to 50) further imply DOC fluxes of 0.8-3.8 Tg C yr^{-1}, orders of magnitude below estimates for coastal and continental margin sediments (121-233 Tg C yr^{-1}, Burdige, 2007; Burdige and Komada, 2015), intertidal sediments (106-416 Tg C yr^{-1}, Maher and Eyre, 2010), deep-sea sediments (~100 Tg C yr^{-1}, Burdige and Komada, 2015), and their minimum summation (327 Tg C yr^{-1}, Pohlabeln et al., 2017). Although it is possible to invoke DOC flux with little concurrent DOS flux, theoretical C:S ratios to bridge ~0.2 Tg S yr^{-1} with 327 Tg C yr^{-1} are difficult to imagine (*i.e.,* >4000). In conclusion, either sulfurized DOS suffers extreme preferential loss over DOC or porewaters are orders of magnitude less significant sources of marine DOM than previously thought.

4.4 | Alternative causes for observed $\delta^{34}S$ heterogeneity

With mixing of biological and sedimentary sources unable to explain a significant set of our marine DOM_{SPE} values (Figure 4), we explore alternative hypotheses that may drive observed heterogeneity. Candidate processes must lower DOM $\delta^{34}S$ values from the photic zone to the deep ocean, while increasing C:S ratios and maintaining constant $\delta^{13}C$ values.

4.4.1 | Mixing with terrestrial organic matter

A third source, with low $\delta^{34}S$ values and high C:S ratios, could mix with phytoplankton DOS to produce the observed values for bulk DOM_{SPE}. Terrestrial organic matter, transported to the ocean by rivers, would be the most likely candidate. However, it is unlikely that this source can explain the observed variation in our dataset. Studies have found that most POC and DOC discharged by rivers is efficiently remineralized within ocean margins (Hedges et al., 2004). Further, our DOM_{SPE} $\delta^{13}C$ values across samples and depths were unambiguously marine, not terrestrial, with a range from -23.2 to -21.5‰ (Figures 2-3). With the lowest $\delta^{34}S$ values observed in samples collected from beyond the photic zone, we exclude mixing with terrestrial organic matter as explaining observed isotopic heterogeneity.

4.4.2 | Exchange between DOS and POS

Current models of the marine sulfur cycle assume that major reservoirs of organic sulfur (phytoplankton, microbes, DOS, and POS) rapidly cycle and exchange, but actual fluxes between pools are unknown (Ksionzek et al., 2016; Moran and Durham, 2019). For example, hypothesized dynamics between DOS and POS include dissolved metabolites aggregating to particles and particles hydrolyzing to enter dissolved phases, but the relative importance of these reactions has not been quantified. However, if POS and DOS exchange is significant, these interactions may drive decreasing DOM_{SPE} $\delta^{34}S$ values observed with depth. Hydrolysis of C-S bonds exhibits a normal kinetic isotope effect (KIE) for some organic sulfur

metabolites (Friedberger and Thornton, 1976; Tcherkez and Tea, 2013). Depth-dependent POS hydrolysis could therefore leave POM increasingly ^{34}S-enriched while DOM becomes ^{34}S-depleted. No profiles of POM $\delta^{34}S$ values exist to test this hypothesis, but a similar pattern of isotope enrichment with depth has been documented for particulate organic nitrogen (PON) in the N Atlantic (Altabet et al., 1991; Casciotti et al., 2008).

4.4.3 | Sulfur isotope fractionation during degradation

Marine DOC concentrations consistently decrease with depth (Hansell et al., 2009), with concurrent increases in C:N, C:P (Hopkinson and Vallino, 2005), and C:S stoichiometry (Figure 2, Ksionzek et al., 2016). These observations imply more efficient removal and more rapid recycling of N, S, and P over C in DOM. Selective removal of labile components may cause isotope fractionation, but this is an unlikely explanation for the observed DOM_{SPE} $\delta^{34}S$ patterns in this study. When sulfur compounds are removed from DOS, they are either (1) reintegrated into S metabolites or (2) salvaged for C skeletons. The first pathway should express no sulfur isotope fractionation due to quantitative removal. This is supported by studies of higher consumers like marine fish that demonstrate no ^{34}S-enrichment with trophic consumption of dietary sulfur (Peterson et al., 1985; Peterson and Fry, 1987). The second pathway is likely to express normal KIEs associated with C-S bond cleavage: for example, when heterotrophic bacteria uptake C_2 and C_3 sulfonates for carbon metabolism and release HSO_3^- (Durham et al., 2019). However, this would cause ^{34}S-enrichment in residual compounds, not depletion. Neither scenario allows for decreasing DOM_{SPE} $\delta^{34}S$ values with depth.

4.4.4 | Selective degradation of ^{34}S-enriched DOS

DOM_{SPE} is comprised of hundreds of compounds, each with a range of characteristic $\delta^{34}S$ values. As each of these components has differential lability, certain compound classes are likely lost preferentially during water-column

remineralization. If there is a positive relationship between compound lability and $^{34}S/^{32}S$ ratio, then the selective loss of ^{34}S-enriched components with depth would cause residual DOS to display increasingly lower $\delta^{34}S$ values, as observed in our data set. We evaluate this hypothesis using a two-reservoir mass balance model. We model two pools of DOS, one that is ^{34}S-enriched and another that is ^{34}S-depleted, and calculate changes in the sulfur isotopic composition of DOS for different initial conditions and remineralization dynamics. As phytoplankton-derived DOM_{SPE} $\delta^{34}S$ values in the surface ocean averaged of 18.4 ± 0.5‰ and deep-water DOM_{SPE} $\delta^{34}S$ values averaged 16.7 ± 0.8‰, we set the model to reproduce this ~3‰ offset. Metabolic sulfur isotope fractionations, as discussed briefly in section 4.1, have only been minimally studied. However, values from both compound-specific and bulk organic sulfur isotope analyses suggest reasonable bounds between 2 and 10‰ for the difference between ^{34}S-enriched and ^{34}S-depleted pools (Kaplan et al., 1963; Trust and Fry, 1992; Oduro et al., 2012; Phillips et al., 2021). We then ask what level of selective loss via mineralization of ^{34}S-enriched components over 3^4S-depleted components is required to drive the isotope heterogeneity observed with depth (Figure 5). The calculation shows that for a system with > 40% initial ^{34}S-enriched DOS and metabolic sulfur isotope fractionation between 2 and 10‰, we must invoke >70% (and often >90%) preferential removal of ^{34}S-enriched components to reproduce our ~3‰ difference in DOM_{SPE} $\delta^{34}S$ values.

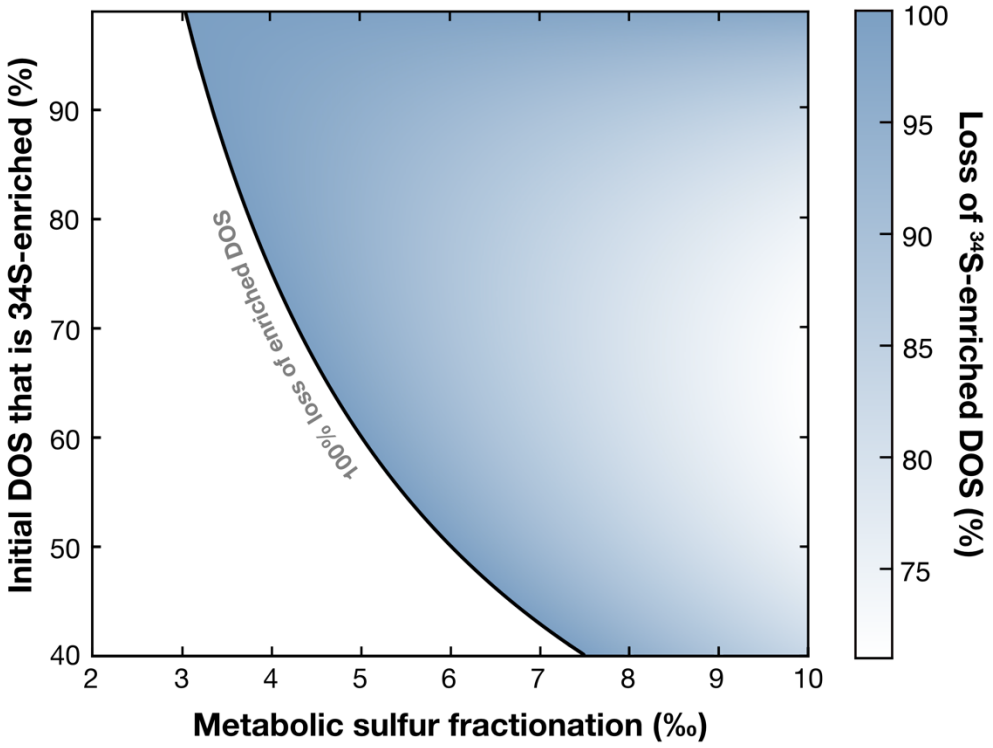

Figure 5 *An isotope mass balance calculation of required preferential loss of ^{34}S-enriched sulfur from initial phytoplankton-derived DOS to drive the δ^{34}S value shift of ~3‰ (from ~19 to 16‰) observed in our global survey of marine DOM$_{SPE}$. The model assumes a percentage range of initial phytoplankton-derived DOS that is ^{34}S-enriched that varies between 40 to 100% and potential metabolic sulfur isotope effects between 2 and 10‰. The results highlight the potential of highly efficient (>70%) removal of ^{34}S-enriched sulfur in DOS to drive our observed isotope heterogeneity.*

Although ^{34}S-enriched and ^{34}S-depleted DOS pools may exist across numerous continuums (*e.g.,* age, lability), we propose sulfur oxidation state as the most likely variable. First, there is reasonable mechanistic evidence to explain preferential loss of reduced over oxidized biotic organic sulfur. Sulfur metabolism below the photic zone is energetically expensive: ATP must be invested to reduce sulfate before organic sulfur metabolites are synthesized (Moran and Durham, 2019). Due

to this energetic cost of assimilating oxidized S, reduced organic sulfur is more biologically valuable. Notably, if these reduced components within DOM_{SPE} have higher $\delta^{34}S$ values than oxidized components, then their efficient, depth-dependent removal would drive our observed isotope changes. Although no studies to our knowledge have measured oxidized metabolites, compound specific sulfur isotope studies of reduced S compounds (*i.e.,* cysteine, methionine, DMSP) suggest that these compounds are naturally ^{34}S-enriched (~19‰; Oduro et al., 2012; Phillips et al., 2021). Further, studies of marine phytoplankton found that 35% of assimilated sulfate was routed to protein synthesis, 40% to low molecular weight (LMW) compounds, 21% to ester-sulfates, and 4% to lipids (Bates et al., 1994), supporting at >40% initial composition of the ^{34}S-enriched pool in primary producers. Taken together, this suggests that there is >70% (and in many scenarios, >90%) preferential loss of reduced over oxidized sulfur by marine heterotrophic bacteria – aligning with estimates that suggest ~95% of remaining marine DOC is refractory (Hansell and Carlson, 2013). This calculation supports increasing evidence that sulfur cycling in marine environments, especially that of organic sulfur, is much more active than canonically considered (Moran and Durham, 2019).

5 I CONCLUSIONS

We developed a more sensitive sulfur isotope EA-IRMS analytical method for marine DOM_{SPE}, enabling concurrent measurements of $\delta^{34}S$ values, $\delta^{13}C$ values, and C:S ratios on ~350 μg DOM. With these first profiles of marine DOM_{SPE} $\delta^{34}S$ values, we conclude that abiotically sulfurized organic matter from sedimentary porewater is at most a small component (<10%) of the marine DOS pool and a negligible component of the oceanic DOM inventory. Sulfurized organic matter is therefore unlikely to be the answer to the long-standing paradox of DOM radiocarbon age. Instead, DOS apparently arises mostly from phytoplankton in the sunlit, surface ocean. We hypothesize that heterotrophic consumption of reduced,

semi-labile organic sulfur from the DOS pool drives the negative correlation between DOM_{SPE} $\delta^{34}S$ values and C:S ratios observed, and their trends with depth. Our mass balance model estimates that > 70% of reduced sulfur would need to be preferentially consumed to drive the ~3‰ shift in DOM_{SPE} $\delta^{34}S$ values from the photic zone to the deep ocean. This implies rapid and efficient cycling of DOS, supporting a paradigm shift that recognizes sulfur, especially biotically produced organic sulfur, as a dynamic and active component of marine biogeochemical cycles.

ACKNOWLEDGEMENTS

We thank the crew, administrative teams, and science parties of the *R/V Atlantic Explorer* and the *R/V Kilo Moana* for their assistance during the Bermuda Atlantic Time Series (BATS) and Hawaii Ocean Time-series (HOT) cruises, especially Rod Johnson and Carolina Funkey. We thank Daniela Osorio Rodriguez and Sijia Dong for their assistance in sample collection aboard the *R/V Sally Ride* and PI Jess Adkins from Caltech. We thank Troy Gunderson from the San Pedro Ocean Timeseries and the crew of the *R/V Yellowfin.* We acknowledge Mike Beman for his assistance in acquiring NE Pacific OMZ samples and Ken Smith for help acquiring the Station M sample used. We are grateful to members and technicians in the Aluwihare lab at Scripps Institution of Oceanography, especially Brandon Stephens and Irina Koester. We acknowledge Usha Lingappa for drafting Figure 1. We thank colleagues for early reviews and conversations about the manuscript, including Hannah Dion-Kirschner and Ted Present. We thank UC Santa Cruz Professor Matthew McCarthy for early conversations and support for the project. Color blind friendly palettes were generated from Paul Tol's online resource. Funding for AAP was provided by NSF OCE Grant 2023676. MS and TD acknowledge funding by the DFG-FAPERJ cooperative project (DI 842/6-1).

SUPPORTING INFORMATION

Materials and Methods:

N Atlantic Gyre: Samples (*n* = 12) of 10 L were collected aboard the *R/V Atlantic Explorer* at BATS Station (31° 40'N, 64° 10'W) during the October 2020 leg of the Bermuda Atlantic Time Series (BATS) cruise.

NE Pacific OMZ: Samples were collected aboard the *R/V Oceanus* on two cruises to the NE Pacific oxygen minimum zone (OMZ) region off the coast of Mexico in April 2017 and June 2018. Samples were collected from five sites across the two cruises: Station 2 (16° 30'N, 107° 12'W; *n*=10), Station 3 (16° 00'N, 110° 00'W; *n*=7), Station 4 (21° 30'N, 109° 30'W; *n*=5), Station 5 (24° 41'N, 113° 17'W; *n*=7), and Station 6 (27° 23'N, 117° 30'W; *n*=1). Station 6 was only sampled in 2017. Stations 3 and 4 were only sampled in 2018. Stations 2 and 5 were sampled in both years. 20 L of seawater was extracted per depth on the 2017 cruise, and 5 L of seawater per sample on the 2018 cruises. One additional sample was collected in April 2018 aboard the *R/V Western Flyer* at Station M (34° 30'N, 123° 00'W; *n*=1): this 15L sample was collected by ROV *Doc Ricketts* 1 m above the seafloor.

NE Pacific and NE Pacific Shelf: Seawater samples for DOM_{SPE} analysis were collected aboard the *R/V Sally Ride* at two stations in the NE Pacific off the coast of Southern California in November 2020: on the shelf (33° 11'N, 118° 37'W; *n* = 7) and offshore (32° 33'N, 120° 31'W; *n* = 12). ~7-9 L of seawater was collected per sample.

N Pacific Gyre: Samples (*n* = 12) were collected aboard the *R/V Kilo Moana* at Station ALOHA (22° 45'N, 158° 00'W) during the November 2020 leg of the Hawaii Ocean Time-series (HOT). 10 L seawater samples were collected for DOM_{SPE} analysis.

San Pedro Basin: Samples (*n*=9) were collected aboard the *R/V Yellowfin* on the February 2021 leg of the San Pedro Ocean Time-series (SPOT) cruise off the coast of Southern California to one station (33° 33'N, 118° 24'W). ~7-9 L seawater were collected for DOM_{SPE} analysis per sample.

S Pacific Gyre: Seawater samples (*n*=7) of 5-7 L were collected aboard the *R/V Ronald Brown* during the first leg of the P18 GO-SHIP (US Global Ocean Ship-based Hydrographics Investigations Program) cruise at a single station (12° 59'S, 103° 00'W) in November to December 2016 off the coast of Peru.

Caeté Estuary and Caeté Estuary Porewater: Water samples were collected by boat in the dry season of October 2018 along a 35 km salinity transect from riverine (1° 1'S, 46° 45'W) to marine (0° 54'S, 46° 36'W), ending at the Amazonian mangrove-fringed estuary near Bragança City (Pará State, Brazil) in the Caeté Estuary, following Call et al. (2019). Porewater samples (~3-6 L) were taken in a tidal creek close to the marine end of the transect, at the mangrove-fringed estuary. Water samples were filtered using a thoroughly pre-rinsed 1.0 μm Causapure filter cartridge (CPR-001-09-DOX, PP, Infiltec).

North Sea Porewater: Porewater from an anoxic intertidal flat were collected in the Northern German Wadden Sea at the Janssand site close to the barrier island Spiekeroog (Seidel et al., 2014). Samples were collected in 10 L acid-cleaned polycarbonate carboys after digging a hole and scooping porewater out of the holes. The samples were filtered through pre-combusted (450°C, 4 hours) glass fiber filters (Whatman 1 μm GMF and 0.7 μm GFF) and solid phase extracted as described by Catalá et al., 2020).

Results:

***N Atlantic Gyre*:** Samples were analyzed between 5 and 4800 m water depth (Figure S1). $\delta^{34}S$ values decreased with depth from a maximum of 18.7‰ in the

surface (5 m) to a minimum value of 14.7‰ below the photic zone. C:S ratios generally increased with depth, from a surface minimum of 191 to a maximum value of 303 in the deep ocean (2000 m). DOM_{SPE} $\delta^{13}C$ values were constant with depth, averaging -22.3 ± 0.1‰.

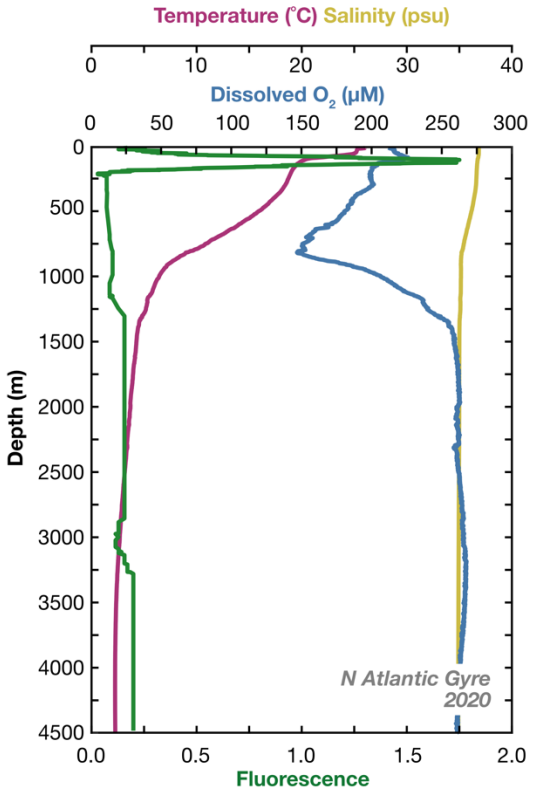

Figure S1 *CTD profile from October 2020 Bermuda Atlantic Time Series cruise at BATS station in the N Atlantic Gyre. Profiles of salinity (psu, yellow line) and temperature (˚C, magenta line) are plotted on the upper x-axis, dissolved oxygen concentration (µM, blue line) on the second upper x-axis and fluorescence (relative fluorescence units) in green on the lower x-axis.*

NE Pacific OMZ: Samples were collected at six stations largely within the upper 250 m of the water column (Figure S2). DOM_{SPE} $\delta^{34}S$ values showed no change with depth in the upper 250 m, averaging 18.7 ± 0.5‰. Deeper samples were

limited, but within error, averaging 17.3 ± 0.9‰. DOM_{SPE} $\delta^{13}C$ values were also constant with depth, averaging -22.2 ± 0.3‰. C:S values generally decreased with depth but had a large range in the surface ocean (< 100m), between 191 and 291. Variations in C:S values and $\delta^{34}S$ values were not related to station number or sampling year. NE Pacific OMZ samples displayed no correlation with dissolved oxygen concentrations, which ranged from ~0 to 250 μM across the sample set (Figure S3). However, samples did show a significant negative correlation between $\delta^{34}S$ values and C:S ratios (R^2 = 0.47, P<.001).

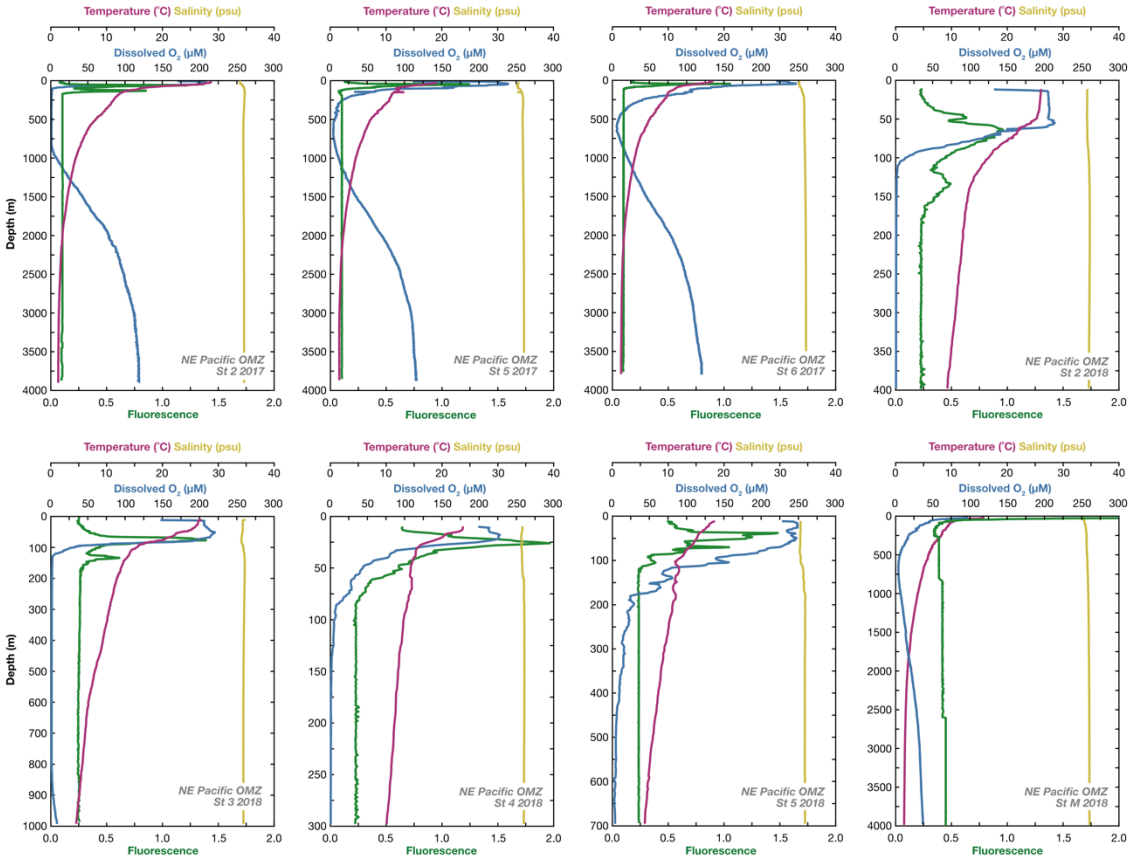

Figure S2 *Physical properties from stations sampled in the NE Pacific OMZ from 2017-2018. Note that while x-axes are constant for each subplot, y-axes are not. Colors and units are the same as Figure S1.*

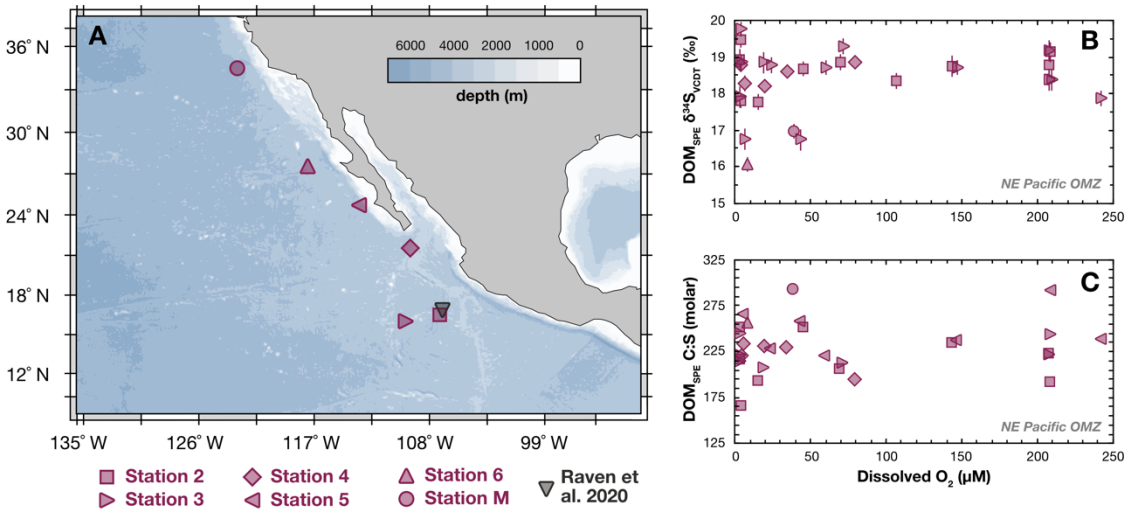

Figure S3 *Map (A) of NE Pacific OMZ sampling locations in this study (magenta shapes), with the sampling site from Raven et al. 2020 marked with a dark grey inverted triangle. Oxygen concentration is plotted against DOM$_{SPE}$ (B) $\delta^{34}S$ values and (C) C:S ratios.*

NE Pacific and NE Pacific Shelf: Samples were analyzed from between 5 and 1275 m on the shelf and between 5 and 3790 m in the coastal ocean (Figure S4). Carbon isotopes were similar across stations, with lower DOM$_{SPE}$ $\delta^{13}C$ values in the upper 100 m (-22.6 ± 0.3‰) than below the photic zone (-22.1 ± 0.1‰). $\delta^{34}S$ values were largely constant in the NE Pacific, averaging 17.7 ± 0.5‰ throughout the water column. Meanwhile, $\delta^{34}S$ values from the NE Pacific shelf decreased from a maximum of 18.8 ± 0.1‰ to 14.8 ± 0.2‰ from surface to deep. DOM$_{SPE}$ C:S ratios fluctuated, with a minimum of 160 ± 4 to a maximum of 275 ± 3.

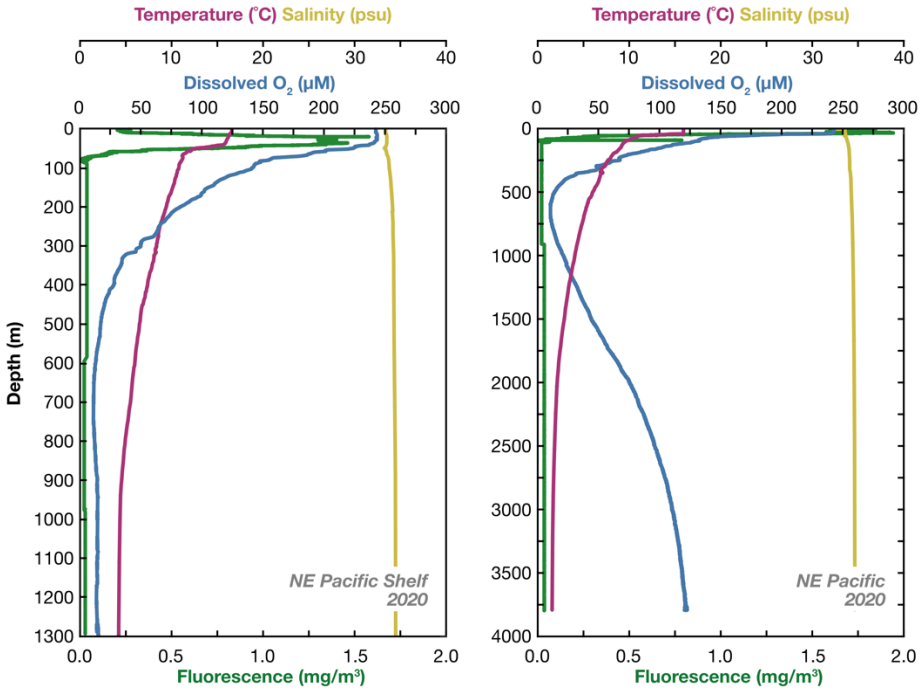

Figure S4 *CTD profile from November 2020 cruise to the NE Pacific and NE Pacific shelf. Note the change of scale in the y axis. Colors and units are the same as Figure S1.*

N Pacific Gyre: Samples were analyzed between 5 and 4800 m (*n* =12; Figure S5). DOM_{SPE} $\delta^{13}C$ values were constant throughout the water column, averaging -22.7 ± 0.1‰. DOM_{SPE} $\delta^{34}S$ values were also fairly constant, with an average of 17.8 ± 0.9‰, but with higher variability. C:S ratios were similarly variable, with an average of 230 ± 25. $\delta^{34}S$ values were also negatively correlated with C:S ratios (R^2 = 0.47, P<.05).

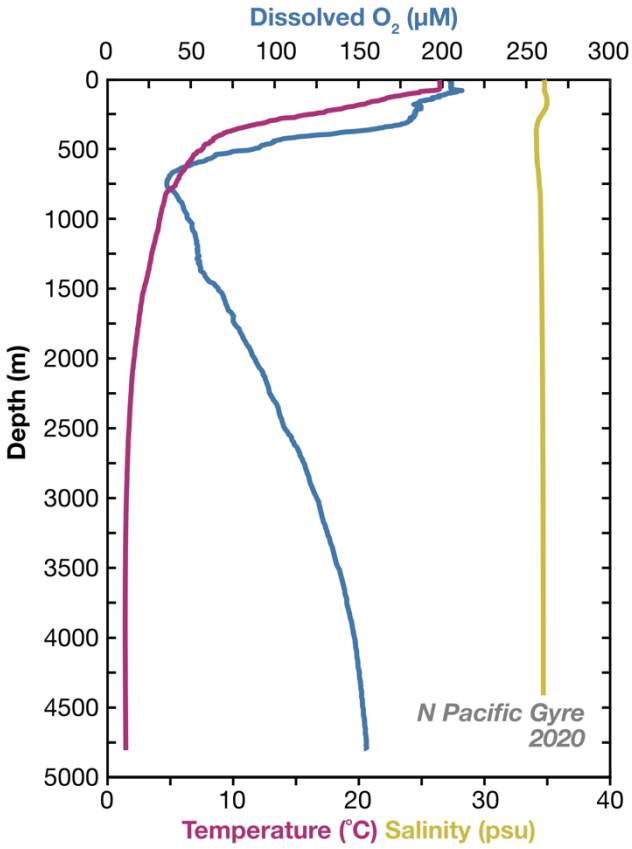

Figure S5 *CTD profile from October 2020 Bermuda Atlantic Time Series cruise at BATS station in the N Atlantic Gyre. Profiles of salinity (psu, yellow line) and temperature (˚C, magenta line) are plotted on the lower x-axis with dissolved oxygen concentration (μM, blue line) on the upper x-axis.*

San Pedro Basin: Samples were analyzed between 2 and 880 m. San Pedro is a persistently hypoxic (<1 mL/L dissolved oxygen) restricted basin off the coast of Los Angeles, Southern California (Figure S6). DOM_{SPE} samples showed no change in $\delta^{13}C$ values, averaging -22.5 ± 0.2‰. In contrast, C:S ratios and $\delta^{34}S$ values were strongly dependent on depth. C:S ratios increased from 153 ± 3 in the surface (2 m) to 287 ± 6 at depth (880 m) while $\delta^{34}S$ values from the same depths decreased from 18.2 ± 0.2‰ to 16.6 ± 0.3‰. C:S and $\delta^{34}S$ values were also significantly negatively correlated (R^2 = 0.71, P<.01).

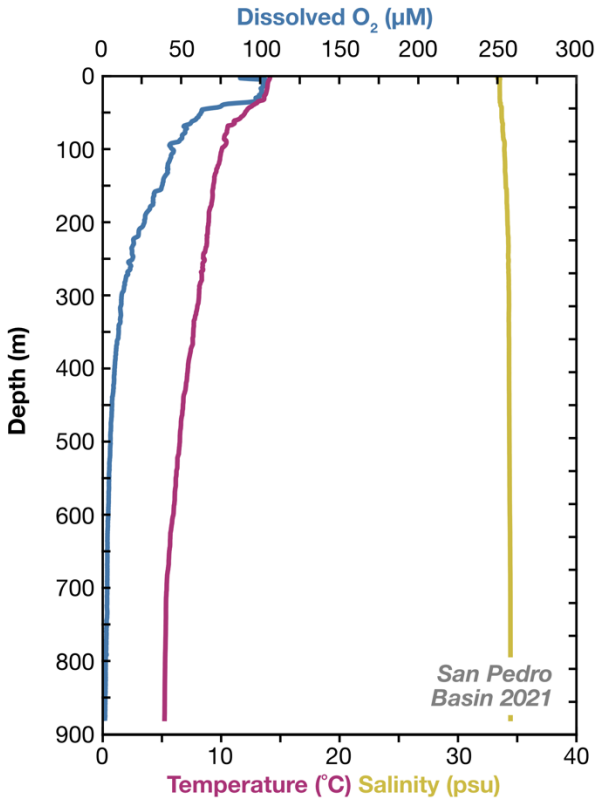

Figure S6 *CTD profile from San Pedro Basin during the February 2021 SPOT cruise. Profiles of salinity (psu, yellow line) and temperature (˚C, magenta line) are plotted on the lower x-axis with dissolved oxygen concentration (μM, blue line) on the upper x-axis.*

S Pacific Gyre: Samples were analyzed between 435 and 4411 m (Figure S7). DOM_{SPE} $\delta^{13}C$ values fluctuated between a minimum of -22.7 ± 0.1‰ and a maximum of -21.5 ± 0.1‰, although without depth dependence. DOM_{SPE} $\delta^{34}S$ values decreased from 17.9 ± 0.2‰ to 16.4 ± 0.2‰ with depth while C:S ratios increased from 235 ± 3 to 277 ± 3.

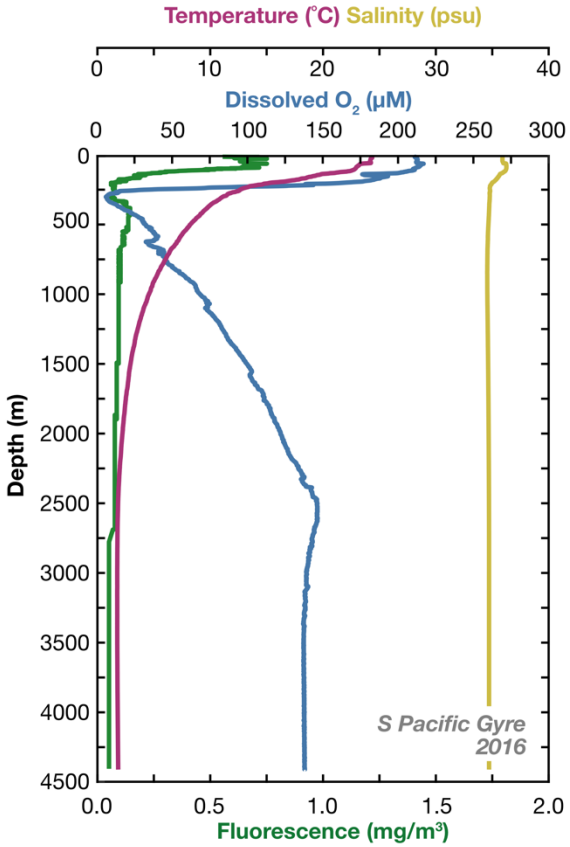

Figure S7 *CTD profile from November 2016 GO-SHIP cruise to the S Pacific Gyre. Colors and units are the same as Figure S1.*

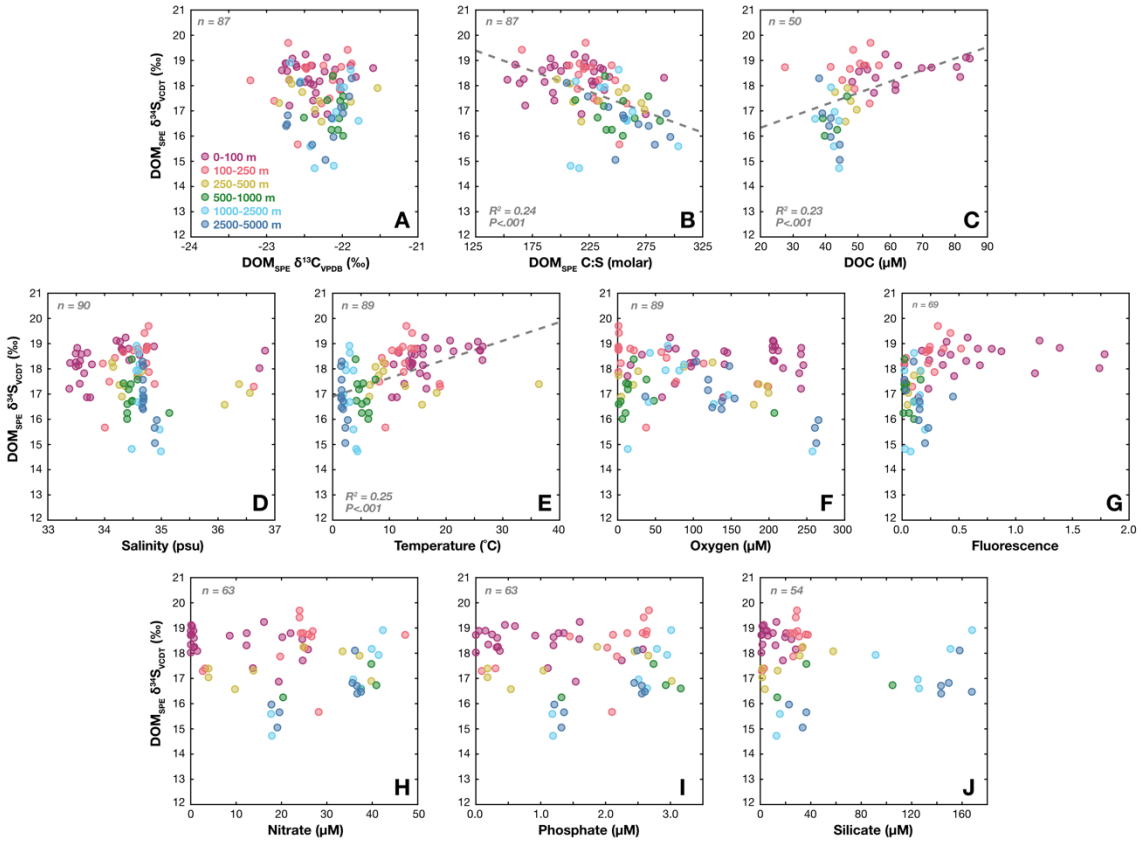

Figure S8 *Metadata analysis of potential correlations between DOM$_{SPE}$ δ^{34}S values against (A) δ^{34}S values, (B) C:S ratios (C) DOC (D) salinity (E) temperature (F) oxygen (G) fluorescence (H) nitrate (I) phosphate and (J) silicate. Only C:S ratios had a significant negative correlation with δ^{34}S values. Temperature and DOC concentration were both positively correlated. However, C:S ratios, δ^{34}S values, temperature, and DOC concentration all also vary with depth. Samples from different depths were binned into 0-100 m (magenta), 100-250 m (pink), 250-500 m (yellow), 500-1000 m (green)m 1000-2500 m (light blue), and 2500-5000 m (dark blue).*

Discussion:

Where does sulfurized organic matter from estuaries go?

Porewater sources were significant sources of DOS (>50%) in water samples from the mangrove-fringed Caeté Estuary in NE Brazil. Here, we hypothesize that benthic fluxes of sulfurized organic matter are significant, but these compounds do not persist in the oxidized, sunlit oceans. In intertidal environments like the Caeté Estuary, sedimentary DOM is exported to shallow depths with sufficient photon flux where photochemical degradation likely chemically removes DOS. This is corroborated by a study of DOM from salt marshes where samples were subjected to solar irradiation. After one month, DOS concentrations had decreased from 13 to 1 μM, indicating that sulfurized DOM is highly photolabile (Gomez-Saez et al., 2017). Mangroves, salt marshes, and other intertidal sediments cover most of the land-ocean transition zone worldwide. Therefore, despite their importance in marine DOM budgets (Dittmar et al., 2006), the impacts of estuarine sulfurized DOS to the open ocean appear short-lived.

Potential outliers in porewater/phytoplankton mixing space

Although our marine dataset overall does not support globally significant porewater sulfurization fluxes to DOS, two samples could have >20% sedimentary inputs: the first is from the N Atlantic Gyre, from 1400 m with a DOM_{SPE} $\delta^{34}S$ value of 14.7± 0.2‰ and a C:S ratio of 216 ± 3. However, this oceanographic context excludes sulfurization sources as it is from the center of the water column and far from sedimentary inputs. The other sample had a DOM_{SPE} $\delta^{34}S$ value of 14.8 ± 0.2‰ and a C:S ratio of 209 ± 3 and was collected from the NE Pacific Shelf, a few meters from the sediment-water interface. This sample is more likely to represent a potential signal from DOS sediment flux. Shelf sediments harbor significant populations of SRB, which are typically active even in the upper few cms (Christensen, 1989). Globally, shelf sediments deliver 121-233 Tg C annually to

the ocean (Burdige et al., 1999; Burdige and Komada, 2015), similar to DOC deliveries from intertidal sediments (106-416 Tg C yr^{-1}; Maher and Eyre, 2010). Future DOS surveys should target additional shelf sediments to determine how robust this finding is. However, if sulfurized DOS fluxes from sediments are indeed significant for the very deepest water column samples above shelf sediments, the effects appear limited – DOS samples from just a few 100 m above the sediment water-interface appeared dominantly phytoplankton-derived.

BIBLIOGRAPHY

Abdulla, H.A., Burdige, D.J., Komada, T., 2020. Abiotic formation of dissolved organic sulfur in anoxic sediments of Santa Barbara Basin. Organic Geochemistry 139, 103879.

al-Farawati, R., Van Den Berg, C.M., 2001. Thiols in coastal waters of the western North Sea and English Channel. Environmental Science & Technology 35, 1902–1911.

Altabet, M.A., Deuser, W.G., Honjo, S., Stienen, C., 1991. Seasonal and depth-related changes in the source of sinking particles in the North Atlantic. Nature 354, 136–139.

Amrani, A., Aizenshtat, Z., 2004. Mechanisms of sulfur introduction chemically controlled: δ34S imprint. Organic Geochemistry 35, 1319–1336.

Anderson, T.F., Pratt, L.M., 1995. Isotopic Evidence for the Origin of Organic Sulfur and Elemental Sulfur in Marine Sediments, in: Geochemical Transformations of Sedimentary Sulfur, ACS Symposium Series. American Chemical Society, pp. 378–396.

Bates, T.S., Kiene, R.P., Wolfe, G.V., Matrai, P.A., Chavez, F.P., Buck, K.R., Blomquist, B.W., Cuhel, R.L., 1994. The cycling of sulfur in surface seawater of the northeast Pacific. Journal of Geophysical Research: Oceans 99, 7835–7843.

Bottrell, S.H., Raiswell, R., 2000. Sulphur Isotopes and Microbial Sulphur Cycling in Sediments, in: Riding, R.E., Awramik, S.M. (Eds.), Microbial Sediments. Springer, Berlin, Heidelberg, pp. 96–104.

Boussafir, M., Gelin, F., Lallier-Verges, E., Derenne, S., Bertrand, P., Largeau, C., 1995. Electron microscopy and pyrolysis of kerogens from the Kimmeridge Clay Formation, UK: Source organisms, preservation processes, and origin of microcycles. Geochimica et Cosmochimica Acta 59, 3731–3747.

Boussafir, M., Lallier-Verges, E., 1997. Accumulation of organic matter in the Kimmeridge Clay formation (KCF): an update fossilisation model for marine petroleum source-rocks. Marine and Petroleum Geology 14, 75–83.

Bradley, A.S., Leavitt, W.D., Johnston, D.T., 2011. Revisiting the dissimilatory sulfate reduction pathway. Geobiology 9, 446–457.

Broek, T., Walker, B., Guilderson, T., McCarthy, M., 2017. Coupled ultrafiltration and solid phase extraction approach for the targeted study of semi-labile high molecular weight and refractory low molecular weight dissolved organic matter. Marine Chemistry 194.

Burdige, D.J., 2007. Preservation of Organic Matter in Marine Sediments: Controls, Mechanisms, and an Imbalance in Sediment Organic Carbon Budgets? Chemical Reviews 107, 467–485.

Burdige, D.J., Berelson, W.M., Coale, K.H., McManus, J., Johnson, K.S., 1999. Fluxes of dissolved organic carbon from California continental margin sediments. Geochimica et Cosmochimica Acta 63, 1507–1515.

Burdige, D.J., Komada, T., 2015. Sediment Pore Waters, in: Biogeochemistry of Marine Dissolved Organic Matter. Elsevier, pp. 535–577.

Call, M., Santos, I.R., Dittmar, T., de Rezende, C.E., Asp, N.E., Maher, D.T., 2019. High pore-water derived CO2 and CH4 emissions from a macro-tidal mangrove creek in the Amazon region. Geochimica et Cosmochimica Acta 247, 106–120.

Carolan, M.T., Smith, J.M., Beman, J.M., 2015. Transcriptomic evidence for microbial sulfur cycling in the eastern tropical North Pacific oxygen minimum zone. Frontiers in Microbiology 6.

Casciotti, K.L., Trull, T.W., Glover, D.M., Davies, D., 2008. Constraints on nitrogen cycling at the subtropical North Pacific Station ALOHA from isotopic measurements of nitrate and particulate nitrogen. Deep Sea Research Part II: Topical Studies in Oceanography, Understanding the Ocean's Biological Pump: results from VERTIGO. 55, 1661–1672.

Catalá, T.S., Rossel, P., Álvarez-Gómez, F., Tebben, J., Figueroa, F., Dittmar, T., 2020. Antioxidant Activity and Phenolic Content of Marine Dissolved Organic Matter and Their Relation to Molecular Composition, in: Frontiers in Marine Science.

Christensen, J.P., 1989. Sulfate reduction and carbon oxidation rates in continental shelf sediments, an examination of offshelf carbon transport. Continental Shelf Research 9, 223–246.

Coppola, A.I., Walker, B.D., Druffel, E.R.M., 2015. Solid phase extraction method for the study of black carbon cycling in dissolved organic carbon using radiocarbon. Marine Chemistry 177, 697–705.

Cuhel, R.L., Waterbury, J.B., 1984. Biochemical composition and short term nutrient incorporation patterns in a unicellular marine cyanobacterium, Synechococcus (WH7803)1. Limnology and Oceanography 29, 370–374.

Dale, A.W., Brüchert, V., Alperin, M., Regnier, P., 2009. An integrated sulfur isotope model for Namibian shelf sediments. Geochimica et Cosmochimica Acta 73, 1924–1944.

de Leeuw, J., Sinninghe-Damste, J., 1990. Organic Sulfur Compounds and Other Biomarkers as Indicators of Palaeosalinity. American Chemical Society 429, 417–443.

Dittmar, T., 2015. Chapter 7 - Reasons Behind the Long-Term Stability of Dissolved Organic Matter, in: Hansell, D.A., Carlson, C.A. (Eds.), Biogeochemistry of Marine Dissolved Organic Matter (Second Edition). Academic Press, Boston, pp. 369–388.

Dittmar, T., Hertkorn, N., Kattner, G., Lara, R.J., 2006. Mangroves, a major source of dissolved organic carbon to the oceans. Global Biogeochemical Cycles 20.

Dittmar, T., Koch, B., Hertkorn, N., Kattner, G., 2008. A simple and efficient method for the solid-phase extraction of dissolved organic matter (SPE-DOM) from seawater. Limnology and Oceanography: Methods 6, 230–235.

Druffel, E.R.M., Williams, P.M., 1992. Importance of isotope measurements in marine organic geochemistry. Marine Chemistry 39, 209–215.

Durham, B.P., Boysen, A.K., Carlson, L.T., Groussman, R.D., Heal, K.R., Cain, K.R., Morales, R.L., Coesel, S.N., Morris, R.M., Ingalls, A.E., Armbrust, E.V., 2019. Sulfonate-based networks between eukaryotic phytoplankton and heterotrophic bacteria in the surface ocean. Nature Microbiology 4, 1706–1715.

Friedberger, M.P., Thornton, E.R., 1976. Solvolysis mechanisms. Sulfur kinetic isotope effects in the hydrolysis of substituted benzyldimethylsulfonium tosylates. Journal of the American Chemical Society 98, 2861–2865.

Gomez-Saez, G., Pohlabeln, A., Stubbins, A., Marsay, C., Dittmar, T., 2017. Photochemical Alteration of Dissolved Organic Sulfur from Sulfidic Porewater. Environmental Science & Technology 51, 14144–14154.

Green, N.W., Perdue, E.M., Aiken, G.R., Butler, K.D., Chen, H., Dittmar, T., Niggemann, J., Stubbins, A., 2014. An intercomparison of three methods for

the large-scale isolation of oceanic dissolved organic matter. Marine Chemistry 161, 14–19.

Grice, K., Schouten, S., Blokker, P., Derenne, S., Largeau, C., Nissenbaum, A., Damsté, J.S.S., 2003. Structural and isotopic analysis of kerogens in sediments rich in free sulfurised Botryococcus braunii biomarkers. Organic Geochemistry 34, 471–482.

Habicht, K.S., Canfield, D.E., 1997. Sulfur isotope fractionation during bacterial sulfate reduction in organic-rich sediments. Geochimica et Cosmochimica Acta 61, 5351–5361.

Hansell, D., Carlson, C., Repeta, D., Schlitzer, R., 2009. Dissolved Organic Matter in the Ocean: A Controversy Stimulates New Insights. Oceanography 22, 202–211.

Hansell, D.A., Carlson, C.A., 2013. Localized refractory dissolved organic carbon sinks in the deep ocean. Global Biogeochemical Cycles 27, 705–710.

Hedges, J.I., Keil, R.G., Benner, R., 2004. What happens to terrestrial organic matter in the ocean? Marine Chemistry 92, 307–310.

Hopkinson, C.S., Vallino, J.J., 2005. Efficient export of carbon to the deep ocean through dissolved organic matter. Nature 433, 142–145.

Jørgensen, B.B., Findlay, A.J., Pellerin, A., 2019. The Biogeochemical Sulfur Cycle of Marine Sediments. Frontiers in Microbiology 10.

Kamyshny, Alexey, Ferdelman, T.G., 2010. Dynamics of zero-valent sulfur species including polysulfides at seep sites on intertidal sand flats (Wadden Sea, North Sea). Marine Chemistry 121, 17–26.

Kaplan, I.R., Emery, K.O., Rittenberg, S.C., 1963. The distribution and isotopic abundance of sulphur in recent marine sediments off southern California. Geochimica et Cosmochimica Acta 27, 297–331.

Ksionzek, K.B., Lechtenfeld, O.J., McCallister, S.L., Schmitt-Kopplin, P., Geuer, J.K., Geibert, W., Koch, B.P., 2016. Dissolved organic sulfur in the ocean: Biogeochemistry of a petagram inventory. Science 354, 456–459.

Lana, A., Bell, T.G., Simó, R., Vallina, S.M., Ballabrera-Poy, J., Kettle, A.J., Dachs, J., Bopp, L., Saltzman, E.S., Stefels, J., Johnson, J.E., Liss, P.S., 2011. An updated climatology of surface dimethlysulfide concentrations and emission fluxes in the global ocean: Global Biogeochemical Cycles 25.

Longnecker, K., Oswald, L., Soule, M.C.K., Cutter, G.A., Kujawinski, E.B., 2020. Organic sulfur: A spatially variable and understudied component of marine organic matter. Limnology and Oceanography Letters 5, 305–312.

Maher, D.T., Eyre, B.D., 2010. Benthic fluxes of dissolved organic carbon in three temperate Australian estuaries: Implications for global estimates of benthic DOC fluxes. Journal of Geophysical Research: Biogeosciences 115.

Matrai, P.A., Eppley, R.W., 1989. Particulate organic sulfur in the waters of the Southern California Bight. Global Biogeochemical Cycles 3, 89–103.

Matrai, P.A., Vetter, R.D., 1988. Particulate thiols in coastal waters: The effect of light and nutrients on their planktonic production. Limnology and Oceanography 33, 624–631.

Mekhtieva, V.L., Pankina, R.G., 1968. Isotopic composition of sulfur in aquatic plants and dissolved sulfates. 5, 624–627.

Moran, M.A., Durham, B.P., 2019. Sulfur metabolites in the pelagic ocean. Nature Reviews Microbiology 17, 665–678.

Newton, R., Bottrell, S., 2007. Stable isotopes of carbon and sulphur as indicators of environmental change: Past and present. Journal of The Geological Society, 164, 691–708.

Oduro, H., Alstyne, K.L.V., Farquhar, J., 2012. Sulfur isotope variability of oceanic DMSP generation and its contributions to marine biogenic sulfur emissions. Proceedings of the National Academy of Sciences 109, 9012–9016.

Paris, G., Sessions, A.L., Subhas, A.V., Adkins, J.F., 2013. MC-ICP-MS measurement of $\delta^{34}S$ and $\Delta^{33}S$ in small amounts of dissolved sulfate. Chemical Geology 345, 50–61.

Peterson, B.J., Fry, B., 1987. Stable Isotopes in Ecosystem Studies. Annual Review of Ecology and Systematics 18, 293–320.

Peterson, B.J., Howarth, R.W., Garritt, R.H., 1985. Multiple Stable Isotopes Used to Trace the Flow of Organic Matter in Estuarine Food Webs. Science 227, 1361–1363.

Phillips, A.A., Wu, F., Sessions, A.L., 2021. Sulfur isotope analysis of cysteine and methionine via preparatory liquid chromatography and elemental analyzer isotope ratio mass spectrometry. Rapid Communications in Mass Spectrometry 35.

Pohlabeln, A.M., Gomez-Saez, G.V., Noriega-Ortega, B.E., Dittmar, T., 2017. Experimental Evidence for Abiotic Sulfurization of Marine Dissolved Organic Matter. Frontiers in Marine Science 4.

Raven, M.R., Fike, D.A., Gomes, M.L., Webb, S.M., 2019. Chemical and Isotopic Evidence for Organic Matter Sulfurization in Redox Gradients Around Mangrove Roots. Frontiers in Earth Science 7.

Raven, M.R., Keil, R.G., Webb, S.M., 2020. Microbial sulfate reduction and organic sulfur formation in sinking marine particles. Science.

Seidel, M., Beck, M., Riedel, T., Waska, H., Suryaputra, I.G.N.A., Schnetger, B., Niggemann, J., Simon, M., Dittmar, T., 2014. Biogeochemistry of dissolved organic matter in an anoxic intertidal creek bank. Geochimica et Cosmochimica Acta 140, 418–434.

Sim, M.S., Bosak, T., Ono, S., 2011. Large Sulfur Isotope Fractionation Does Not Require Disproportionation. Science 333, 74–77.

Sinninghe Damsté, J.S., Kok, M.D., Köster, J., Schouten, S., 1998. Sulfurized carbohydrates: an important sedimentary sink for organic carbon? Earth and Planetary Science Letters 164, 7–13.

Smith, M.W., Zeigler Allen, L., Allen, A.E., Herfort, L., Simon, H.M., 2013. Contrasting genomic properties of free-living and particle-attached microbial assemblages within a coastal ecosystem. Frontiers in Microbiology 4.

Smith, S., Bell, R., Kramer, J., 2002. Metal Speciation in Natural Waters with Emphasis on Reduced Sulfur Groups as Strong Metal Binding Sites. Comparative biochemistry and physiology. Toxicology & pharmacology : CBP 133, 65–74.

Tcherkez, G., Tea, I., 2013. 32S/34S isotope fractionation in plant sulphur metabolism. New Phytologist 200, 44–53.

Thode, H.G., Macnamara, J., Fleming, W.H., 1953. Sulphur isotope fractionation in nature and geological and biological time scales. Geochimica et Cosmochimica Acta 3, 235–243.

Trust, B.A., Fry, B., 1992. Stable sulphur isotopes in plants: a review. Plant, Cell & Environment 15, 1105–1110.

Werne, J.P., Hollander, D.J., Lyons, T.W., Sinninghe Damsté, J.S., 2004. Organic sulfur biogeochemistry: Recent advances and future research directions, in: Sulfur Biogeochemistry - Past and Present. Geological Society of America.

Wing, B.A., Halevy, I., 2014. Intracellular metabolite levels shape sulfur isotope fractionation during microbial sulfate respiration. Proceedings of the National Academy of Sciences 111, 18116–18125.

Chapter 4

DIVERSITY ON SOCIAL MEDIA: A CASE STUDY WITH THE WOMEN DOING SCIENCE INSTAGRAM

Phillips, A.A., Walsh, C.R., Grayson, K.A., Penney, C.E., Husain, F., Women Doing Science Team. Diversity on social media: A case study with the Women Doing Science Instagram. *In Prep.*

ABSTRACT

In the absence of real-life role models, female scientists portrayed in the media may enable young women to imagine themselves as future scientists. Relatable role models are therefore critical for the recruitment and the retention of young women in STEM (science, technology, engineering, and math) and may help improve long-standing racial and gender equity gaps. Both traditional and social media have the potential to expose women to role models, but their representations of women scientists typically reinforce, rather than challenge, gendered characterizations of scientists (e.g., showing women scientists as domestic, emotional, or subordinate). Women Doing Science was created by the authors in June 2018 to address this representation gap by sharing daily photos of international, diverse women in STEM with a description of their research, which often appear in bilingual captions. Since its founding, Women Doing Science has highlighted over 700 women scientists and has become a popular science communication platform with almost 100,000 followers from around the world – primarily women enrolled in undergraduate and graduate STEM degree programs. Here, we evaluate the success of the Women Doing Science Instagram page in portraying international women scientists with diverse racial identities and STEM backgrounds. Furthermore, we explore which aspects of posts (e.g., captions, photos, race, language) drive higher engagement from the audience. We find that

our Instagram audience has higher engagement with posts of women of color, bilingual posts, and posts that break stereotypes associated with women in STEM. Additionally, we find that women of color are more likely to include additional aspects of their identity in their biographies, and that a primary reason our audience follows the page is because of the diversity portrayed in the posts. These results imply the powerful potential for social media platforms like Instagram to host diverse role models for international audiences as they develop their STEM identities.

1 | INTRODUCTION

Internationally, women and minoritized racial and gender groups are underrepresented in science, technology, engineering, and math (STEM) fields (Botella et al., 2019; Shannon et al., 2019), despite the demonstrated benefits of diverse teams in innovation, problem solving, and other key aspects of scientific research(Hong and Page, 2004; Medin and Lee, 2012; Swartz et al., 2019; Hofstra et al., 2020). Recent studies point to the importance of role models for the development of STEM identity and subsequent retention in STEM of individuals from minoritized groups (Steinke, 2017), especially role models who share their gender (González-Pérez et al., 2020) or race (Johnson et al., 2019). Interactions with role models and mentors with intersectional identities are consistently invoked as a priority intervention in improving the diversity of the STEM workforce (McGee, 2019), especially for STEM graduate students. Such interventions have led to some improvements in the racial and gender diversity of STEM graduate students (National Academies of Sciences, 2018). However, women and members of minoritized racial groups remain underrepresented at higher levels (i.e., postdoctoral researchers and faculty). For example, even though female Earth and ocean scientists in the U.S. now earn more doctorates than their male peers each year (Bernard and Cooperdock, 2018), only 27% of U.S. geoscience faculty are women (Ranganathan et al., 2021). STEM fields have even more pronounced

inequities for Black and Hispanic students (Riegle-Crumb et al., 2019) and faculty (Li and Koedel, 2017).

In the absence of real-world mentors who share key aspects of their identities, STEM graduate students from underrepresented groups may find vicarious role models through socio-cultural representations of scientists, such as those in traditional media (e.g., television, movies, magazine; Fujioka, 1999; Steinke, 2017). Significant attention has therefore been given to the way scientists, particularly women in STEM, are portrayed in traditional media. Such women often suffer from stereotyped representations, depicted as subordinates or assistants to male scientists, struggling to balance familial and/or personal obligations, and with increased emphasis on their appearance, sexuality, and domestic qualities compared to their male counterparts (LaFollette, 1982, 1988; Nelkin, 1987; Steinke and Long, 1996; Elena, 1997; Steinke, 1999). For example, in a study of magazine articles, researchers found that the most common portrayal of famous marine biologist and author Rachel Carson was as an “emotional woman” (Losh, 2010). Online media platforms exhibit similar representation issues, with hypersexualized representations of women scientists and general displays of scientists as mostly male, white, able-bodied, middle class, and heterosexual (Mendick and Moreau, 2013). Reports also find that these underwhelming depictions of women scientists decrease aspiring female scientists’ continued interest in science and technology (Microsoft, 2017). Stereotyped and homogenous representations of scientists may therefore have a negative impact on the future diversity of the STEM workforce, perpetuating the underrepresentation of groups who cannot see themselves in the available images of STEM professionals (Steinke, 2017).

Studies have suggested that science educators can weaken these pervasive gender-related stereotypes by highlighting more examples of diverse scientists (Miller et al., 2015), especially via integration of narrative content (Arya and Maul, 2012; Hong and Lin-Siegler, 2012). Social media (e.g., Instagram, YouTube,

Facebook), rather than traditional media (e.g., magazines, film, television), may offer an improved outlet for depictions of women scientists, particularly for younger audiences who tend to prefer online, rather than traditional media, for content. Notably, social media allows individuals to post more frequently than traditional media, resulting in a higher volume of content that could host diverse examples of women scientists. STEM content is also generally growing on social media, with science related Facebook posts up 115% from 2014 to 2017 (Funk et al., 2017). Millions of people worldwide follow science-related pages, which demonstrates the capacity for STEM-related social media to reach wide audiences (Hitlin and Olmstead, 2018). Finally, although studies on the impact of social media STEM content are limited, initial studies have found links to reduced stereotypes: participants who viewed self-portraits ("selfies") of female scientists were less likely to perceive scientists as largely male (Jarreau et al., 2019).

There is a distinct need to deepen our understanding of the ability of social media to depict diverse women scientists and their potential role as vicarious mentors. Women Doing Science (www.instagram.com/women.doing.science) was created in 2018 to address this gap on social media. The movement was founded as an Instagram page with daily photos and biographies of diverse international women scientists and has since expanded to Twitter and Facebook. Since its founding, the Women Doing Science Instagram page (hereafter, Women Doing Science) has reached almost 100,000 followers from around the world and has profiled over 700 women scientists and engineers doing research in the lab, field, and office (Figure 1). Captions (~150-200 words) are submitted by the scientists in the third person, are edited by a Women Doing Science team member, and are often (~3 in 10) translated to a second language (Figure S1-2). The Women Doing Science team, which includes groups focused on translation, recruitment, and science writing, actively aims to showcase scientists with varying identities (e.g., race, location, field of study) to our audience of largely undergraduate and graduate women interested in STEM. In this study, we evaluate the success of Women Doing

Science in this goal, to determine whether our Instagram posts reflect a diverse, international community of women scientists. We also evaluate which aspects of Instagram posts drive higher or lower engagement from the audience and survey Women Doing Science followers for their perceptions of the page. Our results indicate that not only does the Women Doing Science Instagram page show racially diverse international women scientists, but audiences reward these posts with higher engagement and continue to engage due to the page's reputation for racial diversity and ability to inspire belonging in science. This implies the potential for social media, especially visual based platforms like Instagram, to host diverse vicarious role models for international audiences developing their STEM identity.

Figure 1 *Representative example images from the Women Doing Science Instagram page (www.instagram.com/women.doing.science). For caption examples see Figure S1-2. (A) Chemical oceanography PhD student Lauren Kipp (B) Developmental psychology PhD student Nicole Telfer (C) Astrophysics postdoctoral scholar Dr. Sarah Pearson (D) Computational neuroscience PhD student Hajer Nakua (E) Geology postdoctoral scholar Dr. Christine Y Chen (image credit: Kim Huppert) (F) Wildlife research scientist Kyla Garten (G) Conservation biology master's student Callie Veelen (H) Mathematics PhD student Anna Szczekutowicz (I) Junior Paleoartist Ylang Godefroit (J) Cosmochemistry PhD student Soumya Ray (K) Clinical microbiology postdoctoral scholar Ayesha Khan (L) Marine ecology PhD student Lucy Harding (image credit: Nosebroke Productions) (M) Archeological conservator Amanda Imai (N) Wildlife biology masters student Helvi Musdarlia (O) Geobiology PhD student Usha Lingappa (P) Analytical chemistry PhD student Anna Raysyan (Q) Population health science PhD student Nafisa Insan (R) Osteopathic medicine PhD student Lindsey Fitzsimons (S) Medicinal chemistry PhD student Shaneela Hussain (T) Astronomy postdoctoral scholar Dr. Marianne Heida (U) Astrophysics postdoctoral scholar Dr. Emma Osborne (V) Geophysics PhD student Celeste Labedz (W) Developmental biology professor Dr. Ellen Rotherberg (X) Marine biology PhD student Chelsea Bennice and (Y) Bioengineering PhD student Brenda Okereke.*

2 | METHODS

2.1 | Featured scientists survey

A survey designed to collect demographic information (e.g., age, race, field of study, country of origin) was sent to scientists previously featured on the Women Doing Science Instagram page via email. Reminders were sent periodically to encourage participation. The survey introduction stated that responses were voluntary and demographics questions were not mandatory and that respondents

could rescind consent for the use of their information at any time. Racial identity was queried in two ways. First, all subjects were asked whether they were a woman of color (WOC) or a Black or Indigenous woman of color (BIWOC) in two separate questions, allowing scientists to choose one, both, or neither. Responses were separated into BIWOC, WOC who are not Black or Indigenous (hereafter simply "WOC"), and non-WOC (those who responded "no" to each race-related question). We acknowledge that WOC and BIWOC are not universally accepted terms, but we chose to keep these broad self-identifications as more nuanced global racial categories are neither established nor accepted (Morning, 2015). Second, scientists in the United States were asked to report their race according to designated U.S. census categories (American Indian/Alaskan Native, Asian, Black or African American, Native American or other Pacific Islander, or White). Field of study categories were defined from subcategories of the NSF Survey of Earned Doctorates and were later aggregated in order to increase the statistical power of our analyses. Academic career stage was similarly collapsed into pre-graduate school, graduate education (including masters, dental, veterinary and medical students), postdoctoral researchers, and professor/staff scientists. Age groups were adopted following bins used by Instagram's built-in analytics. Finally, scientists were classified by their country of origin.

2.2 | Data from Instagram posts

Reach data (i.e., number of unique views, regardless of whether the viewer follows the Women Doing Science page) was retrieved manually from each post via the Instagram Analytics feature. The first 132 posts did not have reach data, as they were published before Women Doing Science was an Instagram business account, which enables account holders to view post analytics. The number of likes per posts were collected using Instamancer, an open-source project that pulls information about a user's posts from the Instagram public API (https://github.com/ScriptSmith/instamancer). Engagement was defined as the

number of likes divided by reach, a strategy similar to methods used in previous social media science communication studies (Amarasekara and Grant, 2019). This normalized engagement metric served as our primary dependent variable for the study. We did not normalize likes by followers as follower data over time was not available. Furthermore, posts on Instagram often have a significant number of views and likes by users who do not follow the given account as a result of Instagram's private feed and explore algorithms.

Captions from each post were also collected using Instamancer and manually parsed for mentioned themes: outreach, mentoring, STEM identity (*e.g.*, being a scientist, being a female scientist), science communication or policy, racial or ethnic identity (*e.g.,* being a Latina scientist), or the absence of any additional information (*i.e.*, only science). Bilingual captions were classified by language using the R textcat package (Hornik et al., 2013). These bilingual captions were excluded from thematic analyses, as adding in a translation often requires scientists to remove other content from their biography to fit within Instagram's character limit. Images were manually labeled based on the location of the first, featured photo (i.e*.,* field, office, lab, or blackboard) and whether the subjects of the photo were looking directly at the camera or whether the subject was actively "doing" science – a.k.a. an "action shot."

2.3 | Instagram followers survey

A second survey was developed for followers of the Women Doing Science Instagram page and was posted periodically to the account's "stories." Participants were informed that completion of the questionnaire was voluntary, and that consent could be withdrawn at any time. Following consent, participants were asked an identical subset of demographics questions as those to featured scientists, including race, age, and location. Next, survey participants were asked free-response questions regarding their engagement with the Women Doing

Science Instagram page. Finally, participants were asked to rank preferences on Women Doing Science posts and captions, for example, if they preferred to see posts of women scientists who shared their racial identity or who had a range of racial identities. They were also asked whether, following a Women Doing Science post, they ever followed the account of the featured scientist or attempted to communicate directly.

2.4 | Statistical analysis

All analyses were performed in R version 4.0.2 (R Core Team, 2020). Data was visualized across intersections of demographic variables with sufficient sample size: race, age, academic position, and field of study. Two-way ANOVAs (analysis of variance) were performed on normalized engagement data across all demographic variables to determine whether there were differences across categories. Significant main effects were further interrogated using Tukey's pairwise tests. Chi-square tests were applied to caption data to determine whether the proportion of posts explicitly mentioning each theme was different across respondent demographics. Follow-up pairwise proportion tests were performed with a Bonferroni correction for multiple comparisons. Additionally, normalized engagement was analyzed in a series of two-way ANOVAs using presence of a given theme and self-reported demographic variables as factors. Image content was analyzed in a similar fashion – a series of two-way ANOVAs were performed using location of first photo or interaction with the camera as the first factor and self-reported demographic variables. Women Doing Science posts were sorted by engagement and the top, middle and bottom 10% (n_{top} = 31, n_{middle}=27, n_{bottom} = 37) posts were extracted to identify which demographic characteristics drove minimum and maximum engagement. Chi-square tests were used to compare the proportion of demographics across each of the subsets.

Finally, responses from followers about why they follow the page were analyzed using a chi-square test to determine whether preferences about page content differed by race. Recurring topics in free response data from the audience were determined using the topic modeling algorithm *latent Dirichlet allocation* (Blei et al., 2003), which defines topics by defining recurring sets of words within documents. Separate topic modeling analyses were run for the reasons why followers liked the posts and why they followed the page. As some of the resulting topics from each model overlapped, the topics were manually inspected and refined to produce unique categories of themes in the responses. Once topics were defined using the whole sample of responses, individual responses were coded for the presence of the generated topics.

3 | RESULTS

3.1 | Featured scientists survey

The demographics survey emailed to scientists featured on Women Doing Science had 294 unique responses (~50% response rate). Although the survey questions spanned numerous aspects of identity (e.g., disability, sexual orientation, first-generation status), this study will present engagement results on categories with sufficient sample size for statistical analysis: age, race, academic position and field of study (Figure 2). Some survey respondents indicated non-binary gender identity – we will therefore generally refer to people who have been featured as scientists throughout this paper, although it should be noted that a majority identified as female. Survey results indicated that nearly three out of four (72%) featured scientists were graduate students (Figure 2a). Undergraduates accounted for 8% of features while postdocs were 11%, and professors and staff scientists were 9%, respectively. These proportions were similar for WOC, though BIWOC had a significantly higher percentage of graduate students (80%, Figure S3). The most frequent age group of featured scientists was 25-34, accounting for 75% of posts

(Figure 2b). An additional 16% of posts featured scientists aged 18-24, while 8% were 35-44, 1% were 45-54, and <1% were 55+.

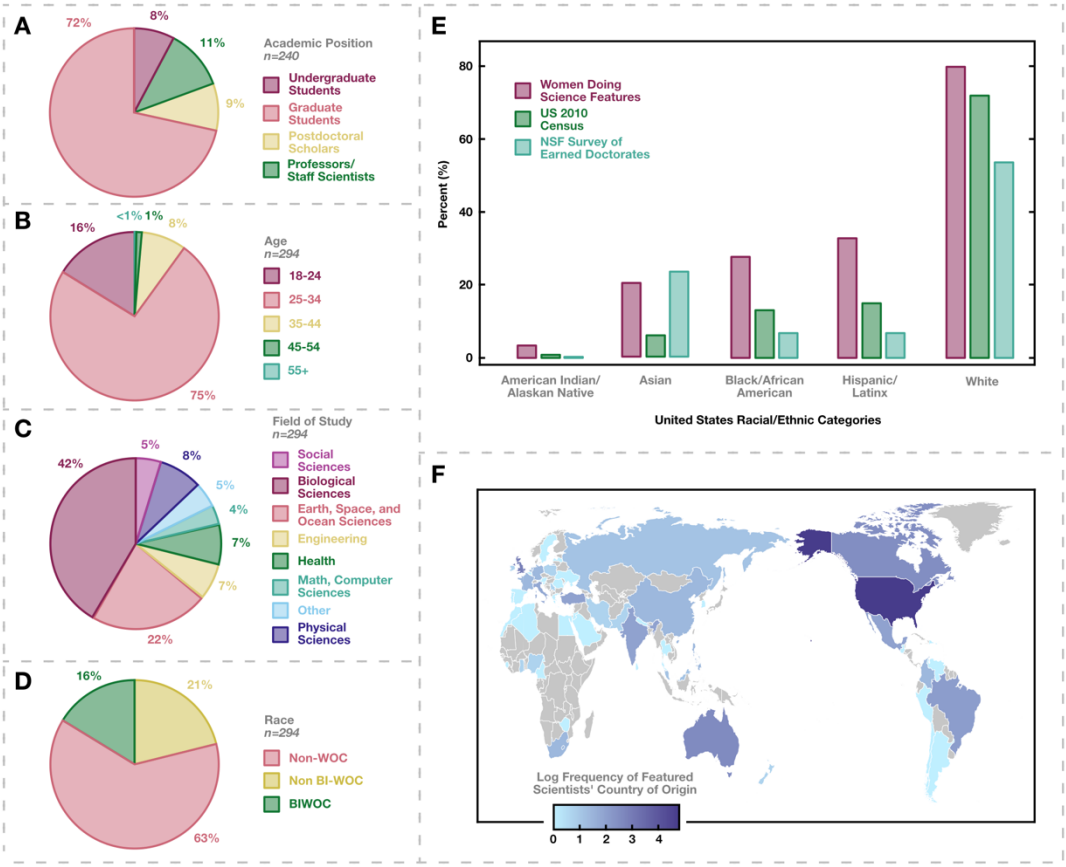

Figure 2 *Results from the demographic survey to scientists featured on the Women Doing Science Instagram page for (A) academic position (B) age (C) field of study and (D) race. (E) Race/ethnicity was also collected for participants from the United States by categories designated by the U.S. Census. Note that unlike the U.S. Census and NSF Survey of Earned Doctorates, respondents to our survey could select multiple racial categories. The magenta bars in (E) therefore sum to greater than 100%. Participants were also asked for their country of origin, with results displayed in a natural log (base e) frequency plot in (F).*

Respondents ranged across fields of study (Figure 2c), with 42% in biological sciences, 22% in earth, space, and ocean sciences, 8% in physical sciences, 7% in engineering, 7% in health and medicine, 5% in social sciences, 4% in mathematics and computer sciences, and 5% in other fields (e.g., education, communication, interdisciplinary studies). There were also differences between non-WOC, WOC, and BIWOC by field of study (Figure S4). Although the proportion of featured scientists in biological sciences was similar (~40%), there were fewer posts about Earth, space, and ocean scientists for WOC (16%) and BIWOC (13%) compared to non-WOC (26%). Both WOC and BIWOC had proportionally higher representation in engineering (11%) compared to non-WOC (4%). WOC had significantly higher proportions of features in health fields (13%) than BIWOC (2%) and non-WOC (7%) while BIWOC had higher representation in physical sciences, social sciences, and other fields (e.g., communication, humanities).

Many survey respondents were from the U.S. (40%, 119 posts, Figure 2f). However, location was generally geographically varied, with 66 unique countries of origin represented. Frequent countries included the UK (17 posts), Australia (12), Canada (12), Brazil (8), Mexico (7), and Turkey (7).

3.2 | Engagement across Instagram posts

Demographic information about our featured scientists was cross referenced with normalized engagement (number of likes divided by number of views). There were no significant differences in engagement across age, field of study, or academic position (Figure S5), even when separated by race (WOC, BIWOC, non-WOC; Figure S6; all $P>.05$). However, race showed a marginally significant effect on engagement, with numerically higher engagement for features of WOC and BIWOC versus non-WOC ($F_{(2,286)} = 2.53$, $P<.1$; Figure 3a). Further chi-square tests of top, middle, and bottom 10% of post engagement found there were differences of race across percentile group ($\chi^2_{(1,19)} = 34.247$, $P<.001$). Bonferroni-corrected

pairwise comparisons showed that there was a larger proportion of non-WOC than BIWOC in all percentile groups (P<.0001 for the bottom percentile group and P<.05 for middle and top) and greater than WOC in the middle (P<.05) and bottom (P<.001) percentile groups. There was no difference in proportions of BIWOC and WOC in any of the percentile groups (all P>.1). Additional follow up pairwise comparisons showed that WOC are more represented in top performing posts compared to bottom percentile posts ($\chi^2_{(1,22)} = 4.271$, P<.05), while non-WOC have a higher proportion of lower performing posts ($\chi^2_{(1,45)} = 34.247$, P<.1; Figure 3d), although these comparisons did not survive correction for multiple comparisons.

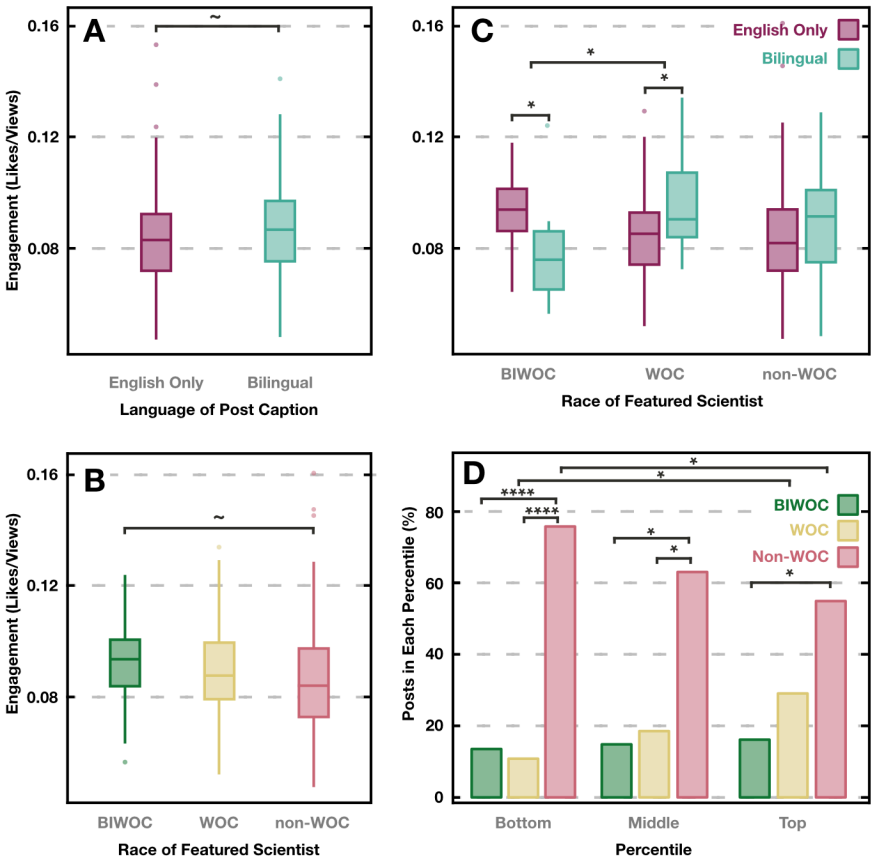

Figure 3 *Engagement of Women Doing Science Instagram posts across (A) language (English only versus bilingual captions) and (B) race (BIWOC, non-BI WOC, versus non-WOC). (C) Engagement across the intersection of race and*

*language. WOC had higher engagement for bilingual posts, but posts of BIWOC had the opposite trend. (D) A breakdown of the bottom 10%, middle 10% and top 10% of posts and their relative proportion of BIWOC, WOC, and non-WOC in each percentile. The proportion of WOC increases from bottom to top percentiles while non-WOC decreases. For all figures ~ indicates P<.1, while * is P<.5, ** is P<.01, *** is P<.001, and **** is P<.0001.*

Bilingual captions, which accounted for 30% of posts, spanned 29 languages. Spanish was the most frequent, with 44 posts. Other romance languages were also common, especially French (17 posts), Portuguese (15) and Italian (9). Other frequent bilingual posts were in Turkish (14), Mandarin (13), German (11), and Arabic (10). Bilingual posts showed a marginally higher engagement than monolingual posts ($t_{(330.58)} = -1.78$, $P<.1$).

It is important to consider, however, that these two effects might interact. When the language of the posts and the race of the featured scientists were entered into a 2x2 ANOVA, there was a significant language by race interaction ($F_{(2,283)} = 3.997$, $P<.05$). Follow-up simple main effect tests revealed that bilingual posts had higher engagement than monolingual posts for WOC ($F_{(1,59)} = 5.182$, $P<.05$), while posts of BIWOC showed the opposite effect, with higher engagement for monolingual posts ($F_{(1,45)} = 5.798$, $P<.05$). There was no difference between monolingual and bilingual posts for non-WOC. However, these effects were not significant after applying multiple comparisons corrections.

Caption content varied by racial identity (Figure 4a). Separate chi-square tests identified differences across race for mentioning outreach ($\chi^2_{(2,199)} = 20.77$, $P<.001$), mentoring ($\chi^2_{(2,165)} = 14.248$, $P<.01$) and racial/ethnic identity ($\chi^2_{(2,199)} = 35.23$, $P<.001$). Follow up Bonferroni-adjusted pairwise proportion tests revealed that BIWOC were more likely to mention outreach ($P<.01$), STEM identity ($P<.0001$) and racial/ethnic identity ($P<0.05$) than WOC. Similarly, BIWOC were

more likely to mention outreach (*P*<.001), mentoring (*P*<.01), STEM identity (*P*<.0001) and racial/ethnic identity (*P*<.0001) than non-WOC. In contrast, posts of non-WOC compared to BIWOC more frequently only discussed science (*P*<0.05). Despite the heterogeneity of caption themes across race, there were no significant effects on engagement (Figure 4b, *P*>.1).

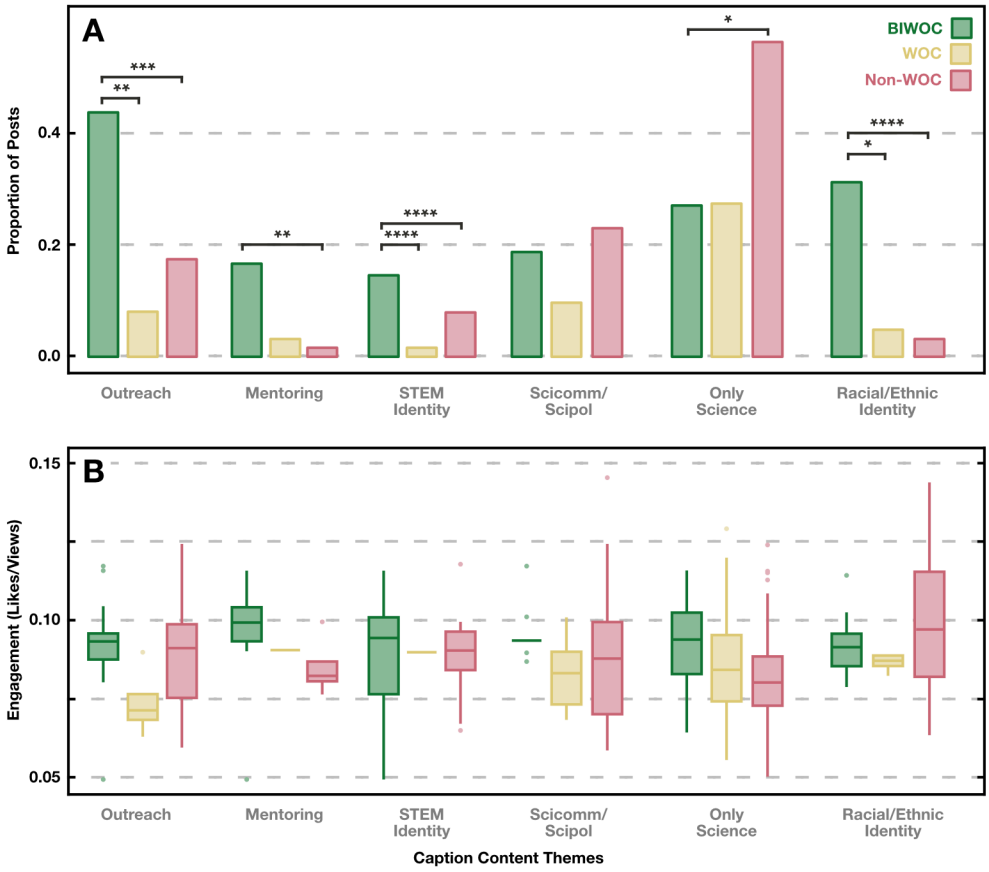

Figure 4 *(A) Frequency and (B) Engagement of Women Doing Science Instagram posts by aggregated caption themes. Proportions reflect the fraction of individuals of a given race who included the respective theme in their post caption. A significantly higher proportion of BIWOC compared to both non-WOC and WOC discussed themes of outreach, STEM identity and racial/ethnic identity, compared to non-WOC discussed mentoring. In contrast, a significantly higher proportion of non-WOC compared to BIWOC only discussed their science, as opposed to any*

*additional aspects of their identity. In contrast, there were no differences in audience engagement across race or topic. For all figures ~ indicates P<.1, while * is P<.5, ** is P<.01, *** is P<.001, and **** is P<.0001.*

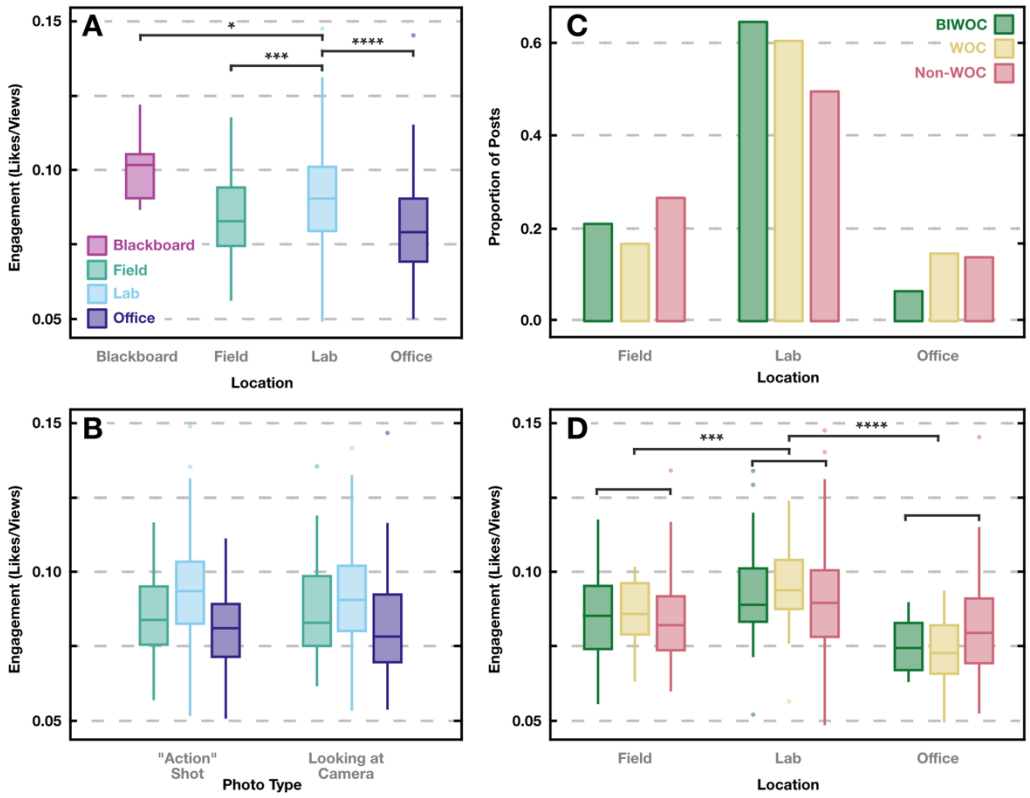

Figure 5 *Engagement of Women Doing Science posts where main photos varied by (A) location and (B) type. Blackboard photos had higher engagement than field photos while lab photos had higher engagement than both field and office photos. Action shots versus looking at camera photos had no significant difference. (C) Proportion of posts by location type for BIWOC, WOC, and non-WOC and (D) their engagement. No new effects were found at the intersection of race and location - only main effects found in (A) were reproduced in (D). For all figures ~ indicates P<.1, while * is P<.5, ** is P<.01, *** is P<.001, and **** is P<.0001.*

Photo locations showed a significant effect on engagement ($F_{(3,474)}$ = 11.332, *P*<.001; Figure 5a), with follow-up Tukey tests showing that scientists at the

blackboard receive higher engagement than photos in the lab ($P<.05$), while photos in the lab outperformed photos in the field ($P<.001$) and office ($P<.0001$). There were no significant differences between action shots and photos where the scientist looks directly at the camera, even across locations (Figure 5b). Proportions of racial identities represented in field, lab, and office posts showed no significant differences by race ($\chi^2_{(6,478)} = 8.547$, $P>.05$; Figure 5c). Similarly, there was no significant race by location interaction effect for engagement (Figure 5d), suggesting that the main effects from Figure 5a did not differ based on the race of the featured scientist.

3.2 | Instagram followers survey

Instagram's business analytics feature was used to understand the basic metrics of the Women Doing Science audience. At the time of study, the Instagram page had 94,490 followers, with 37.3% in the United States, 6.2% in Brazil, 6.1% in India, 4.2% in Mexico, 4.1% in Canada, and the remaining 42.1% distributed between other countries. 83.6% of followers were women and 16.4% were men, with a majority of both men and women between ages 25-34 (50% of followers). Other age categories included 18-24 (25%), 35-44 (16%), 45+ (8%) and 13-17 (1%). We received 259 unique responses to our survey to Women Doing Science Instagram followers survey. 112 respondents were from the United States (43%). Most respondents were between 18-34 years old, matching the demographics of the follower base. Of the response, 24% were WOC and 4% were BIWOC. A majority (>95%) of respondents were female.

Most respondents indicated that they often or always read the captions and "like" Women Doing Science Instagram posts (Figure S7a-b). Over 50% indicated that they have followed a scientist after seeing their feature on Women Doing Science (Figure S7c). Additionally, 9% of respondents have attempted to contact a featured scientist (Figure S7d).

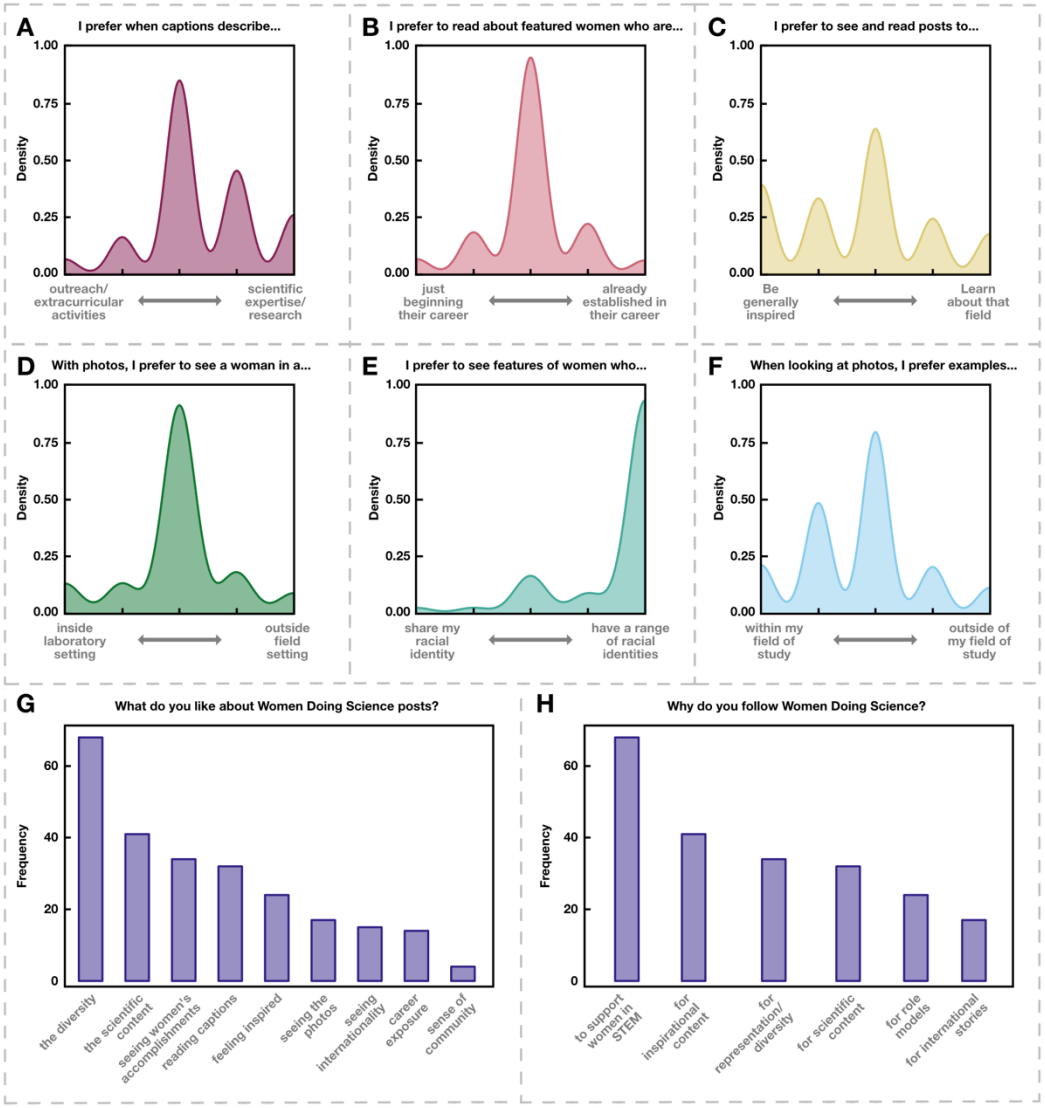

Figure 6 *Results from the survey sent to Women Doing Science Instagram followers. Respondents were asked to rank their preference between two options for a series of questions about engaging with posts' photos and captions (A-F). Participants indicated they were slightly more likely to prefer reading about scientific research over outreach (A), no preference between reading about established versus entry-level scientists (B), no preference between reading for general inspiration over field-specific knowledge (C) no preference between photos of women in the lab versus the field (D), significant preference over seeing women with a range of racial identities rather than sharing the participant's racial*

identity (E) and slight preference so seeing photos from women in the participant's field rather than outside of it. Prior to these specific rankings, participants were asked for free responses to (G) why they like Women Doing Science posts and (H) why they follow Women Doing Science. Responses were grouped by theme and ranked by frequency.

Participants were also asked for free response answers to why they engaged with Women Doing Science posts and why they followed the page. Respondents most often responded that they liked how Women Doing Science posts were diverse, followed by the scientific content, seeing women's accomplishments, reading captions, and being generally inspired (Figure 6g). For reasons they followed Women Doing Science, participants more often mentioned "to support women in STEM," followed by themes of inspiration, diversity, science content, role models, and a sense of community (Figure 6h). Following the free-response section, participants ranked their preference between two options for post/caption content (Figure 6a-f). Participants overwhelmingly preferred to see features of women with a range of racial identities, although a chi-square test identified differences in preference across race ($\chi^2_{(8,234)} = 18.01$, $P<.05$). Specifically, BIWOC were more likely to prefer features of women who share racial identity than non-WOC ($\chi^2_{(1,226)} = 4.631$, $P<.05$). Participants of all races slightly preferred captions describing scientific research over STEM outreach and photos from their field of study over outside of their area. Participants reported no preference between reading about established versus new scientists, seeing photos from a lab versus the field, or reading content for general inspiration or field-specific knowledge.

4 | DISCUSSION

4.1 | Women Doing Science displays diverse, international scientists

Every scientist's story is unique – as noted by a respondent in Kitzinger (2008)'s survey of what female scientists desired from women in STEM in the media: "*you*

can't just have one image that would do everything, and one representation that would solve all the problems." Women Doing Science's aim in representing diverse scientists is to showcase as many individual experiences in STEM as possible and to build an increasingly representative landscape of potential role models for aspiring or current scientists. According to the possible selves theory of identity development, seeing role models who share key aspects of individuals' identities enable individuals to see themselves as potential scientists (that is, to develop a STEM identity), which in turn can motivate behavior and influence career aspirations and selection (Markus and Nurius, 1986; Strahan and Wilson, 2006; Steinke, 2017). It is therefore critical to the goals of Women Doing Science to span diverse identities – across the intersections of career stage, field of study, geography, language, and race.

4.1.1 | Career stage

A majority of featured scientists were graduate students (Figure 2a), reflecting the audience of both Women Doing Science and Instagram itself: young adults aged 18-34, a typical range for masters and doctoral students. Although increasing the diversity of career stages seen on Women Doing Science, particularly at the faculty level, could potentially provide more aspirational role models, there are numerous benefits of primarily showcasing graduate students. The level of commitment, knowledge, and experience in STEM required to undertake graduate study is sufficient to inspire young scientists, whilst remaining an attainable goal. Followers of Women Doing Science indicated that they do not necessarily prefer to see only posts of established career scientists, equally enjoying the stories of scientists beginning their careers (Figure 6b). One survey respondent said, in reference to why they follow Women Doing Science: "*Often when you hear of women in STEM they are of exceptional stories (e.g., Madam Curie) that can be difficult to relate to.*" Sociological research has demonstrated the importance of this perceived feasibility for women developing their STEM identity (Steinke, 2017). Graduate

students may therefore be more effective, vicarious role models in social media spaces than established, tenured faculty, who are more frequently represented in traditional media. Further, adversity faced by faculty members decades prior to their success may no longer be relevant challenges to current students. In addition, graduate student populations are more racially diverse across fields than higher career stages (Liu et al., 2019; American Council of Education, 2019). This is evident in our dataset, with a higher proportion of BIWOC graduate students compared to WOC and non-WOC (Figure S3). Largely featuring graduate students therefore allows Women Doing Science to represent a more racially diverse set of scientists on social media.

4.1.2 | Field of study

Featured scientists on Women Doing Science span academic fields of study, although with clear biases towards disciplines with higher proportions of female graduate students, such as biological sciences and Earth, space, and ocean sciences (National Science Foundation, 2018). The racial diversity of scientists in these frequently featured fields also reflects disciplinary biases. For example, 26% of featured non-WOC are in Earth, space, and ocean sciences, in comparison to 16% for WOC and 13% for BIWOC. Earth, The geosciences are the most white-dominated STEM discipline, with BIWOC just 1.5% of U.S. female PhD earners (Bernard and Cooperdock, 2018). Women Doing Science's order-of-magnitude higher proportion is the result of a deliberate effort, inspired by the numerous team members who are geoscientists, to actively recruit Black and Indigenous women to submit their biographies. For Earth, space, and ocean sciences there is the additional benefit of increased connections through efforts of other active social media accounts like Diverse Geologists, Geo Latinas, and Black in Geoscience. Women Doing Science also sporadically hosts "themed weeks" aimed at specific fields of study that are underrepresented in our posts: for example, "Women in Robotics," "Women in Computer Science," and "Women in Science Policy." These

targeted pushes help balance the steady supply of biologists and Earth scientists that would otherwise more thoroughly dominate Women Doing Science posts.

4.1.3 | Geography and language

Although the relative number of featured scientists from outside the U.S. is low, Women Doing Science posts span 66 countries, representing significant geographical diversity. Given the international diversity of Women Doing Science features, it is unsurprising that post captions also spanned significant language diversity. English has been termed the language of science (Gordin, 2015), but it is not necessarily the most effective language for science communication (Márquez and Porras, 2020). The Women Doing Science team actively seeks to highlight this international diversity by encouraging scientists to translate their biographies. For scientists who wish to translate their biographies but need assistance to do so (*e.g.*, those that speak the language, but do not write in it), the Women Doing Science team includes volunteer translators for Arabic, Farsi, French, German, Hindi, Italian, Mandarin, Portuguese, Spanish, and Turkish. Due to the popularity of Women Doing Science in Latin American countries, the translations team developed submission forms in Spanish and Portuguese, our two most frequent languages and created an Instagram account, Mujeres Haciendo Ciencia (@mujeres.haciendo.ciencia), for posts solely in Spanish and Portuguese. These efforts seem to have tangible effects for those seeking vicarious role models. One audience survey respondent indicated that they follow Women Doing Science because it "*Inspires me that despite all the discrimination and machismo we live in (in Mexico) I can achieve a job like the one you show. That was always my dream but in Mexico you can't expect that if you are a woman.*" Another follower, aged 13-18 from Turkey, mentioned "*Ever since I started following your Instagram I have been more passionate about becoming a scientist. In our country, even though they are very talented, many women are reluctant to choose a career in STEM because they are oppressed by the hidebound society*."

Such responses demonstrate that in representing internationally diverse scientists, Women Doing Science is successfully expanding the range of “possible selves” for young women developing their STEM identity.

4.1.4 | Race and ethnicity

WOC and BIWOC accounted for about one third of Women Doing Science posts (Figure 2d). The geographically specific construction of race makes it hard to evaluate our success in displaying diversity, particularly based on these broad categories. However, our data from U.S. scientists can be leveraged for direct comparisons, such as to the U.S. Census and NSF Survey of Earned Doctorates. Women Doing Science overrepresented minoritized racial groups compared to both metrics, with higher proportions of Black/African American, Native American/Native Alaskan, and Hispanic/Latinx scientists. Notably, Asian American populations in STEM match or exceed their proportion in the U.S. population and are not considered underrepresented by the NSF. The proportion of Asian Americans featured by Women Doing Science exceeds the proportion in the U.S. population, but not the proportion of doctoral degree earners. Both our analysis at the global scale, with 37% of featured scientists identifying as WOC (16% BIWOC), and our comparison of more specific racial and ethnic identities to US census and NSF data, suggest that Women Doing Science posts are racially diverse. It is critical to clarify that this racial diversity is not accidental. Recruitment efforts by the Women Doing Science Diversity team are active and persistent: in periods where our reach lapses, white women dominate the open submissions portal. Features of white women are also purposefully scheduled further behind in the queue to allow space for posts of WOC and BIWOC. Finally, the Women Doing Science team itself is racially diverse; recruitment often starts within a member’s own social media network. Interestingly, this racial diversity impacts caption content significantly: WOC and BIWOC are more likely to mention non-science aspects of their identity in their biographies. Actively choosing to include more than

just their science expands their self-depiction, highlighting the multifaceted nature of identity and providing more aspects for followers to relate to.

4.1.5 | Summary

Women Doing Science posts feature predominantly graduate students from around the world, with significant proportions of non-white scientists. As a case study, Women Doing Science demonstrates the potential for targeted efforts to successfully highlight racially diverse, international women in STEM. Overrepresentation of marginalized groups on social media can inspire a changing view of what a scientist looks like, strengthening the range of visibly attainable STEM identities. The successes and limitations of Women Doing Science also serve as a lesson for other areas of STEM, such as faculty hiring, where active effort in recruitment may alleviate racial gaps. It is crucial that academic systems rise to this challenge, hiring faculty with multifaceted identities to serve as role models for young scientists. By proactively choosing to represent a vision of how the science community *could* look, as opposed to reinforcing existing systems of oppression and marginalization, faculty hiring boards and academic institutions have the potential to provide in person connections to relatable role models for diverse early career scientists. Until this occurs, social media platforms such as Women Doing Science will continue to represent an important, alternative source of vicarious role models and vision for the future of STEM.

4.2 | Instagram audiences reward and seek posts of diverse women in STEM

With the knowledge that Women Doing Science does highlight diverse and international women in STEM, we turn to investigating patterns of engagement from Instagram audiences. The popularity of the page (~100,000 followers) suggests that Women Doing Science fills an important niche in STEM representation on social media. Our audience survey indicated that Women Doing Science followers would most likely reward diverse posts with higher engagement:

"representation/diversity" was cited as the third most frequent reason respondents followed the Instagram page and the most frequent driver of why they "like" Women Doing Science posts (Figure 6g-h). Further, the most skewed response to targeted questions about post content was on racial diversity, with a majority of respondents indicating that they preferred to see photos of women with a range of racial identities (Figure 6e). Interestingly, the definition of "diversity" in free response answers varied, with some citing field of study ("*What struck a chord is the diversity of women that I see here. I had no idea about some of the fields before Women Doing Science*"), some mentioning location ("*I like how diverse the science is… I want to leave my country to get better conditions in science"*) and others citing racial diversity ("*Growing up I never saw WOC in the sciences, it's very empowering to see what other women are doing*") There is no one definition of diversity to Women Doing Science followers – rather they seek posts that represent the multitude of identities expressed across women in STEM.

This nuanced definition of diversity, such as across the intersection of geographic and racial identities, is evident in broad patterns of engagement of Women Doing Science posts. While race and caption language had marginally significant trends, with posts WOC and BIWOC having higher engagement than non-WOC and bilingual captions higher than monolingual captions (Figure 3a-b,d), more significant interactions were found when groups were not aggregated. For instance, for WOC, bilingual posts significantly outperformed those in only English, but for BIWOC the trend was reversed (Figure 3c). Broadly, this demonstrates the complex effect of racial identity and the benefit of studying groups with even the simplest divisions (*i.e.*, Black and Indigenous women versus other WOC). It is possible that these engagement trends suggest different needs of international audiences for social media STEM representation, where U.S. followers that speak English are perhaps more likely to reward posts of BIWOC, whereas non-U.S. followers might engage more with bilingual posts of WOC. Notably, a majority

(64%) of featured BIWOC were from the United States, compared to 25% for other WOC, which may be another influencing factor.

There is also evidence that our audiences view these representations of women in STEM as vicarious role models. Over 50% of followers indicated that they "followed" a featured scientist on Instagram after seeing their post, while 9% indicated they took the increased effort to reach out to the person directly. "Inspiration" and "role models" were also commonly cited as a reason for liking or following the Women Doing Science page (Figure 6g-h). Several audience responses specifically noted the power of the images of women in STEM in helping them feel more secure in their STEM identities: "*Women Doing Science helps with imposter syndrome on bad days*", "*I have no adult that took the STEM path to look up to and understand my options in the future*" and "*Sometimes I need extra encouragement from fellow women who are walking the same path"*. Some explicitly mention role-models, for example: "*I never knew I could have women role models in STEM.*" Similarly, others reported that they follow Women Doing Science to "*feel a greater sense of belonging*", "*have female role models in science*" and to "*feel less alone*."

Women Doing followers not only reward posts of diverse scientists but also seek out diverse scientists in their general social media experience. These narratives add to studies that highlight the power and importance of vicarious role models to cultivate a sense of belonging in STEM (Schmidt and Nixon, 1996; Geena Davis Institute on Gender in Media, 2018). Previous studies of STEM identity development have primarily focused on adolescent girls (Thompson and Windschitl, 2005; Hughes et al., 2013; Tan et al., 2013). However, initial results indicate that for racially diverse doctoral students, being able to recognize key parts of their identity in socio-cultural representations of professionals is just as important to their STEM identity as recognition by others (Herrera et al., 2012). The continued need for inspiration and the higher engagement with diverse potential

role models from our audience of those largely already committed to science highlights the fragility of STEM identity beyond adolescence.

4.3 | Viral posts reflect reactions to STEM stereotypes

Studies have shown that virality of online media is driven by emotional response: posts that spark either high positive arousal (i.e., awe) or high negative arousal (i.e., anger) are much more likely to go viral than other content (Berger and Milkman, 2012). We observed that viral posts on Women Doing Science followed similar trends. High positive or negative arousal were evident in comments, reflecting awe or anger at women who defied or conformed to gendered STEM stereotypes.

Traditional media persistently portrays scientists as stereotypically masculine (*e.g.*, intellectually objective, physically strong, emotionally detached; LaFollette, 1988). Women in STEM are typically presented as passive, dependent, emotional, and more interested in pursuing romance, appearance, or a family than a career (Chimba and Kitzinger, 2010). Unsurprisingly, these gender stereotypes have been shown to decrease young women's interest and participation in STEM (Steinke, 2017; Starr, 2018). These effects are felt beyond adolescence. A recent study surveyed female STEM students and professionals on their ideal portrayal of women scientists in the media and found that images which challenged stereotypes were preferred, opposing the common false dichotomies which portray female scientists as either "frumpy or "sexy," "overly emotional or cold," or "victimized or bitchy" (Chimba and Kitzinger, 2010). Gender schema theory suggests that children organize information about gender in networks of knowledge that influence how they later interpret new information (Liben and Signorella, 1993). These schemata become particularly active when gender is made salient, further emphasizing the stereotyped incompatibility between femininity and success in STEM (Steinke, 2017). Further, most depictions of

scientists in the media do not include people of color. A study analyzing scientists and engineers in popular films from 1991 to 2001 found that some progress has been made on gender parity in recent decades, but nearly three-fourths of scientists were white (Steinke, 2005).

In Women Doing Science posts, we see a trend in which followers "reward" (i.e., engage more with) posts of scientists in traditionally masculine settings and "punish" posts where scientists are depicted as feminine. Broadly, this is manifested in higher engagement for posts at the blackboard or in the lab compared to the field or office (Figure 5). Field photos, such as geologists outside and marine biologists underwater (e.g. Figure 1e,l,x), likely have lower engagement because these disciplines have gender parity at the graduate level (NSF 2018) and posts therefore do not arouse adequate stereotype nonconformity for viewers. Field photos may also have lower engagement due to photos being closer to landscapes than portraits—a study of one million Instagram posts found that visible faces were a highly significant driver for post likes (Bakhshi et al., 2014). Photos of the lab outcompeting photos of in the office may relate to challenging themes of women portrayed as domestic or assistants (Downs, 1981; Moseley and Read, 2002). To further examine the relationship between followers punishing or rewarding stereotypes on Women Doing Science we turn to three "viral" posts, which we define as having a much higher number of likes/comments and >~50% views from non-Women Doing Science followers. Two of these posts sparked high positive arousal through shattering of stereotypes, while the third provoked anger by conforming to typically feminine attributes.

As a first example, a postdoctoral scholar studying computational astrophysics was featured on the Women Doing Science page. She was seen at an oversized lecture-style chalkboard filled with complex equations (Figure 1U). Within hours the post had been viewed by thousands, reaching 7,236 likes (top 1 percentile of posts). Comments reflected the positive emotional arousal of viewers ("*Nice to see*

another astronomer. I admire how you bring the field so much closer to everyone", "*We need more women like this*"). Post viewers rewarded this image of a female scientist confidently standing before a sea of equations, an image that usually conjures white, male mathematicians (e.g., Will from the film *Good Will Hunting* or the famous physicist Richard Feynman). In the context of our previous discussion, it is unsurprising that posts like this one, where scientists are seen at a blackboard as a stark counter to STEM stereotypes, have the highest engagement of any Women Doing Science posts (Figure 5a).

A second viral post, which reached 5,107 likes (top 1 percentile of posts), featured a tenured biology professor in her office, surrounded by stacks of messy papers (Figure 1W). Her biography mentioned the difficulties faced as a scientist in the 1950's, "*...science was an uphill battle, but her supportive family nourished her scientific career.*" She ends her description with a direct quote, rare in Women Doing Science posts: "*It is important to be driven by deep love and inexhaustible curiosity, no matter your gender.*" The presentation of a female scientist as profoundly undomestic was mentioned by multiple viewers in the comments (e.g., "*I love how messy her office is. It gives me inspiration because I'm the same"*), although most were generally inspired and deferential, calling her a "*powerful woman of STEM"*, "*a legend"*, and even "*a rockstar!!"*. This featured professor conjured admiration by breaking stereotypes, discussing familial support in an additive rather than subtractive way and calling on traits of scientists to be specifically non-gendered.

Both above posts went viral due to the positive emotional response from the audience, who viewed these women as "trailblazers." These images of women in STEM in traditionally masculine spaces may boost the STEM identities of those partially committed to science careers, such as graduate students. However, followers of Women Doing Science, who are mostly young adult women in STEM, also punish posts where scientists are displayed as too feminine. Pictures of

women in the lab with visible makeup, with their hair down, or wearing heels often face comments about their appearance or harassment about safety procedures (note that all featured scientists are asked to confirm that they are wearing appropriate PPE for the setting where they are shown). In an extreme example, a post of a biology PhD student in the lab received so much harassment, both in the comments and in her own direct messages, that it was necessary to temporarily remove the post from Instagram. The most inflammatory comments were deleted, but those remaining highlight the anger invoked by her images: "*High school students will think this is the norm. Do we want to pass on unrealistic and potentially unsafe procedures to future researchers?*", "*Really? That is how we are showing women in the chem lab? High heels, open, long hair? Because being pretty is important!...This isn't reality!*", "*The lab can be a runway sometimes…*"

Such comments reflect the complex and fragile relationship women in STEM have with how to present themselves and choices they feel forced to make about their appearance, from which male scientists are exempt (Kitzinger, 2008; Chimba and Kitzinger, 2010). These patterns are not unique to Instagram: a study of science communicators on YouTube found that female hosted channels received higher engagement on videos, but at the cost of more frequent comments on their appearance (Amarasekara and Grant, 2019). Other studies have found that the more people rated a woman as attractive, the less likely they believed her to be a scientist (Banchefsky et al., 2016). Frustratingly, this reinforces the exact false dichotomy (i.e. beauty versus brains) many women in STEM wish to eradicate from the media (Chimba and Kitzinger, 2010). Scientific expertise and attractiveness are not mutually exclusive, but continued stereotyping of women in STEM in the media will reinforce gender schemas that imply otherwise. Notably, some followers of Women Doing Science immediately pushed back against this viral post's negative comments: "...*If you think that curled hair, heels, and makeup detract from the quality of her science then I think you need to update your idea of what a scientist looks like", "Just be yourself! Love the look, love the heels… you're intelligent and*

beautiful". Women Doing Science's goal will always be to represent the many realities of what scientists can look like. These counter comments offer hope that many women in STEM can set aside gender schemas and accept the diversity and individuality of their peers.

5.0 I CONCLUSIONS

The diversity of what women want to see in scientists is as diverse as the women themselves. No one representation will ever be sufficient to encompass all identities. Here, we have shown that Women Doing Science contributes a much-needed platform on social media: a place for diverse women to express their individuality as scientists. We hope these posts expand the range of possible selves for women developing their STEM identities and that lessons from this Instagram project assist other projects in diversifying STEM spaces.

ACKNOWLEDGEMENTS

We would like to specifically thank other Women Doing Science team leaders: Peter Martin, Ana Rita Moreira, Carolina Geoffrey, and Luisa Duque. We are grateful to the incredible followers of Women Doing Science for their support and encouragement and the 700+ scientists who have been featured on the page. We thank Associate Professor Julie Posselt for her informative conversations on survey design and data interpretation. We thank Professor Alex Sessions and members of his lab group for conversations throughout the project.

SUPPORTING INFORMATION

@nafisa_insan is a PhD student in population health sciences at Newcastle University and an ESRC NINE DTP studentship award holder. Nafisa's research focuses on maternal mental health during and after pregnancy in Bangladesh. She aims to understand the barriers, attitudes and views towards mental healthcare for pregnant women within rural areas of Bangladesh, and the social determinants of maternal depression. She has completed a systematic review and meta-analysis on social determinants of antenatal depression in South Asia, with the next step comprising of fieldwork for data collection. This process will include conducting interviews with pregnant women and healthcare providers in Bangladesh. Nafisa will then use quantitative and qualitative methods to determine potential associations and understand any underlying mechanisms. Her goal is to improve maternal healthcare in low- and middle-income countries by creating evidence-based interventions and programs for maternal mental health within low-resource settings. This will involve producing appropriate screening tools, training healthcare providers in screening, diagnosing and treating pregnant women with mental health concerns, and collaborating with organizations to create change in policies and healthcare systems. Nafisa also writes a blog on her PhD journey, providing useful insights into life as a South Asian female PhD student.

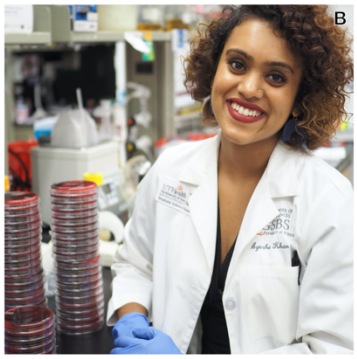

Ayesha Khan, PhD, (@wokescientist) is an infectious diseases scientist & grassroots activist studying antibiotic resistant superbugs while bridging science with social justice. Antimicrobial resistance is the greatest modern public health threat with over 1 million annual deaths, impacting marginalized communities the most, and is set to become the #1 global cause of death by 2050 (CDC, WHO). As a clinical microbiologist, she specializes in the diagnosis of infectious diseases. Ayesha develops accurate and rapid diagnostics that detect emerging pathogens and antibiotic resistant superbugs and find innovative therapies against superbugs in infected patients.This is not only critical in outbreaks, but early detection of superbugs ensures patients receive the right therapy, and aids in curbing global spread. Ayesha works on COVID-19 testing on the frontlines. The second photo shows her excitement from securing COVID tests for her patients. Ayesha also serves as a lead organizer in racial justice movements. The third photo is her leading a protest for Black lives in the Texas Medical Center. Shortly after, Ayesha co-founded the Medical and Science Coalition for Activism with a collective of scientists and health professionals to tackle racism in healthcare and academia. As an Indian Muslim, Ayesha's science is rooted in her community's fight for liberation.

Lucy Harding (@instaloosey) is a 2nd year PhD student at Trinity College Dublin. Lucy's research interests are thermal ecology and ecophysiology with a focus on linking behavior and physiology to the thermal niches of fish. She plans to utilize several research approaches throughout the course of her project such as comparative analyses of large, published datasets to investigate the thermal ranges of ectothermic (cold-blooded) and regionally-endothermic (warm-blooded) marine fish. She also plans to tag marine fish in the wild to explore the thermal range and behavior of ectothermic fish species and conduct lab-based respirometry experiments to study the links between physiology and thermal range of fish. Lucy has worked with collaborators @btwaves in The Bahamas and Cape Cod to tag tiger sharks and blue sharks. The data she collected will provide an insight into the intimate lives of these amazing creatures and will allow her to understand what drives these animals' thermal preferences. Lucy's research is supervised by Dr. Nicholas Payne, as part of The Payne Lab (@thepaynelab).

Figure S1 *Examples of Women Doing Science posts with English only captions, shared with permission from the featured scientists. (A) population health science PhD student Nafisa Insan (B) clinical microbiology postdoctoral scholar Ayesha Khan (C) marine ecology PhD student Lucy Harding.*

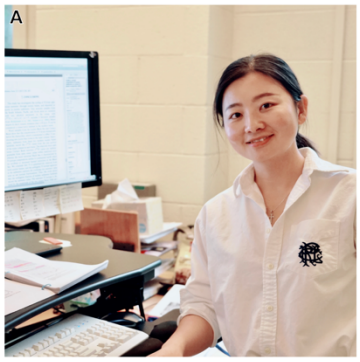

Cheng Cao (@applehekou) is a PhD student in geology at University of North Carolina, Chapel Hill. Her research focuses on the geochemistry of marine carbonate (mostly composed of the mineral calcite). Studying marine minerals left behind in sediments allows Cheng to understand global oxygen content in the past ocean. Climate change has driven the modern ocean to lose 2% of its dissolved oxygen. Ocean models predicts a further 7% loss of dissolved oxygen by the end of this century. To better understand the future, Cheng says we must look to the past. Using geochemical proxies like rare earth elements and isotopes, Cheng tells stories of how the ocean lost oxygen and recovered millions of years ago. She recalls a summer internship at MIT as a pivotal moment for her passion in earth science. "I was the only Chinese undergrad, with no independent research experience. But as I started to delve into the internship I realized, for the first time, how much fun research is."

Cheng Cao（@applehekou）是一名来自北卡罗来纳大学教堂山分校的地质学博士生。 她通过研究沉积物中留下的海洋碳酸盐来了解古海洋中的溶解氧含量。全球气候变化已经让现代海洋失去了2%的溶解氧。同时，已有的海洋模型预测：到本世纪末，海洋中溶解氧的含量将进一步减少7%。为了更好地了解未来，我们必须回顾过去，Cheng说。 通过使用稀土元素和同位素等地球化学手段，Cheng研究了数百万年前海洋如何失去氧气并恢复的过程。 她回忆起在麻省理工学院的暑期实习，那是激发她对地球科学产生浓厚兴趣的关键时刻。 "我还只是一个没有独立科研经验的中国本科生，但是随着实习的推进，我第一次意识到科研是多么有趣。

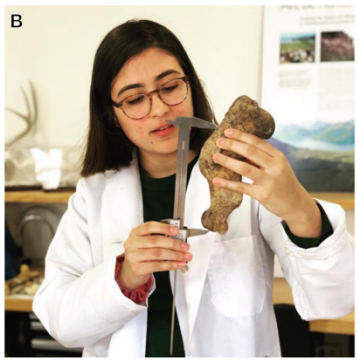

@mmel0n is a first generation latinx student, studying archaeology and anthropology in the zooarchaeology lab at Boston University. Melissa is currently researching a zooarchaeological assemblage (a group of fossils from a particular time and place) of Northern fur seals (Callorhinus ursinus) from Kodiak Island, Alaska. The goal of this research project is to use well-established aging methods to identify the age profiles of the seal pups. By determining if the seals are under four months old, Melissa can infer the presence of breeding seals on Kodiak and challenge previous assumptions about marine mammal dynamics in the North Pacific Ocean. Melissa hopes these results will contribute to our understanding of past fur seal distribution and Native food customs. Melissa is seen in these photos measuring a humerus for a growth curve equation, storing samples, and reading notes on her experiment.

@mmel0n es una estudiante latinx de primera generación que estudia arqueología y antropología en el laboratorio de zooarqueología de la Universidad de Boston. Melissa está investigando un ensamblaje zooarqueológico (un grupo de fósiles de un tiempo en y lugar particular) de lobos marinos del norte (Callorhinus ursinus) de la isla Kodiak, Alaska. El objetivo de este proyecto de investigación es utilizar métodos de envejecimiento bien establecidos para identificar los perfiles de edad de las crías de las focas. Al determinar si las focas tienen menos de cuatro meses, Melissa puede inferir la presencia de focas reproductoras en Kodiak y desafiar suposiciones previas sobre la dinámica de los mamíferos marinos en el Océano Pacífico Norte. Melissa espera que estos resultados contribuyan a nuestra comprensión de la distribución del lobo marino en el pasado y las costumbres de los alimentos nativos. Melissa se ve en estas fotos midiendo un húmero para una ecuación de curva de crecimiento, almacenando muestras y leyendo notas sobre su experimento.

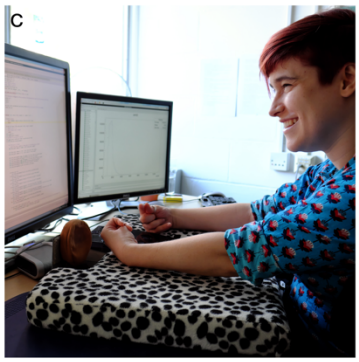

Claire (@geeknproud42) is a member of the High Energy Physics group at the University of Cambridge, searching for evidence of a group of as-yet undiscovered particles. Discovering these particles would complete the model that describes the behavior of the fundamental building blocks of the Universe, the Standard Model. These particles could also resolve some of the open problems in astrophysics such as the nature of dark matter, an unknown substance which is thought to comprise approximately a quarter of the universe. These particles could have properties that mirror those of the particles that we're already familiar with, such as electrons and photons. Claire aims to discover these elusive particles by developing new techniques to differentiate them from the Standard Model particles using data from the Large Hadron Collider at CERN. Due to her physical disability, cerebral palsy, Claire dictates the code she uses to an amanuensis and controls the computer with a joystick and a switch instead of a keyboard and a mouse.

Claire est membre du groupe de physique des hautes énergies de l'université de Cambridge. Elle recherche des preuves d'un groupe de particules encore inconnues. La découverte de ces particules compléterait le modèle standard de la physique des particules qui décrit le comportement des éléments fondamentaux de l'univers. Ces particules inconnues pourraient également résoudre certains des problèmes en suspens en astrophysique, comme la nature de la matière noire, une substance inconnue qui représenterait environ un quart de l'univers. Ces particules pourraient avoir des propriétés qui reflètent celles des particules que nous connaissons déjà comme les électrons et les photons. Claire vise à découvrir ces particules insaisissables en développant de nouvelles techniques pour les différencier des particules du modèle standard à l'aide des données du grand collisionneur de hadrons du CERN. En raison de son handicap physique, la paralysie cérébrale, Claire dicte le code qu'elle utilise à un(e) copiste et contrôle l'ordinateur avec un joystick et un interrupteur au lieu d'un clavier et d'une souris.

Figure S2 *Examples of Women Doing Science posts with bilingual captions, shared with permission from featured scientists: (A) geology PhD student Cheng Cao, whose biography was also posted in Mandarin, (B) archeology undergraduate Melissa Hurtado, whose biography was in English and Spanish (C) Physics PhD student Claire Malone, whose biography was in English and French.*

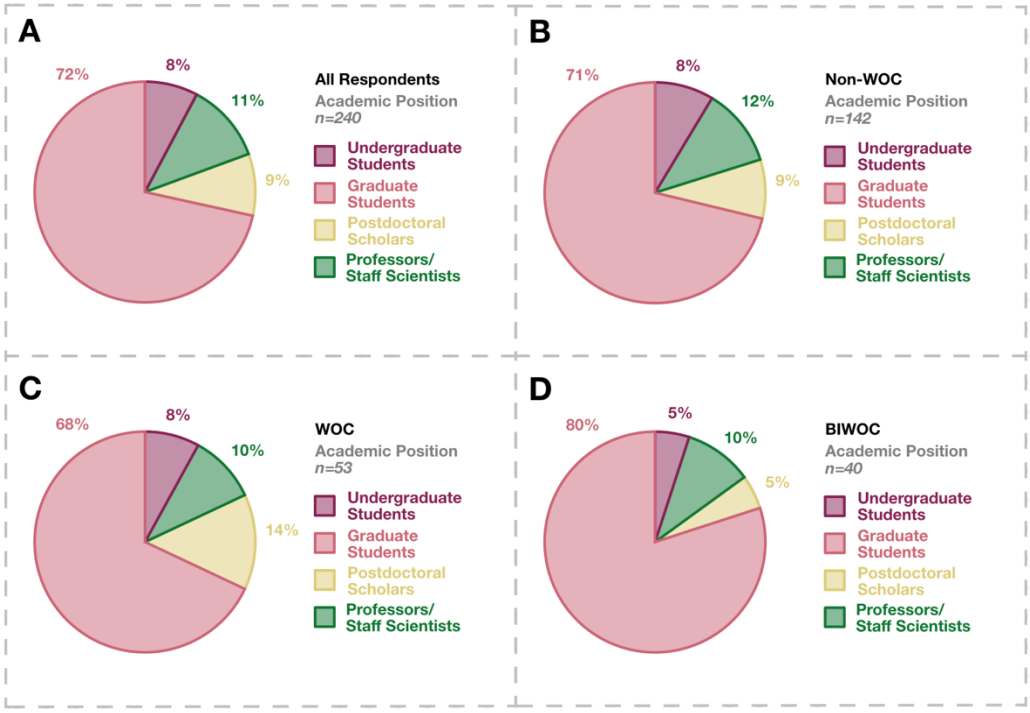

Figure S3 *Results on academic position from the survey sent to featured scientists on Women Doing Science broken down by (A) all respondents, n=240, (B) respondents that did not identify as WOC or BIWOC, n=142, (C) respondents that were WOC but not BIWOC, n=53, and (D) BIWOC, n=40. There were only minor changes across all, non-WOC, and WOC respondents, but BIWOC had a higher proportion of graduate students featured.*

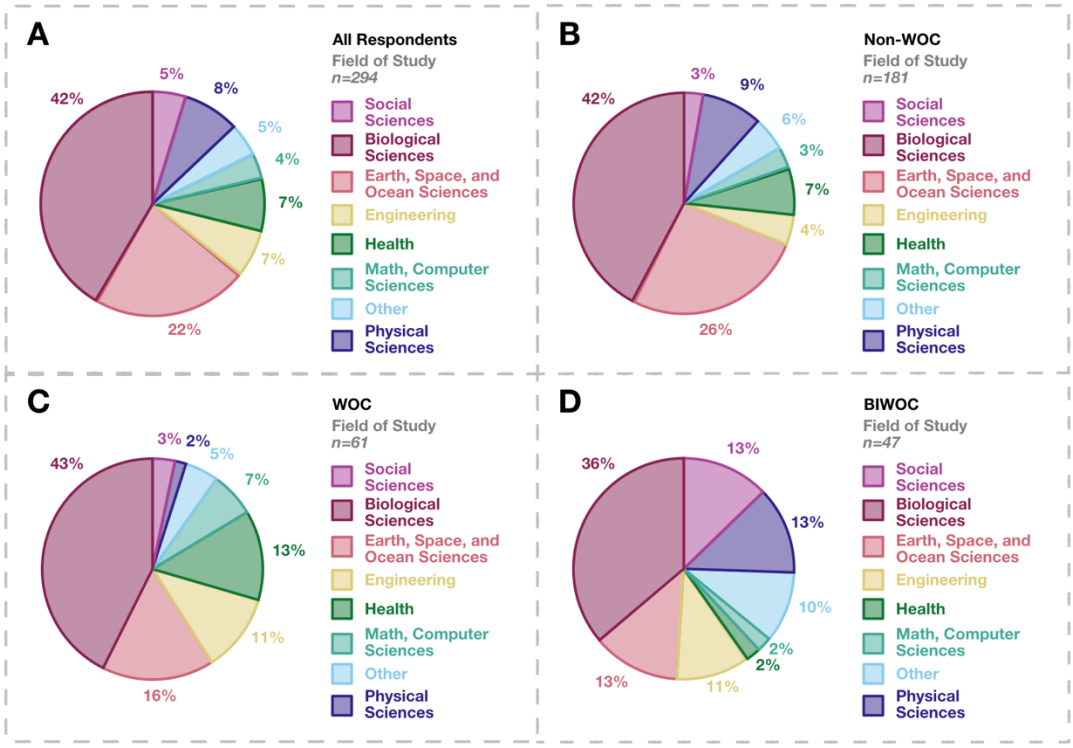

Figure S4 *Results on field of study from the survey sent to featured scientists on Women Doing Science broken down by (A) all respondents, n=294, (B) respondents that did not identify as WOC or BIWOC, n=181, (C) respondents that were WOC but not BIWOC, n=61, and (D) BIWOC, n=47. Note that sample sizes are higher than Figure S1 because scientists outside of academia were included. Non-WOC made up most respondents and therefore matched the overall proportions. WOC and BIWOC had a lower proportion of featured posts in earth, space, and ocean sciences, but higher proportions in engineering. More WOC were featured in health and medicine, while more BIWOC were in other fields like communication and education.*

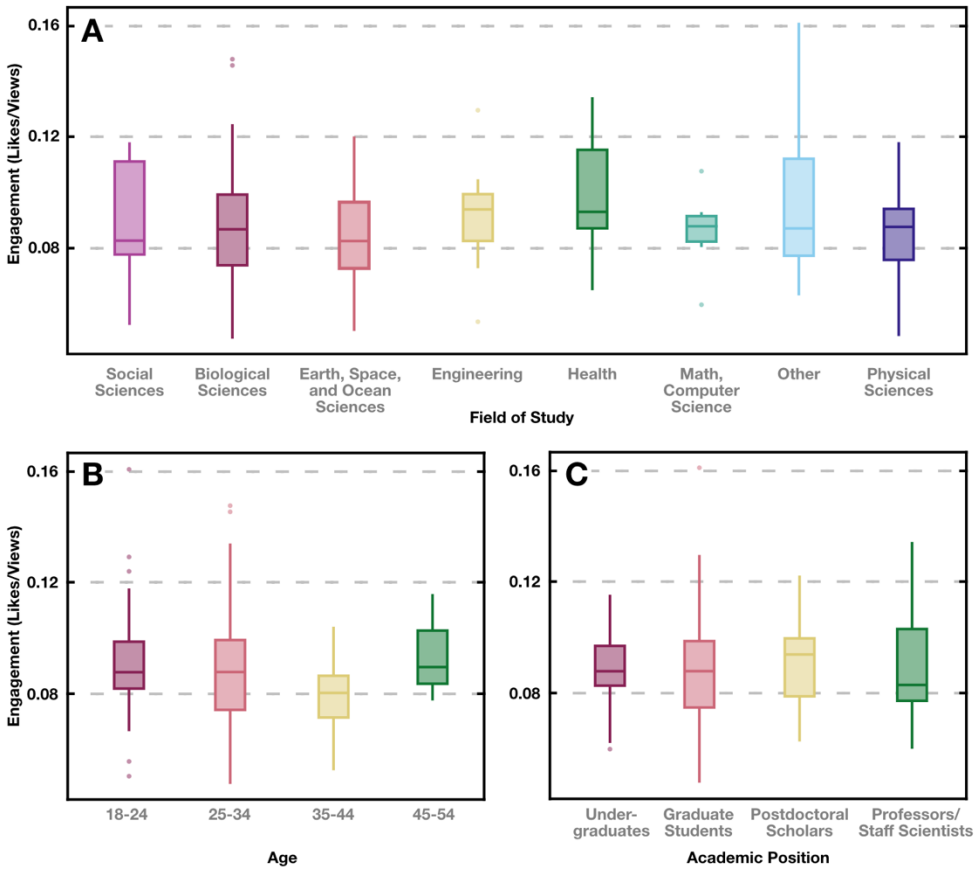

Figure S5 *Engagement of Women Doing Science posts across (A) field of study (B) age of featured scientists and (C) academic position. No significant differences in engagement were found across these categories.*

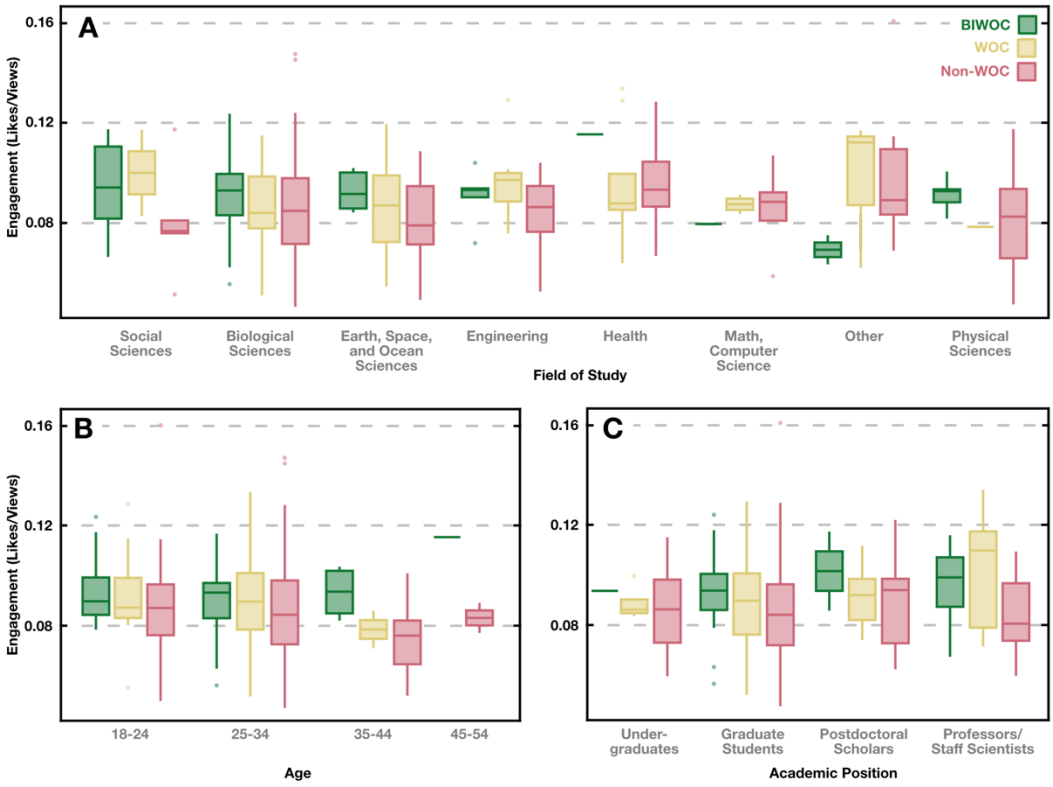

Figure S6 *Engagement of Women Doing Science for WOC, BIWOC and non-WOC by (A) field of study (B) age and (C) academic positions. No significant effects were observed.*

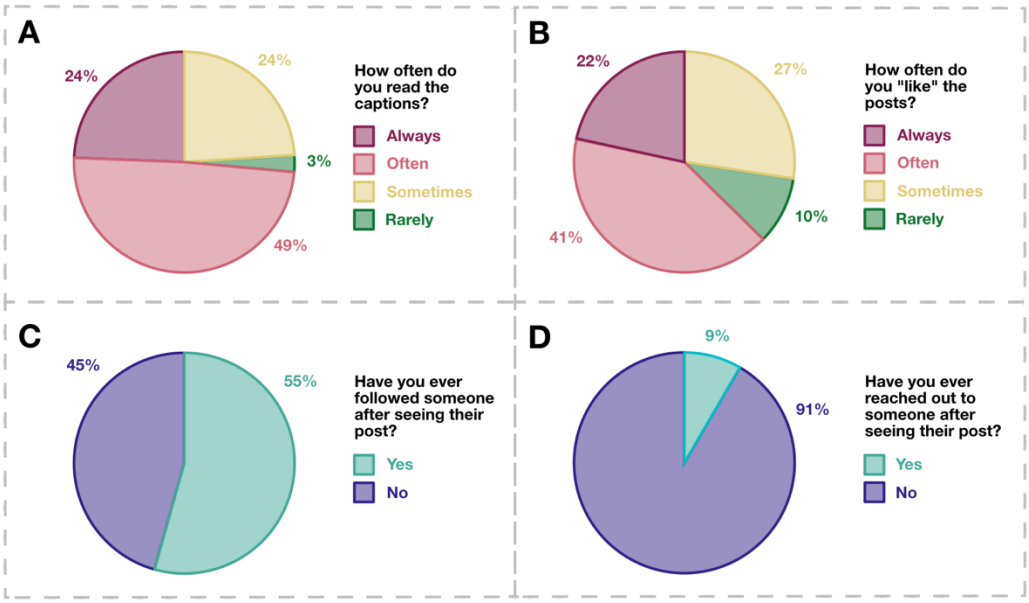

Figure S7 *Results from the survey to Women Doing Science followers for (A) how often they indicated they read Women Doing Science post captions (B) how often they "liked" Women Doing Science posts (C) whether they have ever followed a scientist after seeing their Women Doing Science feature and (D) whether they have ever reached out to someone after seeing their feature.*

BIBLIOGRAPHY

Amarasekara, I., Grant, W.J., 2019. Exploring the YouTube science communication gender gap: A sentiment analysis. Public Understanding of Science 28, 68–84.

Arya, D., Maul, A., 2012. The Role of the Scientific Discovery Narrative in Middle School Science Education: An Experimental Study. Journal of Educational Psychology 104, 1022.

Bakhshi, S., Shamma, D.A., Gilbert, E., 2014. Faces engage us: photos with faces attract more likes and comments on Instagram, in: Proceedings of the SIGCHI Conference on Human Factors in Computing Systems. Presented at the CHI '14: CHI Conference on Human Factors in Computing Systems, ACM, Toronto Ontario Canada, pp. 965–974.

Banchefsky, S., Westfall, J., Park, B., Judd, C.M., 2016. But you don't look like a scientist!: Women scientists with feminine appearance are deemed less likely to be scientists. Sex Roles: A Journal of Research 75, 95–109.

Berger, J., Milkman, K.L., 2012. What Makes Online Content Viral? Journal of Marketing Research 49, 192–205.

Bernard, R.E., Cooperdock, E.H.G., 2018. No progress on diversity in 40 years. Nature Geoscience 11, 292–295.

Blei, D.M., Ng, A.Y., Jordan, M.I., 2003. Latent dirichlet allocation. The Journal of Machine Learning Research 3, 993–1022.

Botella, C., Rueda, S., López-Iñesta, E., Marzal, P., 2019. Gender Diversity in STEM Disciplines: A Multiple Factor Problem. Entropy 21, 30.

Chimba, M., Kitzinger, J., 2010. Bimbo or boffin? Women in science: an analysis of media representations and how female scientists negotiate cultural contradictions. Public Understanding of Science 19, 609–624.

Doctorate Recipients from U.S. Universities, 2018. National Science Foundation.

Downs, A.C., 1981. Sex-Role Stereotyping on Prime-Time Television. The Journal of Genetic Psychology 138, 253–258.

Elena, A., 1997. Skirts in the lab: Madame Curie and the image of the woman scientist in the feature film. Public Understanding of Science (Bristol, England) 6, 269–278.

Fujioka, Y., 1999. Television Portrayals and African-American Stereotypes: Examination of Television Effects when Direct Contact is Lacking. Journalism & Mass Communication Quarterly 76, 52–75.

Funk, C., Gottfried, J., Mitchell, A., 2017. How Americans Get Science News and Information. Pew Research Center.

González-Pérez, S., Mateos de Cabo, R., Sáinz, M., 2020. Girls in STEM: Is It a Female Role-Model Thing? Frontiers in Psychology 11.

Gordin, M.D., 2015. Scientific Babel: How Science was Done Before and After Global English. University of Chicago.

Herrera, F.A., Hurtado, S., Garcia, G.A., Gasiewski, J., 2012. Talented Graduate Students: A Model for Redefining STEM Identity for Talented STEM Graduate Students.

Hitlin, P., Olmstead, K., 2018. The Science People See on Social Media. Pew Research Center.

Hofstra, B., Kulkarni, V.V., Galvez, S.M.-N., He, B., Jurafsky, D., McFarland, D.A., 2020. The Diversity–Innovation Paradox in Science. Proceedings of the National Academy of Sciences 117, 9284–9291.

Hong, H.Y., Lin-Siegler, X., 2012. How learning about scientists' struggles influences students' interest and learning in physics. - PsycNET. Journal of Educational Psychology 104, 469–484.

Hong, L., Page, S.E., 2004. Groups of diverse problem solvers can outperform groups of high-ability problem solvers. Proceedings of the National Academy of Sciences 101, 16385–16389.

Hornik, K., Mair, P., Rauch, J., Geiger, W., Buchta, C., Feinerer, I., 2013. The textcat Package for n -Gram Based Text Categorization in *R*. Journal of Statistical Software 52.

Hughes, R.M., Nzekwe, B., Molyneaux, K.J., 2013. The Single Sex Debate for Girls in Science: a Comparison Between Two Informal Science Programs on Middle School Students' STEM Identity Formation. Research in Science Education 43, 1979–2007.

Jarreau, P.B., Cancellare, I.A., Carmichael, B.J., Porter, L., Toker, D., Yammine, S.Z., 2019. Using selfies to challenge public stereotypes of scientists. PLOS ONE 14, e0216625.

Johnson, I.R., Pietri, E.S., Fullilove, F., Mowrer, S., 2019. Exploring Identity-Safety Cues and Allyship Among Black Women Students in STEM Environments. Psychology of Women Quarterly 43, 131–150.

Kitzinger, J., 2008. Role models in the media: an exploration of the views and experiences of women in science, engineering, and technology. UK Resource Centre for Women in Science, Engineering and Technology, Bradford.

LaFollette, M.C., 1982. Science on Television: Influences and Strategies. Daedalus 111, 183–197.

LaFollette, M.C., 1988. Eyes on the Stars: Images of Women Scientists in Popular Magazines. Science, Technology, & Human Values 13, 262–275.

Li, D., Koedel, C., 2017. Representation and Salary Gaps by Race-Ethnicity and Gender at Selective Public Universities. Educational Researcher 46, 343–354.

Liben, L.S., Signorella, M.L., 1993. Gender-schematic processing in children: The role of initial interpretations of stimuli. Developmental Psychology 29, 141–149.

Liu, S.-N.C., Brown, S.E.V., Sabat, I.E., 2019. Patching the “leaky pipeline”: Interventions for women of color faculty in STEM academia. Archives of Scientific Psychology.

Losh, S.C., 2010. Stereotypes about scientists over time among US adults: 1983 and 2001. Public Understanding of Science 19, 372–382.

Markus, H., Nurius, P., 1986. Possible selves. American Psychologist 41, 954–969.

Márquez, M.C., Porras, A.M., 2020. Science Communication in Multiple Languages Is Critical to Its Effectiveness. Frontiers in Communication 5.

McGee, E., 2019. Mentoring Underrepresented Students in STEMM: A Survey and Discussion. National Academies of Science, Engineering, and Medicine.

Medin, D.L., Lee, C.D., 2012. Diversity Makes Better Science. APS Observer 25.

Mendick, H., Moreau, M.-P., 2013. New media, old images: constructing online representations of women and men in science, engineering and technology. Gender and Education 25, 325–339.

Miller, D.I., Eagly, A.H., Linn, M.C., 2015. Women's representation in science predicts national gender-science stereotypes: Evidence from 66 nations. Journal of Educational Psychology 107, 631–644.

Morning, A., 2015. Ethnic Classification in Global Perspective: A Cross-National Survey of the 2000 Census Round, in: Simon, P., Piché, V., Gagnon, A.A. (Eds.), Social Statistics and Ethnic Diversity, IMISCOE Research Series. Springer International Publishing, Cham, pp. 17–37.

Moseley, R., Read, J., 2002. "Having it Ally ": Popular Television (Post-)Feminism. Feminist Media Studies 2, 231–249.

National Academies of Sciences, E., 2018. Graduate STEM Education for the 21st Century.

Nelkin, D., 1987. Selling Science: How the Press Covers Science and Technology.

R Core Team, 2020. R: The R Project for Statistical Computing. https://www.r-project.org/

Race and ethnicity in higher education: a status report, 2019. . American Council on Education.

Ranganathan, M., Lalk, E., Freese, L.M., Freilich, M.A., Wilcots, J., Duffy, M.L., Shivamoggi, R., 2021. Trends in the representation of women amongst geoscience faculty from 1999-2020: the long road towards gender parity. Earth and Space Science Open Archive.

Riegle-Crumb, C., King, B., Irizarry, Y., 2019. Does STEM Stand Out? Examining Racial/Ethnic Gaps in Persistence Across Postsecondary Fields. Educational Researcher 48, 133–144.

Schmidt, B.M., Nixon, R.M., 1996. Improving girls' attitudes towards science. Public Understanding of Science 5, 255–268.

Shannon, G., Jansen, M., Williams, K., Cáceres, C., Motta, A., Odhiambo, A., Eleveld, A., Mannell, J., 2019. Gender equality in science, medicine, and global health: where are we at and why does it matter? The Lancet 393, 560–569.

Starr, C.R., 2018. “I’m Not a Science Nerd!”: STEM Stereotypes, Identity, and Motivation Among Undergraduate Women. Psychology of Women Quarterly 42, 489–503.

Steinke, J., 1999. Women Scientist Role Models on Screen: A Case Study of Contact. Science Communication 21, 111–136.

Steinke, J., 2005. Cultural Representations of Gender and Science: Portrayals of Female Scientists and Engineers in Popular Films. Science Communication 27, 27–63.

Steinke, J., 2017. Adolescent Girls’ STEM Identity Formation and Media Images of STEM Professionals: Considering the Influence of Contextual Cues. Frontiers in Psychology 8.

Steinke, J., Long, M., 1996. A Lab of Her Own?: Portrayals of Female Characters on Children’s Educational Science Programs. Science Communication 18, 91–115.

Strahan, E.J., Wilson, A., 2006. Temporal comparisons, identity, and motivation: The relation between past, present, and possible future selves. Possible Selves: Theory, Research and Applications 1–16.

Swartz, T.H., Palermo, A.-G.S., Masur, S.K., Aberg, J.A., 2019. The Science and Value of Diversity: Closing the Gaps in Our Understanding of Inclusion and Diversity. The Journal of Infectious Diseases 220, S33–S41.

Tan, E., Barton, A.C., Kang, H., O’Neill, T., 2013. Desiring a career in STEM-related fields: How middle school girls articulate and negotiate identities-in-practice in science. Journal of Research in Science Teaching 50, 1143–1179.

The Scully Effect: I Want to Believe in STEM, 2018. . Geena Davis Institute on Gender in Media.

Thompson, J., Windschitl, M., 2005. “FAILING GIRLS”: Understanding Connections among Identity Negotiation, Personal Relevance, and Engagement in Science Learning from Underachieving Girls. Journal of Women and Minorities in Science and Engineering 11, 1–26.

Why don’t European girls like science or technology?, 2017. . Microsoft.